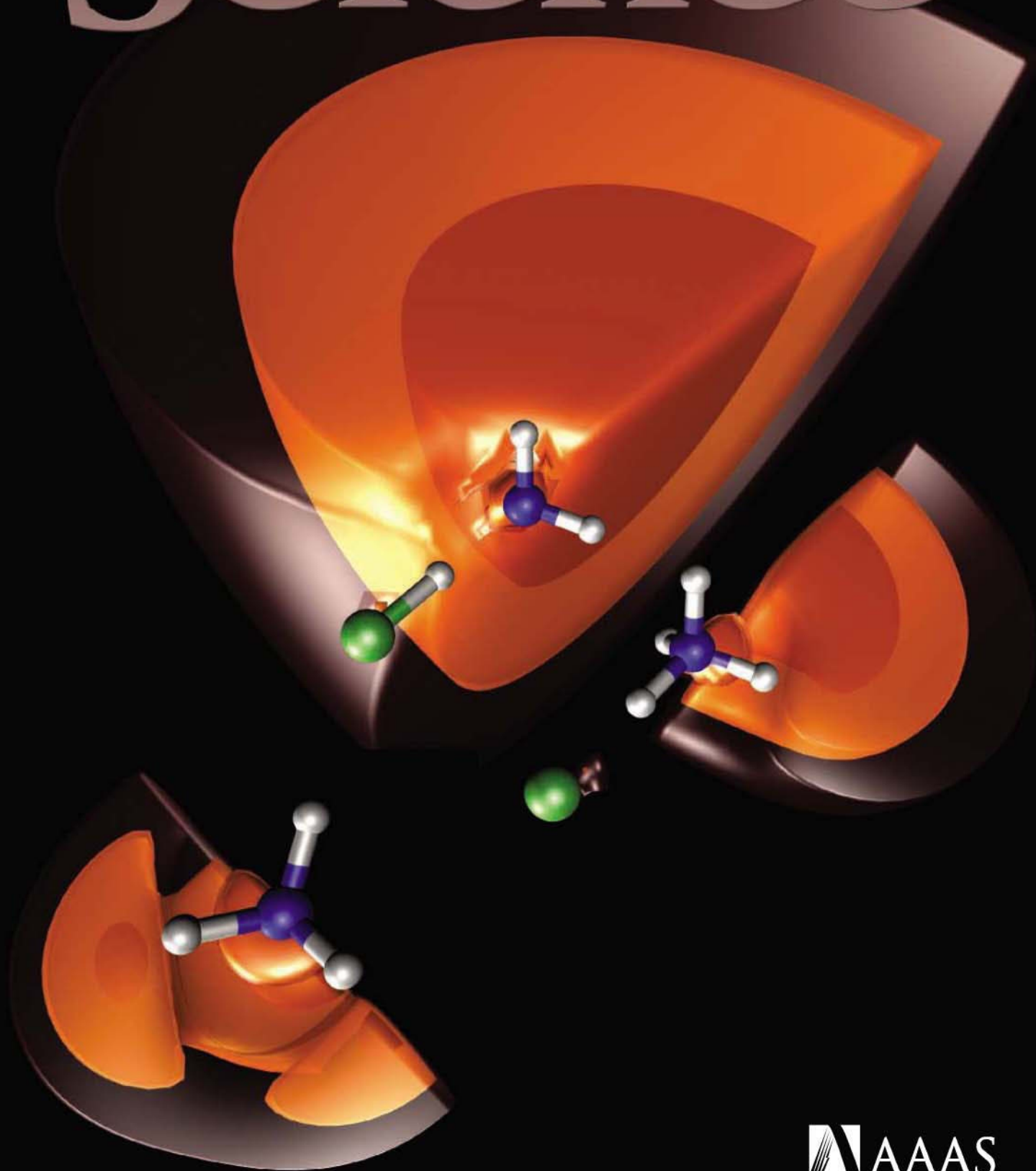
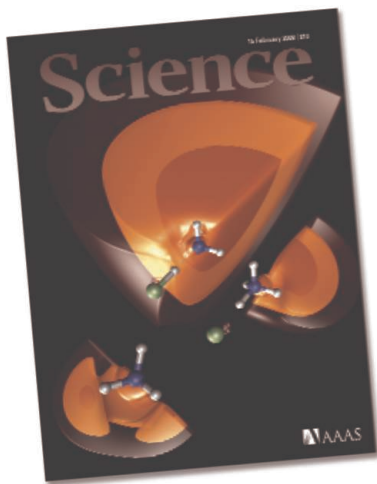


15 February 2008 | \$10

Science





COVER

A depiction of the interaction of an excess electron with the hydrogen-bonded complex $\text{NH}_3 \cdots \text{HCl}$, which induces formation of the ionic pair $\text{NH}_4^+ \text{Cl}^-$ solvated by the excess electron. The image shows the structures of three possible systems and highlights the areas that correspond to 10%, 30%, and 50% of the excess electron. See page 936.

Illustration: Maciej Haranczyk

DEPARTMENTS

- 871 *Science Online*
- 873 *This Week in Science*
- 878 *Editors' Choice*
- 880 *Contact Science*
- 881 *Random Samples*
- 883 *Newsmakers*
- 969 *New Products*
- 970 *Science Careers*

EDITORIAL

- 877 "Glocal" Science Advocacy
by Alan I. Leshner

NEWS OF THE WEEK

- Deaths in Diabetes Trial Challenge a Long-Held Theory 884
- Alien Planetary System Looks a Lot Like Home 885
- >> *Report p. 927*

- Biodefense Watchdog Project Folds, Leaving a Void 886
- U.S. Prepares to Launch Flawed Satellite 886

- Senate Bill Would Scale Up Forest Restoration 887
- SCIENCE SCOPE** 887

- Back-to-Basics Push as HIV Prevention Struggles 888
- Another Side to the Climate-Cloud Conundrum Finally Revealed 889

NEWS FOCUS

- Wolves at the Door of a More Dangerous World 890
- Framework Materials Grab CO_2 and Researchers' Attention 893
- >> *Report p. 939*

- In South Africa, XDR TB and HIV Prove a Deadly Combination 894
- Research Project Mimics TB Transmission

- Joint Mathematics Meeting 898
- Number Theorists' Big Cover-Up Proves Harder Than It Looks
- A Woman Who Counted
- Exact-Postage Poser Still Not Licked



890

LETTERS

- Climate Change: A Titanic Challenge S. C. Sherwood 900
- In Defense of Bed Nets A. Y. Kitua et al.
- Grant Approval and Risky Research: A Nobel Story
J. M. Berg Response M. R. Capecchi
- Making Sense of Scrambled Genomes D. Speijer
Response L. F. Landweber

CORRECTIONS AND CLARIFICATIONS 901

BOOKS ET AL.

- Opting Out?** Why Women Really Quit Careers and Head Home P. Stone, reviewed by P. Moen 903
- Bending the Rules** Morality in the Modern World from Relationships to Politics and War R. A. Hinde, reviewed by B. W. Heineman Jr. 904
- A Taste of the Gonzo Scientist** 905
- >> *Online Feature p. 871*

POLICY FORUM

- Transforming Environmental Health Protection 906
- F. S. Collins, G. M. Gray, J. R. Bucher

PERSPECTIVES

- Making Strong Fibers** 908
- H. G. Chae and S. Kumar
- Homo economicus** Evolves 909
- S. D. Levitt and J. A. List
- Combating Impervious Bugs** 910
- R. P. Novick
- >> *Report p. 962 and Science Express Report by Liu et al.*
- On Mixing and Demixing** 912
- J. M. Ottino and R. M. Lueptow
- Green with Complexity** 913
- S. Naeem >> *Report p. 952*
- Sidestepping Mutational Meltdown** 914
- E. A. Shoubridge and T. Wai >> *Report p. 958*



903



SCIENCE EXPRESS

www.sciencexpress.org

APPLIED PHYSICS

Sr Lattice Clock at 1×10^{-16} Fractional Uncertainty by Remote Optical Evaluation with a Ca Clock

A. D. Ludlow et al.

Two clocks based on optical transitions in single trapped ions set 4 kilometers apart are able to keep time within a fractional error of 1×10^{-16} , better than the standard atomic clock.

10.1126/science.1153341

MICROBIOLOGY

A Cholesterol Biosynthesis Inhibitor Blocks *Staphylococcus aureus* Virulence

C.-I. Liu et al.

A drug for controlling cholesterol may be useful as an antibiotic for multi-drug-resistant *Staphylococcus* because of unexpected structural similarities among critical proteins.

10.1126/science.1153018

MEDICINE

Neurokinin 1 Receptor Antagonism as a Possible Therapy for Alcoholism

D. T. George et al.

A drug that inhibits a neural signaling pathway linked to behavioral stress may be a useful therapy in preventing relapse in alcoholics.

10.1126/science.1153813

DEVELOPMENTAL BIOLOGY

Generation of Pluripotent Stem Cells from Adult Mouse Liver and Stomach Cells

T. Aoi et al.

Induced pluripotent stem cells are generated by direct reprogramming of adult liver and stomach cells without retroviral integration into specific sites in the genome.

10.1126/science.1154884

TECHNICAL COMMENT ABSTRACTS

EVOLUTION

Comment on "The Latitudinal Gradient in Recent Speciation and Extinction Rates of Birds and Mammals" 901

J. A. Tobias, J. M. Bates, S. J. Hackett, N. Seddon

[full text at www.sciencemag.org/cgi/content/full/319/5865/901c](http://www.sciencemag.org/cgi/content/full/319/5865/901c)

Response to Comment on "The Latitudinal Gradient in Recent Speciation and Extinction Rates of Birds and Mammals"

J. T. Weir and D. Schluter

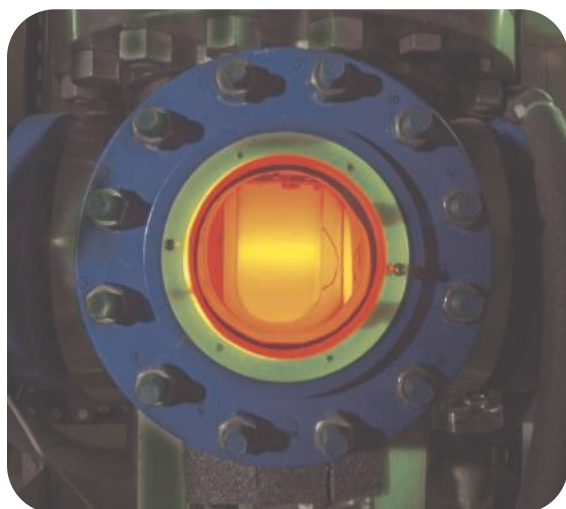
[full text at www.sciencemag.org/cgi/content/full/319/5865/901d](http://www.sciencemag.org/cgi/content/full/319/5865/901d)

REVIEW

CELL BIOLOGY

Adapting Proteostasis for Disease Intervention 916

W. E. Balch, R. I. Morimoto, A. Dillin, J. W. Kelly



933

BREVIA

CLIMATE CHANGE

Emergence of Anoxia in the California Current Large Marine Ecosystem 920

F. Chan et al.

Extreme oxygen deficits in the northern California Current system caused widespread anoxia, killing benthic invertebrates on the continental shelf of Oregon during 2006.

RESEARCH ARTICLE

MEDICINE

Identification of Host Proteins Required for HIV Infection Through a Functional Genomic Screen 921

A. L. Brass et al.

An RNAi screen identified 237 new and 38 known human proteins required for HIV infection, including ones used in Golgi transport and in viral integration and transcription.

REPORTS

ASTRONOMY

Discovery of a Jupiter/Saturn Analog with Gravitational Microlensing 927

B. S. Gaudi et al.

A system of two giant planets orbiting a star has been discovered through their gravitational deflection of light from more distant stars.

>> *News story p. 885*

APPLIED PHYSICS

Imaging Phonon Excitation with Atomic Resolution 930

H. Gawronski, M. Mehlhorn, K. Morgenstern

Maps of the second derivative of the scanning tunneling microscope current with respect to voltage reveal atomic-scale variations in the surface vibrational modes of metals.

CONTENTS continued >>

REPORTS CONTINUED...

PHYSICS

Spin-Dependent WIMP Limits from a Bubble Chamber 933

E. Behnke et al.

Experiments with a stabilized bubble chamber, consisting of a buried superheated liquid, limit the abundance of weakly interacting massive particles, a dark-matter candidate.

CHEMISTRY

Electron-Driven Acid-Base Chemistry: Proton Transfer 936 from Hydrogen Chloride to Ammonia

S. N. Eustis et al.

Spectroscopy and simulations show that binding an excess electron to HCl helps it fully transfer its proton to ammonia, facilitating this type of acid-base reaction in a vacuum.

CHEMISTRY

High-Throughput Synthesis of Zeolitic Imidazolate Frameworks and Application to CO₂ Capture 939

R. Banerjee et al.

Microporous metallic-organic frameworks with two types of linkers between the metal atoms in a tetrahedral lattice can take up large amounts of CO₂ at ambient conditions. >> *News story p. 893*

GEOCHEMISTRY

Rogue Mantle Helium and Neon 943

F. Albarède

Anomalously high ratios of ³He to ⁴He in the recycled basalts under ocean islands may result from helium diffusing in from more pristine, primitive mantle.

EVOLUTION

The Premetazoan Ancestry of Cadherins 946

M. Abedin and N. King

A close unicellular relative of metazoans unexpectedly contains 23 genes for a cell adhesion protein, suggesting a role for the protein in the evolution of multicellularity.

ECOLOGY

A Global Map of Human Impact on Marine Ecosystems 948

B. S. Halpern et al.

A meta-analysis shows that human activities have altered virtually all ocean ecosystems, at least to some extent, documenting those areas needing the most protection.

ECOLOGY

Effects of Predator Hunting Mode on Grassland Ecosystem Function 952

O. J. Schmitz

An ecosystem containing actively hunting spiders shows lower plant diversity but higher primary production than one with spiders that sit and wait to ambush their prey.

>> *Perspective p. 913*

BIOCHEMISTRY

Axle-Less F₁-ATPase Rotates in the Correct Direction 955

S. Furuie et al.

A molecular rotary motor continues to rotate in the correct direction even when its shaft is deleted, leaving only the rotor head sitting on top of the shaft housing.

GENETICS

A Mouse Model of Mitochondrial Disease Reveals Germline Selection Against Severe mtDNA Mutations 958

W. Fan et al.

Developing mouse oocytes that harbor highly deleterious mitochondrial DNA mutations are eliminated, minimizing negative impact on population fitness.

>> *Perspective p. 914*

MEDICINE

Metal Chelation and Inhibition of Bacterial Growth in Tissue Abscesses 962

B. D. Corbin et al.

An immune cell-derived protein binds metal ions in infected abscesses, depriving the bacteria of the essential nutrients magnesium and zinc and reducing their growth.

>> *Perspective p. 910*

PSYCHOLOGY

The Critical Importance of Retrieval for Learning 966

J. D. Karpicke and H. L. Roediger III

Students recalled words they had learned the previous week more effectively if they were tested repeatedly in the interim than if they spent the time studying.



ADVANCING SCIENCE. SERVING SOCIETY

SCIENCE (ISSN 0036-8075) is published weekly on Friday, except the last week in December, by the American Association for the Advancement of Science, 1200 New York Avenue, NW, Washington, DC 20005. Periodicals Mail postage (publication No. 484460) paid at Washington, DC, and additional mailing offices. Copyright © 2008 by the American Association for the Advancement of Science. The title SCIENCE is a registered trademark of the AAAS. Domestic individual membership and subscription (51 issues): \$144 (\$74 allocated to subscription). Domestic institutional subscription (51 issues): \$770; Foreign postage extra: Mexico, Caribbean (surface mail) \$55; other countries (air assist delivery) \$85. First class, airmail, student, and emeritus rates on request. Canadian rates with GST available upon request, GST #1254 88122. Publications Mail Agreement Number 1069624. SCIENCE is printed on 30 percent post-consumer recycled paper. Printed in the U.S.A.

Change of address: Allow 4 weeks, giving old and new addresses and 8-digit account number. Postmaster: Send change of address to AAAS, P.O. Box 96178, Washington, DC 20090-6178. Single-copy sales: \$10.00 current issue, \$15.00 back issue prepaid includes surface postage; bulk rates on request. Authorization to photocopy material for internal or personal use under circumstances not falling within the fair use provisions of the Copyright Act is granted by AAAS to libraries and other users registered with the Copyright Clearance Center (CCC) Transactional Reporting Service, provided that \$20.00 per article is paid directly to CCC, 222 Rosewood Drive, Danvers, MA 01923. The identification code for Science is 0036-8075. Science is indexed in the Reader's Guide to Periodical Literature and in several specialized indexes.

CONTENTS continued >>>

SCIENCE NOW

www.sciencenow.org DAILY NEWS COVERAGE

The Tiredness of the Long-Distance Runner

Leaky calcium channels may cause muscle fatigue, and a new drug could boost performance.

I Hear You, My Monkey Brother

A region of the monkey brain responds preferentially to the voices of other monkeys.

Taking the Heat Off Coral

A natural ocean “thermostat” is counteracting the effects of climate warming.



Stopping cell death.

SCIENCE SIGNALING

www.stke.org THE SIGNAL TRANSDUCTION KNOWLEDGE ENVIRONMENT

PERSPECTIVE: Cell Stress Gives a Red Light to the Mitochondrial Cell Death Pathway

M. E. Guicciardi and G. J. Gores

A prefoldin protein and insulin-like growth factor-binding protein act at the mitochondrion to inhibit apoptosis.

TEACHING RESOURCE: Quantitative Models of Mammalian Cell Signaling Pathways

R. Iyengar

Prepare a graduate-level class covering mathematical modeling of mammalian signaling pathways.



SCIENCE ONLINE FEATURE

THE GONZO SCIENTIST: Can Scientists Dance?

Our intrepid reporter organized the first-ever “Dance Your Ph.D.” contest to answer the question—and has video to show for it.

www.sciencemag.org/sciext/gonzoscientist



Overcoming that phony feeling.

SCIENCE CAREERS

www.sciencecareers.org CAREER RESOURCES FOR SCIENTISTS

In Person: Finding Opportunities in a Dysfunctional Job Market

B. Allen

To find hidden value in the job market, you have to cast a wide net.

No, You're Not an Impostor

L. Laursen

Getting over the feeling that you're a phony takes an accurate self-appraisal.

Tooling Up: Put Some Muscle Into Your Marketing Materials

D. Jensen

Powerful writing can move your job application to the top of the pile.

From the Archives: How to Get a Job in Academia

A. Fazekas

What the hiring committee is looking for depends on the type of institution.

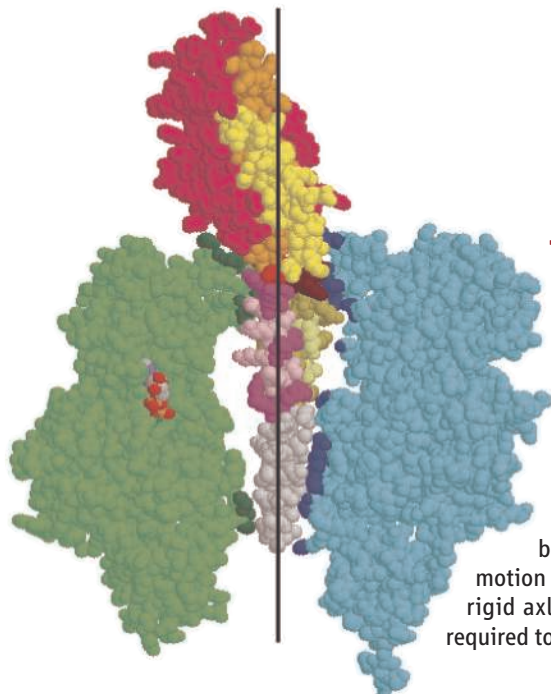
SCIENCE PODCAST

Download the 15 February *Science* Podcast to hear about the discovery of a Jupiter/Saturn analog, anoxia in the California Current marine ecosystem, extensively drug-resistant tuberculosis, dancing scientists, and more.

www.sciencemag.org/about/podcast.dtl



Separate individual or institutional subscriptions to these products may be required for full-text access.



<< Molecular Rotary Motor

F_1 -adenosine triphosphatase is an ATP-driven rotary motor in which a central subunit rotates inside a static cylinder. The stator provides a hydrophobic sleeve for the bottom of the rotor that could act as a bearing so that force from ATP hydrolysis can be converted to a torque. **Furuike *et al.*** (p. 955) truncated the shaft to leave just a rotor head on top of the concave rotor orifice. Surprisingly, the head rotated in the correct direction, but the average rotary speeds were low and the motion sometimes irregular. Although a fixed pivot and a rigid axle improve the efficiency of the motor, neither is required to achieve rotation.

Detecting Less Massive Extrasolar Planets

Astronomers have discovered a large number and variety of planets orbiting stars far from our solar system. Most of these detections were of bodies with masses much larger than the heaviest objects in the solar system, largely because methods for detecting them are only sensitive to massive orbiting bodies. **Gaudi *et al.*** (p. 927; see the news story by **Kerr**) report their observation of two planets with masses less than that of Jupiter orbiting a star of mass half that of our Sun. The discovery was made possible by an improved form of gravitational lensing in which light from distant stars is bent by the planetary system on its way to Earth.

Pinning Down WIMP Detectability

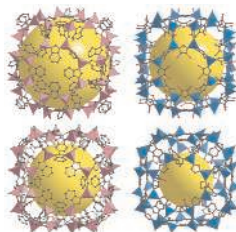
Most of the universe is thought to be composed of dark matter, and novel ways are being sought to detect and characterize it. One strong candidate for dark matter are so-called weakly interacting massive particles (WIMPs), which interact through weak force and gravity but do not interact with electromagnetic radiation. **Behnke *et al.*** (p. 933) show that bubble chambers, which consist of superheated liquids that yield a train of bubbles from the heat produced as a particle passes through them, can be tuned to provide some limits on the abundance of WIMPs. One challenge was stabilizing the chamber for long-term measurements (most particle physics detections last for milliseconds). The cross sections measured for spin-dependent WIMP coupling do not support a recent claim of dark-matter detection.

Proton Transfer Charged Ahead

Proton transfer from hydrogen chloride to ammonia is a prototypical acid-base reaction and is known to proceed not only in solution but in dense gaseous mixtures as well. However, careful studies have shown that when isolated HCl and NH_3 molecules pair up in vacuum, they form a hydrogen-bonded complex that keeps the shared proton more closely associated with chloride. **Eustis *et al.*** (p. 936; see the cover) applied photoelectron spectroscopy and theoretical simulations to explore the perturbations necessary to induce full proton transfer, and found that one driver can be the binding of an excess electron. The resulting complex is characterized as a neutral NH_4 Rydberg radical species polarized by an adjacent Cl^- anion.

Capturing CO_2 with Organic Zeolite Analogs

Porous metal-organic framework compounds are useful for gas sorption, and a wide variety of compounds could be made, especially if different linkers between metal atoms were incorporated within the same material. However, the expectation might be that two products, each with only one of the linkers, would be favored in a mixed system. Despite this potential drawback, **Banerjee *et al.*** (p. 939; see the news story by **Service**) show that a combinatorial



microsynthetic approach that uses Zn(II) or Co(II) centers and imidazolate and related linkers generates a large number of crystalline products with tetrahedral frameworks and zeolitic topologies. Of the 25 structures, 10 have heterolinkers and 5 have previously unobserved topologies. Three of the products show exceptional thermal stability (up to 390°C), along with high selectivity for CO_2 versus CO , as well as high CO_2 uptake at ambient conditions.

Staying in the Fold

A cell's proteins are continually subjected to stresses that could promote their misfolding and aggregation. In addition, a wide variety of diseases are caused by the misfolding and aggregation of key proteins. **Balch *et al.*** (p. 916) now review the so-called proteostasis machinery, which the cell uses to combat these problems. The authors highlight the potential for manipulation of the proteostasis machinery in future efforts to treat misfolding diseases.

Getting a Handle on HIV Host Factors

Because the HIV-1 virus encodes only a handful of its own proteins, it must exploit multiple host cell processes to ensure completion of its life-cycle. Thus, many potential host factors could influence HIV infection, which for the most part remain unknown. **Brass *et al.*** (p. 921, published online 10 January; see the 11 January news story by **Cohen**) used a genome-wide small interfering RNA functional screen to identify a large number of HIV-dependency factors, some known, but

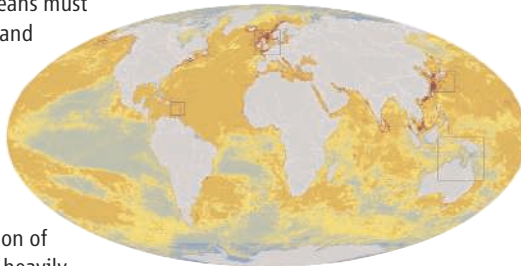
Continued on page 875

Continued from page 873

many unknown. Several of the genes were studied further and played roles in viral entry, integration, biosynthesis, and assembly, as well as in the later stages of infection.

Oceans Under Threat

In order to assign regional priorities to global-scale marine resource management, the type and extent of human impacts on the world's oceans must be assessed. Through quantitative, global, and high-resolution analyses of the cumulative impact of 17 of the most urgent land- and ocean-based threats to all marine ecosystems, **Halpern *et al.*** (p. 948) show that no areas of the ocean are untouched by human activities. A third of the oceans are heavily impacted, and the spatial distribution of impacts is highly heterogeneous. The most heavily affected ecosystems are continental shelves, rocky reefs, coral reefs, seagrass beds, and seamounts.



Cadherins on the Road to Multicellularity

How early organisms made the transition from unicellularity to multicellularity is unknown, although certain genes have been implicated as important players in this process. One such group is the cadherin family of genes that function in cell adhesion and cell-cell signaling. By examining the genome of the unicellular choanoflagellate *Monosiga brevicollis*, **Abedin and King** (p. 946) show that the genome of *M. brevicollis* contains 23 expressed cadherin genes—as many as several multicellular animals. At least two of the cadherins localized to the actin-filled microvilli of the protozoan feeding collar, where they may participate in the recognition and capture of bacterial prey.

The Spider and the Grasshopper

How do predators control ecosystem dynamics? **Schmitz** (p. 952; see the Perspective by **Naeem**) studied spiders and their grasshopper prey in a meadow ecosystem, and identified predator hunting mode and prey response as determinants of ecosystem function. Actively hunting spider species (which grasshoppers largely ignored) reduced plant species diversity and enhanced aboveground net primary production, litter quality, and nitrogen mineralization rates, whereas sit-and-wait ambush spider species (which grasshoppers avoided) had opposite effects. Top predators in marine and terrestrial ecosystems are among the fastest disappearing elements of biodiversity, and understanding their role in local ecosystem functioning may help to predict the effects of their loss.

Filtering Out the Bad from the Less Bad

Maternally inherited mitochondrial DNA (mtDNA) mutations are implicated in a variety of human diseases including cardiomyopathy and neurodegenerative disorders. It has been assumed that mtDNA mutations are randomly segregated by genetic drift within the female germ line. **Fan *et al.*** (p. 958; see the Perspective by **Shoubridge and Wai**) created a sophisticated mouse model that allowed them to monitor the fates and phenotypic effects of mtDNAs containing mutations of varying severity. Surprisingly, the most pathogenic mtDNA mutation was quickly eliminated from the female germ line, whereas a moderately deleterious mtDNA mutation continued to be transmitted through multiple generations. Thus, the female germ line filters out the most deleterious mtDNA mutations prior to conception, thereby minimizing their impact on population fitness.

Practice, Practice, Practice!





Artur Rubinstein's response when asked the way to Carnegie Hall in Manhattan may in fact apply to other forms of study as well. **Karpicke and Roediger** (p. 966) examined undergraduates tasked with learning the meanings of 40 words in Swahili. Repeated testing of already learned words enhanced long-term recall when assessed 1 week later, whereas repeated studying had no beneficial effects. Testing required students to retrieve the English-Swahili word associations, which suggests that encoding, although critical for the formation of a memory, may not be sufficient for its retention or consolidation.

CREDIT: HALPERN ET AL.

EASY FOR FUSIONS



Monomeric tags for protein labeling

-  Cyan fluorescent protein
TagCFP
ex/em = 458/480 nm
-  Green fluorescent protein
TagGFP
ex/em = 482/505 nm
-  Yellow fluorescent protein
TagYFP
ex/em = 508/524 nm
-  Red fluorescent protein
TagRFP
ex/em = 555/583 nm
-  Far-red fluorescent protein
TagFP635
ex/em = 588/635 nm

Evrogen JSC
Tel: +7(495) 336 6388
Fax: +7(495) 429 8520
www.evrogen.com



Alan I. Leshner is chief executive officer of the American Association for the Advancement of Science and executive publisher of *Science*.

“Glocal” Science Advocacy

HERE WE GO AGAIN. ON 4 FEBRUARY, PRESIDENT BUSH RELEASED HIS FISCAL YEAR (FY) 2009 budget request to the U.S. Congress, and the news for research funding is once again mixed. Some agencies, such as the National Science Foundation and the Department of Energy’s Office of Science, are proposed for very substantial increases, but others, such as the National Institutes of Health (NIH), are slated for flat funding or worse. This news comes after a dismal FY 2008 science funding outcome. If the new Bush budget proposal is adopted, U.S. research will see its fifth consecutive year of decreased support (in inflation-adjusted constant dollars) as compared to the increasing research investments by other nations. The news is important not only for the U.S. scientific community but also for its many international collaborators.

What can be done about it? The traditional approach used by U.S. scientific societies and citizen advocacy groups has been en masse descents on Capitol Hill to plead with Congress for better treatment. This scheme has sometimes worked in the past, as Congress often provided larger increases for science than those proposed by the president. But the “attack on the Hill” has been marginally effective in recent years, and last year it didn’t seem to work at all. So simply following the same game plan this year risks another failure.

We should take up “glocal” science advocacy to complement the traditional approach. This strategy involves taking a global issue and making it meaningful to society at the local level. Scientists and citizen advocates should recruit their nonscience friends and neighbors to promote science funding to decision-makers. Recruiting efforts can be as simple as discussing science-related issues at dinner parties or as ambitious as meeting with community groups, school boards, or city council members. The appeal should be locally focused for two important reasons: Policy-makers often seem to listen better in their home districts, where they are less distracted by the press of life on Capitol Hill; and they need to see clearly that science funding is not only a national but a local issue for all their constituents, not just those who are scientists.

This approach has long been urged by such leaders as former Congressman John Porter (R–IL), who with Senators Arlen Specter (R–PA) and Tom Harkin (D–IA) led the successful efforts on the Hill to double the NIH budget during 1998–2003. But glocal science advocacy is not a strategy that is easily implemented. To make it work, the scientific community needs to change the way it relates to friends and neighbors about the scientific enterprise. That will require finding more effective ways to persuade them that science is not only fascinating but also central to them as individuals, because most major societal issues have a science component to them. On the other side, scientists must respond to concerns about how scientific advances will affect personal lives and things that matter in the community. The high visibility of embryonic stem cell research and the study of evolution exemplify the need for better public engagement and dialogue about the underlying science and its implications.

Glocal science advocacy will be a learned skill for scientists and nonscientists, so training programs are needed to help scientists better engage with the public and foster this approach. Some organizations, such as Stanford University’s Aldo Leopold Leadership Program, Research!America’s Paul G. Rogers Society for Global Health Research, and the American Association for the Advancement of Science, have good programs that can help guide scientists to become effective communicators, but many more need preparation of this kind. Every U.S. scientist should embrace glocal science advocacy as a meaningful part of the job. If the scientific community does not expand its efforts and try new approaches to influence investment in research, it risks, as Einstein put it, proving that insanity is “doing the same thing over and over again and expecting a different outcome.”

– Alan I. Leshner

10.1126/science.1155656



ECOLOGY/EVOLUTION

The More the Merrier

The relationship between the number of species in an ecological community and the functional aspects of the ecosystem is usually studied experimentally by observing the effects of random changes in diversity. However, a study of rocky intertidal pools reveals that the nonrandom variation in species diversity that is characteristic of natural habitats yields better predictions of functional effects than experiments in which the species composition is altered randomly. Bracken *et al.* quantified the effects of both kinds of variation in seaweed diversity on nutrient dynamics (nitrogen uptake) in a set of tide pools in which the number of species increased as disturbance (caused by heavy surf) decreased. The effects of natural realistic variation were compared with the effects of artificial diversity gradients established by random groupings of species. Increased diversity in the “real-world” pools was associated with higher rates of nutrient acquisition by the plants, whereas the artificial communities showed no relationship. These results present new challenges for experimental ecologists studying the consequences of biodiversity loss in ecosystems. — AMS

Proc. Natl. Acad. Sci. U.S.A. **105**, 924 (2008).



MOLECULAR BIOLOGY

Wobble and Superwobble

In most cases, more than one triplet codon can specify an amino acid—at one extreme, leucine can be encoded by any of six nucleotide triplets. Degenerate codons tend to vary at the third position, which was the basis for Francis Crick’s wobble hypothesis: Each codon must be recognized by its cognate transfer RNA (tRNA) through an anticodon that is strictly complementary at the first two positions, but can use nonstandard base-pairing in the third, or wobble, position. Applying these complementarity rules indicates that a minimum of 32 tRNAs would be needed to read all 64 possible triplet codons. Yet in human mitochondria and plant plastids, there are fewer than 32 distinct tRNAs, leading to the suggestion that tRNAs with U in their wobble position might be able to make up for the deficit by pairing with any of the four bases at the third position of the codon—via a so-called superwobble.

Plastids in tobacco plants have two tRNA genes that code for the amino acid glycine (Gly): tRNA^{Gly}(GCC), which can decode GGC and GGU Gly codons, and tRNA^{Gly}(UCC), which, according to the superwobble hypothesis, should be able to decode both its regular Gly codons, GGA and GGG, and also GGC and GGU. Rogalski *et al.* support this idea by individually

knocking out both tRNA^{Gly} genes and showing that only the superwobble tRNA is essential for cell survival. Although tRNA^{Gly}(UCC) suffices for accurate reading of the code through superwobble, translation efficiency nonetheless seems to be reduced, explaining why superwobble is rarely selected for in genetic systems. — GR

Nat. Struct. Molec. Biol. **15**, 10.1038/nsmb1370 (2008).

BIOMATERIALS

Seeping into Cartilage

Polymer nanoparticles have been explored for more accurate delivery of drugs to improve efficacy and reduce toxicity within the body. For tissues lacking vasculature, such as articular cartilage, the challenge is to get the drug through the dense extracellular matrix (ECM) via a localized injection without removal in the synovial fluid. Rothenfluh *et al.* synthesized poly(propylene sulfide) (PPS) particles, ranging in size from 20 to 200 nm, that could potentially be used to deliver hydrophobic drugs such as aggrecanase inhibitors used to treat osteoarthritis. The PPS particles were decorated with a peptide sequence obtained from a five-generation phage panning process, where cloning enhances the population of sequences that best bind to a target tissue. For the best sequence obtained, binding tests with the target peptide

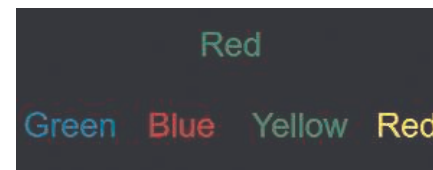
and a related scrambled sequence showed that binding was sequence-specific to collagen II $\alpha 1$. Not only were the smallest particles able to enter the ECM, but the targeting peptide then caused them to bind to the collagen matrix, thus turning a barrier into a reservoir that persisted for more than 96 hours. — MSL

Nat. Mater. **7**, 10.1038/nmat2116 (2008).

PHYSIOLOGY

A Neural Vulnerability to Hypertension

Rising blood pressure is a typical stress response—usually a healthy and adaptive reaction to dangerous situations that increases one’s chances of survival. However, individuals with excessive stressor-evoked blood pressure increases are at risk for developing cardiovascular disease later in life.



Green is the correct choice.

In an fMRI study of undergraduates charged with choosing the word that names the color of a target word (a Stroop color-word interference

CREDITS (TOP TO BOTTOM): J. SONES; INSET: C. HARTLEY; ADAPTED FROM GIANAROS ET AL., *J. NEUROSCI.* **28**, 990 (2008)

task), Gianaros *et al.* connect stressor processing with the brainstem cardiovascular control mechanisms regulating blood pressure. People with higher stressor-evoked blood pressure reactivity displayed more activation of the amygdala, especially in the dorsal part that contains the central nucleus. Individuals showing greater blood pressure reactivity also had a lower amygdala gray matter volume, which itself predicted greater amygdala activation. In addition, greater stressor-evoked blood pressure reactivity was correlated with stronger functional connectivity between the amygdala and an area in the brainstem, called the pons, which is critical for blood pressure control, as well the perigenual anterior cingulate cortex (pACC). As in the amygdala, greater activation of the pACC was associated with lower pACC gray matter volume. These results indicate a role for the amygdala and some of its projection areas in mediating individual differences in autonomic stress responses and hence vulnerability to psychological stressors. — PRS
J. Neurosci. **28**, 990 (2008).

CHEMISTRY

Tracking Surface Shakes

Two-dimensional infrared (2D-IR) spectroscopy has recently proven useful for tracking chemical dynamics through shifts in detected molecular vibrations. The "2D" refers not to a spatial framework but rather to the initial and final sets of mode populations that are simultaneously monitored at different vibrational frequencies. Bredenbeck *et al.* extend this technique to achieve surface specificity by combining it with sum frequency generation (SFG). This latter, well-established class of spectroscopy affords a background-free signal arising from the additive mixing of two different frequencies of light at an interface—a process that fails to build intensity in a bulk 3D environment where the polarizations of stacked molecular layers cancel one another out. The authors applied their SFG 2D-IR hybrid to the characterization of vibrational energy flow in the hydrophobic alkyl tails protruding from a water-dodecanol interface. — JSY

J. Am. Chem. Soc. **130**, 10.1021/ja710099c (2008).

BIOCHEMISTRY

What's It All Good For?

Enzyme kinetics is a subject dreaded by all but hard-core biochemists. Purifying proteins and measuring product generated or substrate consumed at varying concentrations of enzyme and substrate—not to mention the characterization of competitive and noncompetitive inhibitors—and then integrating these data within a mecha-

nistic scheme that spits out rate constants... well, this is not the stuff that dreams are made of, and neither is reading someone else's enzyme kinetics papers.

Umejiego *et al.* have applied this kind of information (a random order of substrate binding and a rate-limiting hydrolysis of the covalent enzyme intermediate) in designing a small-molecule screen for inhibitors of the enzyme inosine-5'-monophosphate dehydrogenase (IMPDH). Why should we care? Because IMPDH salvages purines in order to supply guanine in the human pathogen *Cryptosporidium parvum*, and because the *C. parvum* enzyme differs enough from human IMPDH to serve as a drug target. By screening under kinetically defined conditions where the conserved IMP site was occupied, whereas the less conserved NAD site was empty, they managed to fish out 10 candidates from a starting pool of 44,000 compounds. Four of these were more potent inhibitors of *C. parvum* growth than the standard drug paromomycin in a cell culture assay. — GJC
Chem. Biol. **15**, 70 (2008).

CHEMISTRY

DNA's Self-Regard

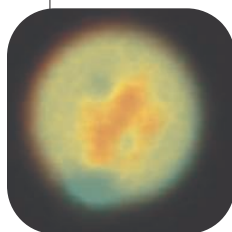
Recognition of double-stranded (ds) DNA sequences is usually thought to require some unwinding of the double helix to expose the bases

for interactions with single-stranded nucleic acid sequences or with proteins. Thus, it would be reasonable to assume that recognition between dsDNA sequences in solution would require processes involving single-stranded DNA, such as triple-helix formation. Baldwin *et al.* examined a binary mixture of two different dsDNA

DNA segregation in spherulite.

sequences of identical length (294 base pairs) and GC base proportion (50%) in electrolytic solution under minor osmotic stress. Under conditions of low fluorescent labeling to avoid quenching, liquid-crystalline spherulites form, and the two DNAs within these structures prefer to self-associate rather than mix. The authors suggest, based on their recent theoretical work, that association between identical DNAs is favored as this arrangement maintains registry of the phosphate backbone and surrounding counterions; different sequences result in small changes in pitch that can disrupt these interactions and extract an energetic penalty. Other mechanisms may also operate, but dsDNA recognition occurs in the presence of intervening solution. — PDS

J. Phys. Chem. B **112**, 1060 (2008).



Use your mouse to order
your KO mice
CLICK ON IT

TEXAS INSTITUTE FOR GENOMIC MEDICINE

713-677-7429 | 888-377-TIGM

1200 New York Avenue, NW
Washington, DC 20005

Editorial: 202-326-6550, FAX 202-289-7562

News: 202-326-6581, FAX 202-371-9227

Bateman House, 82-88 Hills Road
Cambridge, UK CB2 1LQ

+44 (0) 1223 326500, FAX +44 (0) 1223 326501

SUBSCRIPTION SERVICES For change of address, missing issues, new orders and renewals, and payment questions: 866-434-AAAS (2227) or 202-326-6417, FAX 202-842-1065. Mailing addresses: AAAS, P.O. Box 96178, Washington, DC 20090-6178 or AAAS Member Services, 1200 New York Avenue, NW, Washington, DC 20005

INSTITUTIONAL SITE LICENSES please call 202-326-6755 for any questions or information

REPRINTS: Author Inquiries 800-635-7181

Commercial Inquiries 803-359-4578

PERMISSIONS 202-326-7074, FAX 202-682-0816

MEMBER BENEFITS AAAS/Barnes&Noble.com bookstore www.aaas.org/bn; AAAS Online Store <http://www.apisource.com/aaas/> code MKB6; AAAS Travels: Betchart Expeditions 800-252-4910; Apple Store www.apple.com/epstore/aaas; Bank of America MasterCard 1-800-833-6262 priority code FAA3YU; Cold Spring Harbor Laboratory Press Publications www.cshlpress.com/affiliates/aaas.htm; GEICO Auto Insurance www.geico.com/landingpage/go51.htm?logo=17624; Hertz 800-654-2200 CDP#343457; Office Depot <https://bsd.office depot.com/portalllogin.do>; Seabury & Smith Life Insurance 800-424-9883; Subaru VIP Program 202-326-6417; VIP Moving Services <http://www.vipmayflower.com/domestic/index.html>; Other Benefits: AAAS Member Services 202-326-6417 or www.aaasmember.org.

science_editors@aaas.org (for general editorial queries)

science_letters@aaas.org (for queries about letters)

science_reviews@aaas.org (for returning manuscript reviews)

science_bookrevs@aaas.org (for book review queries)

Published by the American Association for the Advancement of Science (AAAS), *Science* serves its readers as a forum for the presentation and discussion of important issues related to the advancement of science, including the presentation of minority or conflicting points of view, rather than by publishing only material on which a consensus has been reached. Accordingly, all articles published in *Science*—including editorials, news and comment, and book reviews—are signed and reflect the individual views of the authors and not official positions of view adopted by AAAS or the institutions with which the authors are affiliated.

AAAS was founded in 1848 and incorporated in 1874. Its mission is to advance science and innovation throughout the world for the benefit of all people. The goals of the association are to: foster communication among scientists, engineers and the public; enhance international cooperation in science and its applications; promote the responsible conduct and use of science and technology; foster education in science and technology for everyone; enhance the science and technology workforce and infrastructure; increase public understanding and appreciation of science and technology; and strengthen support for the science and technology enterprise.

INFORMATION FOR AUTHORS

See pages 634 and 635 of the 1 February 2008 issue or access www.sciencemag.org/about/authors

EDITORIAL SUPERVISOR SENIOR EDITOR Phillip D. Szurromi; **SENIOR EDITOR/PERSPECTIVES** Lisa D. Chong; **SENIOR EDITORS** Gilbert J. Chin, Pamela J. Hines, Paula A. Kiberstis (Boston), Marc S. Lavine (Toronto), Beverly A. Purnell, L. Bryan Ray, Guy Riddiough, H. Jesse Smith, Valda Vinson, David Voss; **ASSOCIATE EDITORS** Jake S. Yeston, Laura M. Zahn; **ONLINE EDITOR** Stewart Willis; **ASSOCIATE ONLINE EDITORS** Robert Frederick, Tara S. Marathe; **BOOK REVIEW EDITOR** Sherman J. Suter; **ASSOCIATE LETTERS EDITOR** Jennifer Sills; **EDITORIAL MANAGER** Cara Tate; **SENIOR COPY EDITORS** Jeffrey E. Cook, Cynthia Howe, Harry Jach, Barbara P. Ordway, Trista Wagener; **COPY EDITORS** Lauren Kmeck, Peter Mooreside; **EDITORIAL COORDINATORS** Carolyn Kyle, Beverly Shields; **PUBLICATIONS ASSISTANTS** Ramatoulaye Diop, Chris Filiatreau, Joi S. Branger, Jeffrey Hearns, Lisa Johnson, Scott Miller, Jerry Richardson, Brian White, Anita Wynn; **EDITORIAL ASSISTANTS** Carlos L. Durham, Emily Guya, Patricia M. Moore, Jennifer A. Seibert; **EXECUTIVE ASSISTANT** Sylvia S. Kihara; **ADMINISTRATIVE SUPPORT** Maryrose Madrid

NEWS SENIOR CORRESPONDENT Jean Marx; **DEPUTY NEWS EDITORS** Robert Coontz, Eliot Marshall, Jeffrey Mervis, Leslie Roberts; **CONTRIBUTING EDITORS** Elizabeth Colutta, Polly Shulman; **NEWS WRITERS** Yudhijit Bhattacharjee, Adrian Cho, Jennifer Couzin, David Grimm, Constance Holden, Jocelyn Kaiser, Richard A. Kerr, Eli Kintisch, Andrew Lawler (New England), Greg Miller, Elizabeth Pennisi, Robert F. Service (Pacific NW), Erik Stokstad; **INTERN** Elsa Youngsteadt; **CONTRIBUTING CORRESPONDENTS** Jon Cohen (San Diego, CA), Daniel Ferber, Ann Gibbons, Robert Irlin, Mitch Leslie, Charles C. Mann, Virginia Morell, Evelyn Strauss, Gary Taubes; **COPY EDITORS** Rachel Curran, Linda B. Felaco, Melvin Gattling; **ADMINISTRATIVE SUPPORT** Scherraine Mack, Fannie Groom; **BUREAU** New England: 207-549-7755, San Diego, CA: 760-942-3252, FAX 760-942-4979, Pacific Northwest: 503-963-1940

PRODUCTION DIRECTOR James Landry; **SENIOR MANAGER** Wendy K. Shank; **ASSISTANT MANAGER** Rebecca Doshi; **SENIOR SPECIALISTS** Jay Covert, Chris Redwood; **SPECIALIST** Steve Forrester; **PREFLIGHT DIRECTOR** David M. Tompkins; **MANAGER** Marcus Spiegel; **SPECIALIST** Jessie Mudjitaba

ART DIRECTOR Kelly Buckheit Krause; **ASSOCIATE ART DIRECTOR** Aaron Morales; **ILLUSTRATORS** Chris Bickel, Katharine Sultiff; **SENIOR ART ASSOCIATES** Holly Bishop, Laura Creveling, Preston Huey, Nayomi Kevittiyagala; **ASSOCIATE** Jessica Newfield; **PHOTO EDITOR** Leslie Blizard

SCIENCE INTERNATIONAL

EUROPE (science-int.co.uk) **EDITORIAL/INTERNATIONAL MANAGING EDITOR** Andrew M. Sugden; **SENIOR EDITOR/PERSPECTIVES** Julia Fahrenkamp-Uppenbrink; **SENIOR EDITORS** Caroline Ash, Stella M. Hurltle, Ian S. Osborne, Stephen J. Simpson, Peter Stern; **EDITORIAL SUPPORT** Deborah Dennison, Rachel Roberts, Alice Whaley; **ADMINISTRATIVE SUPPORT** John Cannell, Janet Clements, Jill White; **NEWS: EUROPE NEWS EDITOR** John Travis; **DEPUTY NEWS EDITOR** Daniel Clery; **CONTRIBUTING CORRESPONDENTS** Michael Balter (Paris), John Bohannon (Vienna), Martin Eisenrnik (Amsterdam and Paris), Gretchen Vogel (Berlin); **INTERN** Elizabeth Quill

ASIA Japan Office: Asca Corporation, Eiko Ishioka, Fusako Tamura, 1-8-13, Hirano-cho, Chuo-ku, Osaka-shi, Osaka, 541-0046 Japan; +81 (0) 6 202 6272, FAX +81 (0) 6 202 6271; asca@os.gulf.or.jp; **ASIA NEWS EDITOR** Richard Stone (Beijing: rstone@aaas.org); **CONTRIBUTING CORRESPONDENTS** Dennis Normile (Japan: +81 (0) 3 391 0630, FAX 81 (0) 3 5936 3531; dnormile@gol.com); Hao Xin (China: +86 (0) 10 6307 4439 or 6307 3676, FAX +86 (0) 10 6307 4358; cindyhao@gmail.com); Pallava Bagla (South Asia: +91 (0) 11 2271 2896; pbagla@vsnl.com)

AFRICA Robert Koenig (contributing correspondent, rob.koenig@gmail.com)

FULFILLMENT SYSTEMS AND OPERATIONS (membership@aaas.org); **DIRECTOR** Waylon Butler; **CUSTOMER SERVICE SUPERVISOR** Pat Butler; **SPECIALISTS** Laurie Baker, Latoya Casteel, LaVonda Crawford, Vicki Linton; **DATA ENTRY SUPERVISOR** Cynthia Johnson; **SPECIALISTS** Tarrica Hill, Erin Layne, Sheila Thomas

BUSINESS OPERATIONS AND ADMINISTRATION DIRECTOR Deborah Rivera-Wienhold; **ASSISTANT DIRECTOR, BUSINESS OPERATIONS** Randy Yi; **SENIOR FINANCIAL ANALYSTS** Michael LoBue, Jessica Tierney; **FINANCIAL ANALYST** Nicole Nicholson; **RIGHTS AND PERMISSIONS: ADMINISTRATOR** Emilie David; **ASSOCIATE** Elizabeth Sandler; **MARKETING DIRECTOR** John Meyers; **MARKETING MANAGERS** Allison Pritchard, Darryl Walter; **MARKETING ASSOCIATES** Aimee Aponte, Alison Chandler, Mary Ellen Crowley, Marcia Leach, Julianne Wielga, Wendy Wise; **INTERNATIONAL MARKETING MANAGER** Wendy Sturley; **MARKETING EXECUTIVE** Jennifer Reeves; **MARKETING/MEMBER SERVICES EXECUTIVE** Linda Rusk; **SITE LICENSE SALES DIRECTOR** Tom Ryan; **SALES MANAGER** Russ Edra; **SALES AND CUSTOMER SERVICE** Mehan Dossani, Iqum Edo, Kiki Forsythe, Catherine Holland, Phillip Smith, Philip Tsolakidis; **ELECTRONIC MEDIA: MANAGER** Elizabeth Harman; **PROJECT MANAGER** Trista Snyder; **ASSISTANT MANAGER** Lisa Stanford; **SENIOR PRODUCTION SPECIALIST** Walter Jones; **PRODUCTION SPECIALISTS** Nichole Johnston, Kimberly Oster

ADVERTISING DIRECTOR WORLDWIDE AD SALES Bill Moran

PRODUCT (advertising@aaas.org); **CONSUMER & SPONSORSHIP SALES MANAGER** Tina Morra: 202-326-6542; **MIDWEST RICK Bongiovanni**: 330-405-7080, FAX 330-405-7081; **WEST COAST/W. CANADA** Teola Young: 650-964-2266; **EAST COAST/ CANADA** Christopher Breslin: 443-512-0330, FAX 443-512-0331; **UK/EUROPE/ASIA** Michelle Field: +44 (0) 1223-326-524, FAX +44 (0) 1223-325-532; **JAPAN** Mashy Yoshikawa: +81 (0) 33235 5961, FAX +81 (0) 33235 5852; **SENIOR TRAFFIC ASSOCIATE** Deandra Simms

COMMERCIAL EDITOR Sean Sanders: 202-326-6430

CLASSIFIED (advertise@sciencecareers.org); **US: RECRUITMENT SALES MANAGER** Ian King: 202-326-6528, FAX 202-289-6742; **INSIDE SALES MANAGER: MIDWEST/CANADA** Daryl Anderson: 202-326-6543; **NORTHEAST** Alexis Fleming: 202-326-6578; **SOUTHEAST** Tina Burks: 202-326-6577; **WEST** Nicholas Hintibidze: 202-326-6533; **SALES COORDINATORS** Erika Foad, Rohan Edmondson, Shirley Young; **INTERNATIONAL: SALES MANAGER** Tracy Holmes: +44 (0) 1223 326525, FAX +44 (0) 1223 326532; **SALES** Mariuum Huda, Alex Palmer, Alessandra Sorgente; **SALES ASSISTANT** Louise Moore; **JAPAN** Mashy Yoshikawa +81 (0) 33235 5961, FAX +81 (0) 33235 5852; **ADVERTISING PRODUCTION OPERATIONS MANAGER** Deborah Tompkins; **SENIOR PRODUCTION SPECIALISTS** Robert Buck, Amy Hardcastle; **SENIOR TRAFFIC ASSOCIATE** Christine Hall; **PUBLICATIONS ASSISTANT** Mary Lagnaoui

AAAS BOARD OF DIRECTORS **RETIRING PRESIDENT, CHAIR** John P. Holdren; **PRESIDENT** David Baltimore; **PRESIDENT-ELECT** James J. McCarthy; **TREASURER** David E. Shaw; **CHIEF EXECUTIVE OFFICER** Alan I. Leshner; **BOARD** John E. Dowling, Lynn W. Enquist, Susan M. Fitzpatrick, Alice Gast, Linda P. B. Katchi, Cherry A. Murray, Thomas D. Pollard, Kathryn D. Sullivan



ADVANCING SCIENCE. SERVING SOCIETY

SENIOR EDITORIAL BOARD

John I. Brauman, *Chair, Stanford Univ.*
Richard Lockard, *Harvard Univ.*
Robert May, *Univ. of Oxford*
Marcia McClut, *Monterey Bay Aquarium Research Inst.*
Linda Partridge, *Univ. College London*
Vera C. Rubin, *Carnegie Institution*
Christopher R. Somerville, *Carnegie Institution*
George M. Whitesides, *Harvard Univ.*

BOARD OF REVIEWING EDITORS

Joanna Aizenberg, *Harvard Univ.*
R. McNeill Alexander, *Leeds Univ.*
David Altschuler, *Broad Institute*
Arturo Alvarez-Buylla, *Univ. of California, San Francisco*
Richard Amasino, *Univ. of Wisconsin, Madison*
Angelika Amon, *MIT*
Meinrat O. Andreae, *Max Planck Inst., Mainz*
Kristi S. Anseth, *Univ. of Colorado*
John A. Bargh, *Yale Univ.*
Cornelia I. Bargmann, *Rockefeller Univ.*
Marisa Bartolomei, *Univ. of Penn. School of Med.*
Ray H. Baughman, *Univ. of Texas, Dallas*
Stephen J. Benkovic, *Penn State Univ.*
Michael J. Bevan, *Univ. of Washington*
Ton Bisseling, *Wageningen Univ.*
Mina Bissell, *Lawrence Berkeley National Lab*
Peter Borik, *EMBL*
Dianna Bowles, *Univ. of York*
Robert W. Boyd, *Univ. of Rochester*
Paul M. Brakefield, *Leiden Univ.*
Dennis Bray, *Univ. of Cambridge*
Stephen Buratowski, *Harvard Medical School*
Jillian M. Buriak, *Univ. of Alberta*
Joseph A. Burns, *Cornell Univ.*
William P. Butz, *Population Reference Bureau*
Peter Carmeliet, *Univ. of Leuven, VIB*
Gerbrand Cedar, *MIT*
Mildred Cho, *Stanford Univ.*
David Clapham, *Children's Hospital, Boston*
David Clary, *Oxford University*

J. M. Claverie, *CNRS, Marseille*
Jonathan D. Cohen, *Princeton Univ.*
Stephen M. Cohen, *EMBL*
Robert H. Crabtree, *Yale Univ.*
F. Fleming Crim, *Univ. of Wisconsin*
William Cumberland, *Univ. of California, Los Angeles*
George O. Daley, *Children's Hospital, Boston*
Jeff L. Dangl, *Univ. of North Carolina*
Edward DeLong, *MIT*
Emmanouil T. Dermitzakis, *Wellcome Trust Sanger Inst.*
Robert Desimone, *MIT*
Dennis Discher, *Univ. of Pennsylvania*
Scott C. Doney, *Woods Hole Oceanographic Inst.*
Peter J. Donovan, *Univ. of California, Irvine*
W. Ford Doolittle, *Dalhousie Univ.*
Jennifer A. Doudna, *Univ. of California, Berkeley*
Julian Downward, *Cancer Research UK*
Dennis Duboule, *Univ. of Geneva/EPPFL Lausanne*
Christopher Dye, *WHO*
Richard Ellis, *Cal Tech*
Gerhard Ertl, *Fritz-Haber-Institut, Berlin*
Douglas H. Erwin, *Smithsonian Institution*
Mark Estelle, *Indiana Univ.*
Barry Everitt, *Univ. of Cambridge*
Paul G. Falkowski, *Rutgers Univ.*
Ernst Fehr, *Univ. of Zurich*
Tom Fenichel, *Univ. of Copenhagen*
Alain Fischer, *INSERM*
Scott E. Fraser, *Cal Tech*
Chris D. Frith, *Univ. College London*
Wulfram Gerstner, *EPPFL Lausanne*
Charles Godfray, *Univ. of Oxford*
Christian Haass, *Ludwig Maximilians Univ.*
Niels Hansen, *Technical Univ. of Denmark*
Dennis L. Hartmann, *Univ. of Washington*
Chris Hawkesworth, *Univ. of Bristol*
Martin Heimann, *Max Planck Inst., Jena*
James A. Hendler, *Rensselaer Polytechnic Inst.*
Ray Hilborn, *Univ. of Washington*
Ove Hoegh-Guldberg, *Univ. of Queensland*
Ronald R. Hoy, *Cornell Univ.*
Evelyn L. Hu, *Univ. of California, Santa Barbara*
Olli Ikkala, *Helsinki Univ. of Technology*
Meyer B. Jackson, *Univ. of Wisconsin Med. School*

Stephen Jackson, *Univ. of Cambridge*
Steven Jacobsen, *Univ. of California, Los Angeles*
Peter Jonas, *Universität Freiburg*
Daniel Kahne, *Harvard Univ.*
Gerard Karsenti, *Columbia Univ. College of P&S*
Bernhard Keimer, *Max Planck Inst., Stuttgart*
Elizabeth A. Kellog, *Univ. of Missouri, St. Louis*
Alan B. Krueger, *Princeton Univ.*
Lee Kump, *Penn State Univ.*
Mitchell A. Lazar, *Univ. of Pennsylvania*
Virginia Lee, *Univ. of Pennsylvania*
Anthony J. Leggett, *Univ. of Illinois, Urbana-Champaign*
Michael J. Lenardo, *NIH*
Norman L. Letvin, *Beth Israel Deaconess Medical Center*
Olle Lindvall, *Univ. Hospital, Lund*
John Lis, *Cornell Univ.*
Richard Lockard, *Harvard Univ.*
Ke Lu, *Chinese Acad. of Sciences*
Andrew P. MacKenzie, *Univ. of St. Andrews*
Raul Madariaga, *Ecole Normale Supérieure, Paris*
John M. Mather, *Univ. of Pennsylvania*
Michael Malm, *King's College, London*
Virginia Miller, *Washington Univ.*
Yasushi Miyashita, *Univ. of Tokyo*
Richard Morris, *Univ. of Edinburgh*
Edward Moser, *Univ. of Science and Technology*
Naoto Nagasawa, *Univ. of Tokyo*
James Nelson, *Stanford Univ. School of Med.*
Timothy W. Nilsen, *Case Western Reserve Univ.*
Roeland Nolte, *Univ. of Mijmegen*
Helga Nowotny, *European Research Advisory Board*
Eric N. Olson, *Univ. of Texas, SW*
Erin O'Shea, *Harvard Univ.*
Elinor Ostrom, *Indiana Univ.*
Jonathan T. Overpeck, *Univ. of Arizona*
John Pendry, *Imperial College*
Philippe Poulin, *CNRS*
Molly Power, *Univ. of California, Berkeley*
Mary Przeworski, *Univ. of Chicago*
David J. Read, *Univ. of Sheffield*
Les Real, *Emory Univ.*
Colin Renfrew, *Univ. of Cambridge*
Trevor Robbins, *Univ. of Cambridge*
Barbara A. Romanowicz, *Univ. of California, Berkeley*
Nancy Ross, *Virginia Tech*

Edward M. Rubin, *Lawrence Berkeley National Lab*
J. Roy Sambles, *Univ. of Exeter*
Jürgen Sandkühner, *Medical Univ. of Vienna*
David S. Schimel, *National Center for Atmospheric Research*
David W. Schindler, *Univ. of Alberta*
Paul Schulz, *Albert-Ludwigs-Universität*
Georg Schulze-Lefert, *Max Planck Inst., Cologne*
Terrence J. Sejnowski, *The Salk Institute*
David Sibley, *Washington Univ.*
Montgomery Slatkin, *Univ. of California, Berkeley*
George Somero, *Stanford Univ.*
Joan Steitz, *Yale Univ.*
Elisbeth Stern, *ETH Zürich*
Thomas Stocker, *Univ. of Bern*
Jerome Strauss, *Virginia Commonwealth Univ.*
Glenn Telling, *Univ. of Kentucky*
Marc Tessier-Lavigne, *Genentech*
Michel van der Kooij, *Astronomical Inst. of Amsterdam*
Derek van der Kloot, *Univ. of Toronto*
Bert Vogelstein, *Johns Hopkins Univ.*
Christopher A. Walsh, *Harvard Medical School*
Graham Warren, *Yale Univ. School of Med.*
Colin Watts, *Univ. of Dundee*
Detlef Weigel, *Max Planck Inst., Tübingen*
Jonathan Weissman, *Univ. of California, San Francisco*
Ellen D. Williams, *Univ. of Maryland*
Ian A. Wilson, *The Scripps Res. Inst.*
Jerry Workman, *Stowers Inst. for Medical Research*
John R. Yates III, *The Scripps Res. Inst.*
Jan Zaenen, *Leiden Univ.*
Martin Zatz, *NIH*
Huda Zoghbi, *Baylor College of Medicine*
Maria Zuber, *MIT*

BOOK REVIEW BOARD

John Aldrich, *Duke Univ.*
David Bloom, *Harvard Univ.*
Angela Creager, *Princeton Univ.*
Richard Swedner, *Univ. of Chicago*
Ed Wasserman, *DuPont*
Lewis Wolpert, *Univ. College London*

You Go, Gill!

Behind every male leader, there's a female calling the shots. At least that's true in one type of African fish, according to research that contradicts previous notions about male-determined hierarchy.

The cichlid fish *Neolamprologus pulcher* lives in groups in Lake Tanganyika in southeastern Africa. Each social group contains one breeding pair and about 20 other males and females that look after the young and ward off predators. When the alpha male dies or is displaced, another comes forward to breed with the alpha female.

Behavioral ecologist Sigal Balshine of McMaster University in Hamilton, Canada, and colleagues removed the alpha males from 18 free-living cichlid groups in Zambia and watched as males fought for the head spot. In the end, however, the decision wasn't up to the males. The alpha female would only accept a mate larger than she. If the largest male in her own group was still too small, she selected a mate from another group. Testosterone levels, aggressive behavior, and genetic relationships had no impact on her choice.

"It turned out that females were the linchpin. That was the surprise," says Balshine, lead author of the study, which was published online last month in the *Proceedings of the Royal Society B*.

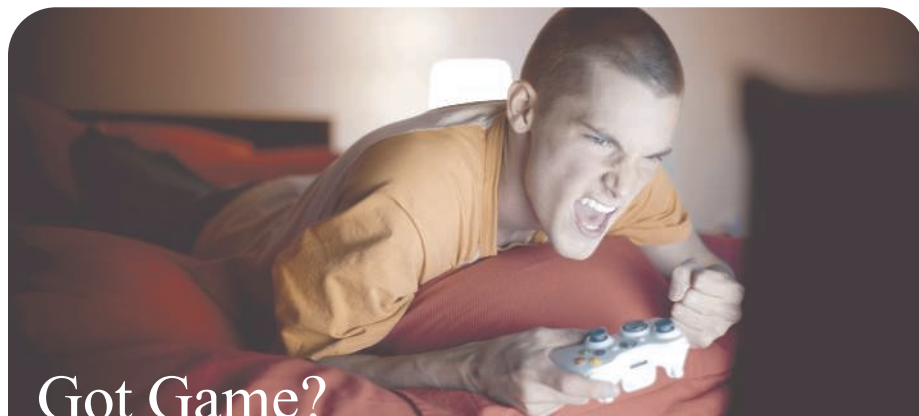


Evolutionary ecologist Peter Buston of the Estación Biológica de Doñana in Spain says the study is the first to show a role for females in determining male status. "This is almost certain to occur in other species," he notes.

An Epic Journey

In the summer of 2003, a leatherback sea turtle set out from the Indonesian coast to forage for food. A year later, she finally settled down to a feast of jellyfish along the Oregon coast, having completed one of the longest recorded migrations by a marine vertebrate.

During nesting season, female leatherbacks lay thousands of eggs in the sands of tropical beaches, then swim out to sea. Until now, scientists didn't know where they went or how long they stayed away. But in the summer of 2003, ecologist Scott Benson of the Southwest



Got Game?

Just like cocaine, video games trigger reward centers of the brain. A new study suggests that men feel the game buzz more than women do, which could explain why men are more prone to game addiction.

Researchers at the Stanford University School of Medicine recruited 22 college students—11 men and 11 women—to play a computer game while the scientists imaged their brains using functional magnetic resonance.

As men played, the reward and addiction circuitry in their brains was more active than in the female participants. And the more the men won, the stronger their brain activity. The women's responses were less intense and didn't correlate with winning. The results "lay the foundation for why men are more likely to play games to the point of addiction," says Stanford neuroscientist Allan Reiss, who led the study, published online 14 January in the *Journal of Psychiatric Research*.

That men's nucleus accumbens, the "ground zero of addiction research" in the brain, is more active during gaming is "very interesting," says neuroscientist Lawrence Cahill of the University of California, Irvine. What's more, Cahill adds, it uncovers pronounced sex differences in the human brain, which could "impact every corner of neuroscience and clinical work."

Fisheries Science Center in Moss Landing, California, and colleagues outfitted nine female western Pacific leatherbacks nesting in Papau, Indonesia, with tracking devices.

They expected all the turtles to migrate to the same region, just as eastern Pacific leatherbacks had been shown to do.

These turtles, however, had other plans. Some headed northeast toward the eastern North Pacific; others turned west toward the South China Sea. One kept going along an "epic journey" that took her to Oregon. After several months of dining on jellyfish, the turtle headed toward Hawaii for the winter, returning toward Oregon the following spring. By the time her tracking device stopped working in April 2005, the turtle had traveled 20,558 km over 647 days.

Benson says the leatherback study underscores the scale of efforts needed to protect the endangered species. "This is an animal that doesn't recognize international borders," he says. "It's a global mariner that needs global attention."

One Wei or Another

Earning a name for yourself in science can be a struggle. Imagine how much harder it would be if your name was routinely confused with several others. That often happens to researchers with Asian names, many of which may share the same English transliteration.

To address the issue, the American Physical Society (APS) will let authors with Chinese, Japanese, or Korean names include the Asian spellings (in parentheses after the English equivalent) on papers in the society's journals, including *Physical Review Letters*. An editorial announcing the policy in December noted that at least eight different Chinese names (shown at left) are transcribed as Wei Wang. "I think this is a great way to show that science is an international matter," says Wei Wang (王伟), a particle physicist at the University of Wisconsin, Madison. Adds Wei Wang (王巍), a biophysicist at the University of California, San Diego, "All the journals should do the same thing."

王伟
王薇
王维
王蔚
汪卫
汪玮
汪威
汪巍



<< Two Cultures

DECONSTRUCTING SUDOKU. As Thomas Snyder prepares to defend his title as the world's best Sudoku player, he sees a parallel between the scientific thought process and his puzzle-solving prowess. "It's the systematic way you break apart a problem into little pieces that are more approachable," says Snyder, a bioengineering postdoc at Stanford University in Palo Alto, California, who works on novel methods of automated DNA synthesis and sequencing.

Snyder, 27, claimed his crown last year in Prague, Czech Republic, and he's hoping to repeat the achievement in April in Goa, India. Last fall, he captured the first-ever U.S. Sudoku championship in Philadelphia, Pennsylvania.

Despite the recognition and the occasional cash prize—the U.S. title was worth \$10,000—Snyder says it's hard to balance puzzle competitions with his lab work. "I don't know if this is a hobby I can continue too long," he says.

IN BRIEF

Computer scientists **Edmund Clarke** of Carnegie Mellon University in Pittsburgh, Pennsylvania, **E. Allen Emerson** of the University of Texas, Austin, and **Joseph Sifakis** of the French national research agency in Grenoble are co-winners of the 2007 A. M. Turing Award from the Association for Computing Machinery. They will share the \$250,000 prize for helping to develop "model checking," an automated process for spotting errors in computer hardware and software.

Physicist and millionaire **Bill Foster** last week cleared one hurdle in his bid to win a seat in the U.S. House of Representatives by squeaking past his closest Democratic rival to win the party's nomination for the 14th Congressional

District in Illinois. The seat was most recently held by former Speaker of the House, Republican Dennis Hastert, who retired last year. Foster, who worked at Fermilab from 1984 to 2006, faces a tough contest ahead: The Republican nominee, Jim Oberweis, is a businessman with deep pockets. Stay tuned.

MOVERS

REACHING FOR THE MOON. A longtime NASA manager, exploration buff, and astronomer trained at Harvard University will help launch a new moon-focused center at Ames Research Center in Mountain View, California. David Morrison will serve as interim director of the Lunar Science Institute, which will coordinate the agency's various moon-research efforts and fund a new generation of lunar researchers.

Morrison, 67, has been "a pillar of the planetary-research community," says Ames Director S. Pete Worden, citing his work on the Mariner, Voyager, and Galileo robotic missions.



"His communication and management skills are just the talents we need to ensure early success for the institute." Morrison, now a senior scientist at Ames's Astrobiology Institute, says he plans to

step aside for "a real lunar scientist" once the new institute is up and running. "I've never written a lunar paper," he adds.

Got a tip for this page? E-mail people@aaas.org



Three Q's

Last month, German scholars discussed the results of an 8-year project examining the conduct of the German research funding agency, the Deutsche

Forschungsgemeinschaft (DFG), from 1920 to 1970 with a focus on the Nazi years (1933–1945). **Ulrich Herbert**, a historian at the University of Freiburg, shared some of the findings with *Science*.

Q: DFG's funding of egregious Nazi research, such as Mengele's twin experiments at Auschwitz, was already known. What was the most surprising finding from your project?

The transition to National Socialism for most areas of research was not a very dramatic step. In 1933, Nazis

came into leadership positions, but there was no specific Nazi agenda. Instead, contrary positions and voices were simply eliminated.

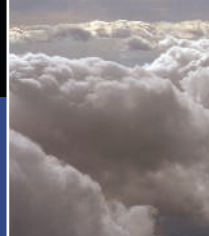
Q: Was German research particularly susceptible to Nazi ideology?

We found that the research community was seized by the same radical patriotism as the rest of society after the First World War. ... There was similar research on race, nationalism, and the heritability of criminal tendencies in Scandinavia, France, and the United States at the

time—but it was part of a pluralistic discourse. The decisive difference [in Germany] was that after 1933, the researchers who challenged Nazi views did not receive any more support.

Q: You also examined DFG's postwar history. Were there any surprises?

I found it interesting that German biology into the 1970s still had not recovered from the expulsion of Jewish scientists. But the DFG [never said] to researchers living in exile, "Please come back." The idea didn't occur to anyone.



CLINICAL RESEARCH

Deaths in Diabetes Trial Challenge a Long-Held Theory

Medical treatment is often anchored in conjecture and instinct, and every so often a rigorous study proves common wisdom wrong. That happened last week when the U.S. National Heart, Lung, and Blood Institute (NHLBI) in Bethesda, Maryland, suspended a major component of a 10,000-person clinical trial that examined whether strong measures to bring blood sugar down to normal levels could prevent heart attacks and strokes in people with diabetes. There were more deaths, including fatal heart attacks, in the intensive-treatment group than among those who received standard care and had higher glucose levels. “We had every reason to believe this intervention would help,” says Denise Simons-Morton, who oversaw the trial at NHLBI. Instead, the study screeched to a halt 18 months earlier than planned.

What went wrong? Researchers aren’t sure—in fact, they’re not even sure that bringing about a steep decline in blood sugar is harmful over the long term. An odd but consistent pattern in a handful of studies designed to control diabetes suggests that aggressive treatment worsens complications in the short term but reduces them as time passes. Indeed, a small study published last week in the *New England Journal of Medicine* (NEJM) reported that aggressive glucose, cholesterol, and blood pressure control led to slightly more deaths among diabetics after 4 years—the same period as the halted NHLBI trial—but after 13 years, the intensively treated group was better off.

The NHLBI study aspired to something unprecedented. Even when doctors and patients try to reduce high glucose levels in diabetes, rarely do they bring glucose down to normal levels—a goal considered more trouble than it’s worth. Now, scientists realize, it may also be dangerous for some people with

higher-than-normal blood sugar.

The halted trial, Action to Control Cardiovascular Risk in Diabetes (ACCORD), focused on older people with diabetes at high risk of dying from heart disease. Investigators in the United States and Canada recruited 10,251 people with type 2 diabetes who fit



UNEXPECTED RESULTS

Treatment	Aggressive	Standard
Total deaths	257	203
Death rate per year	1.4%	1.1%

Upset. A glucose-reduction trial was halted when researchers found that volunteers receiving aggressive therapy were more likely to die.

this description. Blood sugar was assessed by hemoglobin A1c, a measure of sugar inside blood cells. A healthy A1c is less than 6%.

After nearly 4 years, 257 people in intensive treatment, whose A1c averaged 6.4%, had died, compared with 203 in standard care, whose A1c was on average 7.5%. This translates to a death rate of 1.4% per year in the intensive group and 1.1% per year in the standard-care group. The deaths had various causes—surgical complications, sepsis, strokes. But many were heart attacks. NHLBI has declined to release the number of cardiovascular deaths until the findings are published, saying only that it was higher in the intensive-treatment cohort. Puzzlingly, nonfatal heart attacks were about 10% less common, however. Is this because those people had a lower chance of surviving their heart attacks and were dying instead? “That’s an interesting conjecture,” says Simons-Morton. “Don’t put those words in my mouth.”

Although endocrinologists have believed for years that the lower the glucose level, the better off the patient, there have been hints

that the relationship is more complicated. In the 1990s, a Department of Veterans Affairs (VA) study found that 32% of volunteers in an intensive glucose-reduction arm suffered cardiovascular events, compared with 20% in the standard-care arm. With only 153 men participating, though, the study wasn’t big enough to estimate optimum glucose levels, and VA researchers launched a much larger study of 1792 patients. Results will be unveiled in June at the annual meeting of the American Diabetes Association. In a conference call last Friday, the group monitoring the VA study agreed to continue it as is.

At the University of Pittsburgh in Pennsylvania, epidemiologist Trevor Orchard has been a minority voice arguing against pushing blood sugar in diabetics down to normal levels, especially if cardiovascular risk is significant. “You get increased atherosclerosis in diabetes, but—and this is the key—it’s perhaps more likely to be stable and less likely to rupture” and cause a heart attack, he says. That’s because the plaques include extra sugar that toughens them. Post-mortems of people with diabetes back this up, he says, as do studies that have looked for and found little or no relationship between A1c and cardiovascular problems in type 2 diabetes, including the 20-year UK Prospective Diabetes Study, which failed to establish a firm connection.

One theoretical hazard of ACCORD, says Orchard, is that “by dramatically reducing blood glucose levels,” the investigators “have effectively removed a stabilizing influence on these plaques.” There’s no question that lowering blood sugar is essential in diabetes, he emphasizes—but going below an A1c of 7% may be risky for precisely the kind of people in ACCORD, those with heart disease or at high risk for it. In younger people who haven’t had diabetes as long and whose hearts are healthy, the consequences of normal glucose may be different.

But dramatically reducing glucose could have other effects, too. “We had to use every possible medication out there” to get blood sugar down, says endocrinologist Vivian Fonseca of Tulane University in New Orleans, who participated in ACCORD. One treatment, insulin, often causes periods of low blood sugar, which can increase heart rate and have other untoward effects on the cardiovascular system. ▶



Finally, there's the unanswerable question of what would have happened had the study continued. Although Fonseca supported stopping it, he also believes that "when you intervene in a high-risk population, you may transiently worsen things" before they improve. A small study he conducted in the 1980s, he says, showed that trying to control diabetes

initially led to more pain from nerve damage in patients before the pain subsided; scientists have made similar observations with eye damage associated with diabetes.

"We do not know the molecular mechanisms behind" this phenomenon, says endocrinologist Oluf Pedersen of the Steno Diabetes Center in Gentofte, Denmark, who

recorded it himself in his study published last week in *NEJM*.

Still, says Pedersen, the ACCORD study was perhaps too ambitious. "Many of us without diabetes do not have an A1c of 6," he says of ACCORD's target. "My A1c is 6.3, ... [and] I'm superhealthy."

—JENNIFER COUZIN

ASTRONOMY

Alien Planetary System Looks a Lot Like Home

After finding nearly 250 alien-looking extrasolar planets, astronomers using a powerful new observing technique have spotted a planetary system—a star and two giant planets—that bears a striking resemblance to our own solar system. "This bodes well for there being a larger number of Earth-like planets" than previous observations had suggested, says planetary dynamicist Jack Lissauer of NASA's Ames Research Center in Mountain View, California. And it "bodes well for astrobiology," too.

The new technique, known as gravitational microlensing, involves a star's gravity bending the light of a more distant star behind it the way a magnifying lens bends light, explains astronomer Scott Gaudi of Ohio State University in Columbus. Gaudi heads an aggregation of four collaborations—OGLE, μ FUN, PLANET, and RoboNet—

consisting of 69 colleagues from 11 countries, including some amateur astronomers. They used telescopes at 11 observatories spread around the Southern Hemisphere to watch continuously as microlensing brightened a star from late March well into April of 2006. As a star slowly drifted in front of a more distant one, observers recorded brief brightenings superimposed on the weeks-long brightening and dimming of the merged image of the two stars.

Calculating from the number, timing, and magnitudes of the subsidiary peaks, the group reports on page 927 the discovery of two planets orbiting the nearer star. The star has only half the mass of the sun, they calculate. The inner planet has a mass about 71% that of our Jupiter and lies about 2.3 times farther from its star than Earth is from the sun (2.3 astronomical units, or

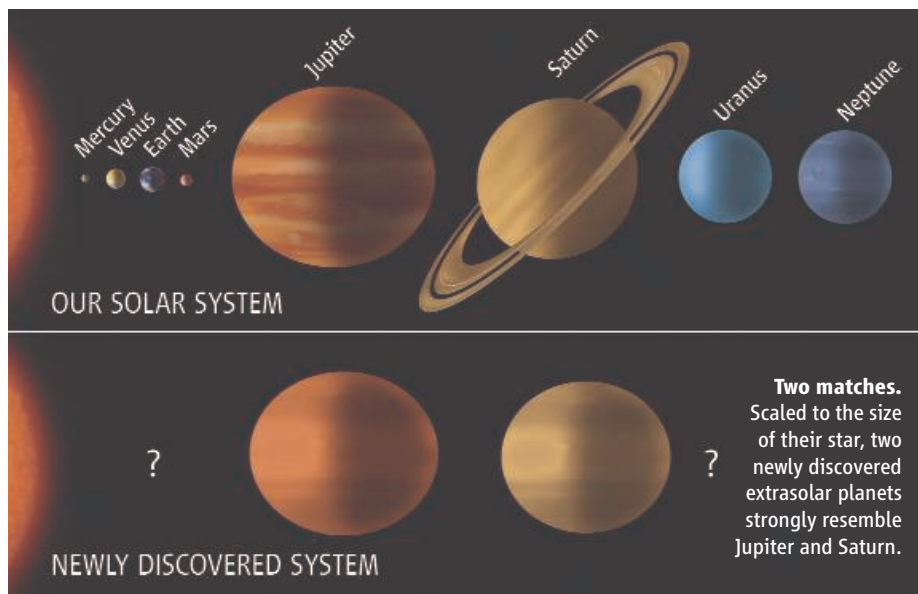
2.3 AU); Jupiter is 5.2 AU from the sun. The outer planet is about 90% as massive as Saturn and lies 4.6 AU from the star, whereas Saturn is 9.5 AU from the sun.

The result, the group writes, is a planetary system that "bears a remarkable similarity to our own solar system," only scaled down. The ratio of the planets' masses and the ratio of their distances from the star are similar to those of Jupiter and Saturn. The ratio of the larger planet's mass to that of the star is close to the Jupiter-sun ratio. Even the warmth that the dimmer but nearer star sheds on the planets is similar to what the sun sheds on Jupiter and Saturn.

The resemblance isn't perfect, Gaudi says, but it certainly beats the competition. Apart from a few lone exo-Jupiters, most known extrasolar planets are too massive or too close to their stars to be reminiscent of anything in the solar system (*Science*, 21 June 2002, p. 2124). Microlensing is currently the only way to detect Saturn-mass planets at Saturn-like distances from their stars, and this microlensing detection of a giant planet is the first in which astronomers could have detected a second, Saturn-like planet. "That suggests these things might be quite common," says Gaudi.

Other researchers agree. "This is a really neat story," says astrophysicist Alan Boss of the Carnegie Institution of Washington's Department of Terrestrial Magnetism in Washington, D.C. Given the striking resemblance to the solar system, "there's lots of room" between the star and the inner detectable planet for an Earth-like planet or two nestled in life's environmental comfort zone, he says. And microlensing is potentially capable of detecting analogs of all the solar system planets except Mercury.

—RICHARD A. KERR



BIOSAFETY

Biodefense Watchdog Project Folds, Leaving a Void

An activist who has been both loathed and lauded for his criticism of safety at the United States's booming biodefense labs is closing his doors. Edward Hammond, director of the Austin, Texas–based watchdog group called the Sunshine Project, earlier this month posted a note on his Web site saying he is suspending operations. For 8 years, he has survived on a shoestring budget, he says, and he has had enough.

The news may come as a relief to microbiologists and university officials who have been subjected to Hammond's relentless probing. But even some of those scientists say Hammond has had a positive influence. Virologist C. J. Peters of the University of Texas Medical Branch in Galveston says that



Muckraker. Ed Hammond's digging into safety at biodefense labs found problems.

although Hammond was a “pest” who often exaggerated risks to the public, his work has “made the community more careful” about biosafety. “I think the country works best with watchdogs,” he says. “I am, strangely, sad to see him go.”

Hammond's causes included destroying smallpox stocks and sharing flu strains, but his greatest impact may be his scrutiny of the U.S. biodefense labs that sprang up after the 2001 anthrax attacks. He filed open-records requests for the minutes of nearly 400 institutional boards that oversee

safety at biology labs (*Science*, 6 August 2004, p. 768). This revealed that some met infrequently, if at all. And last summer, after Hammond uncovered an unreported infection and other safety violations at Texas

A&M University in College Station, federal authorities suspended the lab's biodefense research. A few months later, Congress held a hearing on safety at biodefense labs and called for stricter oversight.

Despite these accomplishments, Hammond says he had had enough of a “totally consuming” job on a budget “well under \$100,000 a year” cobbled together from small foundation grants. (The Sunshine Project's other staffer in Germany was part-time, he says.) Last year's fund-raising didn't go particularly well, he says, and “I hit my breaking point.” He says he hasn't figured out what he'll do next; for now, he's planning to spend a couple of years in Bogotá, with his wife, a Colombia-born attorney, and young daughter.

Some observers, meanwhile, are lamenting the Sunshine Project's demise. “[Hammond] called attention to very real problems in the way that biosecurity has been funded and research reviewed,” says Gigi Kwik Gronvall of the Center for Biosecurity of the University of Pittsburgh Medical Center in Baltimore, Maryland. “There's no one else I know of that will look over at that level of detail and keep things transparent.”

—JOCELYN KAISER

EARTH OBSERVING

U.S. Prepares to Launch Flawed Satellite

The U.S. government is planning to fly an Earth-observing satellite that will be essentially colorblind, at least as far as the oceans are concerned.

The NPP satellite is a prototype for the \$12 billion National Polar-orbiting Operational Environmental Satellite System (NPOESS), a series of satellites to be launched between 2013 and 2022. In 2006, scientists learned that there was a problem with the filter on one of NPP's instruments, VIIRS, which will prevent it from accurately measuring ocean color, a window into how sea life responds and contributes to fluctuating atmospheric and ocean carbon. But officials with NASA and the National Oceanic and Atmospheric Administration (NOAA) rebuffed a request last fall from scientists to correct the problem out of concern that working on the filter could jeopardize the other 21 parameters that VIIRS measures, including clouds, the extent of ice sheets, and forest cover. Last month, NOAA announced that a glitch in the system to regulate the satellite's temperature would push back the mission by 8 months, to 2010, prompting scientists to ask the government to use the delay to at least

conduct a risk-benefit analysis of correcting the filter problem.

Last week, NOAA officials told *Science* that they have no plans to do such an analysis or to alter the timetable to accommodate any changes to VIIRS's filters. Instead, says NPOESS manager Dan Stockton, the agency will try to fix the ocean-color problem “for the

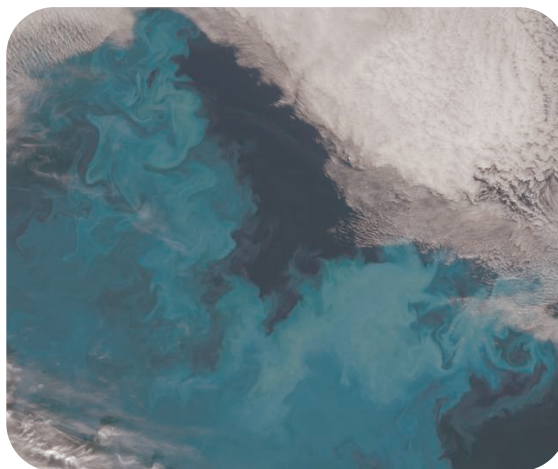
first NPOESS” mission set to launch in 2013.

Scientists fear that the flaws in NPP will disrupt the longitudinal record on ocean color, because two experimental NASA craft now providing good data are near or beyond their 5-year design life. Color data from a European satellite have been difficult to use, and an Indian sensor has yet to be launched, they add.

“Are we going to [make it] to NPOESS [in 2012]? I don't think so,” says David Siegel, a marine scientist at the University of California, Santa Barbara.

But Art Charo, who follows the issue for the U.S. National Academies' National Research Council, points out that the ocean-color community is at least better off than other climate specialties that had instruments removed from NPOESS in 2006 and don't know whether they will be restored (*Science*, 31 August 2007, p. 1167). “With such a tight budget environment, it's a question of triage,” he says.

—ELI KINTISCH



Bloomin' brilliant. NASA's 9-year-old Terra is living on borrowed time but still provides good data for studies of plankton blooms.

CREDITS (TOP TO BOTTOM): COURTESY OF E. HAMMOND; GSFC/NASA



Teamwork. A new bill emphasizes collaborations to reduce fire risk, using tools such as prescribed burns.

ECOLOGY

Senate Bill Would Scale Up Forest Restoration

Focus on the whole forest and think big. That's the intent of a bill, introduced in the U.S. Senate last week, that would direct the Forest Service to fund large, collaborative projects to reduce fire risk, improve forest health, and stimulate economic development. "It's going to be more holistic, and Lord knows we need it," says Jerry Franklin of the University of Washington, Seattle. Although they praise the bill, scientists and environmentalists say there is still room for improvement.

Fires have taken an ever-larger toll on forests, communities, and the Forest Service budget. The Healthy Forests Restoration Act of 2003 was designed to lessen the risk of conflagrations by expediting projects to thin forests and clear out flammable undergrowth. But the projects have typically been small and picked in a scattershot fashion, says Laura McCarthy of The Nature Conservancy in Santa Fe, New Mexico. Environmentalists have also objected to the logging of old-growth trees, revenues from which helped fund the projects.

Under the new bill, S. 2593, the Forest Service would solicit proposals from collaborations involving regional Forest Service staff, local groups, and nongovernmental organizations. Each project would encompass at least 20,000 hectares, although only part of the landscape might be treated. In addition to lessening fire risk, the 10-year projects should benefit the ecosystems by improving fish and wildlife habitat, for example, and clearing out invasive species. Another goal is to stimulate local economies by selling the small wood removed from forests to sawmills. With the guidance of a new science advisory board, the secretary of the U.S. Department of Agriculture would pick up to 10 such projects a year.

To help pay for the work, the bill authorizes \$40 million a year for 10 years. That amount is equivalent to recent increases to the service's "hazardous fuels" reduction program, which has a budget of \$320 million in fiscal year 2008. These funds would have to be matched by the partners in the collaboration. The bill calls for 15 years of monitoring for social, economic, and ecological impacts, but observers note that monitoring is often the first part of a project budget to be cut. "That's one of the things that everybody gives lip service to," says Rick Brown of Defenders of Wildlife in Washington, D.C. "This bill moves us toward thinking that monitoring is part of the job."

The bill isn't perfect, supporters say. Wally Covington of Northern Arizona University in Flagstaff thinks the projects should be at least 40,000 hectares to make ecological planning as strategic as possible. Covington also cautions that smaller areas may not provide enough wood to support local mills and bioenergy plants. Randi Spivak of the American Lands Alliance, an advocacy group in Washington, D.C., and others would like to see specific protections for old-growth trees, as well as tighter constraints on road building in project areas.

The bipartisan bill has a powerful array of sponsors. It was introduced by Jeff Bingaman (D-NM), who chairs the Energy and Natural Resources Committee, and the ranking minority member, Pete Domenici (R-NM). Co-authors include the chair of the relevant appropriations subcommittee, which means there's a shot at actually funding the measure. A companion bill, H.R. 5263, was introduced in the House last week, albeit with less powerful backers. Hearings are planned for this spring.

—ERIK STOKSTAD

Cyclotron Shuttered

A disappointing budget has forced the U.S. National Science Foundation (NSF) to scuttle experiments and is causing labs to shut down machines. Officials at the National Superconducting Cyclotron Laboratory (NSCL), an NSF-funded facility at Michigan State University in East Lansing, have decided to turn off the lab's two cyclotrons from May to September. The omnibus budget bill, signed into law in December, failed to contain an expected \$1 million boost, to \$19.5 million. As a result, officials can afford to run the machines, which produce radioactive nuclei for nuclear physics experiments, for only 3000 hours in fiscal year 2008 instead of the 4000 hours scheduled, says NSCL Director Konrad Gelbke. The lab will lay off six to eight of its 200 scientists and technicians, and 10 or more experiments will be postponed or canceled. NSCL "may be the optimal place to do some experiments," says physicist Samuel Tabor of Florida State University in Tallahassee, "but if we can't do them here, [other] people will find ways to get them done."

NSF Director Arden Bement says the tight 2008 budget is also forcing the agency to make 1000 fewer grants than it had hoped and to award 230 fewer graduate research fellowships. A new program to study the societal impact of research investments will be delayed a year, he adds, and ongoing programs to support undergraduate research and middle school math teachers will shrink.

—ADRIAN CHO AND JEFFREY MERVIS

It's Not Just Size That Matters

The oversight board for the U.S. National Science Foundation (NSF) has quietly bowed out of a long-running debate about how best to satisfy scientists. In 2000, the National Science Board told agency officials to boost the size of the typical research grant, even at the expense of the number and duration of grants. As a result, average grant size grew by 40% over the next 5 years as NSF's overall budget rose modestly, leading to lower success rates for grantees as the number of awards held steady. That triggered another board review, which led to last week's decision. "We think it should be left up to each discipline, based on the attitudes of the community it serves," says President Emeritus Ray Bowen of Texas A&M University in College Station, who chairs the board panel that oversaw the review.

—JEFFREY MERVIS

RETROVIRUS MEETING

Back-to-Basics Push as HIV Prevention Struggles

BOSTON—At the big annual AIDS conference held in the United States, new drug studies once dominated the agenda. But last week at the 15th Conference on Retroviruses and Opportunistic Infections (CROI), treatment took a back seat to prevention. Many powerful anti-HIV drugs now exist, but few attempts to obstruct HIV infection have succeeded. Results presented at CROI, which ran from 3 to 6 February, continued the string of bad news and prompted much soul-searching about how to invigorate the ailing vaccine search. A few sessions did, however, relieve some of the gloom with reports on new ways to stop HIV's spread from mother to child and new insights into how HIV causes an infection and destroys the immune system.

Vaccine researcher Ronald Desrosiers, head of the New England Primate Research Center in Southborough, Massachusetts, sparked debate by criticizing the funding priorities at the U.S. National Institutes of Health (NIH) in Bethesda, Maryland. NIH devotes nearly one-third of the roughly \$600 million it spends annually on AIDS vaccine research to developing and testing products in humans, yet, Desrosiers asserted, no product now under development has “any reasonable hope of being effective.” “Has NIH lost its way in the vaccine arena?” asked Desrosiers, who argued for more basic research. “I think it has.” (*ScienceNOW*, 5 February: sciencenow.org/content/full/2008/205/1.)

The beleaguered AIDS vaccine field took a serious hit last September, when researchers halted a clinical trial of a promising AIDS vaccine after an interim analysis revealed that it offered no protection against HIV. More disconcerting still, some evidence suggests that preexisting antibodies against an adenovirus strain, Ad5, used in the Merck and Co. vaccine to carry HIV genes, may somehow have made people *more* susceptible to the AIDS virus (*Science*, 16 November 2007, p. 1048). Data from Susan Buchbinder, an epidemiologist at the San Francisco Department of Public Health in California and co-chair of the study, offered some reassurance that the vaccine did not cause harm. Circumcision protects men from HIV, and uncircumcised men with high levels of Ad5 antibodies appear to have become

infected more readily. “The effect of circumcision seemed at least as strong if not stronger than Ad5 [antibodies],” said Buchbinder. Although it's difficult to unravel cause and effect in post-hoc analyses, Buchbinder said: “I don't think at the end of the day that Ad5 was associated with increased infection.”

In another blow to the prevention field, Connie Celum of the University of Washington, Seattle, revealed unexpected results from a study aimed at reducing susceptibility to HIV infection by treating preexisting infection with

through breast milk. “The data are very exciting, but there are caveats,” said Michael Thigpen of the U.S. Centers for Disease Control and Prevention in Atlanta, Georgia, which sponsored one of the studies. Babies can develop resistance to the drugs, which can limit treatment options if they do become infected.

Some intriguing data came from studies of a new type of immune actor, discovered just 2 years ago, called Th17 cells. HIV targets and destroys CD4 white blood cells; Th17 cells are a subset of CD4 cells that secrete interleukin-

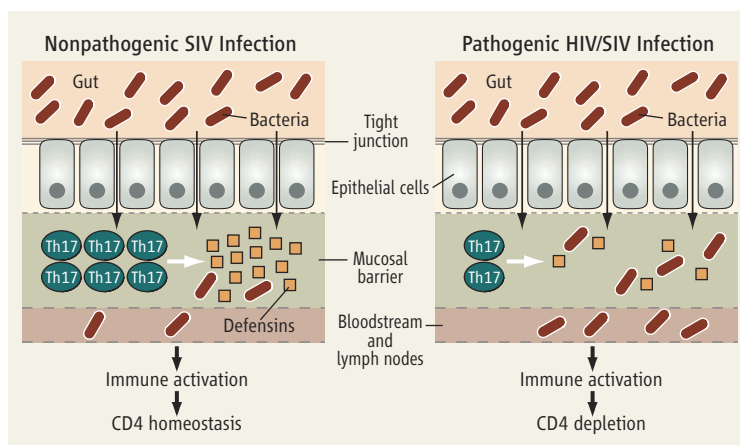
17. Three labs reported that in monkeys and humans, destruction of Th17 cells in the gut make it “leaky,” allowing gut microbes, or pieces of them, to flood into the bloodstream. The researchers contend that this turns up the immune system, “activating” CD4 cells that then prematurely die or become targets for HIV themselves. In one study, said Barbara Cervasi, a postdoc in Guido Silvestri's lab at the University of Pennsylvania, Th17 cells were profoundly depleted in the gastrointestinal tracts of HIV-infected people and SIV-infected macaques—species that both develop AIDS—but

not in SIV-infected sooty mangabeys that suffer no harm from that virus. “People assume that high [HIV or SIV levels] lead to activation,” said Silvestri. “What if it's the opposite and activation causes the problems?”

In the final session, George Shaw of the University of Alabama, Birmingham, reported that his group had sequenced the HIV envelope gene in 102 recently infected people. HIV-infected people carry many genetic variants of the virus, but a single one established an infection and dominated in 80% of the subjects, Shaw and co-workers found. Although other studies have shown that a “bottleneck” occurs in sexual transmission of HIV, allowing few viruses to infect, this is the first study to clarify just how few. Four other new studies have had similar findings, said Shaw.

Shaw, who hopes to discover and target HIV variants that are especially good at transmission, said this work is good news for vaccine researchers. “If all you've got to deal with is one virus,” said Shaw, “surely it shouldn't be so difficult to develop a vaccine.”

—JON COHEN



Gutty virus. Several studies suggest that the AIDS virus causes immune “activation” by destroying Th17 cells, a CD4 subset that resides in the gastrointestinal tract and secretes “defensins” that prevent bacteria from entering the bloodstream and lymph nodes.

herpes simplex virus-2 (HSV-2). Infection with HSV-2, which causes genital ulcers, makes a person two to three times more vulnerable to HIV infection through sex. In a multi-country study involving more than 3000 people, Celum found that treatment with the anti-HSV-2 drug acyclovir did not reduce HIV transmission. Over the course of 18 months, 75 people who received acyclovir became infected with HIV versus 64 who received a placebo. “This is a surprising, disappointing, and important result,” said Celum. “Many people thought this was going to be a slam dunk.”

Celum said the problem wasn't linked to a failure to take acyclovir and that the treatment did reduce genital ulcers—although not as much as in earlier trials. That means intervention might work with a more powerful anti-HSV-2 drug or an effective HSV-2 vaccine, she said.

On a more positive note, two studies of thousands of HIV-infected pregnant women in several developing countries showed for the first time that anti-HIV drugs given to their babies could prevent transmission of the virus

GLOBAL WARMING

Another Side to the Climate-Cloud Conundrum Finally Revealed

Clouds have always given climate modelers fits. The clouds in their models are crude at best, and in the real world, researchers struggle to understand how clouds are responding to—and perhaps magnifying—greenhouse warming. As a result, cloud behavior is the biggest single source of uncertainty in climate prediction. But two new studies now show that much of the worry about clouds' role in the warming has been misdirected. Clouds' response to global temperature changes may be much quicker and more direct—and thus easier to study—than experts have thought.

"It's a little bit of good news," says climate researcher Brian Soden of the University of Miami in Florida. "People have been working on [the cloud problem] for 2 decades or more, and we haven't done a lot to decrease the uncertainty. I'm a little more optimistic now about making progress on this problem."

Researchers have always considered the cloud problem a matter of feedbacks. In a positive feedback, increasing greenhouse gases warm the surface, and the warmer surface then feeds back somehow to overlying clouds. The nature of the feedback remains mysterious, but if it's positive, it would decrease global cloud cover. With fewer clouds reflecting solar energy back into space, more energy would reach Earth, amplifying the initial warming. But Earth's surface and especially its oceans are slow to warm, so cloud feedbacks operate over decades—or so scientists assumed.

Two groups have recently looked at just how quickly model clouds actually respond to an increase in greenhouse gases. Climate researchers Jonathan Gregory and Mark

Webb, both of the Hadley Centre for Climate Prediction and Research in Exeter, U.K., report in the January *Journal of Climate* (issue 1) that model clouds, at least, can respond quickly to added carbon dioxide—in months, not decades. In most of the models examined, the classic cloud feedback driven by change at the surface played only a minor role. The real action took place where the clouds themselves were, up in the air. Added carbon dioxide absorbs more long-wave energy radiating from the surface; the air holding that carbon dioxide warms, and clouds evaporate, letting more solar radiation in.

In follow-up work in press in *Geophysical Research Letters*, climate researchers Timothy Andrews and Piers Forster, both of the University of Leeds, U.K., extend and refine the analysis of Gregory and Webb. In seven models, they doubled carbon dioxide while holding the global surface temperature constant and watched how atmospheric temperatures respond. The classic, slow cloud response is only half of previous estimates, they find, and most of the cloud response is fast.

Scientists "have been looking at the incorrect part of the problem," says Forster. Properly accounting for fast response is important when modeling rising temperatures under the strengthening greenhouse, Webb and Gregory argue. And because it is fast and therefore has been going on for decades, notes Gregory, researchers may be able to tease the newly appreciated cloud response out of observations and improve their models faster than they have the past few decades.

—RICHARD A. KERR



At risk. Greenhouse gases can directly reduce cloud cover and magnify warming.

Standards: An Evolving Story

The Florida Board of Education will decide next week whether to approve new science standards that for the first time in the state's history would require the teaching of evolution. Nine counties have passed resolutions against the document, saying that evolution is not a proven fact, and two of the eight members of the politically appointed board have spoken out against it. But scientists say a statewide signature campaign and an endorsement from science curriculum expert Lawrence Lerner of the Thomas B. Fordham Institute in Washington, D.C., which gave the current standards an F in a nationwide assessment, bode well for their cause. A 19 February vote in favor of the standards would be "a great victory" in keeping creationist ideology out of public schools, says Eugenie Scott of the National Center for Science Education in Oakland, California.

—YUDHIJIT BHATTACHARJEE

Interesting Findings

Most U.S. medical schools are struggling with how to handle institutional conflicts of interest, according to a new survey by the Association of American Medical Colleges (AAMC) and other researchers. The survey, published this week in the *Journal of the American Medical Association*, found that only 38% of 86 medical schools have responded to a 2001 recommendation from AAMC to adopt a policy on institutional conflict of interest. Such conflicts arise when a university has a financial stake in research—for example, having patents on a drug that its researchers are testing. Ethicists say such conflicts should be disclosed to patients in clinical trials, along with any conflicts involving the investigators themselves.

A school's delay may reflect the fact that managing institutional conflicts is "extremely complicated," says Susan Ehringhaus of AAMC in Washington, D.C. AAMC and another group will issue "more detailed advice" this spring, Ehringhaus says.

—JOCELYN KAISER

Hello, Columbus

After years of delay, a 7-hour spacewalk by two astronauts, and a nudge from a robotic arm, the 10-ton Columbus laboratory module slipped into position aboard the international space station 11 February and is being prepared for research. The docking marked the start of the \$2 billion orbiting lab's ability to host substantial science experiments. Columbus will be joined in March by another lab module built by Japan.

—ANDREW LAWLER

Wolves at the Door of a More Dangerous World

Weeks away from being removed from the endangered species list, wolves in the northern Rockies may soon be hunted once more

Three weeks ago, while tracking Yellowstone National Park's gray wolf (*Canis lupus*) packs from the air, wildlife biologist Douglas Smith darted wolf number 637, a young female from the Cougar Creek pack. Then, handling her on the ground for monitoring, he noticed that she had only three legs, probably after getting caught in a coyote trap outside the park's boundaries. Smith, leader of the park's wolf project, fears that 637's misfortune could be a harbinger of things to come, because gray wolves here are soon slated to be removed from the endangered species list. The new ruling from the U.S. Fish and Wildlife Service (USFWS) has been in the works for 5 years and is expected to be published at the end of this month in the *Federal Register*; it would go into effect 30 days later. Wolves on park grounds would still be protected, but "what will happen when they travel outside the boundaries?" asks Smith. "There's a good chance some are going to end up like this one, trapped or killed by hunters."

Smith isn't the only one worried about the future for wolves in the northern Rocky Mountains when they lose the protective shield of the federal Endangered Species Act. Yet at first glance, the announcement would seem cause for celebration. After all, wolves were intentionally driven to extinction in this region less than 100 years ago. Now, following successful reintroductions and management, their population hovers around 1500 animals.

But some of those who have worked to restore the wolf say the new ruling is like the proverbial wolf in sheep's clothing: It turns wolf management over to state and tribal agencies that plan to actively reduce the canid's numbers. The state management plans, already approved by USFWS, will allow trophy hunting and trapping of wolves, plus lethal control of those that harm

livestock or eat too many deer and elk. Last year, Idaho Governor C. L. Otter promised to "bid for that first ticket [hunting tag] to shoot a wolf myself," although he later said that Idaho would manage a viable wolf population. Most controversially, each state is required to maintain a population of only 100 wolves and 10 breeding pairs. That means wolf numbers could drop to a mere 300 and still be considered "recovered," although most wolf watchers think a tally of 500-plus animals is more likely.

So instead of popping champagne corks, as usually happens when a species is brought back from the brink, conservation groups are preparing legal briefs to challenge the ruling. They charge that it's based on politics, not science.

But USFWS officials say they are convinced their science is sound. "That is what the law mandates," says Edward Bangs, wolf recovery coordinator at USFWS in Helena, Montana, referring to the 1994 federal environmental impact statement that established the minimum numbers for recovery. "We've looked at every minute bit of science." He adds that the wolf's biologi-



Pushing boundaries. Yellowstone's wolves don't stay inside the park, as these partial estimates of their movements show.



cal resilience gives him the most hope for their continued success. "Every year, about 23% of the population is killed by people legally and illegally, and yet the wolves are still growing at 24% a year. Biologically, they couldn't be any easier. But politically, wolves are the most difficult to manage."

Hunted with passion

Before Lewis and Clark, some 350,000 wolves inhabited the lower 48 states, preying on bison, deer, and elk, according to genetic studies. As pioneers decimated the bison, wolves turned to livestock, and settlers and the federal government fought back with guns and poison. Ironically, it was the job of USFWS to wipe out wolves. They succeeded by the 1930s, extirpating the canids from more than 95% of their historic range. "Wolves were hunted and killed with more passion than any other animal in U.S. history," says a USFWS publication.

Placed on the federal endangered species list in 1974, gray wolves began making a comeback in the 1980s, when a few Canadian wolves (the Canadian population may be as high as 60,000) crossed the border and settled in Montana. In the 1990s, USFWS brought 66 Canadian and 10 Montana wolves to Yellowstone and a separate area in Idaho. Ranchers, farmers, and hunters fought the restoration, but USFWS surveys showed that many Americans wanted this top predator back on the landscape. "For many people, wolves are

SOURCE: MONTANA FISH, WILDLIFE, AND PARKS INFORMATION SERVICES DIVISION



Top dog. Some hunters worry that wolves may compete with them for elk and deer.

the symbol of Yellowstone,” says Bangs. “They think that we should find a way to live with wolves,” although he adds that this idea is more prevalent among city dwellers who don’t live near wolves.

The reintroductions, which cost a total of \$27 million over 33 years, have been hailed worldwide as great successes, particularly in Yellowstone, where the wolves are helping to bring back a more balanced ecosystem (*Science*, 27 July 2007, p. 438). They also serve as key subjects in a natural laboratory for scientists. Research has shown the ecological benefits of reintroduction, many scientists say: “The most trenchant message from conservation science in the last decade comes from studies about the role of top predators in maintaining the health of ecosystems,” says Michael Soulé, a professor emeritus at the University of California (UC), Santa Cruz.

With abundant prey and open territory, the reintroduced wolves rocketed back, doubling their numbers in the first few years. Young wolves regularly disperse in neighboring states such as Utah and Oregon, although packs have not yet been established there. And although the wolves are currently considered an endangered species, USFWS is allowed to manage them, which includes killing or relocating them. The agency removes packs that have spread into problem areas and has killed about 700 wolves since 1987.

Given the wolf’s recovery, it’s now time for the next step, says Bangs: removing

wolves from the Endangered Species List. To gauge scientists’ reactions to the delisting and the minimum population target, USFWS “surveyed 80 scientists around the world,” says Bangs. “Between 75% and 80% of them thought that this goal [of 300 wolves] was good enough, although I, personally, think it is too low. But the broad consensus was that this definition represents a minimum viable population.” Bangs adds that the “states have already committed to managing for more than the minimum, so that there will be a cushion” of about 45 breeding pairs and more than 450 wolves.

That’s still a reduction of about two-thirds of their numbers. Indeed, traces of earlier attitudes toward wolves linger. Many ranchers, farmers, and hunters despise the canids because they kill livestock and pets and compete for elk and deer. Posters put up by antiwolf groups label the wolf “The Saddam Hussein of the Animal World.” Terry Cleveland, director of the Wyoming Game and Fish Department, says that “state law requires us to have an aggressive management plan for wolves,” although he adds that this will include monitoring as well as hunting. Outside of the greater Yellowstone area, wolves will be classified as predatory animals. That means that, once delisted, they can be killed without a hunting license and by many methods,

including intentionally running over them with a car or in “wolf-killing contests.” Cleveland says that “our floor wolf population here will be roughly 150 wolves. The ceiling has yet to be determined.”

Idaho, too, plans a hunting season for its 700-some wolves, and populations will be thinned in areas of high conflict, says Steve Nadeau, a large carnivore manager for Idaho’s Fish and Game Department. “But we’re going to go slow and conservative to see how the harvest works.” In Montana, where about 400 wolves reside, the numbers are also certain to drop because the plan describes wolves as a

“species in need of management.” Carolyn Sime, the wolf program coordinator for Montana’s Fish, Wildlife, and Parks Department, says that “when there are at least 15 breeding pairs, hunting and trapping could occur.”

The wildlife agencies insist they’re not planning to send the canids back to the brink. “We manage big game for a living, and we’re good at it,” says Nadeau. “We’ll do a good job with the wolves, too. The whole world is watching, and we know it.”

The states’ plans to treat wolves as big game animals available for trophy hunting may actually end up helping the canids, suggests Bangs. He expects hunters will likely become some of wolves’ staunchest supporters, “just as they are now for mountain lions and black bears.”

“The whole world is watching, and we know it.”

**—STEVE NADEAU,
IDAHO FISH AND
GAME DEPARTMENT**



Born to run. Reintroduced wolves are recolonizing their old territories.

Battling over the numbers

Despite Bangs's description of broad support for the delisting among the USFWS survey of scientists, many university scientists and conservation organization researchers interviewed by *Science* find the plan premature and unwise. In particular, they object to the notion that a population of 300 wolves is viable. "They don't even need a scientist to tell them that," says Robert Wayne, an evolutionary biologist at UC Los Angeles, whose lab has reconstructed the past genetic history of North America's gray wolves. In a letter he sent to USFWS last February in response to the service's request for his comments on the delisting proposal, Wayne wrote that the recovery goal "severely underestimates the number of wolves required for maintaining a genetically healthy, self-sustaining meta-population." He also notes that the delisting proposal makes no effort to assure that the populations in the three states and Canada are interconnected via corridors so that the wolves can mix genetically and form a metapopulation. He and others argue that such a metapopulation was one of the goals of the original 1987 federal wolf recovery plan.

The lack of gene flow most threatens the 171 wolves in Yellowstone National Park, which are all descendants of the first 41 released there between 1995 and 1997. Without new wolves, the population's genetic health is certain to decline, says Wayne and his graduate student Bridgett vonHoldt, who analyzed the genealogy and genetic viability of the Yellowstone wolves last year. They note that recent studies of a highly inbred population of Swedish wolves indicate that within 60 years, the Yellowstone wolves will begin suffering from "significant inbreeding depression," which will lead to a lower population. "It will be the equivalent of having one less pup a year," says Wayne.

But Bangs counters that the Endangered Species Act requires only that wolf numbers stay above the threatened or endangered level. "It isn't about maintaining genetic diversity," he says. If inbreeding problems arise, new wolves can always be reintroduced to the park later. "Connectivity can happen through a ride

in the back of a truck," he says. That attitude dismays vonHoldt. "The impact is there on the horizon for anyone to see," she says. "Why create a problem for others to solve down the line? Why not fix the recovery plan now?"

"Basically, the goals of the USFWS's wolf recovery plan aren't in sync with the latest thinking in conservation science," says Carlos Carroll, a wildlife biologist with the Klamath Center for Conservation Research in Orleans, California, who has modeled the restored wolf populations. "Biologists have moved away from the idea of a minimum viable population [MVP] to a more comprehensive population analysis." The problem with MVP numbers, he adds, is that "wildlife managers focus solely on that number," as they are in the three states. Instead, he and other researchers say that management plans need to include the "range of factors that might threaten a population and determine ways to make it more resilient to unexpected events," such as a new disease.

"We will most certainly lose some of our wolves."

**—DOUGLAS SMITH,
YELLOWSTONE WOLF PROJECT**

"That 300 figure reflects old thinking; new data suggest that several thousand wolves" may be needed before delisting should be considered, says Carroll. He and others note that USFWS delisted the Great Lakes gray wolves only last year in Michigan, Wisconsin, and Minnesota, when the population totaled 4000 individuals. (Although all three states now consider wolves as big game animals, none has yet initiated a hunting season.)

And then there are the wolves of Yellowstone. Smith and others have monitored them for 13 years, collecting data that should help settle long-standing issues such as how great an impact wolves have on prey populations and how natural wolf populations fluctuate. None of the states' plans makes special provisions or buffer zones to protect these wolves; one of Montana's proposed wolf-hunting zones abuts the park's boundary. Six of the park's 11 wolf packs travel outside the park's boundaries every year (see map, p. 890); and two of these six do so for extensive periods of time, largely in pursuit of elk, the wolves' main prey. "They'll get into trouble," predicts Smith. "I support delisting. But [this] concerns me, because the parks' mission is one of protection

and preservation. And we will most certainly lose some of our wolves."

State wildlife managers make no promises on this issue, saying that wolves in their territory are fair game. "The Yellowstone wolves will be treated the same as elk that also travel outside of the park and are hunted," says Sime. Counters Smith, "These are park wolves; most spend 99.9% of their time here, yet they may get killed on that one trip outside. The public knows them as individuals. Which state official is going to take the call when someone's favorite wolf is shot?" Further, the loss of park wolves to hunters will "squander our research."

Many scientists would prefer to see the wolves remain on the endangered list until they reach a point at which they can be self-sustaining without the need for heavy human management. "It's frustrating," says Sylvia Fallon, an ecologist with the Natural Resources Defense Council in Washington, D.C. "Having a natural population of wolves is achievable and sustainable, and we're close to being there. But now, they're going to be knocked back down. We have to stop the delisting."

Environmental organizations are already running ads decrying the planned delisting and have joined forces to ask for an injunction against USFWS's proposal as soon as it is published. They have also already filed a lawsuit to try to block another USFWS ruling, published in late January, that would essentially let the three states begin lethal management of the wolves (although not a public hunting season), even if the delisting is blocked in court.

Conservationists argue that wolves should stay on the land and fulfill their ecological niche where possible. But for that to happen, people must accept the presence of wolves—and change their behavior accordingly, says Timmothy Kaminski, a wildlife biologist with the Mountain Livestock Cooperative in Augusta, Montana. Otherwise, a sad, repetitive scenario ensues, with wolves moving onto the same ranchlands, killing cattle, and then being killed, over and over. "Wolves are here; grizzly bears and mountain lions are here. You can't turn your cows out into a mountain pasture without being as vigilant as an elk," says Kaminski. "This is no longer a 20th century landscape."

—VIRGINIA MORELL

CREDIT: AP

CHEMISTRY

Framework Materials Grab CO₂ And Researchers' Attention

Porous solids have become a rich playground for chemists, who can tailor the materials' makeup for use in gas storage, filtering, and catalysis

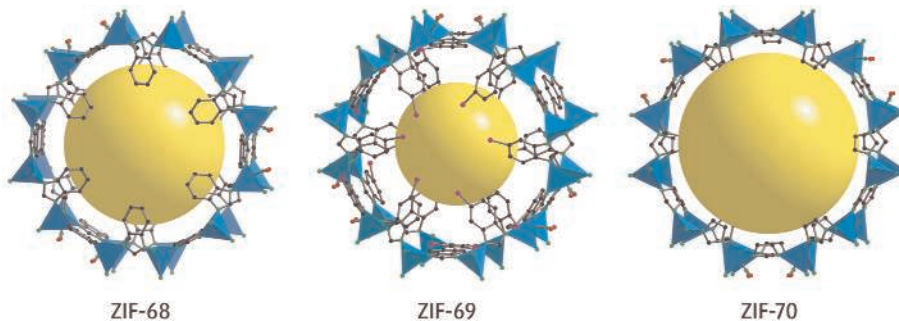
In most synthetic chemistry projects, researchers struggle to stitch molecules together one bond at a time. Not so in the lab of Omar Yaghi, a chemist at the University of California (UC), Los Angeles. Yaghi and his colleagues work to find just the right set of conditions so that entire networks of materials fabricate themselves when given the go-ahead.

In the late 1990s, Yaghi first worked out the formula for creating a family of highly porous, yet stable, crystalline materials known as metal organic frameworks. MOFs have a Tinkertoy-like construction with metals that serve as the hubs and connecting struts made from organic compounds. By tweaking his recipe, Yaghi and others have since made thousands of such porous crystals. That's made MOFs and related compounds one of the hottest playgrounds in chemistry, and Yaghi their greatest inventor. "His work is terrific," says Thomas Mallouk, a chemist at Pennsylvania State University in State College. "He does beautiful fundamental science that is knocking on the door of important applications."

On page 939, Yaghi and colleagues report a new robotic high-throughput scheme for creating MOF relatives known as zeolitic imidazolate frameworks (ZIFs). And Mallouk and others say that the work is again an important blend of fundamental research and a critical application: materials that might help coal-fired power plants filter out carbon dioxide from their smokestacks. Mallouk calls the new work "very clever" because Yaghi and his colleagues have designed their hubs and linkers to mimic the construction of zeolites, a family of natural porous compounds widely used as catalysts and filters in industry. But because ZIFs are stable at high temperatures and are easier to tailor by adding desired chemical functional groups, they may prove even more useful in the long run.

Attempts to gain control over open-framework materials have a long and frustrating history. The frameworks are synthesized in solution and can take on a wide variety of structures depending on the hubs and linkers used. For decades, however, researchers

found that their frameworks almost always collapsed when they removed the solvent. Equally troubling, they found it nearly impossible to make large pores, as multiple networks would form simultaneously and interpenetrate one another. Yaghi and colleagues solved both of these problems in the late 1990s. They increased the strength of their frameworks by selecting starting materials that preferentially assembled into a network of rigid prisms and cages. They also worked out designs that keep separate frameworks from interpenetrating. It's been off to the races ever since.



Carbon traps. Cagelike zeolitic imidazolate frameworks and their kin excel at straining carbon dioxide out of a mixture of gases, a knack that could lead to CO₂ scrubbers for power-plant smokestacks.

One key race is to create a MOF that can store hydrogen for use in future fuel-cell cars. High-pressure gas tanks do the job fairly well. But pressurizing gases is a big energy drain and can create a hazard if the gas tank is punctured in a crash. By filling part of the tank with a MOF's cagelike network built with hydrogen-absorbent metal hubs and organic struts, however, it is possible—at least in theory—to store more of the gas at a lower pressure. Slightly raising the temperature or releasing the pressure then liberates the gas. Yaghi's group and Jeffrey Long's group at UC Berkeley both recently created MOFs that can hold up to 7.5% of their weight in hydrogen, better than a benchmark for hydrogen storage set by the U.S. Department of Energy. Unfortunately, they only do so at 77 kelvin (−196°C), making them impractical for real-world use.

In July 2007, researchers led by William Goddard III of the California Institute of

Technology in Pasadena reported in the *Journal of the American Chemical Society* that adding lithium to a MOF should make it possible to store 6% of its weight in hydrogen at room temperature. Long says many groups are working on it, but "it's not trivial." Lithium, he points out, tends to hold strongly to solvent molecules after synthesis, and removing the solvent requires so much energy that it typically blows apart the framework.

Other MOF applications are pushing ahead as well. Several of the new ZIFs appear to have a strong preference for binding CO₂. Yaghi suspects that carbon-rich benzene rings in their struts act as valves that let CO₂ molecules pass in and out of the pores. Once inside, the CO₂'s carbon atoms, which have a partial positive charge, readily bind to nitrogen atoms in the framework, which carry a partial negative charge. Yaghi says ZIFs could be used to capture CO₂ in power-plant smokestacks. Once full, the ZIFs can be removed, and the ensuing pres-

sure drop would release the CO₂ from the pores, allowing the ZIFs to be reused. MOFs are also being looked at as filters for a variety of hydrocarbons.

Other teams are beginning to explore using the porous solids as scaffolds for catalysts. By tuning the materials to allow certain gases inside easily while excluding others, researchers can control which compounds in a mixture gain access to a catalytic metal atom inside. Because the materials are solids, they can easily be recovered and reused after running a reaction, unlike many highly active catalysts that must be separated from a solution. With all the possible ways to construct MOFs and their many applications, today dozens of groups around the world are streaming into the field. "Interest in these materials has been increasing extremely rapidly," says Long. "The trajectory is still going way upward."

—ROBERT F. SERVICE



◀ **Tricky diagnosis.** X-rays, like this one taken in Port Elizabeth, show TB infection, but tests to distinguish normal from drug-resistant TB can take weeks.

DRUG-RESISTANT TUBERCULOSIS

In South Africa, XDR TB and HIV Prove a Deadly Combination

Since the 2005–2006 outbreak of extensively drug-resistant TB in KwaZulu-Natal, health experts have been grappling with how to detect and treat the disease

CAPE TOWN, SOUTH AFRICA—A gaunt man with dark, deep-set eyes nods toward the uniformed security guards at the gate and the nurses who wear double-thick “respirator” masks when they make their rounds. The cheerless ward, surrounded by a 3-meter fence, is “more like a prison than a hospital,” he says. “Many patients are depressed; they don’t want to be here,” the chief nurse tells a visitor as a TV soap opera drones in a nearby room.

That feeling is understandable. The two dozen men and women in the isolated ward are undergoing harsh and possibly futile treatment for the often lethal, contagious, and stigmatized disease that has brought them to Brooklyn Chest Hospital: extensively drug-resistant tuberculosis (XDR TB). The emergence over the past 2 years of the disease—which is even more difficult to treat effectively when patients are coinfecting with HIV, as many are—is posing complex medical, ethical, and scientific issues in South Africa, the site of the largest and deadliest XDR TB outbreak to date. Last year, more than 500 cases of XDR TB were diagnosed here, and the total number was probably far higher.

On the medical front, the challenges include treating an infection that resists even last-ditch medications and finding the best ways to prevent hospital transmission of the disease (see sidebar, p. 897). Among the research challenges are identifying new drug targets and

rapid diagnostics, as well as investigating the molecular evolution of the TB strains that led to the emergence of this new threat. The main ethical quandary is the extent to which hospitals can or should isolate XDR TB patients against their will or force them to take potentially life-saving yet toxic drugs—perhaps for years.

Few warning signs

In August 2006, researchers made headlines at the annual AIDS meeting in Toronto, Canada, with a report that a new strain of TB, apparently resistant to almost all known drugs, had emerged in South Africa. The cases had been detected in 2005–2006 in the poor, mainly Zulu community of Tugela Ferry in South Africa’s KwaZulu-Natal (KZN) Province; nearly all the victims were also coinfecting with HIV. Especially alarm-

ing was the fatality rate: 52 of 53 patients had died within a median of 16 days after being tested for TB (*Science*, 15 September 2006, p. 1554).

XDR TB caught health care workers off guard and sparked fears of a new wave of “killer TB” outbreaks—especially in countries with high rates of HIV infection—that could jeopardize the progress in global TB control. The outbreak provided a “wake-up call,” says Mario Raviglione, director of the World Health Organization’s (WHO’s) Stop TB Department, which had first discussed the emergence of XDR TB of Tugela Ferry and elsewhere at a meeting in May 2006. WHO quickly formed a global XDR TB task force that soon made recommendations for dealing with the threat. These include better TB and HIV/AIDS control and stricter management of drug-resistant TB, as well as better laboratory services and more extensive surveillance.

Although the Tugela Ferry outbreak was startling, XDR TB wasn’t brand-new. Sporadic cases had been reported in the United States, Latvia, Russia, and elsewhere; WHO and the U.S. Centers for Disease Control and Prevention in Atlanta, Georgia, had first defined the strain in a March 2006 article. Nor was the new bug totally unexpected, given the poor record of treating TB in many countries. After multidrug-resistant (MDR) strains of TB surfaced a couple of decades ago, some scientists had warned, it was only a matter of time before new strains, resistant to even more drugs, would emerge.

MDR TB first garnered widespread attention in the 1990s, when researchers and clinicians around the globe began identifying an alarming number of cases that were resistant to at least two of the four standard drugs used to treat TB. Suddenly, the already arduous task of treating TB became even more difficult and expensive. MDR TB can take as long as 2 years to treat, compared with 6 to 8 months for drug-sensitive TB. Costs run 3 to 100 times higher, depending on the country and the drug-resistance pattern. WHO now estimates that of the 8 million cases of active TB diagnosed each year, more than 400,000 are MDR. Cases tend to be concentrated in regions where inadequate health-care services make it harder to ensure that patients can follow the lengthy drug regimen.

Resistance can arise when patients fail to complete their therapy, thereby giving the TB bacteria



an opportunity to mutate to evade the drugs. That's why a cornerstone of TB therapy has long been directly observed treatment—short course (DOTS), which focuses on supervised adherence to a fixed combination of anti-TB drugs. However, DOTS does not require drug-resistance testing, meaning that many undiagnosed MDR TB patients have been treated by an ineffective DOTS drug regimen that may have allowed those MDR TB strains to develop even further drug resistance. To help address that problem, WHO in March 2006 began recommending what's called the "DOTS-Plus" protocol—which calls for using second-line TB drugs for people with confirmed or presumed MDR TB—for some high-incidence countries.

"The major challenge is to see that TB patients stay on the treatment regimen," says Karin Weyer, head of the TB program at South Africa's Medical Research Council (MRC). Lindiwe Mvusi, who heads the South African Health Department's TB Program Directorate, estimates that at least 20% of the country's MDR TB patients are defaulting, making it more likely that some may eventually end up with XDR TB. Because XDR TB is resistant to most of the second-line drugs that are used to treat MDR TB (including fluoroquinolone-category medications as well as either amikacin, capreomycin, or kanamycin), clinicians have few options, other than trying older drugs or new combinations of drugs.

Paul van Helden, co-director of the Centre of Excellence in Biomedical TB Research at Stellenbosch University, questions whether the DOTS drug protocols are always the best approach in high-incidence TB countries such as South Africa. He believes more investigations are needed to determine the best mixture of drugs to treat MDR and XDR TB in different regions.

At this point, no one knows exactly how many cases of XDR TB there are globally, because most go undiagnosed and are not reported. WHO recently estimated that XDR TB may infect about 27,000 people a year in at least 41 countries. But this is just an educated guess, based on a percentage of the MDR TB cases diagnosed each year. Later this month, a new WHO report will give a more detailed picture of the spread of drug-resistant TB.

Flash point at Tugela Ferry

In retrospect, it's not surprising that the 2005–2006 outbreak occurred in KZN Province, which includes areas of extreme poverty. Although for centuries tuberculosis has been called The White Plague, in South Africa it is predominantly a disease of black

Africans, a byproduct of poverty, poor health care, and—perhaps most perniciously—a high HIV infection rate. About 5.5 million South Africans are HIV-infected, about 11% of the population, with the highest infection rate in KZN. The combination of drug-resistant TB and HIV is especially dangerous because the weakened immune systems of HIV-infected persons make them more vulnerable to TB and also more difficult to treat.

The Tugela Ferry outbreak was detected when doctors at Church of Scotland (COS) Hospital began investigating the unexpectedly high mortality rate among TB-HIV-coinfected patients. Drug-sensitivity tests revealed that not only was MDR TB rampant, but even more

in many South African communities. He argues that the current South African statistics are unreliable and the extent of the problem underestimated because "there has been a marked underreporting of XDR TB."

But other TB experts, including Weyer and Mvusi, regard Tugela Ferry as atypical, in large part because its mortality rate has not been matched anywhere else in South Africa. Mvusi says there were 183 confirmed deaths from XDR TB in South Africa last year, but 342 XDR TB patients were still under treatment—giving hope that some cases can be managed. Although the Eastern Cape and KZN provinces had the most XDR TB cases, the strain has been found in all nine South



Isolation. The new XDR TB ward at Brooklyn Chest Hospital in Cape Town is guarded around the clock and surrounded by a high chain-link fence. A patient who tested positive for XDR TB awaited treatment at a rural hospital in Tugela Ferry in 2006 (right).

patients had the superresistant XDR strain. Before then, few clinicians tested for drug resistance because it was expensive and time-consuming. That has changed over the last 2 years; today, many South Africans who test positive for TB are started on first-line drugs while being tested for drug resistance.

Since the initial reports, a total of 217 XDR TB cases have been found in Tugela Ferry, with a mortality rate of 84% between June 2005 and last March. Paul Nunn, the TB-HIV and drug-resistance coordinator at WHO's Stop TB Department, calls the Tugela Ferry outbreak "the worst of its kind" worldwide, in terms of the number of cases, fatality rate, and the high ratio of XDR to MDR cases.

Was Tugela Ferry the harbinger of other severe XDR TB outbreaks or an anomaly resulting from an unusual convergence of risk factors? Gerald Friedland of Yale University School of Medicine—whose research group reported the outbreak at the 2006 AIDS conference as part of its collaboration with physician Anthony Moll's COS hospital staff and other institutions—wonders that interlinked HIV and XDR TB epidemics could "create a firestorm"

African provinces. Many of those XDR TB patients were HIV-infected and many others had defaulted on TB drug regimens.

Searching for origins

In the wake of the Tugela Ferry outbreak, scientists have been using molecular fingerprinting techniques to analyze thousands of old, frozen TB samples to try to reconstruct the history of XDR TB's emergence in South Africa. At the University of KwaZulu-Natal, A. Willem Sturm's team discovered that XDR isolates of the KZN strain had existed undetected as far back as 2001. About 9% of the province's 2634 MDR TB cases had actually been XDR infections.

XDR isolates dating back to 2001 were also found in western South Africa, where biologists at Stellenbosch University's TB research center are conducting a retrospective analysis of thousands of TB samples. They are also cooperating with the Broad Institute and Harvard School of Public Health in Boston to sequence and compare the genomes of several drug-resistant TB strains isolated here (*Science*, 9 November 2007, p. 901).

Research Project Mimics TB Transmission

PRETORIA, SOUTH AFRICA—A half-century ago, Richard L. Riley of Johns Hopkins University in Baltimore, Maryland, and others set up an innovative experiment at a Baltimore Veterans Administration Hospital: venting air exhaled by tuberculosis (TB) patients in a six-bed ward into an “exposure chamber” housing 150 guinea pigs. The challenge was to prove that TB can be transmitted by tiny airborne droplets and that individual patients vary greatly in how infectious they are to others.

But Riley’s classic experiments did not test the effectiveness of interventions such as air filters and bacteria-killing ultraviolet lights that aim to reduce airborne TB transmission. They also took place before the emergence of drug-resistant TB strains and the AIDS epidemic, two key factors that influence airborne spread of TB and patient susceptibility in Africa’s crowded hospital wards.

This spring, South African and U.S. researchers will use a hospital setup similar to Riley’s to investigate those and other variables in TB transmission at the new Airborne Infection Research (AIR) Facility in the coal-mining city of Witbank. In helping to plan the studies, TB researcher Edward Nardell of Harvard School of Public Health in Boston consulted with his mentor Riley before his death in 2001 along with scientists at South Africa’s Medical Research Council (MRC) and the U.S. Centers for Disease Control and Prevention in Atlanta, Georgia.

Research at the new facility will focus on patients who are coinfecting with HIV and drug-resistant TB, Nardell says. The goal is to “tease out the importance of infectious source strength, microbial resistance to environmental interventions, and the critical importance of microbial genotype and host factors” in airborne transmission, says Nardell.

Lindiwe Mvusi, the chief TB official in South Africa’s health department, hopes the AIR experiments will yield more data on the best ways to block airborne transmission of TB. During the deadly extensively drug-resistant



Transmission. Air from a TB ward is vented into guinea-pig cages (*above*) at an experimental facility in Witbank.

(XDR) TB outbreak in Tugela Ferry in 2005–2006 (see main text), hospital transmission was a major factor. Eight hospital staff members later died from drug-resistant TB (half of them from XDR TB, the other half from multidrug-resistant TB) before ventilation was improved and other control steps were taken.

Although the experimental setup is complex, Nardell says Riley’s model is the only one developed so far that accurately mimics airborne TB transmission in hospital wards. Other efforts to simulate hospital conditions by exposing lab animals to artificially aerosolized TB bacteria have failed to simulate the natural infection process.

The AIR experiments will expose as many as 360 guinea pigs at a time to air vented directly from a six-bed TB unit. Preliminary experiments last year validated the model, Nardell says, showing the same sorts of infections found in humans. Karin Weyer, who heads MRC’s TB program, agrees that AIR is “an ideal model for studying environmental infection control.”

—R.K.

Meanwhile, other groups are searching for faster and cheaper ways to detect XDR TB, as well as new drugs to treat it. Testing for resistance to second-line drugs can take up to 2 months using the standard techniques, by which time patients may have been treated with the wrong drugs.

In South Africa and elsewhere, clinical trials of new, molecular-based tests for drug resistance are already under way by MRC, in cooperation with the Foundation for Innovative New Diagnostics in Geneva, Switzerland. If WHO validates the results, approval seems likely for a German firm’s test that can quickly detect MDR TB and is being modified to detect XDR TB. Other groups are also testing their own molecular-based techniques.

Drugs for treating XDR TB are much further away, although several trials are under way. For now, doctors prescribe older TB drugs such as capreomycin and ADT that have not been used in typical second-line drug regimens.

Despite the daunting challenges, there is some reason to hope that XDR TB patients can be effectively treated, if not cured. In contrast to the Tugela Ferry outbreak, Iqbal Master, chief of medicine for drug-resistant TB at King George V Hospital in Durban, says

two-thirds of the 133 XDR TB patients who were in King George V Hospital during 2007 were still alive at the year’s end. Researchers in Latvia suggest that up to 30% of XDR TB cases that are not HIV-infected could be effectively treated. That is good news for patients but poses problems for medical officials who must decide whether and how to separate XDR TB patients from others during the lengthy treatment period.

The isolation debate

“We were caught off guard by XDR TB,” concedes Marlene Poolman, the deputy director for TB control at the Western Cape province’s health department in Cape Town. No cases were diagnosed until the end of 2006, and the following year, the number of XDR TB admissions at Brooklyn Chest Hospital soared to 72. “Virtually overnight, we had to convert an empty ward into a new XDR unit.” The chain-link fence and 24-hour guards were added in October after several patients left the hospital and had to be returned under court order.

Involuntary isolation or confinement of XDR TB patients is controversial, allowed in some nations only if the disease is found to pose

an immediate threat to public health. WHO recommends separating XDR TB patients from others, especially in regions with high HIV prevalence, and South Africa’s health department has adopted that policy.

But even high fences and guards at some specialized TB hospitals in South Africa haven’t kept all patients inside. In December 2007, 20 XDR TB patients and 28 MDR TB patients in another ward cut a hole in the fence and fled a TB hospital in Port Elizabeth. A month later, eight of those patients had not returned, despite court orders.

Mvusi says overcrowding at some hospitals and clinics, especially in high-incidence areas such as KZN, has made it difficult to separate XDR TB patients. King George V Hospital had a waiting list of 120 drug-resistant TB patients at the end of last year. Many of those were being treated as outpatients.

Master says the caseload is challenging the health care system. If patients with M(X)DR TB survive their entire 2-year treatment regimens and still test positive for drug-resistant TB, Master asks, “What do you do then? You can’t put everyone in the hospital for an indefinite period.”

—ROBERT KOENIG

Number Theorists' Big Cover-Up Proves Harder Than It Looks

Every integer is either even or odd. Not the deepest of mathematical theorems, to be sure. But number theorists have molded it into conjectures that challenge the intellect, including one the redoubtable Paul Erdős declared “perhaps my favorite problem.”

In an invited address at the joint meetings, mathematician Carl Pomerance of Dartmouth College described recent progress in the theory of coverings: collections of number sequences that, taken together, include every single integer—zero, positive, and negative—stretching toward infinity. The research includes computer-intensive investigations into the nature of prime numbers (integers that can't be broken down into smaller factors), including an Internet-wide attack on a poser known as the Sierpiński problem.

“There is a flurry of activity right now,” Pomerance says. Jeffrey Lagarias, a mathematician at the University of Michigan, Ann Arbor, agrees. “Covering questions are perennially important,” he says. The fact that the problems are simple to state yet notoriously tough to solve, he adds, “illustrates how little we know about the integers.”

In the even-odd covering, each of the two covering sequences has the same step size, namely 2. One starts at 0, the other at 1. You can also cover the integers with sequences of step size 3 (starting at 0, 1, and 2) or of any other size. The game gets interesting when each sequence has a different step size, or modulus. For example, every integer fits into one (or more) of the following five arithmetic progressions: step sizes 2 and 3 starting at 0, step

sizes 4 and 6 starting at 1, and step size 12 starting at 11 (see figure, below).

There are infinitely many essentially different ways to cover the integers using 2, 3, or 4 as the smallest step size. But above that, things get dicey. The Hungarian mathematician Paul Erdős's “favorite problem,” dating back to about 1950, is to prove that there are coverings with a smallest step size as large as you like. But the record starting step size for any covering to date is a mere 36.

That record was set last year by PACE Nielsen of the University of Iowa in Iowa City. Nielsen's 36 topped the record 25 established in 2006 by Jason Gibson, now at Eastern Kentucky University in Richmond. Gibson's paper presented a new way of looking for coverings and concluded with pages of starting points and step sizes for the arithmetic progressions starting at step size 25. Nielsen also gave a systematic procedure for his new covering, but he didn't describe the cover explicitly. For good reason: Nielsen estimates his approach produces a covering with more than 10^{40} different progressions—“too many to list individually with current computer resources,” he wryly notes.

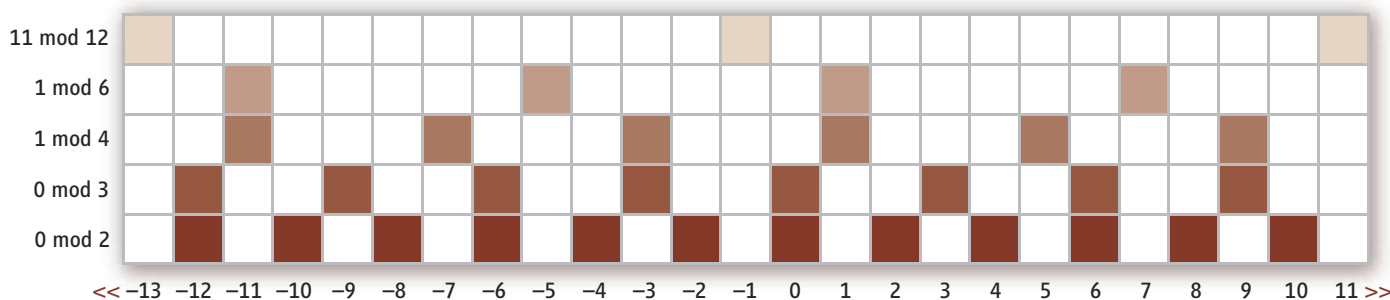
The outrageous number of progressions in Nielsen's covering, and presumably any beyond it, is not a surprise, according to Pomerance. He and colleagues have proved another conjecture, first formulated in 1973 by Erdős and John Selfridge of the University of Illinois, Urbana-Champaign, which implies that coverings with large smallest step size must have extremely many step sizes to compensate for the wide gaps between covered numbers.

Coverings have no immediate “real world” applications, but they do carry implications for number theory, a branch of mathematics deeply entwined with practical issues of computing and computer security. Many key algorithms in cryptography, for example, are based on probing large numbers for primality.

One byproduct of coverings is a method of generating sequences that are guaranteed to avoid primes. It got its start in 1960, when the Polish mathematician Waclaw Sierpiński of the University of Warsaw used the theory of coverings to show that there are infinitely many values of k for which every number of the form $2^k + 1$ (i.e., $k + 1, 2k + 1, 4k + 1, 8k + 1$, and so on) is nonprime, or composite. In 1973, Selfridge showed that the smallest composite number Sierpiński's result describes is the one formed when $k = 78,557$. He conjectured that for all smaller values of k , the sequence $k + 1, 2k + 1, 4k + 1, 8k + 1, \dots$ contains at least one prime.

Selfridge's idea was easy to check for most small values of k , but a few holdouts still stymie mathematicians. In 2002, Louis Helm of the University of Michigan, Ann Arbor, and David Norris of the University of Illinois, Urbana-Champaign, launched an online effort to put the problem to rest. At the time there were 17 small values of k for which no prime had been found, so they called the project “Seventeen or Bust” and put it on the Web at the address seventeenorbust.com.

Today, only six small values of k remain unsettled. The most recent value to bite the dust is $k = 33,661$. Last October, Sturle Sunde of the University of Oslo, a contributor to Seventeen or Bust, reported a computation showing that $2^n \times 33661 + 1$ is prime when $n = 7,031,232$. Earlier calculations mistakenly reported the number as composite, but double-checking confirmed its prime status. Sunde's prime, which weighs in at

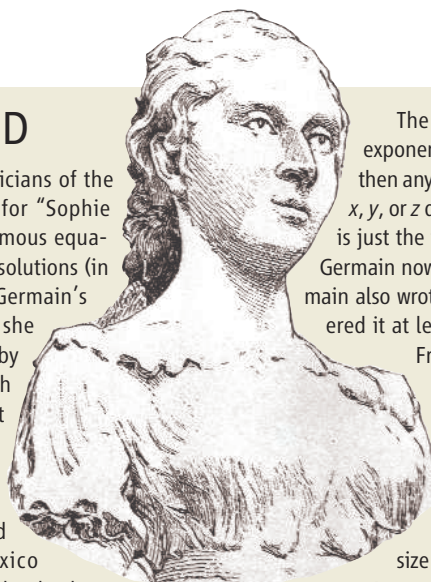


Mod squad. Progressions with small step sizes, like these five sequences, cover the integers handily, but the problem gets trickier as the gaps increase.

A WOMAN WHO COUNTED

Sophie Germain was one of the great mathematicians of the early 19th century. Number theorists laud her for “Sophie Germain’s theorem,” an insight into Fermat’s famous equation $x^n + y^n = z^n$ aimed at establishing its lack of solutions (in positive integers) for certain exponents. Oddly, Germain’s fame for her theorem stems not from anything she herself published but from a footnote in a treatise by her fellow Parisian Adrien-Marie Legendre, in which he proved Fermat’s Last Theorem for the exponent $n = 5$. Now, two mathematicians have found that Germain did far more work in number theory than she has ever been given credit for.

Poring over long-neglected manuscripts and correspondence, David Pongelley of New Mexico State University in Las Cruces and Reinhard Laubenbacher of Virginia Polytechnic Institute and State University in Blacksburg have discovered that Germain had an ambitious strategy and many results aimed at proving not just special cases of Fermat’s Last Theorem but the whole enchilada. “What we thought we knew [of her work in number theory] is actually only the tip of the iceberg,” Pongelley said at a session on the history of mathematics.



The theorem in Legendre’s footnote asserts that if the exponent n is a prime number satisfying certain properties, then any solution to $x^n + y^n = z^n$ must have one of the numbers x , y , or z divisible by n . Pongelley and Laubenbacher report this is just the first of numerous theorems in a long manuscript by Germain now housed at the Bibliothèque Nationale in Paris. Germain also wrote another bulky manuscript on the subject and covered it at length in a letter to the German mathematician Carl Friedrich Gauss. In the three sources, Germain elaborated programs for proving, first, that all primes satisfy the necessary properties; and second, that exponents n cannot divide any of the numbers x , y , or z . Together, those two results would have proved Fermat’s Last Theorem. Along the way, she showed that any counterexample would involve numbers “whose size frightens the imagination,” as she put it to Gauss.

A proper Hollywood ending would have Germain’s proof of Fermat’s Last Theorem take precedence over Andrew Wiles’s monumental accomplishment of 15 years ago. However, Pongelley notes, that’s not how the story goes. Much of Germain’s approach was rediscovered later by others and found to fall short of its goal. Nonetheless, Pongelley says, the fact that she had developed far more than a single footnoted theorem “calls for a reexamination of the scope and depth of her work.” —B.C.

2,116,617 digits, is currently the 10th-largest known prime on the books. The meatiest prime number currently on record is a 9,808,358-digit monster of the type known as a Mersenne prime, $2^{32,582,657} - 1$.

Exact-Postage Poser Still Not Licked

Quick: What’s the largest amount of postage it’s impossible to pay exactly using 41-cent and 26-cent stamps? What if you have a supply of 58-cent stamps as well?

Stumped? So are mathematicians—at least when the numbers are large and there are more than three different stamps involved. But using techniques from computational algebraic geometry, researchers have recently made stunning progress in solving large cases of what they call the linear Diophantine problem of Frobenius. Should inflation take the price of stamps into 10-digit territory, mathematicians are confident they can quickly solve the impossible postage problem with as many as a dozen different denominations of stamps.

That such a simple-sounding problem turns out to be so hard is part of the Frobenius problem’s appeal, says Matthias Beck of San Francisco State University in California. “It has a certain flair to it,” he says. Moreover, “all kinds of mathematical areas connect to it,” including number theory and theoretical

computer science.

The problem, named for the 19th century German mathematician who popularized it, was first posed by the English mathematician James Sylvester in 1884, as a money-changing problem. Sylvester showed that if two denominations, A and B , have no common factor, then the largest amount that cannot be formed is given by the formula $AB - A - B$. This makes the 41/26-cent problem a snap; the reader will find the answer pleasantly surprising.

Mathematicians have proved that with three or more stamps, there is no simple, Sylvester-style formula for the largest impossible amount. In fact, researchers have shown that the problem is what computer scientists call NP-hard: Any algorithm powerful enough to give an efficient general solution would automatically solve an entire class of problems, including everything that currently underlies the cryptographic security of Internet transactions.

Various researchers found practical but complicated algorithms for the three-stamp problem in the 1970s and ’80s. In 1992, Ravi Kannan, now at Yale University, showed that there are theoretically efficient algorithms for each fixed number of denominations, but his approach is so

wildly impractical that “nobody has yet dared to implement it,” Beck notes.

Nevertheless, researchers are chipping away at the problem. In a special session devoted to the Frobenius problem at the San Diego math meetings, Stan Wagon of Macalester College in St. Paul, Minnesota, reported that he and three colleagues had created an algorithm that works remarkably fast: It solves typical four-stamp problems with 100-digit numbers in under a second and solves up to 11 stamps with 10-digit numbers in under 2 days. Bjarke Rounne of the University of Aarhus in Denmark has

pushed the envelope even further. Based on techniques from a branch of mathematics called computational algebraic geometry, Rounne’s algorithm knocks off in seconds the four-stamp problem with numbers up to 10,000

digits long and extends what’s feasible with 10-digit numbers to 13 stamps.

Neither algorithm comes close to cracking Frobenius: A practical solution would be able to handle hundreds of 100-digit numbers without batting an eye. Still, other researchers are impressed. “Stan’s algorithm was already a big leap,” Beck says. “Bjarke has taken this to the next level. ... I wouldn’t be surprised if he comes up with something even better.”

—BARRY CIPRA





LETTERS

edited by Jennifer Sills

Climate Change: A Titanic Challenge



R. KERR'S NEWS FOCUS STORY "HOW URGENT IS CLIMATE change?" (23 November 2007, p. 1230) is an excellent summary of the challenges facing action on climate change, and the reasons why we are unfortunately already committed to substantial warming. However, the multidecadal time lags in the climate system, infrastructure, and political sphere do not by themselves compel action now rather than, say, 5 years from now. Greater urgency comes from the rapid growth rate (especially in the developing world) of the very infrastructure that is so problematic. Mitigating climate change is often compared to turning the Titanic away from an iceberg. But this "Titanic" is getting bigger and less maneuverable as we wait—and that causes prospects to deteriorate nonlinearly, and on a time scale potentially much shorter than the time scale on which the system itself responds.

STEVEN C. SHERWOOD

Department of Geology and Geophysics, Yale University, New Haven, CT 06520, USA.

The Untapped Potential of Bed Nets

AFTER READING THE NEWS FOCUS STORY "Battling over bed nets" by L. Roberts (26 October 2007, p. 556), we wish to emphasize that the higher the percentage of coverage of a population with insecticide-treated nets, the more mosquitoes will be killed and the greater the reduction in the infective mosquito population (1). Coverage targeted only at children and pregnant women achieves good, but not perfect, personal protection for those categories (2), but it has little impact on the vector population. This was the main basis of the plea by Jeffrey Sachs and collaborators (3) for community-wide, not just targeted, distribution.

As Dr. Lengeler admits in the story, one can legitimately criticize the Tanzanian social marketing and vouchers scheme for only achieving 35% coverage of all Tanzanian children. In fact, coverage was considerably worse in rural areas, where the main burden of malaria exists (4). In the past, when funding for malaria control was very limited, it was reasonable to

accept the need for partial cost-recovery of the price of nets, even from very poor rural people. Fortunately, this is no longer the case; the cost of a sustained program of long-lasting insecticidal net (LLIN) distribution, including replacement for worn-out nets, throughout lowland rural tropical Africa would be easily affordable by rich countries for far less than their citizens spend on cat flea control (5)! Regarding concerns about sustainability, distribution of LLINs is comparable to vaccination programs, and these are sustained remarkably well in Tanzania and many other African countries. Roberts describes Jeffrey Sachs as an impatient man, and he is right to be impatient with a system that leaves thousands of children to die when the world has the technology and resources to massively reduce this toll.

ANDREW Y. KITUA,^{1*} LEONARD MBOERA,¹
STEPHEN M. MAGESA,¹ CAROLINE A. MAXWELL,²
CHRISTOPHER F. CURTIS²

¹National Institute for Medical Research, Dar es Salaam, Tanzania. ²London School of Hygiene and Tropical Medicine, London WC1E 7HT, UK.

*To whom correspondence should be addressed. E-mail: akitua@hotmail.com

References

1. S. M. Magesa *et al.*, *Acta Trop.* **49**, 97 (1991).
2. S. Soremekun *et al.*, *Trop. Med. Int. Health* **9**, 664 (2004).
3. A. Teklehaimanot, J. D. Sachs, C. F. Curtis, *Lancet* **369**, 2143 (2007).
4. S. Hay, C. A. Guerra, A. J. Tatem, P. M. Atkinson, R. W. Snow, *Nat. Rev. Microbiol.* **3**, 81 (2003).
5. M. K. Rust, *Trends Parasit.* **21**, 232 (2005).

A Nobel Lesson: The Grant Behind the Prize

IN THE NEWS OF THE WEEK STORY "A KNOCK-out award in medicine" (12 October 2007, p. 178), which describes the groundbreaking work leading to this year's Nobel Prize in physiology or medicine, G. Vogel writes, "Indeed, in the early 1980s, [Mario] Capecchi's grant application was rejected by the National Institutes of Health in Bethesda, Maryland, with the advice that he should forget the idea." While this has been widely reported, it is factually incorrect. Members of the study section that reviewed the competing renewal application that included the first description of Capecchi's proposed experiments on homologous recombination (among other projects) did express skepticism about the likelihood of success of these experiments. However, the application was funded by NIH's National Institute of General Medical Sciences with an initial budget that was 19% higher than the previous year and with a duration of 5 years, indicating strong support from the Institute. The flexibility of the NIH grant system allowed Capecchi to use some of the funds to support the research that led to his Nobel Prize-winning discoveries.

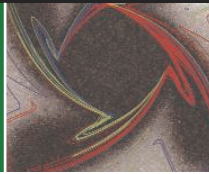
JEREMY M. BERG

Director, National Institute of General Medical Sciences, National Institutes of Health, Bethesda, MD 20892-6200, USA. E-mail: bergj@mail.nih.gov

Response

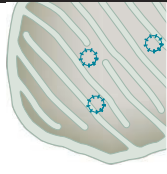
I BELIEVE THE STATEMENT BY BERG IS MIS-leading. The grant application of 1980 contained three projects. The members of the study section liked the first two projects, which were unrelated to gene targeting, but they were unequivocally negative in their response to the third project, in which I proposed to develop gene targeting in mammalian cells. Not only

CREDIT: JUPITER IMAGES



Countering segregation

912



Mutation filter

914

did they suggest that the gene targeting project was not worthy of pursuit, but they lowered my grant score from a 1.00 (the score given to my previous grant application) to a 1.39. I consider this a poor score, not an outstanding score as indicated by Berg. The message of the study section was clear: Work on the first two projects and drop the third.

Despite this clear message, I chose to put almost all of my effort into the third project. It was a big gamble. Had I failed to obtain strong supporting data within the designated time frame (4 years), our NIH funding would have come to an abrupt end and we would not be talking about gene targeting today. Fortunately, within 4 years we obtained strong supporting evidence for the feasibility of gene targeting in mammalian cells, and in 1984 I submitted our renewal grant to extend our gene targeting program to mammalian cells and also to mouse embryonic stem cells and the generation of mice with targeted mutations. Dispelling any doubt that I misinterpreted the original 1980 pink sheet, the pink sheet for the 1984 renewal grant started, "We are glad that you didn't follow our advice."

I have been very careful not to state that the study section disapproved the grant, but rather that they disapproved the gene targeting project. My point in retelling this story has not been to question NIH's funding. Rather, it has been to provide a well-documented case of the delicate balance that study sections must negotiate between their responsibility to prudently allocate their funds and their responsibility to encourage innovative (i.e., "risky") projects with potentially very high rewards.

MARIO R. CAPECCHI

Howard Hughes Medical Institute, University of Utah School of Medicine, Salt Lake City, UT 84112-5331, USA. E-mail: mario.capecchi@genetics.utah.edu

Making Sense of Scrambled Genomes

IN HER INTERESTING PERSPECTIVE, APTLY called "Why genomes in pieces?" (19 October 2007, p. 405), L. F. Landweber discusses possible explanations for the existence and maintenance of evolutionary puzzling modes of gene expression, as exemplified by the fully

scrambled mitochondrial (mt) genome of *Diplonema papillatum* (1) and a set of nuclear transfer RNAs in the red alga *Cyanidioschyzon merolae* that are split in half (2). I wondered why Landweber did not discuss the recent model (3, 4) that explains the spread of another example of gene splitting: pan-editing of kinetoplastid mt messengers. Diplonemids, the kinetoplastid's sister group, have extensively scrambled mt genes and "guideRNA-like" molecules that are postulated to help in selection of the correct ligation partners. Freshwater eukaryotes such as diplomemids and kinetoplastids do not necessarily have to be parasitic to be confronted with changes in the environment that release large parts of the mt genome from all selective pressure (5). This implies that a population could lose these parts as a result of strong intraspecific competition. Gene scrambling would minimize the danger of irreversible loss of those mt genes

not under selective pressure (3, 4). This model explains the phylogenetic distribution and rapid spread of extensive editing early on in the kinetoplastid lineage (6). The same model can be applied to gene scrambling in diplomemids, as it is not essential that the gene segments are physically linked in one molecule. Gene scrambling solutions to ecological challenges are neither neat nor elegant, but nevertheless seem to be favored by selection processes.

DAVE SPEIJER

Medical Biochemistry, Academic Medical Center, University of Amsterdam, Meibergdreef 15, 1105 AZ Amsterdam, Netherlands. E-mail: D.Speijer@amc.uva.nl

References

1. W. Marande, G. Burger, *Science* **318**, 415 (2007).
2. A. Soma *et al.*, *Science* **318**, 450 (2007).
3. D. Speijer, *IUBMB Life* **58**, 91 (2006).
4. D. Speijer, in *RNA Editing*, U. Goring, Ed. (Springer Verlag, Berlin, 2007), pp. 199-227.
5. T. Cavalier-Smith, *Trends Genet.* **13**, 6 (1997).
6. L. F. Landweber, W. Gilbert, *Proc. Natl. Acad. Sci. U.S.A.* **91**, 918 (1994).

Response

SPEIJER OFFERS, TO MY KNOWLEDGE, THE FIRST plausible explanation for why possession of a chaotically organized genome, a hallmark of some microbial eukaryotes, may actually confer increased evolutionary fitness. He proposes a model in the context of extensive RNA

CORRECTIONS AND CLARIFICATIONS

Brevia: "Arabidopsis CLV3 peptide directly binds CLV1 ectodomain," by M. Ogawa *et al.* (18 January, p. 294). In the last sentence of the penultimate paragraph, the peptide/protein names are incorrectly identified. The correct sentence is "The relative binding affinities of the CLV3 and CLE peptides for the ectodomain of CLV1 and related receptors may, together with the location and timing of expression of these components, form the basis for the physiological importance of these signals in the SAM and other tissues."

Brevia: "The 160-kilobase genome of the bacterial endosymbiont *Carsonella*," by A. Nakabachi *et al.* (13 October 2006, p. 267). The scale in the Fig. 1 inset should have been 25 μm instead of 50 μm .

TECHNICAL COMMENT ABSTRACTS

COMMENT ON "The Latitudinal Gradient in Recent Speciation and Extinction Rates of Birds and Mammals"

Joseph A. Tobias, John M. Bates, Shannon J. Hackett, Nathalie Seddon

Weir and Schluter (Reports, 16 March 2007, p. 1574) used variation in the age distribution of sister species to estimate that recent rates of speciation decline toward the tropics. However, this conclusion may be undermined by taxonomic biases, sampling artifacts, and the sister-species method, all of which tend to underestimate diversification rates at low latitudes.

Full text at www.sciencemag.org/cgi/content/full/319/5865/901c

RESPONSE TO COMMENT ON "The Latitudinal Gradient in Recent Speciation and Extinction Rates of Birds and Mammals"

Jason T. Weir and Dolph Schluter

Tobias *et al.* suggest that taxonomic uncertainty, an underestimated correction for the lag-time to speciation, and the sister-species method undermine our estimates of speciation rates at tropical latitudes. However, our estimates incorporated a correction for taxonomic uncertainty and are robust to small increases in the lag-time correction. Contrary to the claim of Tobias *et al.*, we find no indication that the sister-species method underestimates tropical diversification rates.

Full text at www.sciencemag.org/cgi/content/full/319/5865/901d

editing in kinetoplastid protozoa (1, 2) and the scrambled mitochondrial (mt) genomes of their sister diplomids, but the reasoning may extend more broadly to other highly deconstructed genomes, even the most elaborately scrambled cases in ciliated protozoa (3).

The new model requires no evolutionary novelty, as originally proposed (4, 5)—though the benefits from alternative splicing or accelerated evolution probably influenced the evolution of some discontinuous systems. Instead, a spread-out life-insurance plan—one that squirrels away essential gene pieces all over the genome—may be all it takes to bring even a highly scattered genetic architecture to

evolutionary fixation. With each gene segment present on its own DNA circle, *Diplonema* mtDNA (6) is maximally scrambled. This challenges Speijer's model, which depends on linkage of myriad tiny pieces to protect each other (7). Guide RNA genes, essential for RNA editing, can also be on individual DNA minicircles. However, kinetoplastid mtDNA is interlocked (8), and so the circles may still be physically linked.

The large, scrambled genomes of ciliates such as *Oxytricha* (*Sterkiella*) offer an extreme test-bed for the proposed protective effect of genome scrambling. *Oxytricha trifallax* has two nuclei, with a ~1-Gb germline genome giving rise to a 50-Mb somatic genome after destroying 95% and descrambling the 5% remaining (3). How such an uncanny system could arise and be so successful across the globe fits Speijer's model rather well: *Oxytricha*'s germline genome is usually unexpressed, and genes in the somatic genome are physically unlinked and prone to loss after generations of asexual growth. The only way to regenerate the somatic genome is to recoup all the pieces from the germ line. An observed evolutionary trend supports increased levels of fragmentation and

scrambling over time, with accompanying dispersal across unlinked loci (9).

There is accidental elegance in this argument to explain an evolutionary advantage of unsculpted genomes. Before embracing its panselctionism, however, an important caveat is that some protists may accumulate slightly deleterious mutations during extended periods of asexual growth, and this would influence their inner organization (or lack thereof).

LAURA F. LANDWEBER

Department of Ecology and Evolutionary Biology, Princeton University, Princeton, NJ 08544, USA.

References and Notes

1. D. Speijer, *IUBMB Life* **58**, 91 (2006).
2. D. Speijer, in *RNA Editing*, U. Goring, Ed. (Springer Verlag, Berlin, 2007), pp. 199–227.
3. M. Nowacki *et al.*, *Nature* **451**, 153 (2008).
4. L. F. Landweber, W. Gilbert, *Nature* **363**, 179 (1993).
5. L. F. Landweber, *Science* **318**, 405 (2007).
6. W. Marande, G. Burger, *Science* **318**, 415 (2007).
7. Dispersed tRNA genes may usually protect against mtDNA loss (1, 2), but kinetoplasts bear no mt tRNAs, instead editing nuclear-imported ones (10) to accommodate the mt genetic code.
8. L. Simpson, J. Berliner, *J Protozool.* **21**, 382 (1974).
9. W.-J. Chang, P. D. Bryson, H. Liang, M. K. Shin, L. F. Landweber, *Proc. Natl. Acad. Sci. U.S.A.* **102**, 15149 (2005).
10. J. D. Alfonzo, V. Blanc, A. M. Estévez, M. A. Rubio, L. Simpson, *EMBO J.* **18**, 7056 (1999).

Letters to the Editor

Letters (~300 words) discuss material published in *Science* in the previous 3 months or issues of general interest. They can be submitted through the Web (www.submit2science.org) or by regular mail (1200 New York Ave., NW, Washington, DC 20005, USA). Letters are not acknowledged upon receipt, nor are authors generally consulted before publication. Whether published in full or in part, letters are subject to editing for clarity and space.



From physics to nutrition

For careers in science, turn to *Science*
www.ScienceCareers.org

- Search Jobs
- Career Advice
- Job Alerts
- Resume/CV Database
- Career Forum
- Graduate Programs

All features **FREE** to job seekers.

Science Careers
From the journal *Science* AAAS



From physics to nutrition

For careers in science, turn to *Science*
www.ScienceCareers.org

- Search Jobs
- Career Advice
- Job Alerts
- Resume/CV Database
- Career Forum
- Graduate Programs

All features **FREE** to job seekers.

Science Careers
From the journal *Science* AAAS

SOCIOLOGY

It's Constraints, Not Choices

Phyllis Moen

When I directed the Sociology Program at the National Science Foundation in the late 1980s, the (then) director, Erich Bloch, requested a report from me about women in science. Bloch, an engineer, was interested in gaining an understanding of the gender gap. Why were there so few women in the top echelons of the sciences? In engineering? What were the trends and prospects for the future? Why weren't women scientists and engineers receiving more grants from the NSF?

I did a quick review of the literature, called experts in the field and at NSF, and prepared a brief report. The gist of my conclusions included the requisite discussion of "leaky pipelines," starting wide and narrowing with each turn. Evidence shows a steady decline in girls and women at every stage: a shift away from science-related interests in grade school; avoidance of preparatory high school courses; rejection or abandonment of college majors, graduate programs, and postdoctoral fellowships in science and engineering; not obtaining or remaining in tenure-track professorships. The explanations offered by the experts made sense: a hostile, or at best unfriendly, cultural climate; little encouragement; too few role models; relations based on gender stereotypes as well as overt and subtle discrimination; and, a thread interwoven throughout, choices made in the face of (current or anticipated future) work and family strains and conflicts.

Pamela Stone, a professor of sociology at the City University of New York, addresses this topic on a wider canvas, looking not just at women scientists and engineers but also at professional women in a variety of fields who have left their jobs. We have all read or heard media reports on the "opt out" revolution. Stone seeks to promote understanding of it by going deep rather than wide, choosing in-depth interviewing over survey methods to better capture the layers of complexity and contradictions behind simple



explanations. Her sample consists of 54 high achievers, a range of lawyers, physicians, professors, and engineers from across the United States who are married, mothers, and have left

their career jobs. They are women who already traveled far through their respective occupational pipelines: women who "made it" in their professions and who had strong prospects for rising still further up status ladders. Why did they choose to leave their jobs? The book's title, *Opting Out? Why Women Really Quit Careers and Head Home*, presages Stone's

doubts about this so-called trend in women returning en masse to hearth and home.

Social scientists have documented the work and family pressures women experience, as well as the costs to women's careers of scaling back or leaving the workforce. But until now no one has systematically investigated the actual dropouts. Thus all the analyses of the stress experienced by employed women (including my own) tend to underestimate the presence, depth, and consequences of such chronic strains.

Stone's decision to study professionals makes sense. This is the group best equipped to manage conflicts and strains at work and at

home by, for example, hiring an au pair or housekeeper. When married to other successful professionals, they are often able to afford to exit the workforce. And they are the segment of the female population most apt to spearhead change in the broader society, one reason for ongoing media fascination with the opting-out phenomenon.

Stone shows that these highly educated women are also knowledgeable about the latest evidence on child development. They believe they can best facilitate their children's optimal development, but not when they themselves are in a constant time bind. She chronicles as well their professional abilities and dedication to their jobs. One of them, a publicist, talks about 100% women: "I give 100 percent. I was very, very good at what I did. But I can't give it both places, and I wanted to be really, really good at being a mother."

Often there is a precipitating event that brings on such insights: another pregnancy, a husband's career shift that requires relocation,

a sick child, an automobile accident, a new (nonsupportive) boss, an increased need to travel on the job. For other women, exits are preceded by the slow, steady toll of too much to do, too little sleep, and too often careening from one deadline, meeting, or pediatrician appointment to the next. Their stories do not reflect a shift in values; opting out is not about their desire to return to the Ozzie and Harriet family of the 1950s. Stone lets the women speak for themselves, providing a deft analysis of the impossibilities they face.

It is often remarked that economists explain how people make choices, whereas sociologists explain why people have few choices to make. Ever the sociologist, Stone talks about the "illusion of choice" that is perpetuated in the very phrase "opting out," as well as by the women themselves, who tend to view their dilemma as reflecting private troubles, not public issues. By contrast, Stone faults the taken-for-granted work policies that are based on a career mystique of continuous, full-time (or more) work as the only path to security and success. Given the way jobs and career paths are structured, it is difficult if not impossible for women (or men) to manage effectively as professionals, as part of a dual-earning couple, and as parents without burning out. Stone concludes that the women she studied did not opt out, but were

Opting Out?

Why Women Really Quit Careers and Head Home

by Pamela Stone

University of California Press, Berkeley, 2007.
313 pp. \$24.95, £14.95.
ISBN 9780520244351.

The reviewer, coauthor with Patricia Roehling of *The Career Mystique: Cracks in the American Dream*, is at the Department of Sociology, University of Minnesota, 909 Social Sciences Building, 267 19th Avenue South, Minneapolis, MN 55455, USA. E-mail: phylmoen@umn.edu

CREDIT: JOE SUTLIFF

effectively pushed out—given the absence of options permitting jobs that can be configured and reconfigured (in terms of assignments, expectations, and hours) in ways compatible with raising a family.

Back to the future: What we found in terms of the gender gap in NSF grant awards in the late 1980s was, in fact, an application gap. NSF funded women scientists' research in the same proportion as men's, of those who applied for research funding. The crux was that far fewer women than men submitted proposals.

Since then, I have continued talking with women at professional meetings. Many have in fact submitted a proposal for NSF or other federal research support, often early in their careers. But when it was not funded, many of them gave up. Most scholars who do receive grants have also had unsuccessful proposals. But they applied again (and again) with honed, even more scientifically sound and more compelling proposals, until they were successful. Did the women who gave up do so by "choice" because structural forces provide neither the encouragement nor the resources required to do the hard work of reworking, revising, and persevering in submitting applications? Proposal writing may have been buried in the myriad of tasks for professors trying to manage and integrate their own careers with their obligations as mentors, models, spouses, parents, and children of aging parents.

Nearly 20 years later, little has changed in professional career expectations and trajectories. For example, people can opt out of demanding jobs, but they cannot opt back in. Nor can most scale back on job demands or work fewer hours, unless they are close to retirement (and even then not always). Reading Stone's book, I recalled a senior government official who in the mid-1980s said to me, "Women simply have to choose. Do they want careers or families?" It is not by accident that women who have achieved prominence in their field are disproportionately never married or divorced (or else married to a man who has dialed down his own career). They are also more likely to be childfree, have only one child, or have started their families later in life.

Women are not the only ones wanting career flexibility. Aging baby-boomers are looking for ways to keep working, drop out for a brief time, or shift their focus. Most older employees don't want to continue putting in the long hours so often required in their professions. Yet they, like Stone's sample of mothers, often have only two options: continue as is or leave the workforce.

Science and engineering, the professions,

businesses, and governments all thrive on innovation. They are improved when people are willing to take a different perspective, challenge conventional wisdom, and respond to what no longer works by trying something new. Stone's account in *Opting Out?* highlights the need for employees to be able to customize their career paths. Which universities, centers, corporations, and agencies will develop increased work-time flexibilities and creative possibilities that offer employees meaningful engagement at every stage of their lives? Meeting that challenge will benefit families, businesses, and societies alike.

10.1126/science.1153865

BEHAVIORAL SCIENCE

The In-Group Rules

Ben W. Heineman Jr.

In *Bending the Rules*, Robert Hinde addresses the controversial and timely subject of how the behavioral sciences apply to the study of morality. In contrast to moral philosophers who focus "on how people ought to behave," he concentrates on "how they *think* they should behave and how they *actually* behave."

For Hinde, an emeritus research professor at Cambridge University with expertise in ethology, primatology, and developmental psychology, moral codes are "essentially social matters; precepts are meaningless unless accepted by the group to which one belongs." The propensity of people to divide their world into "in-groups and out-groups," he argues, leads to "moral" behavior within the group but a bending of that code (hence the title) when dealing with the "other." Morality is a product of biological and cultural evolution: the interplay—in specific settings, societies, and historical moments—between

The reviewer is at the Beifer Center for Science and International Affairs, John F. Kennedy School of Government, Harvard University, 79 JFK Street, Cambridge, MA 02138, USA. E-mail: ben.heineman@ge.com

the two opposing human potentials of selfish assertiveness (to win inevitable human competition) and "prosociality" (to facilitate group cohesion, in part to win competition against other groups).

As a behavioral scientist, Hinde concludes that what is seen as right may differ with the situation. Thus, there is no single moral answer, and "there are no general objective tests for morality except that most actions, to be moral, must be conducive to group harmony." As chair of the British Pugwash Group (which is dedicated to the social responsibility of scientists), Hinde does not, however, wish to be a "relativist," without his own moral perspective. And neither would have Sir Joseph Rotblat, a Pugwash founder and 1995 Nobel Peace Prize winner (who was to be a coauthor but died in 2005).

Beyond answering descriptive questions about how individuals acquire a moral outlook, Hinde attempts in three ways to introduce his normative views. First, he submits that using scientific methods (from biology, ethology, psychology, sociology, and anthropology) can help us understand the "other" in different groups and cultures and that under-



Wartime goodwill. Frederice Villiers's imaginative depiction of the spontaneous beginning of the 1914 Christmas Truce, when German and English troops on the Western Front observed an unofficial temporary cessation of hostilities.

CREDIT: ILLUSTRATED LONDON NEWS, 9 JANUARY 1915

A TASTE OF THE GONZO SCIENTIST

How would you interpret your Ph.D. thesis in dance form? This was the challenge posed during the 2008 *Science* "Dance Your Ph.D." contest that took place 18 January in Vienna, Austria. The 12 dances—based on theses ranging from particle physics to prehistoric archaeology—were divided into three categories depending on the professional status of the principal

dancer: graduate students, postdocs, and professors. Before the contest began, each dancer was given 60 seconds to summarize his or her research to a panel of

four judges—an astronomer, an anthropologist, a science communicator, and a professional dancer—who then scored the dances on an 80-point scale of artistic, scientific, and physical creativity. Winners received a year's subscription to *Science*.

The three winning dances prove that there are many ways to communicate a doctoral dissertation with your body. In the student category, Brian Stewart (University of Cambridge) depicted his thesis on prehistoric archaeology (1) as a highly stylized hunt of an antelope (above) played by fellow Oxford University grad student Giulia Saltini-Semerari. Like a Shirley Temple of the molecular biology era, the winning postdoc, Nicole-Claudia Meisner (Novartis Institutes for Biomedical Research, Vienna) interpreted her Ph.D. (2) on mRNA regulation with a tap dance.

See www.gonzoscientist.org

The showstopper was Giulio Superti-Furga, the scientific director of the Center for Molecular Medicine in Vienna. Accompanied by his Ph.D. students Adriana Goncalves and Evren Karayel, he won the professor category by turning his dissertation on human developmental genetics (3) into an epic pop-ballet medley that brought the house down. We congratulate the winners.



—JOHN BOHANNON

References

1. B. Stewart, *Refitting Repasts: A Spatial Exploration of Food Processing, Cooking, Sharing and Disposal at the Duneveld Midden Campsite, South Africa*, thesis, Univ. of Oxford, 2008.
2. N.-C. Meisner, *mRNA Stability Regulation as a Drug Target: mRNA Stability Cross-Screening and Molecular Mechanisms in Post-Transcriptional Regulation Resolved by Quantitative Biology*, thesis, Univ. of Salzburg, 2005.
3. G. Superti-Furga, *Transcription Factors Involved in Development and Growth Control: Regulation of Human G-Globin and Fos Gene Expression*, thesis, Univ. of Zurich, 1991.

10.1126/science.1155902

standing can dampen conflict. This is an important and powerful point. (Imagine if U.S. policy-makers had had much deeper and nuanced views of Vietnam and Iraq before extensive military intervention.) But Hinde offers no detailed studies of how long-standing conflicts—for example, in Northern Ireland, in the Middle East, or on the Korean Peninsula—have been, or can be, ameliorated with improved understanding of the other's culture and values. The failure to explore the point with any historical and institutional concreteness robs it of power.

Second, the author argues that there are certain moral principles found in all cultures. These pancultural principles contrast with precepts—rules and values for guiding behavior that are found in different cultures. Hinde does not develop a set of universal principles but instead primarily asserts the evolutionary existence of one: the "Golden Rule of Do-as-you-would-be-done-by." This principle, he holds, is a constant in intragroup relations over time and around the globe and can form the basis for more harmonious intergroup relations. Whether such a pancultural principle exists and has consistent meaning is for experts to debate. Yet even to accept the principle as universal is to take but one step in a journey of a thousand miles to practical implications in a conflict-ridden world. Hinde recognizes that the group basis of

morality causes the golden rule to be ignored when dealing with out groups. And, indeed, the foundation of the Pugwash Group was due, in part, to the horrific 20th-century death toll from intergroup and international conflicts involving ethnic, religious, ideological, or national differences.

Third, in a series of chapters Hinde offers a set of personal, but quite general, ethical perspectives on law, personal relationships, physical sciences, medicine, politics, business, and war. He sketches the value tensions in these fields: e.g., between genetic engineering for therapeutic purposes or for self-improvement; a politician's conflicting responsibilities to constituents, party, and conscience; between a business's decision to focus solely on profit or to also consider its impact on society; between a

society's own moral code and the violation of that code in war. These descriptions (which make up much of the book) touch important moral problems from the perspective of an informed and humane citizen. But they are hardly the detailed, nuanced studies of social relationships and social structures that Hinde advocates as a behavioral scientist and that are needed to plan effective change.

The author's own ethical views on the issues are also quite summary. It is important, for example, to establish and abide by rules of law in international relations, to ameliorate the deleterious impact of pure market forces by practicing corporate social responsibility, to abolish the arms trade, and to eliminate weapons of mass destruction. But Hinde's general prescriptions do not reflect the complex, detailed, and fact-based ethical and public policy analyses and debates on these subjects in universities and in the public and private sectors around the globe.

Hinde's normative efforts provide a reflective overview of why certain contemporary ethical issues are important, but, in the end, they fail to help us gain deep understanding about how to resolve those issues. Hinde's most fervent moral point—that humanity must recognize common traits, celebrate interconnectedness, and value individuals from all cultures equally (Al Qaeda?)—runs against his fundamental behavioral-science point that morality and the bending of moral codes arise from the enduring dynamic within and between in groups and out groups.

At the end of *Bending the Rules*, Hinde acknowledges that many argue scientific description does not lead to ethical prescription. Because its scientific and moral perspectives are so loosely and summarily connected, the book does not effectively rebut that claim, despite its noble aspirations.

10.1126/science.1153415

Bending the Rules

Morality in the Modern World from Relationships to Politics and War

by Robert A. Hinde, with contributions from Sir Joseph Rotblat

Oxford University Press, Oxford, 2007. 287 pp.

\$29.95, £14.99.

ISBN 9780199218974.

TOXICOLOGY

Transforming Environmental Health Protection

Francis S. Collins,^{1†} George M. Gray,^{2*} John R. Bucher^{3*}

In 2005, the U.S. Environmental Protection Agency (EPA), with support from the U.S. National Toxicology Program (NTP), funded a project at the National Research Council (NRC) to develop a long-range vision for toxicity testing and a strategic plan for implementing that vision. Both agencies wanted future toxicity testing and assessment paradigms to meet evolving regulatory needs. Challenges include the large numbers of substances that need to be tested and how to incorporate recent advances in molecular toxicology, computational sciences, and information technology; to rely increasingly on human as opposed to animal data; and to offer increased efficiency in design and costs (1–5). In response, the NRC Committee on Toxicity Testing and Assessment of Environmental Agents produced two reports that reviewed current toxicity testing, identified key issues, and developed a vision and implementation strategy to create a major shift in the assessment of chemical hazard and risk (6, 7). Although the NRC reports have laid out a solid theoretical rationale, comprehensive and rigorously gathered data (and comparisons with historical animal data) will determine whether the hypothesized improvements will be realized in practice. For this purpose, NTP, EPA, and the National Institutes of Health Chemical Genomics Center (NCGC) (organizations with expertise in experimental toxicology, computational toxicology, and high-throughput technologies, respectively) have established a collaborative research program.

EPA, NCGC, and NTP Joint Activities

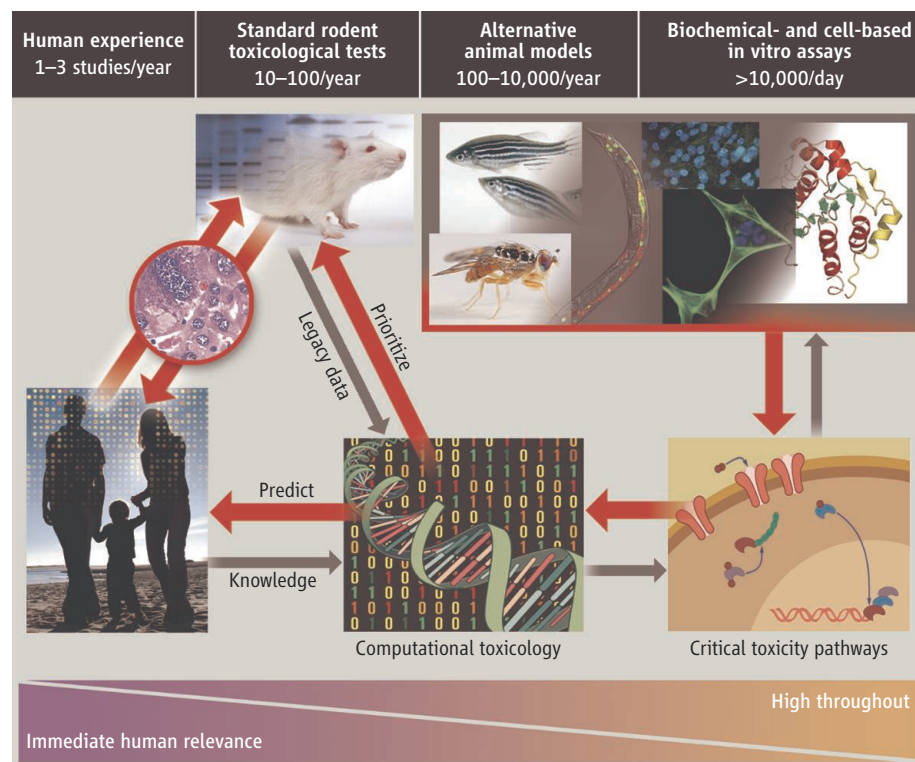
In 2004, the NTP released its vision and roadmap for the 21st century (1), which established initiatives to integrate high-

throughput screening (HTS) and other automated screening assays into its testing program. In 2005, the EPA established the National Center for Computational Toxicology (NCCT). Through these initiatives, NTP and EPA, with the NCGC, are promoting the evolution of toxicology from a predominantly observational science at the level of disease-specific models *in vivo* to a predominantly predictive science focused on broad inclusion of target-specific, mechanism-based, biological observations *in vitro* (1, 4) (see figure, below).

Toxicity pathways. *In vitro* and *in vivo* tools are being used to identify cellular responses after chemical exposure expected to result in adverse health effects (7). HTS methods are a primary means of discovery for drug development, and screening of >100,000 compounds per day is routine (8). However, drug-discovery HTS methods traditionally test compounds at one concentra-

We propose a shift from primarily *in vivo* animal studies to *in vitro* assays, *in vivo* assays with lower organisms, and computational modeling for toxicity assessments.

tion, usually between 2 and 10 μM , and tolerate high false-negative rates. In contrast, in the EPA, NCGC, and NTP combined effort, all compounds are tested at as many as 15 concentrations, generally ranging from ~ 5 nM to ~ 100 μM , to generate a concentration-response curve (9). This approach is highly reproducible, produces significantly lower false-positive and false-negative rates than the traditional HTS methods (9), and facilitates multiassay comparisons. Finally, an informatics platform has been built to compare results among HTS screens; this is being expanded to allow comparisons with historical toxicologic NTP and EPA data (<http://ncgc.nih.gov/pub/openhts>). HTS data collected by EPA and NTP, as well as by the NCGC and other Molecular Libraries Initiative centers (<http://mli.nih.gov/>), are being made publicly available through Web-based databases [e.g., PubChem (<http://pubchem.ncbi.nlm.nih.gov/>)]. In addition,



Transforming toxicology. The studies we propose will test whether high-throughput and computational toxicology approaches can yield data predictive of results from animal toxicity studies, will allow prioritization of chemicals for further testing, and can assist in prediction of risk to humans.

¹Director, National Human Genome Research Institute (NHGRI), National Institutes of Health, Bethesda, MD 20892; ²Assistant Administrator for the Office of Research and Development, U.S. Environmental Protection Agency, Washington, DC 20460; ³Associate Director, U.S. National Toxicology Program, National Institute of Environmental Health Sciences (NIEHS), Research Triangle Park, NC 27709, USA.

*The views expressed here are those of the individual authors and do not necessarily reflect the views and policies of their respective agencies.

†Author for correspondence. E-mail: francisc@mail.nih.gov

efforts are under way to link HTS data to historical toxicological test results, including creating relational databases with controlled ontologies, annotation of the chemical entity, and public availability of information at the chemical and biological level needed to interpret the HTS data. EPA's DSSTox (Distributed Structure Searchable Toxicity) effort is one example of a quality-controlled, structure-searchable database of chemicals that is linked to physicochemical and toxicological data (www.epa.gov/ncct/dsstox/).

At present, more than 2800 NTP and EPA compounds are under study at the NCGC in over 50 biochemical- and cell-based assays. Results from the first study, in which 1408 NTP compounds were tested for their ability to induce cytotoxicity in 13 rodent and human cell types, have been published (10). Some compounds were cytotoxic across all cell types and species, whereas others were more selective. This work demonstrates that titration-based HTS can produce high-quality in vitro toxicity data on thousands of compounds simultaneously and illustrates the complexities of selecting the most appropriate cell types and assay end points. Additional compounds, end points, and assay variables will need to be evaluated to generate a data set sufficiently robust for predicting a given in vivo toxic response.

In 2007, the EPA launched ToxCast (www.epa.gov/ncct/toxcast) to evaluate HTS assays as tools for prioritizing compounds for traditional toxicity testing (5). In its first phase, ToxCast is profiling over 300 well-characterized toxicants (primarily pesticides) across more than 400 end points. These end points include biochemical assays of protein function, cell-based transcriptional reporter assays, multicell interaction assays, transcriptomics on primary cell cultures, and developmental assays in zebrafish embryos. Almost all of the compounds being examined in phase 1 of ToxCast have been tested in traditional toxicology tests. ToxRefDB, a relational database being created to house this information, will contain the results of nearly \$1 billion worth of toxicity studies in animals.

Another approach to identifying toxicity pathways is exploring the genetic diversity of animal and human responses to known toxicants. The NCGC is evaluating the differential sensitivity of human cell lines obtained from the International HapMap Project (<http://www.hapmap.org/>) to the 2800 compounds provided by NTP and EPA. Similarly, NTP has established a Host Susceptibility Program to investigate the genetic basis for differences in disease response using various mouse strains

(<http://ntp.niehs.nih.gov/go/32132>); cell lines derived from these animals will be evaluated at the NCGC for differential sensitivity to the compounds tested in the HapMap cell lines. The resulting collective data sets will be used to develop bioactivity profiles that are predictive of the phenotypes observed in standard toxicological assays and to identify biological pathways which, when perturbed, lead to toxicities. The ultimate goal is to establish in vitro "signatures" of in vivo rodent and human toxicity. To assist, computational methods are being developed that can simulate in silico the biology of a given organ system.

The liver is the most frequent target of more than 500 orally consumed environmental chemicals, based on an analysis of the distribution of critical effects in rodents by organ, in the EPA Integrated Risk Information System (IRIS) (www.epa.gov/iris). The goal of the recently initiated Virtual Liver project (www.epa.gov/ncct/virtual_liver.html) is to develop models for predicting liver injury due to chronic chemical exposure by simulating the dynamics of perturbed molecular pathways, their linkage with adaptive or adverse processes leading to alterations of cell state, and integration of the responses into a physiological tissue model. When completed, the Virtual Liver Web portal and accompanying query tools will provide a framework for incorporation of mechanistic information on hepatic toxicity pathways and for characterizing interactions spatially and across the various cells types that comprise liver tissue.

Targeted testing. The NRC committee report (7) proposes in vitro testing as the principal approach with the support of in vivo assays to fill knowledge gaps, including tests conducted in nonmammalian species or genetically engineered animal models. A goal would be to use genetically engineered in vitro cell systems, microchip-based genomic technologies, and computer-based predictive toxicology models to address uncertainties.

Dose-response and extrapolation models. Dose-response data and extrapolation models encompass both pharmacokinetics (the relation between exposure and internal dose to tissues and organs) and pharmacodynamics (the relation between internal dose and toxic effect). This knowledge can aid in predicting the consequences of exposure at other dose levels and life stages, in other species, or in susceptible individuals. Physiologically based pharmacokinetic (PBPK) models provide a quantitative simulation of the biological processes of absorption, distribution, metabolism, and elimination of a substance in animals or humans. PBPK models are being

created to evaluate exposure-response relation for critical target organ effects (11). These can be combined with models that measure changes in cells in target tissues under different test substance concentrations. This will help to determine the likelihood of adverse effects from "low-dose" exposure, as well as to assess variation among individuals in specific susceptible groups.

Making It Happen

Elements of this ongoing collaboration and coordination include sharing of databases and analytical tools, cataloging critical toxicity pathways for key target organ toxicities, sponsoring workshops to broaden scientific input into the strategy and directions, outreach to the international community, scientific training of end users of the new technologies, and support for activities related to the requirements for national and international regulatory acceptance of the new approaches. It is a research program that, if successful, will eventually lead to new approaches for safety assessment and a marked refinement and reduction of animal use in toxicology. The collective budget for activities across the three agencies that are directly related to this collaboration has not yet been established. Future budgets and the pace of further development will depend on the demonstration of success in our initial efforts. As our research strategy develops, we welcome the participation of other public and private partners.

References and Notes

1. NTP, *A National Toxicology Program for the 21st Century: A Roadmap for the Future* (NTP, NIEHS, Research Triangle Park, NC, 2004); (<http://ntp.niehs.nih.gov/go/vision>).
2. NTP, *Current Directions and Evolving Strategies: Good Science for Good Decisions* (NTP, NIEHS, Research Triangle Park, NC, 2004); (http://ntp.niehs.nih.gov/ntp/Main_Pages/PUBS/2004CurrentDirections.pdf).
3. J. R. Bucher, C. Portier, *Toxicol. Sci.* **82**, 363 (2004).
4. R. Kavlock *et al.*, *Toxicol. Sci.*, published online 7 December 2007, 10:1093/toxsci/kfm297, in press.
5. D. Dix *et al.*, *Toxicol. Sci.* **95**, 5 (2007).
6. NRC, *Toxicity Testing for Assessment of Environmental Agents: Interim Report* (National Academies Press, Washington, DC, 2006).
7. NRC, *Toxicity Testing in the 21st Century: A Vision and a Strategy* (National Academies Press, Washington, DC, 2007).
8. D. A. Pereira, J. A. Williams, *Br. J. Pharmacol.* **152**, 53 (2007).
9. J. Inglese *et al.*, *Proc. Natl. Acad. Sci. U.S.A.* **103**, 11473 (2006).
10. M. Xia *et al.*, *Environ. Health Perspect.*, published online 22 November 2007, 10.1289/ehp.10727, in press.
11. W. A. Chiu *et al.*, *J. Appl. Toxicol.* **27**, 218 (2007).
12. We thank R. Tice (NIEHS), R. Kavlock (EPA), and C. Austin (NCGC and NHGRI), without whose contributions this manuscript would not have been possible. This research was supported in part by the Intramural Research programs of the NHGRI, EPA, and NIEHS.

10.1126/science.1154619

Making Strong Fibers

Han Gi Chae and Satish Kumar

Today's polymeric and carbon fibers are up to 10 times as strong as those available half a century ago (see the figure, left and middle panels). High-performance polymeric fibers find applications in textiles such as firefighter clothing, bulletproof vests, and cables requiring stiffness and strength in tension; high-performance carbon fibers find applications in structural composites, for example, in airplanes, satellites, and tennis rackets. Even stronger fibers can be made using carbon nanotubes. These fibers will be lighter than existing fibers and may increase the performance of airplanes, space vehicles, and many sports and leisure goods.

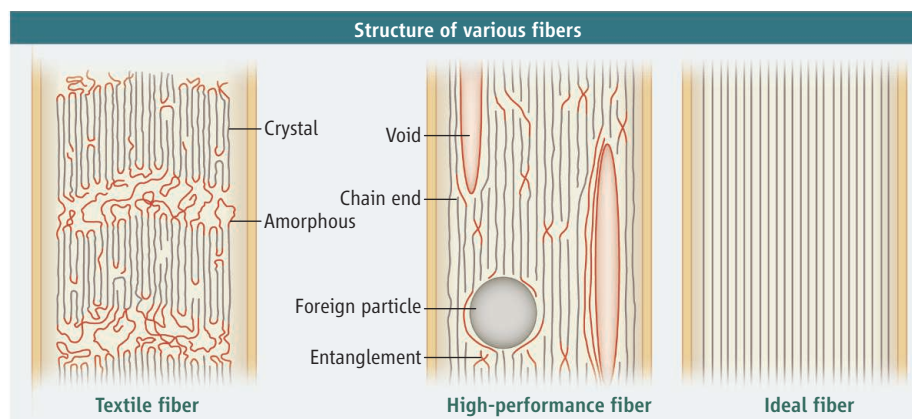
In applications such as advanced textiles and structural composites, high-performance polymeric and carbon fibers have two key advantages over high-strength bulk materials such as steel. First, as a result of their low density, the specific strength (strength divided by density) of polymeric and carbon fibers is 5 to 10 times that of high-strength bulk materials. Second, fibers can be more easily processed into complex shapes (*1*).

One reason that fibers can have higher strength than bulk materials is that they can be processed with small diameters, which minimizes defects. The diameters of current commercial high-performance polymeric fibers range from 10 to 15 μm , and those of carbon fibers range from 5 to 10 μm ; making fibers with even smaller diameters will further increase the strength.

Innovations in polymer synthesis and fiber processing have been critical for making high-performance fibers. The first high-performance fiber, Kevlar was developed in the 1960s at DuPont, a company with a long history in fiber synthesis. In the 1980s, polyethylene, first synthesized in the 1930s, was processed into a high-performance commercial fiber (with the trade names Spectra and Dyneema), based on gel-spinning technology invented at DSM in the Netherlands (*2*). The high-strength polymeric fiber Zylon, based on rigid-rod polymer research that began in the 1970s at the U.S. Air Force Research Laboratory, was commercialized in 1998 by Toyobo in Japan (*3*). High-strength polyacry-

The authors are in the School of Polymer, Textile and Fiber Engineering, Georgia Institute of Technology, Atlanta, GA 30332, USA. E-mail: satish.kumar@ptfe.gatech.edu

Research toward carbon nanotube fibers that are light yet extremely strong is progressing rapidly.



Schematic structures of various fibers. With decreasing disorder and defect density, the fiber strength increases (left to right). **(Left)** Typical commodity textile fiber contains amorphous and crystalline regions as well as voids and foreign particles; tensile strength, ~ 0.5 GPa. **(Middle)** High-performance polymer fibers contain chain ends, entanglements, voids, and defects; tensile strength, ~ 5 GPa. The structure of currently produced carbon nanotube fibers resembles this structure. In addition, carbon nanotube fibers often contain foreign particles in the form of catalysts. **(Right)** On the basis of predicted strain to failure (*15*), ideal carbon nanotube fibers without defects or entanglements will have a specific tensile strength of 70 N/tex; for a single-wall carbon nanotube fiber a diameter of 2 nm, this would translate to a tensile strength of 70 GPa.

lonitrile-based carbon fibers were developed by optimizing parameters such as the polyacrylonitrile-copolymer composition, fiber spinning, and polyacrylonitrile stabilization and carbonization (*4*). Other high-strength fibers include silicon carbide, alumina, glass, and alumina borosilicate fibers (*1*); however, these fibers have relatively high densities.

Kevlar, Zylon, Spectra, Dyneema, and the carbon-fiber precursor polyacrylonitrile are all processed from solutions typically containing 5 to 20 weight percent (wt %) of polymer (*1, 5*). The rest of the mass is the solvent. Solvent removal disrupts the structure and worsens tensile properties. Entanglements, chain ends, voids, and foreign particles act as stress concentration points, lowering strength (see the figure, middle panel). Conversion of polyacrylonitrile to carbon involves heat treatment under tension in air and then in an inert environment (*4*). During this process, $\sim 40\%$ of the mass is lost in the form of gases. Gas diffusion, particularly at high temperature, also disrupts and degrades the structure and lowers strength.

Carbon nanotube fibers can also be processed from liquid media (*6, 7*). Alternatively, they may be pulled from nanotube "forests" (*8*) or drawn as an aerogel fiber from the gas phase in a reactor (*9, 10*). The latter process appears to be particularly prom-

ising. The resulting fiber consists mostly of flattened double-walled nanotubes with diameters of 5 to 10 nm and a length of about 1 mm. The specific strength of this fiber is up to 2.5 times that of the strongest commercial fiber today.

The method used to make this fiber eliminates two problems encountered in the formation of high-strength polymeric and polyacrylonitrile-based carbon fibers: the solvent and gas removal. However, some key challenges need to be ironed out. The catalyst particles must be eliminated from the fiber; drawing conditions must be optimized to eliminate entanglements between carbon nanotubes; and conditions must be tuned so that the growth of a given carbon nanotube is not terminated and that the fiber is pulled at the rate at which nanotubes are growing.

The structure of carbon nanotube fibers is similar to that of high-strength polymeric fibers (see the figure, middle panel). Both types of fibers are strong and stiff along the fiber axis in tension, but relatively weak in axial compression and transverse to the fiber axis (*11*). However, carbon nanotube fibers are electrically and thermally conducting, whereas current high-strength polymeric fibers are insulators of both heat and electricity. Potential applications of carbon nanotube fibers will thus be those requiring high

strength and stiffness in tension, high energy absorption, and electrical and thermal conductivity. The low density of these fibers would provide further weight savings.

Carbon nanotubes can also act as a nucleating agent for polymer crystallization and as a template for polymer orientation (12). No other nucleating agents are as narrow and long as a single-wall carbon nanotube. The tensile strength of a poly(vinyl alcohol) film tripled with the addition of 1 wt % of single-wall carbon nanotubes (13). Similarly, incorporation of 1 wt % of carbon nanotubes in polyacrylonitrile increased the tensile strength and modulus of the resulting carbon fiber by 64% and 49%, respectively (14). Polyacrylonitrile/carbon nanotube composites have good tensile and compressive properties. Next-generation

carbon fibers used for structural composites will thus likely be processed not from polyacrylonitrile alone but from its composites with carbon nanotubes.

If processing conditions can be developed such that all carbon nanotube ends, catalyst particles, voids, and entanglements are eliminated, this would result in a continuous fiber with perfect structure, low density, and tensile strength close to the theoretical value. Such a carbon nanotube fiber could have 10 times the specific strength of the strongest commercial fiber available today. However, many challenges have to be overcome to achieve this goal.

References

1. K. K. Chawla, *Fibrous Materials* (Cambridge Univ. Press, Cambridge, 1998).
2. P. Smith, P. J. Lemstra, *J. Mater. Sci.* **15**, 505 (1980).

3. H. G. Chae, S. Kumar, *J. Appl. Polym. Sci.* **100**, 791 (2006).
4. M. L. Minus, S. Kumar, *JOM* **57**, 52 (2005).
5. V. B. Gupta, V. K. Kothari, Eds., *Manufactured Fibre Technology* (Chapman & Hall, New York, 1997).
6. L. M. Ericson *et al.*, *Science* **305**, 1447 (2004).
7. P. Miaudet *et al.*, *Nano Lett.* **5**, 2212 (2005).
8. M. Zhang, K. R. Atkinson, R. H. Baughman, *Science* **306**, 1358 (2004).
9. K. Koziol *et al.*, *Science* **318**, 1892 (2007); published online 15 November 2007 (10.1126/science.1147635).
10. M. Motta, A. Moiala, I. A. Kinloch, A. H. Windle, *Adv. Mater.* **19**, 3721 (2007).
11. V. V. Kozey, H. Jiang, V. R. Mehta, S. Kumar, *J. Mater. Res.* **10**, 1044 (1995).
12. M. L. Minus, H. G. Chae, S. Kumar, *Polymer* **47**, 3705 (2006).
13. Z. Wang, P. Ciselii, T. Peijs, *Nanotechnology* **18**, 455709 (2007).
14. H. G. Chae, M. L. Minus, A. Rasheed, S. Kumar, *Polymer* **48**, 3781 (2007).
15. T. Dumitrica, M. Hua, B. I. Yakobson, *Proc. Natl. Acad. Sci. U.S.A.* **103**, 6105 (2006).

10.1126/science.1153911

ECONOMICS

Homo economicus Evolves

Steven D. Levitt and John A. List

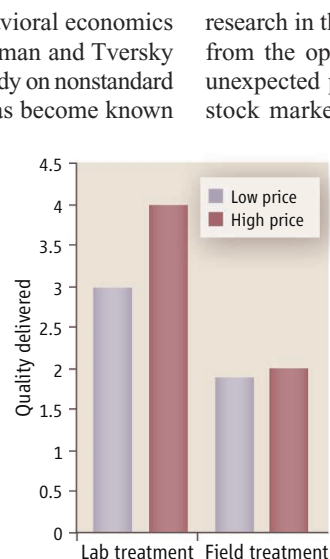
The discipline of economics is built on the shoulders of the mythical species *Homo economicus*. Unlike his uncle, *Homo sapiens*, *H. economicus* is unwaveringly rational, completely selfish, and can effortlessly solve even the most difficult optimization problems. This rational paradigm has served economics well, providing a coherent framework for modeling human behavior. However, a small but vocal movement in economics has sought to dethrone *H. economicus*, replacing him with someone who acts “more human.” This insurgent branch, commonly referred to as behavioral economics, argues that actual human behavior deviates from the rational model in predictable ways. Incorporating these features into economic models, proponents argue, should improve our ability to explain observed behavior.

The roots of behavioral economics date back to Adam Smith, who viewed decisions as a struggle between “passions” and an “impartial spectator”—a “moral hector who, looking over the shoulder of the economic man, scrutinizes every move he makes” (1). Simon’s (2) pioneering analysis of bounded rationality represents an early attempt to incorporate cognitive limitations into economic models, as did later work on bias and altruism (3–5).

The watershed for behavioral economics came in the 1970s. Kahneman and Tversky carried out the landmark study on nonstandard preferences (6), or what has become known as “loss aversion” or the “endowment effect,” i.e., that losses loom larger than gains in decision-making. In a similar spirit, models of social preferences, such as human reciprocity, inequity aversion, and altruism (7–9), and modeling of temporal decision-making (10) have substantially influenced economic research. These theoretical approaches are buttressed by an entire body of empirical evidence drawn from laboratory experiments that lends strong support to their critical modeling assumptions and findings.

Most of this research eschews a narrow conception of rationality, while continuing to embrace precisely stated assumptions that produce a constrained optimization problem. A less “scientific,” and in our view less productive line of

Economic models can benefit from incorporating insights from psychology, but behavior in the lab might be a poor guide to real-world behavior.



Selfish subjects. Quality as a function of price offered for sports trading cards of different quality (13). (Left) Results of offering high (\$65) and low (\$20) prices in a laboratory setting. (Right) Results in a natural environment with the sellers unaware they were participating in an experiment. Dealers in the lab provide much higher quality on average for the same offer, and respond to generous offers in the lab by increasing the quality of the goods. This suggests that dealers behave far more selfishly in natural settings than in the lab.

research in this area approaches the problem from the opposite direction: Observing an unexpected pattern of behavior (e.g., lower stock markets on rainy days in New York City), one looks for a psychological theory consistent with that behavior (in this case, seasonal affective disorder). Given the wide array of psychological explanations from which to choose, however, a researcher undertaking such a task has virtually unlimited freedom to explain any observed behavior *ex post facto*.

Perhaps the greatest challenge facing behavioral economics is demonstrating its applicability in the real world. In nearly every instance, the strongest empirical evidence in favor of behavioral anomalies emerges from the lab. Yet, there are many reasons to suspect that these laboratory findings might fail to generalize to real markets. We have recently discussed (11) several factors, ranging from the properties of the situation—such as the nature and extent of scrutiny—to individual expectations and the type of actor involved. For

The authors are in the Department of Economics, University of Chicago, Chicago, IL 60637, USA. E-mail: jlist@uchicago.edu

example, the competitive nature of markets encourages individualistic behavior and selects for participants with those tendencies. Compared to lab behavior, therefore, the combination of market forces and experience might lessen the importance of these qualities in everyday markets.

Recognizing the limits of laboratory experiments, researchers have turned to “field experiments” to test behavioral models (12). Field experiments maintain true randomization, but are carried out in natural environments, typically without any knowledge on the part of the participant that their behavior is being scrutinized. Consequently, field experiments avoid many of the important obstacles to generalizability faced by lab experiments.

Some evidence thus far suggests that behavioral anomalies are less pronounced than was previously observed in the lab (13) (see the figure). For example, sports card dealers in a laboratory setting are driven strongly by positive reciprocity, i.e., the seller provides a higher quality of good than is necessary, especially when the buyer offers to pay a generous price. This is true even though the buyer has no recourse when the seller delivers low quality in the lab experiment. Yet, this same set of sports card traders in a natural field experiment behaves far more selfishly. They provide far lower quality on average when faced with the same buyer offers and increase quality little in response to a generous offer from the buyer.

Other field data yield similar conclusions. For example, farm worker behavior is consistent with a model of social preferences when workers can be monitored (14). Yet, this disappears when workers cannot monitor each other, which rules out pure altruism as the underlying cause. Being monitored proves to be the critical factor. Similar data patterns are observed in work that explores the endowment effect (15).

Stigler (16) wrote that economic theories should be judged by three criteria: generality, congruence with reality, and tractability. We view the most recent surge in behavioral economics as adding fruitful insights—it makes sense to pay attention to good psychology. At the very least, psychological insights induce new ways to conceptualize problems and provide interesting avenues of research. In their finest form, such insights provide a deeper means to describe and even shape behaviors. One important practical example involves savings decisions, where it has been shown that decision-makers have a strong tendency to adhere to whatever plan is presented to them as the default option, regardless of its characteristics. With this tendency in mind, Madrian and Shea (17) worked with a Fortune 500 company to change the default option for the firm’s retirement plans, dramatically influencing asset allocations. The changes in behavior induced by changing default rules dwarf more “rational” approaches to influence

choice such as information provision or financial education.

Behavioral economics stands today at a crossroads. On the modeling side, researchers should integrate the existing behavioral models and empirical results into a unified theory rather than a collection of interesting insights, allowing the enterprise to fulfill its enormous potential. To be empirically relevant, the anomalies that arise so frequently and powerfully in the laboratory must also manifest themselves in naturally occurring settings of interest. Further exploring how markets and market experience influence behavior represents an important line of future inquiry.

References

1. N. Ashraf, C. F. Camerer, G. Lowenstein, *J. Econ. Perspect.* **19**, 131 (2005).
2. H. A. Simon, *Q. J. Econ.* **69**, 99 (1955).
3. R. H. Strotz, *Rev. Econ. Stud.* **23**, 165 (1956).
4. G. S. Becker, *The Economics of Discrimination* (Univ. of Chicago Press, Chicago, 1957).
5. G. S. Becker, *J. Polit. Econ.* **82**, 1063 (1974).
6. D. Kahneman, A. Tversky, *Econometrica* **47**, 263 (1979).
7. M. Rabin, *Am. Econ. Rev.* **83**, 1281 (1993).
8. E. Fehr, K. Schmidt, *Q. J. Econ.* **114**, 817 (1999).
9. J. Andreoni, J. Miller, *Econometrica* **70**, 737 (2002).
10. D. Laibson, *Q. J. Econ.* **112**, 443 (1997).
11. S. D. Levitt, J. A. List, *J. Econ. Perspect.* **21**, 153 (2007).
12. G. W. Harrison, J. A. List, *J. Econ. Lit.* **42**, 1009 (2004).
13. J. A. List, *J. Polit. Econ.* **114**, 1 (2006).
14. O. Bandiera, R. Iwan Rasul, I. Barankay, *Q. J. Econ.* **120**, 917 (2005).
15. J. A. List, *Q. J. Econ.* **118**, 41 (2003).
16. G. Stigler, *Essays in the History of Economics* (Univ. of Chicago Press, Chicago, 1965).
17. B. C. Madrian, D. F. Shea, *Q. J. Econ.* **116**, 1149 (2001).

10.1126/science.1153640

MEDICINE

Combating Impervious Bugs

Richard P. Novick

Staphylococcus aureus has always been a serious human pathogen, and during recent decades it has become more serious owing to its acquisition of antibiotic resistance. In the past few years, a new strain of methicillin-resistant *S. aureus* (MRSA), known as USA300, and its close relatives, have emerged that are not only resistant to antibiotics but are more virulent and highly contagious. MRSA is presently spreading throughout the world, in hospitals and also in community settings where people are in close contact (1–3). Indeed, in the

United States, MRSA infections now account for more deaths each year than AIDS (4). But two reports, by Corbin *et al.* on page 962 in this issue (5), and by Liu *et al.* in *Science Express* (6), are cause for some cautious optimism about new therapeutic approaches to treat such infections.

Both studies describe possible strategies for interfering with the ability of *S. aureus* to thwart attacks that are mounted by the immune system during infection. Bacteria defend against lethal reactive oxygen species (ROS) produced by neutrophils, immune cells that are mobilized to sites of infection. Corbin *et al.* show that calprotectin, a well-known mammalian calcium-binding protein, chelates manganese (Mn²⁺), which the bac-

Host and bacterial proteins essential for bacterial survival offer new avenues for developing nonantibiotic-based treatments for infections.

terium requires for growth and for detoxifying ROS. Liu *et al.* report that certain cholesterol-lowering drugs have an entirely unexpected activity against *S. aureus*—blocking synthesis of staphyloxanthin, the pigment that imparts the organism’s characteristic color (aureus means “golden” in Latin) and also chemically detoxifies ROS.

Staphylococcal infection is an especially serious health threat in individuals with weakened immune systems, impaired circulation (as with diabetics), and surgical wounds. In deep-tissue sites, staphylococci can be life-threatening, even in otherwise healthy individuals. Staphylococcal abscesses form when the host immune system recognizes certain bacterial products, including cell wall components

The author is at the Kimmel Center for Biology and Medicine, New York University School of Medicine, New York, NY 10016, USA. E-mail: novick@saturn.med.nyu.edu

MATERIALS SCIENCE

On Mixing and Demixing

Julio M. Ottino and Richard M. Lueptow

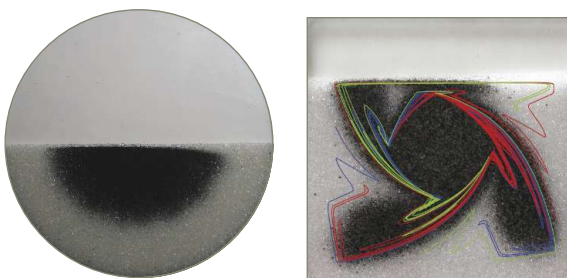
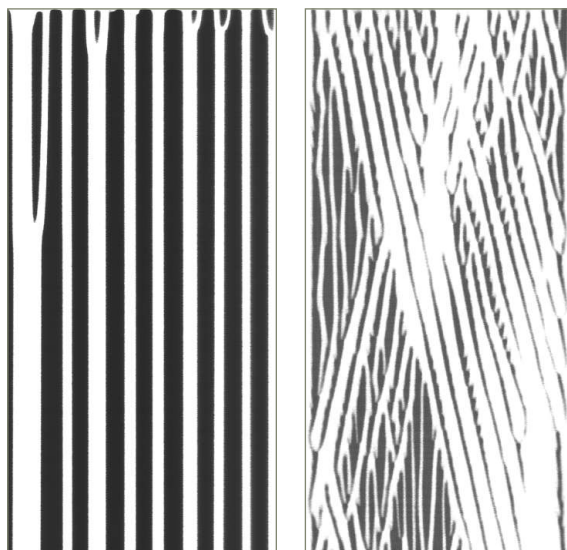
Trying to mix two dissimilar granular materials—such as light and heavy or small and large particles—may lead to counterintuitive results: Putting more and more energy into mixing may actually result in more and more demixing (1–5). The robust and varied patterns resulting from demixing (see the first figure) have long puzzled practitioners and researchers alike. How can one mix something that does not want to mix? Recently, Shi *et al.* have devised a conceptual approach that may allow for the mixing of dissimilar granular materials based on the fundamental physics of granular flow (6).

The first studies of granular mixing were of an engineering nature: “How can we mix this?” This targeted approach was successful in many practical applications. However, it provided few insights into the causes of demixing and did not yield general solutions to new segregation problems encountered in the processing of pharmaceuticals, dry chemicals, ceramics, minerals, polymers, and powdered or granular foodstuffs.

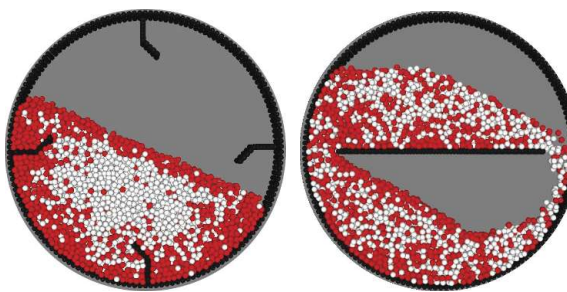
The origin of demixing seems counterintuitive at first glance: One might expect particles tumbling down a slope to mix as they flow. Nevertheless, simple cases of demixing can be explained in terms of the percolation of small particles through interstices between large particles or due to “buoyancy” differences between light and heavy particles. The small or heavy particles drift to lower portions of the flowing layer and thus fall out of the flowing layer earlier than large or light particles (see the first figure, bottom left).

Other segregation patterns can occur for various combinations of particle sizes and densities (7), whether the

J. M. Ottino is in the Northwestern Institute on Complex Systems, Department of Chemical and Biological Engineering, and Department of Mechanical Engineering, Northwestern University, Evanston, IL 60208, USA. R. M. Lueptow is in the Department of Mechanical Engineering, Northwestern University, Evanston, IL 60208, USA. E-mail: jm-ottino@northwestern.edu; r-lueptow@northwestern.edu



Demixing patterns. (Top) Upon rotation, a long cylindrical tumbler partially filled with a homogeneous mixture of two sizes of particles will segregate into bands. Space (horizontal) and time (vertical from top to bottom) plots show coarsening (left) and waves (right), depending on the rotational speed and interstitial fluid (19). (Bottom) In a circular tumbler, small particles segregate into a semicircular pattern (dark) surrounded by large particles (light) within one or two rotations (left) (7); in a square tumbler, similar particles segregate into a lobed pattern outlined by unstable manifolds (right) (20).



Mixing and demixing. In simulations of bidisperse mixtures of particles with different densities, short baffles added to the wall of the tumbler do little to enhance mixing (left), whereas a central baffle truncates the flowing layer, leading to good mixing (right) (6).

Insights into the physics of mixing are leading to methods for avoiding segregation of different particles.

particles are surrounded by air or wholly immersed in a liquid (8). Predicting these patterns is challenging, because granular matter provides an example of “more is different” (9): The behavior of one or a few elements does not capture the behavior of many elements, so that segregation patterns cannot be deduced from the behavior of individual particles.

In recent years, there has been a surge of systematic studies of granular flow under a wide range of experimental conditions, including, for example, how flow is affected by the interstitial fluid, the adhesive properties of the particles, and changes in gravity (10). Other studies have investigated the rheology of granular flows in an attempt to develop appropriate constitutive relations (11). Typical solutions to combat segregation driven by this understanding have fallen into two classes: change the particles or change the process. Changing the particles may involve controlling interparticle adhesion (12) or balancing the differences in size and density. Changing the process may involve geometrical changes (such as adding internal obstructions called “baffles”) or operational changes (such as varying the tumbler speed).

These systematic studies have led to interesting results on the process side. For example, small particles need time to migrate through the flowing layer; thus, if the flow is interrupted before the particles have percolated to the bottom of the flowing layer, the particles do not segregate completely and segregation can be prevented. This relatively simple observation can be applied to devise systems that counteract segregation.

McCarthy and co-workers have implemented this approach using the concept of a “zigzag chute” (6). Imagine heavy and light particles flowing down a chute made up of “zigs” that are downward and rightward and “zags” that are downward and leftward. Heavy particles drift downward in the zig portion and end up lower in the flowing layer, but become the upper portion of the flowing layer in the subsequent zag

CREDITS: FIRST FIGURE (TOP PANELS) FROM (19), COPYRIGHT AMERICAN PHYSICAL SOCIETY; (BOTTOM LEFT PANELS) W. MEIER/EXXONMOBIL; (BOTTOM RIGHT PANEL) FROM (20), COPYRIGHT AMERICAN PHYSICAL SOCIETY; SECOND FIGURE FROM (6), COPYRIGHT AMERICAN PHYSICAL SOCIETY.

portion of the chute, thus thwarting demixing. The idea is reminiscent of droplets in zigzagging channels aimed at generating chaotic mixing in the drops (13).

Extensions of the zigzagging idea have practical consequences. Baffles have long been used in mixing tumblers, but were designed by trial and error. Usually, short baffles were attached to the outer wall of the container (see the second figure, left). In fact, the best mixing is achieved with long internal baffles (see the second figure, right) (6).

Physical understanding, computational and theoretical approaches (14–16), and experimental capabilities (17) are now sufficiently mature so that mixing or demixing can

be designed into a system with a reasonable probability of success. The next challenge is extending the ideas to three dimensions. Recent theoretical work on mixing a single class of particles in three-dimensional tumblers (18)—a far simpler case than mixing two classes of particles—suggests an explosive increase in the richness of problems that may be encountered when tackling mixing and demixing of granular materials.

References

1. J. B. Knight *et al.*, *Phys. Rev. Lett.* **70**, 3728 (1993).
2. M. E. Mobius *et al.*, *Nature* **414**, 270 (2001).
3. T. Shinbrot, F. J. Muzzio, *Phys. Rev. Lett.* **81**, 4365 (1998).
4. S. B. Savage, C. K. K. Lun, *J. Fluid Mech.* **189**, 311 (1988).
5. S. Ulrich *et al.*, *Phys. Rev. E* **76**, 042301 (2007).
6. D. Shi *et al.*, *Phys. Rev. Lett.* **99**, 148001 (2007).
7. K. M. Hill *et al.*, *Complexity* **10**, 79 (2005).
8. N. Jain *et al.*, *Phys. Rev. Lett.* **86**, 3771 (2001).
9. P. W. Anderson, *Science* **177**, 393 (1972).
10. A. Brucks *et al.*, *Phys. Rev. E* **75**, 032301 (2007).
11. G. D. R. MiDi, *Eur. Phys. J. E* **14**, 341 (2004).
12. H. Li, J. J. McCarthy, *Phys. Rev. Lett.* **90**, 184301 (2003).
13. M. R. Bringer *et al.*, *Phil. Trans. Roy. Soc. London A* **362**, 1087 (2004).
14. M. Moakher *et al.*, *Powder Tech.* **109**, 58 (2000).
15. D. C. Rapaport, *Phys. Rev. E* **75**, 031301 (2007).
16. S. W. Meier *et al.*, *Adv. Phys.* **56**, 757 (2007).
17. S. L. Conway *et al.*, *Chem. Eng. Sci.* **60**, 7091 (2005).
18. www.maths.leeds.ac.uk/~rsturman/pwi_mixing.html
19. S. J. Fiedor, J. M. Ottino, *Phys. Rev. Lett.* **91**, 244301 (2003).
20. S. W. Meier *et al.*, *Phys. Rev. E* **74**, 031310 (2006).

10.1126/science.1152849

ECOLOGY

Green with Complexity

Shahid Naeem

Why the sky is blue is a matter of basic physics, but why land is green is a much trickier question. The obvious response is that land is green because it is covered with plants. This answer, however, raises the question of why land is covered with plants in the face of omnipresent herbivory, which in turn raises the question of why herbivory is omnipresent in the face of omnipresent carnivory? Why land is green, or what governs primary productivity, is one of the most basic yet astonishingly complex questions in ecological research. Like a Russian matryoshka doll, each answer uncovers another question. On page 952 of this issue, Schmitz (1) adds to the complexity; given omnipresent carnivory, he finds that behavioral traits affect greenness. This result has profound implications for ecological and environmental research.

Before the 1960s, the question of greenness was largely the domain of ecologists who paid little heed to biodiversity. At its simplest level, greenness measures the density of autotrophs like plants and algae that use solar energy to turn inorganic matter into organic matter. This primary productivity is usually cited in grams of carbon fixed per unit area per year.

The yin to this yang is consumption by heterotrophs that consume and cycle organic matter back to its inorganic constituents. All ecosystem functions, including primary pro-

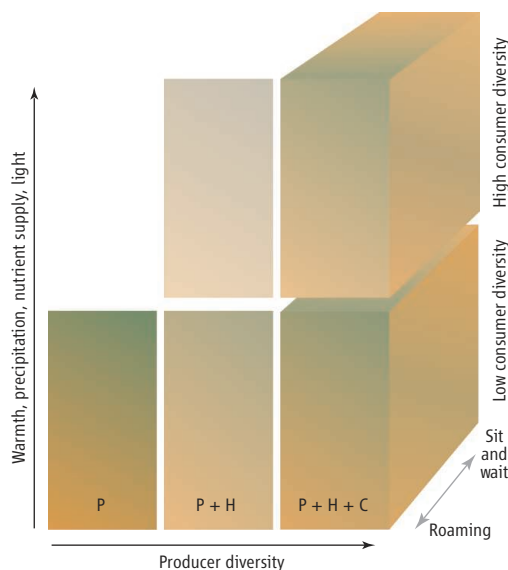
duction, decomposition, nitrogen mineralization, nutrient cycling, and energy flow, are driven by the balance between autotrophy and heterotrophy. Primary production, because it is the starting point in ecosystem function, is more intensely studied than other ecosystem functions.

At present, terrestrial global primary production clocks in at 59.22 petagrams (10^{15} g) of carbon fixed per year, almost a quarter of which is appropriated by humans as food, biofuel, and building materials (2). Not surprisingly, the principle determinants of greenness were considered to be climate and geography, with animals and microorganisms playing a minor role.

Predators, by affecting prey behavior, can change both plant diversity and productivity in an ecosystem.

But Hairston *et al.* suggested that there was another layer to the question (3, 4). They argued that herbivory should reduce the green world to a barren one, were it not for carnivory.

Although Hairston *et al.* dramatically expanded the complexity of the question of greenness, even deeper layers were unmasked in the 1990s when researchers discovered that biodiversity could also influence greenness. Trophic levels ignore biodiversity, grouping species into layers with producers on the bottom, then primary consumers, secondary consumers, and so on to the top, with each level only about 10% of the biomass of the level below it.



Hunting green. The greenness of ecosystems (rectangles) varies according to abiotic factors such as warmth, precipitation, nutrient supply rates, and light (vertical axis), but other influences are at work. Greenness in a system with only plants (P) is reduced by herbivory (P+H), but carnivory (P+H+C) restores greenness by suppressing herbivory. Increasing producer diversity (from left to right) can increase greenness. High and low levels of consumer (herbivore and carnivore) diversity can also affect greenness if diversity improves the efficiency of one level's exploitation of another. Schmitz suggests that carnivore behavior, in particular its hunting mode, adds a new dimension to ecosystem greenness (the rightmost rectangles become blocks). The degree to which carnivores roam or sit and wait for prey affects herbivore impacts on greenness.

Each trophic level, in theory, can suppress the level below it, leading to a cascade of influences on primary production. In the 1990s, however, some controversial studies on biodiversity and ecosystem function (BEF) argued that diversity within trophic levels could also affect ecosystem function. The bulk of this work suggested that plant diversity improved primary production (5). Recent research suggests that diversity in higher trophic levels has similar effects (more consumer diversity, more consumer biomass) (6, 7). Thus, consumer biodiversity at each trophic level can affect the downward trophic control over primary production (8).

Schmitz now adds animal behavior to the layers of complexity (see the figure). In an elegant experiment, he established a series of 14 replicate grassland ecosystems: outdoor cages containing plants (grasses and forbs), herbivores (grasshoppers), and predators (spiders), controlling for everything among the replicates with the exception of one manipulated factor. In half the replicates, he swapped a “sit and wait” ambush predatory spider (*Pisaurina mira*) for an actively roaming predatory spider (*Phidippus rimator*).

One would think that such a minor change would amount to nothing. Surprisingly, a number of significant changes occurred. A 14% reduction in plant diversity, 33% increases in nitrogen mineralization, and, most important, a 163% increase in aboveground primary productivity occurred in the replicates containing *P. rimator*, the active hunter.

Schmitz suggests that the active roaming of *P. rimator* did not alter grasshopper foraging because it left little in the way of persistent cues to its whereabouts. In contrast, *P. mira*'s more sedentary behavior caused a chronic shift in grasshopper foraging because its persistent cues to its whereabouts led grasshoppers to favor the safety provided by the dominant plant.

Such nonconsumption effects of predators due to behavioral responses of prey occur widely (9); thus, these findings have far-reaching implications. The findings also touch upon trait-based forecasting of biodiversity's influence on ecosystem function. Phylogenetic, metabolic, morphological, reproductive, and stoichiometric species traits can all be used to forecast the response of species to environmental change and to predict how such change impacts ecosystem function (10–12). Schmitz adds behavioral traits to the list of traits currently used.

More work is needed, but the importance of this study should not be underestimated. In addition to the usual limitations imposed by small-scale, short-term, simplified studies,

the relevant behavioral traits are simply not known for millions of species. Consider a typical biodiversity inventory in which researchers collected 1649 individuals in 21 families comprising 20 to 69 species, at various altitudes in a single study in Sulawesi, Indonesia (13). For BEF forecasting, one might imagine deriving phylogenetic, morphological, stoichiometric, and perhaps even reproductive traits from the spider corpses, but not behavioral traits. Despite such limitations, workers in community, ecosystem, food web, and BEF research, as well as in conservation and environmental biology, need to test Schmitz's proposal that hunting mode and prey response play prominent roles in predicting production.

The greenness of land is everything—primary production is Earth's fuel injection system, feeding 6.7 billion people, keeping oxygen at 21%, and regulating greenhouse gases. Despite our having converted 40% of Earth's terrestrial surface to maximize production for

human consumption, the world is actually less green than it could be (2). We have a long way to go in a short time if we are to better understand what governs greenness. Including consumer behavior in our theoretical and empirical work gets us closer to the answer.

References

1. O. J. Schmitz, *Science* **319**, 952 (2008).
2. H. Haberl *et al.*, *Proc. Natl. Acad. Sci. U.S.A.* **104**, 12942 (2007).
3. N. G. S. Hairston, F. E. Smith, L. B. Slobodkin, *Am. Nat.* **106**, 421 (1960).
4. S. D. Fretwell, *Oikos* **50**, 291 (1987).
5. D. U. Hooper *et al.*, *Ecol. Monogr.* **75**, 3 (2005).
6. B. J. Cardinale *et al.*, *Nature* **443**, 989 (2006).
7. B. Worm *et al.*, *Science* **314**, 787 (2006).
8. J. E. Duffy, *Oikos* **99**, 201 (2002).
9. E. L. Preisser, D. I. Bolnick, M. F. Benard, *Ecology* **86**, 501 (2005).
10. M. Solan *et al.*, *Science* **306**, 1177 (2004).
11. D. E. Bunker *et al.*, *Science* **310**, 1029 (2005).
12. P. B. McIntyre, L. E. Jones, A. S. Flecker, M. J. Vanni, *Proc. Natl. Acad. Sci. U.S.A.* **104**, 4461 (2007).
13. A. Russell-Smith, N. E. Stork, *J. Trop. Ecol.* **10**, 545 (1994).

10.1126/science.1154770

MEDICINE

Sidestepping Mutational Meltdown

Eric A. Shoubridge and Timothy Wai

Mouse mitochondrial DNA with severe mutations is not passed down to later generations, but the selection process is unclear.

One benefit of sexual reproduction is the ability to shuffle genes and repair DNA damage during germ cell differentiation. Genetic recombination during the formation of egg and sperm cells in mammals thus permits the generation of genetic diversity and the continuous removal of deleterious mutations from the population (1). Mitochondria in mammalian cells harbor their own DNA (mtDNA), but unlike nuclear DNA, the mitochondrial genome is transmitted asexually from mother to child, and thus does not benefit from genetic recombination. How mtDNA avoids the accumulation of deleterious mutations remains unknown. Selection against pathogenic mtDNA mutations in the germ line is thought to be weak or nonexistent, as transmission in human pedigrees can largely be accounted for by random genetic drift (2, 3). However, relatively few mtDNA mutations are responsible

for human mitochondrial diseases (4). On page 958 of this issue, Fan *et al.* (5) show in a mouse model that mtDNA avoids the accumulation of severe deleterious mutations in its protein-coding genes by selecting against them during oocyte maturation.

The mitochondrial genome codes for a few essential protein components of organelle's respiratory machinery as well as transfer and ribosomal RNAs. It is currently not possible to mutate mammalian mtDNA at will, so to investigate the transmission of mutations in protein-coding genes of the mitochondrial genome, Fan *et al.* first had to select for such mutations in a murine cell line. They identified two pathogenic mutations on the same mtDNA molecule (mitochondria generally harbor several circular mtDNA molecules): a severe mutation in a gene encoding a subunit of complex I (ND6) that shifts the reading frame of the gene and completely abolishes the complex's enzymatic activity, and a milder mutation in a gene encoding a complex IV subunit (COI) that reduces the complex's enzymatic activity by 50%. The mutations were introduced into mouse embryonic stem cells, and a cell line

The authors are at the Montreal Neurological Institute and Department of Human Genetics, McGill University, Montreal, Quebec H3A 2B4, Canada. E-mail: eric@ericpc.mni.mcgill.ca

was identified that contained the two original mutations. These cells were injected into normal blastocysts to create chimeric animals. A single female (founder) was obtained whose mtDNAs all had the COI mutation (homoplasmic). About half of these mtDNAs carried the severe ND6 mutation. Strikingly, the ND6 frameshift mutation was completely eliminated in successive generations, but the animals remained homoplasmic for the COI mutation and developed a cardiomyopathy. Analysis of oocytes from the founder female showed that the frameshift mutation was selected against during oocyte maturation, which suggests that there is strong purifying selection in the germ line for severe mtDNA mutations.

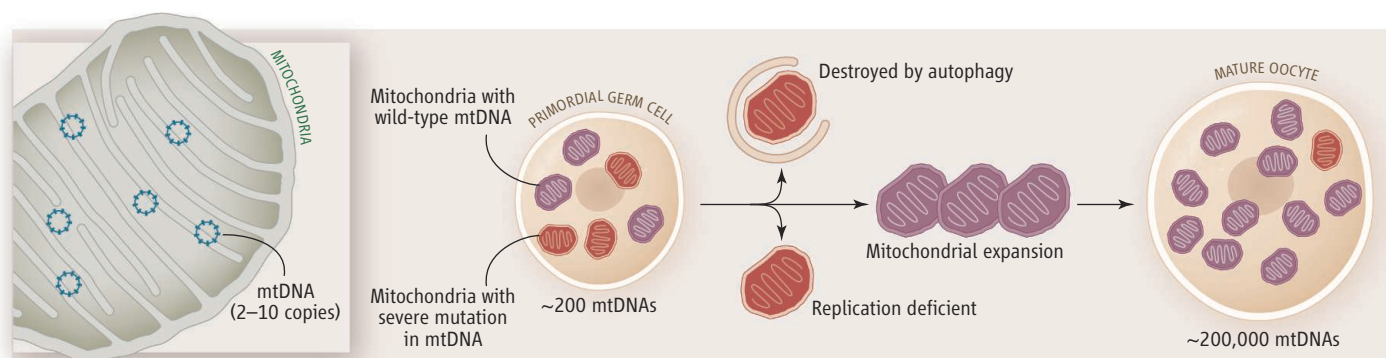
Using a completely different strategy, Stewart *et al.* (6) reached a similar conclusion. They mated female mice carrying a mutation

could occur by apoptosis (cell death) of the developing oocytes, perhaps triggered by increased production of reactive oxygen species that occurs in response to mutations. However, it is very difficult to see how the mechanism could be acting at the cellular level, as mtDNAs carrying the frameshifted ND6 gene, representing a low proportion of the gene, are rapidly eliminated (low amounts of mtDNA with this severe mutation could not possibly produce a cellular phenotype). In fact, even the founder female, 50% of whose mtDNAs contained the frameshifted ND6 gene, had only a modest complex I deficiency.

It seems much more likely that selection occurs at the level of the organelle. How might this occur? At least two mechanisms are possible (see the figure). Mitochondria harboring mutant mtDNAs could be targeted for

plasmoly. This is in contrast to mitochondrial genes that do not encode proteins (but code for tRNAs, which make up the majority of human pathogenic mutations). Presence of the latter mutations typically must exceed 80% for expression of a biochemical phenotype (4). Purifying selection could occur simply by making replication of mtDNA in the most dysfunctional mitochondria less efficient. This might, for instance, involve less efficient import of proteins necessary for mitochondrial biogenesis in organelles with a lowered membrane potential. The importance of starting such a selection process in early germline development is that it can act on multiple rounds of mtDNA replication.

The evolutionary necessity to filter severe germline mutations could explain three hitherto unexplained observations in mtDNA biol-



Gene filter. Mitochondrial DNAs with severe mutations are filtered out of the female germ line during oogenesis. Two possible pathways are shown.

in the gene encoding the mtDNA polymerase with wild-type males, and tracked the evolution of mtDNA mutations that were caused by the defective polymerase in successive generations. Although mtDNA mutations in the original mutator strain were randomly distributed, with an average of 30 mutations per genome, a significant bias against non-synonymous mutations in protein-coding genes was observed as early as the second generation, suggesting a filter that prevents the transmission of deleterious germline mtDNA mutations.

Must mutations in mitochondrial DNA be severely deleterious to be subject to selection? Although Fan *et al.* observed that the milder COI mutation was retained through successive generations, it was always homoplasmic, so the ability to filter it out was never put to the test. Although mtDNA experiences a genetic bottleneck in the transmission from mother to offspring (2), which is responsible for the random, but rapid, segregation of mtDNA sequence variants between generations, this cannot explain the bias against transmitting deleterious genes. Fan *et al.* suggest that selec-

tion could occur by apoptosis (cell death) of the developing oocytes, perhaps triggered by increased production of reactive oxygen species that occurs in response to mutations. There is some evidence that this process can be selective (7). A second possibility simply involves a relative selective advantage to wild-type mtDNAs during the expansion of mitochondria that occurs in oogenesis. MtDNA has a curious natural history during the development of the female germ line. A mature oocyte contains about 200,000 copies of mtDNA (8), with one or two copies per organelle. These mtDNA copies are apportioned, without mtDNA replication, to cells of the early embryo. By the time mtDNA replication resumes, new primordial germ cells contain about 100 mitochondria (8) and about 200 copies of mtDNA (9).

The relatively low copy number of mtDNA per organelle in a primordial germ cell might be important to expose the most severe mutations to selection. For mutations in protein-coding genes, expression of a phenotype (such as reduction in the amount of functional protein) is directly proportional to the proportion of mutant versus wild-type genes present in a cell's mtDNA (hetero-

ogy: the large number of mtDNAs in the mature oocyte (a genetic device to distribute mtDNAs in the early embryo), the absence of mtDNA replication during early embryonic development (ensuring multiple rounds of mtDNA replication in primordial germ cells), and the reduction in mtDNA copy number per organelle (exposing severe mutations to strong selection). Still, there are some severe mutations in protein-coding genes of the mitochondrial genome, such as those in *ATP6*, that are associated with early-onset lethal human disease (4). How do they escape selection?

References

1. J. Felsenstein, *Genetics* **78**, 737 (1974).
2. J. P. Jenuth, A. C. Peterson, K. Fu, E. A. Shoubridge, *Nat. Genet.* **14**, 146 (1996).
3. P. F. Chinnery *et al.*, *Trends Genet.* **16**, 500 (2000).
4. R. W. Taylor, D. M. Turnbull, *Nat. Rev. Genet.* **6**, 389 (2005).
5. W. Fan *et al.*, *Science* **319**, 958 (2008).
6. J. B. Stewart *et al.*, *PLoS Biol.* **6**, e10 (2008).
7. R. Scherz-Shouval, Z. Elazar, *Trends Cell Biol.* **17**, 422 (2007).
8. L. Cao *et al.*, *Nat. Genet.* **39**, 386 (2007).
9. L. M. Cree *et al.*, *Nat. Genet.* **40**, 249 (2008).

10.1126/science.1154515

Adapting Proteostasis for Disease Intervention

William E. Balch,¹ Richard I. Morimoto,² Andrew Dillin,³ Jeffery W. Kelly^{4*}

The protein components of eukaryotic cells face acute and chronic challenges to their integrity. Eukaryotic protein homeostasis, or proteostasis, enables healthy cell and organismal development and aging and protects against disease. Here, we describe the proteostasis network, a set of interacting activities that maintain the health of proteome and the organism. Deficiencies in proteostasis lead to many metabolic, oncological, neurodegenerative, and cardiovascular disorders. Small-molecule or biological proteostasis regulators that manipulate the concentration, conformation, quaternary structure, and/or the location of protein(s) have the potential to ameliorate some of the most challenging diseases of our era.

Proteostasis refers to controlling the concentration, conformation, binding interactions (quaternary structure), and location of individual proteins making up the proteome by readapting the innate biology of the cell, often through transcriptional and translational changes (Fig. 1). Proteostasis thus influences specific cellular functions and enables differentiated cells to change their physiology for successful organismal development and aging in the face of constant intrinsic and environmental challenges to prevent disease onset. Proteostasis is influenced by the chemistry of protein folding/misfolding and by numerous regulated networks of interacting and competing biological pathways (Fig. 1) that influence protein synthesis, folding, trafficking, disaggregation, and degradation (1–8). Herein, we examine a growing body of evidence suggesting that adapting the cellular proteostasis network by using “proteostasis regulators” (Fig. 1) can partially correct proteostatic deficiencies that contribute to a broad range of human diseases, some that present at birth, but most upon aging.

Proteostasis Maintenance During Development and Aging

The competition between cellular protein folding and degradation, often referred to as protein quality control, is one of many processes influencing proteostasis. The additional components of the proteostasis network (Fig. 1) are in place to achieve proteome maintenance with

alternatives in addition to degradation. Protein folding *in vivo* is accomplished through interactions between the folding polypeptide chain and macromolecular cellular components, including multiple classes of chaperones and folding enzymes—interactions that minimize aggregation (Fig. 2) (3). Metabolic enzymes also influence cellular protein folding efficiency

because the organic and inorganic solutes produced by a given compartment affect polypeptide chain solvation through noncovalent forces, including the hydrophobic effect, that influences the physical chemistry of folding. Metabolic pathways also produce small-molecule ligands that can bind to and stabilize the folded state of a specific protein(s), enhancing folding by shifting folding equilibria (9, 10). Whether a given protein folds in a certain cell type depends on the distribution, concentration, and subcellular localization of chaperones, folding enzymes, metabolites, and the like (3).

Temporal cellular proteostasis adaptation is necessary as a result of the presence of an ever-changing proteome during development and the presence of new proteins and the accumulation of misfolded proteins upon aging. Because the fidelity of the proteome is challenged during development and aging, and by exposure to pathogens that demand high protein folding and trafficking capacity, cells use stress sensors and inducible pathways to respond to a loss of proteostatic control. These include the heat shock response (HSR) (11) that regulates cytoplasmic proteostasis and the unfolded protein response (UPR) (2, 12) that helps maintain exocytic

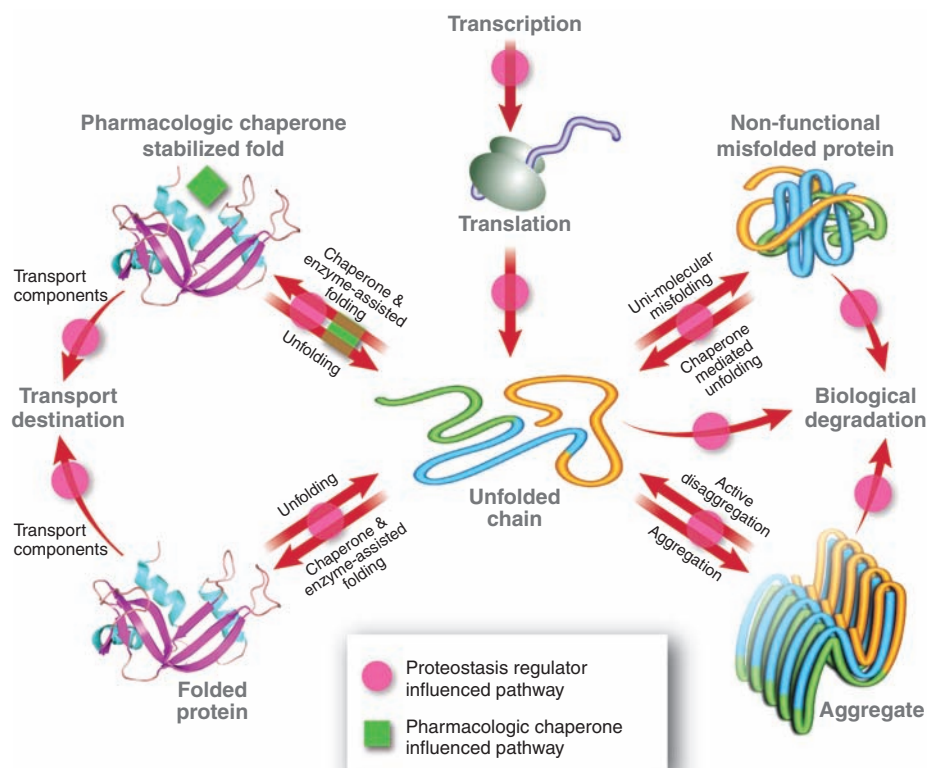


Fig. 1. A proteostasis network comprising pathways represented by the red arrows. Imbalances in proteostasis often lead to disease and, therefore, proteostasis regulators (magenta circles) that manipulate the proteostasis pathways/network can restore protein homeostasis and ameliorate both loss- and gain-of-function diseases. A finite population of the folded conformational ensemble is required for pharmacological chaperones (green squares) to enhance folding and trafficking, through a mechanism distinct from the innate biological pathways influenced by proteostasis regulators (ribonuclease A is shown; Protein Data Bank ID, 2BLP).

¹Department of Cell Biology and the Institute for Childhood and Neglected Diseases, The Scripps Research Institute, 10550 North Torrey Pines Road, La Jolla, CA 92037, USA.

²Department of Biochemistry, Molecular Biology, and Cell Biology, Rice Institute for Biomedical Research, Northwestern University, 2205 Tech Drive, Hogan 2-100, Evanston, IL 60208–3500, USA. ³Salk Institute for Biological Studies, 10010 North Torrey Pines Road, La Jolla, CA 92037, USA.

⁴The Skaggs Institute for Chemical Biology and the Department of Chemistry, The Scripps Research Institute, 10550 North Torrey Pines Road, La Jolla, CA 92037, USA.

*To whom correspondence should be addressed. E-mail: jkelly@scripps.edu

pathway proteostasis. Recent experiments reveal that some cells possess a proteostasis maintenance capacity that can be exceeded when a new misfolding-prone protein appears (13). An age-associated decline in proteostatic control in concert with an increase in protein oxidation and modification that exacerbates aggregation challenges the maintenance of proteostasis during aging, offering a partial explanation for why many diseases are age onset (14–17). Much of the current knowledge about proteostasis results from studying cells under optimal growth conditions, but how proteostasis is accomplished in the face of nutritional or environmental challenges, especially upon aging, remains to be established.

Proteostasis Maintenance Is Linked to Healthy Aging

Misfolding-prone proteins challenge proteostasis within and outside the cell. The inability to restore proteostasis leads to diseases conveniently categorized as loss- or gain-of-function disorders (18). Loss-of-function diseases, including cystic fibrosis and Gaucher disease, are typically caused by inherited mutations leading to inefficient folding and excessive degradation (9, 19). Gain-of-toxic-function diseases, on the other hand, appear to arise when aggregation-associated proteotoxicity dominates over clearance inside and/or outside the cell (6, 18). The latter maladies, often associated with aging, include Parkinson's disease, Huntington's disease, amyotrophic lateral sclerosis, and Alzheimer's disease. Emerging evidence suggests that proteostasis is controlled by signaling pathways that also influence longevity and youthfulness (Fig. 3) (6, 20–23). Therefore, treatments aimed at restoring proteostasis to alter the clinical course of multiple aging-associated disorders of complex etiology could also influence longevity. Emerging strategies to restore proteostasis in both loss- and gain-of-function diseases by manipulating the innate biology of the cell are outlined below.

Protein Replacement, the Current Therapeutic Strategy

Loss-of-function diseases are currently treated by intravenous administration of a wild-type version of the deficient protein to restore function. However, the scope of protein replacement therapy as a general solution is limited because the injected protein must find its way to the appropriate cell type and to the relevant subcellular compartment through an endocytic trafficking pathway. In enzyme replacement therapy for lysosomal storage diseases like Gaucher disease, less than 5% of the injected enzyme makes it to the target organelle (the lysosome). Although protein replacement therapy is effective for some loss-of-proteostasis diseases, alternative approaches are clearly necessary, especially for brain disorders, because recombinant proteins do not cross the blood-brain barrier.

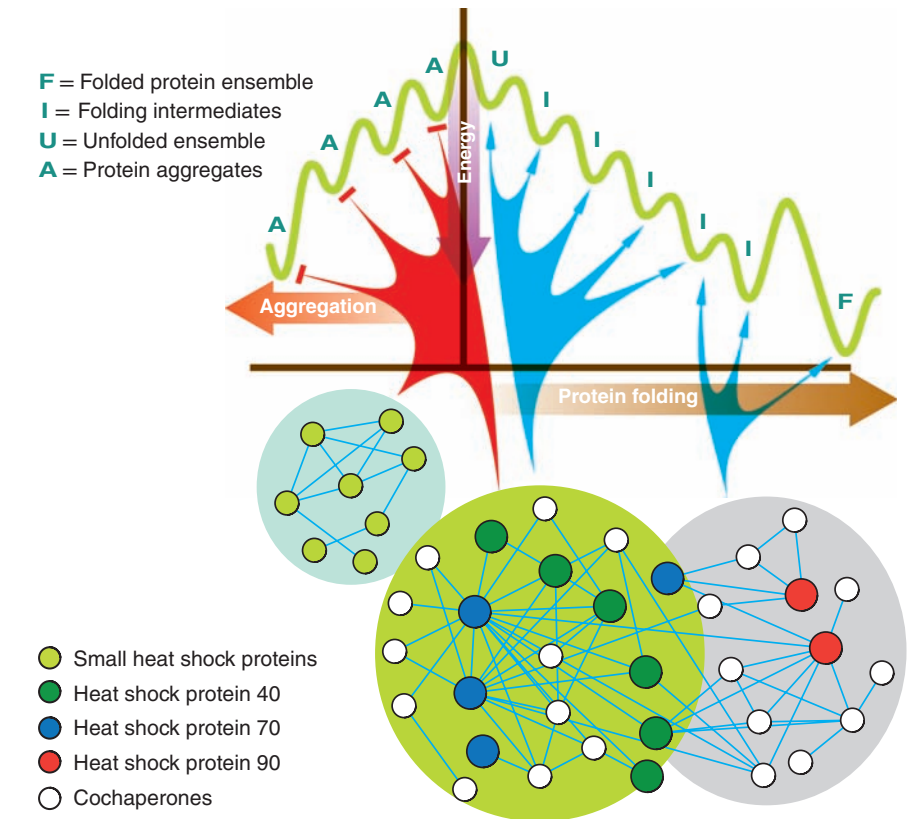


Fig. 2. The chaperone/cochaperone–assisted folding and aggregation prevention pathways, one component (red arrow) of the proteostasis network depicted in Fig. 1. Many chaperones and cochaperones interact with each other (depicted by the interaction map) and the polypeptide undergoing structure acquisition (indicated by the arrows to the structures on the folding free-energy coordinate) to produce a low-energy functional protein fold while avoiding aggregation.

Protein Stabilization to Remedy Loss- or Gain-of-Function Diseases

Two emerging therapeutic strategies offer promise to ameliorate gain- or loss-of-function diseases. For the latter, a so-called pharmacologic chaperone that binds to and stabilizes the folded, functional form of a mutant protein and shifts the folding equilibria away from degradation and aggregation may be useful (Fig. 1) (9). Pharmacologic chaperoning increases the concentration and proper localization of the protein by coupling more of the folded state to the trafficking pathway (Fig. 1), a pathway that strongly influences proteostasis (3). Pharmacologic chaperones are currently being evaluated in phase II clinical trials for Gaucher and Fabry diseases (24) and may prove useful for cystic fibrosis.

Small molecules that bind to the folded functional state of a protein can also impose kinetic stability on it, preventing its denaturation and misassembly into cytotoxic aggregates (10). These so-called “kinetic stabilizers” are currently being evaluated in placebo controlled clinical trials to stabilize transthyretin against amyloidogenesis associated with familial amyloid polyneuropathy, a gain-of-toxic-function disease (24).

Adapting the Proteostasis Network to Restore Normal Physiology

In contrast to the protein replacement and pharmacologic chaperone/kinetic stabilizer approaches, a more general therapeutic strategy to restore proteostasis may be to use small molecules or biologicals [small interfering RNA (siRNA), cDNA, or protein] to manipulate the concentration, conformation, and/or the location of a given protein or family of proteins by re-adapting the innate biology of the cell. This can be accomplished by altering the proteostasis network, including protein synthesis, folding, trafficking, disaggregation, and degradation pathways (Fig. 1) (1–8, 25–28). Proteostasis regulators often function by manipulating signaling pathways and/or the transcription and translation of components of a given pathway(s) composing the proteostasis network, including the HSR and UPR. Below we provide evidence that both loss- and gain-of-function diseases associated with defective proteostasis can be remedied with proteostasis regulators.

Proteostasis Regulators in Loss-of-Function Disease Cell Lines

Proteomic analysis of the chaperones required to fold the cystic fibrosis transmembrane conduct-

ance regulator (CFTR) chloride channel reveals that the $\Delta F508$ CFTR cystic fibrosis-associated mutant is trapped as a folding intermediate in the endoplasmic reticulum (ER), sequestering more chaperones and cochaperones than wild-type CFTR (27). Readjusting the chaperone folding pathway with an siRNA proteostasis regulator directed against one cochaperone (Aha 1) restores partial folding, trafficking, and >50% of wild-type halide conductance, possibly by adjusting the Hsp-90/Aha-1 folding cycle to match the altered folding kinetics of $\Delta F508$ CFTR (19, 27). Proteostasis regulators and pharmacologic chaperones are expected to act synergistically in cystic fibrosis, owing to their distinct mechanisms of action (Fig. 1).

Several small-molecule proteostasis regulators have recently been discovered that partially restore enzyme homeostasis in multiple cellular models of loss-of-function lysosomal storage diseases. The proteostasis regulators diltiazem and verapamil appear to function by inhibiting L-type Ca^{2+} channels in the plasma membrane, decreasing intracytoplasmic Ca^{2+} levels, which leads to increased transcription and translation of numerous cytoplasmic and ER chaperones, including BiP and Hsp40, that enhance the folding, trafficking, and activity of lysosomal enzymes (29). Thus, proteostasis regulators can augment the capacity of the cell to fold damaged proteins in both cystic fibrosis and lysosomal storage diseases (Figs. 1 and 2) (27, 29).

Ameliorating Gain-of-Toxic-Function in Organismal Disease Models

RNA interference (RNAi)-based proteostasis regulators that readjust disaggregase and chaperone levels, through manipulation of aging signaling pathways (Fig. 3) substantially delay the onset of the gain-of-toxicity phenotype in *Caenorhabditis elegans* models of Alzheimer's and Huntington's diseases (6, 20–23). Genetic and biochemical evidence implicates A β and polyglutamine aggregation as the cause of neurotoxicity in Alzheimer's and Huntington's diseases, respectively, through a mechanism(s) that remains obscure (30).

RNAi-induced reduction of insulin growth factor signaling (Fig. 3) allows the DAF-16 transcription factor to enter the nucleus, extending the life span of the Alzheimer's *C. elegans* model by a factor of almost 2 and substantially delaying age-onset aggregation-associated toxicity in this cytoplasmic A β 1-42 aggregation model (6, 21). The HSF-1 transcriptome is also required for this protection and appears to predominantly regulate a disaggregation activity, while DAF-16 seems to regulate a backup active aggregation pathway that converts highly toxic A β oligomers into less toxic amyloid fibrils (6). Proteostasis regulators that enhance both the disaggregase and active aggregation pathways and/or related activities represent promising therapeutic strategies for gain-of-function proteotoxicity diseases (Figs. 1 and 3).

Huntington's disease is the prominent member of a family of gain-of-toxic-function diseases caused by an expansion of a contiguous polyglutamine tract beyond a threshold length, resulting in protein aggregation in the cytoplasm and neurotoxicity, with an age of onset that inversely correlates with the length of the polyglutamine repeat (20). RNAi directed against the proteostasis regulator *age-1* (a phosphoinositide-3 kinase) in the insulin signaling pathway (Fig. 3) mediates slowing of the aging process and an increase in chaperone expression levels in Q_{82} expressing worms, conferring protection from proteotoxicity, and demonstrating that the adaptable biology of proteostasis can ameliorate polyQ proteotoxicity (20).

That the *age-1* proteostasis regulator rebalances the chaperone network to restore proteostasis in

the Huntington's disease worm model follows from observations that overexpressing certain chaperones, including Hsp70, Hsp40, and CCT, suppresses aggregation-associated proteotoxicity in numerous neurodegenerative disease models (31–35). Moreover, a number of small-molecule proteostasis regulators, including the natural product celastrol (25), function by activating HSF-1 (heat shock factor 1), leading to cytoplasmic chaperone up-regulation, lending support to the idea that it is possible to “naturally” rebalance proteostasis.

Restoring Proteostasis in Metabolic Diseases

Proteostasis defects that arise from ER folding deficiencies may be at the core of metabolic syndrome and type II diabetes (36). In the leptin-deficient ob/ob mouse model of severe obesity and

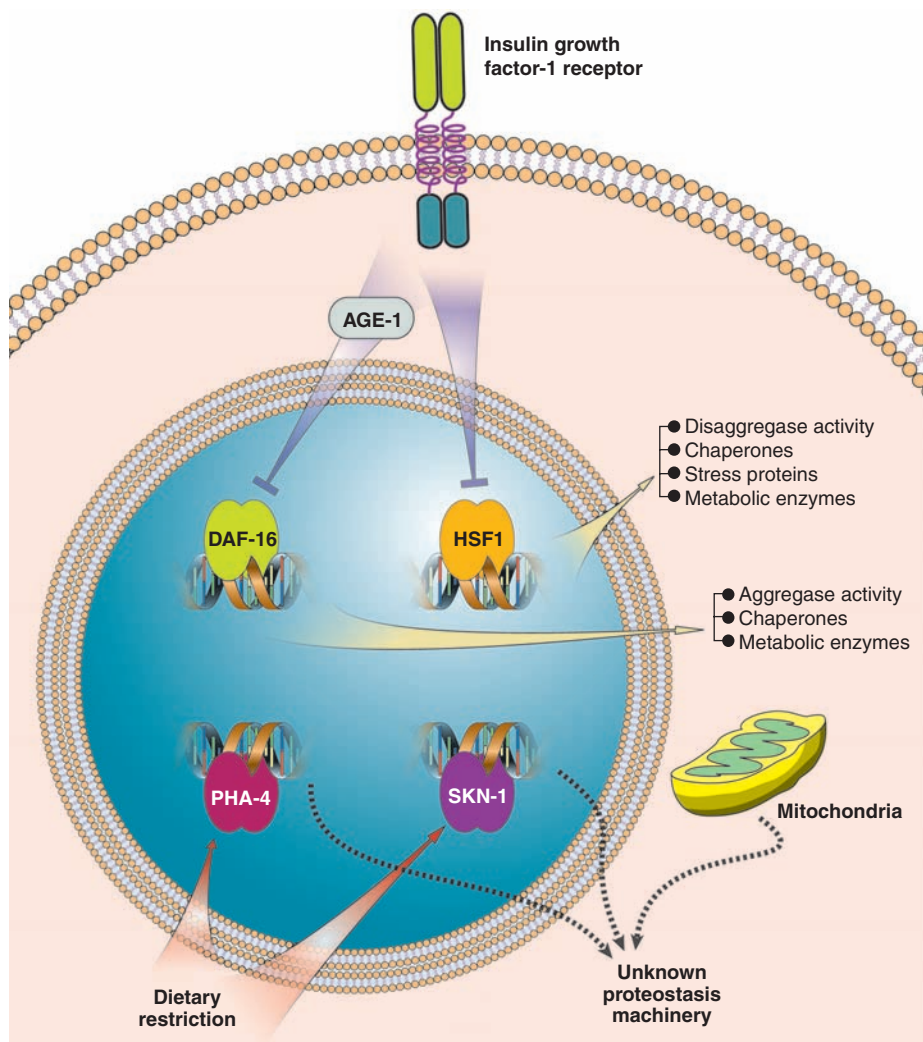


Fig. 3. Signaling pathways that control longevity and youthfulness strongly influence proteostasis. The insulin growth factor-1 receptor signaling pathway negatively regulates the activity of the transcription factors DAF-16 and HSF-1. HSF-1 regulates the transcription of stress response proteins, including chaperones, as well as a protein disaggregase activity. DAF-16 also mediates chaperone expression and appears to regulate an active aggregase activity. The dietary restriction pathway is known to suppress proteotoxicity in rodent models, which suggests that this pathway(s) (40, 41) also influences proteostasis. In a fourth mechanism, a decline in the flux through the mitochondrial electron transport chain results in extended life span; however, the links to proteostasis, if any, are unknown.

insulin resistance, the complex disease-associated traits are ameliorated by enhancing ER folding capacity using 4-phenylbutyrate (4-PBA) and taurine-conjugated ursodeoxycholic acid (36). Oral administration of these small molecules reversed hyperglycemia, increased glucose tolerance, decreased stress inside the ER in response to misfolding, and improved insulin receptor signaling. Notably, lipid accumulation in the liver also is resolved (36). 4-PBA has been used to partially restore the proteostasis of many misfolding-prone soluble and transmembrane proteins traversing the exocytic pathway, including CFTR, where it is currently being tested in clinical trials to treat cystic fibrosis (24). Although the term “chemical chaperone” has been used as a catch-all category for compounds of unknown mechanism of action like 4-PBA (37) and compounds that clearly influence folding by acting as osmolytes, it is likely that molecules used in this study (including 4-PBA) fall in the proteostasis regulator category mechanistically, that is, they re-adjust the biological folding and trafficking machinery to increase insulin and insulin receptor folding and trafficking, known to play a major role in metabolic syndrome and type II diabetes.

Decreasing Folding/Trafficking Capacity as a Therapeutic Strategy for Infectious Diseases and Cancer

Manipulation of the proteostasis network by mammalian viruses represents an ancient requirement. Protein folding and trafficking down-regulation may prevent the occurrence of resistance in viral disease because enhanced folding and trafficking capacity is required for viral replication and assembly. For example, coadministration of Hsp90 inhibitors with antiviral drugs prevented the appearance of drug-resistant poliovirus strains in cell culture (38). Using proteostasis down-regulators that selectively target the folding of viral proteins or the synthesis of bacterial proteins that confer resistance may provide a general antiviral/antibacterial strategy by enabling control over the evolution of drug resistance (38).

A number of lines of evidence suggest that rapidly proliferating tumor cells require an increased protein folding and trafficking capacity to maintain basic physiology (39). Chaperone inhibitors, especially Hsp90 inhibitors, decrease cell proliferation in animal models, possibly by diminishing folding capacity, and are currently in phase II clinical trials for cancer (24). Thus, the facilitation of pathogen propagation and resistance, as well as proliferation of cancer cells by a high proteostasis capability, may be the principal reason that proteostasis capacity is closely matched to demand in most cells (13, 39), but this does not mean that restoring

the decreased proteostasis capacity in the aged to normal young-adult levels will predispose one to disease.

Slowing the Emergence of Complex Age-Onset Diseases

Aging challenges proteome homeostasis because of decreasing cellular proteostasis capacity and increasing protein damage (14–17). Given the central role of the proteome in physiology, proteostasis regulators may alleviate some of the defects facing the proteome of aged individuals and indirectly delay the onset of complex diseases of unknown etiology, such as a subset of autoimmune diseases and disorders like inclusion body myositis. Perhaps more intriguing is the possibility that restoring proteostasis capabilities to young-adult levels could reverse age-dependent imbalances that have very subtle phenotypes. In support of this idea, up-regulating proteostasis activities by the HSF-1 and DAF-16 transcription factors results in both an increased longevity of worms harboring misfolding-prone proteins and an increased ability to prevent aggregation-associated proteotoxicity (6, 20). Even if longevity is not increased in humans, restoring or maintaining proteostasis should increase the quality of life by delaying the onset and/or decreasing the impact of late-onset diseases.

Outlook

Alterations in the chemistry and biology of proteostasis, mediated by proteostasis regulators, are now established to ameliorate loss- and gain-of-function phenotypes in patient-derived cell lines or in organismal models of human diseases. The data show that the innate pathways composing the cellular proteostasis network can be rebalanced to slow the age-dependent decline in proteostatic control, preventing disease. Unlike pharmacological chaperones and kinetic stabilizers, which are protein and disease specific, one proteostasis regulator can reestablish proteostasis in multiple related diseases, as demonstrated by their efficacy in several lysosomal storage disease cell lines. Proteome repair, mediated by proteostasis regulators, has the potential to change the practice of medicine.

References and Notes

1. Y.-C. Tang, H.-C. Chang, M. Hayer-Hartl, F. U. Hartl, *Cell* **128**, 412 (2007).
2. D. Ron, P. Walter, *Nat. Rev. Mol. Cell Biol.* **8**, 519 (2007).
3. R. L. Wiseman, E. T. Powers, J. N. Buxbaum, J. W. Kelly, W. E. Balch, *Cell* **131**, 809 (2007).
4. E. D. Werner, J. L. Brodsky, A. A. McCracken, *Proc. Natl. Acad. Sci. U.S.A.* **93**, 13797 (1996).
5. C. Queitsch, T. A. Sangster, S. Lindquist, *Nature* **417**, 618 (2002).
6. E. Cohen, J. Bieschke, R. M. Perciavalle, J. W. Kelly, A. Dillin, *Science* **313**, 1604 (2006).
7. R. I. Morimoto, *Genes Dev.* **12**, 3788 (1998).

8. B. Bukau, J. Weissman, A. Horwich, *Cell* **125**, 443 (2006).
9. J. Q. Fan, S. Ishii, N. Asano, Y. Suzuki, *Nat. Med.* **5**, 112 (1999).
10. P. Hammarstrom, R. L. Wiseman, E. T. Powers, J. W. Kelly, *Science* **299**, 713 (2003).
11. S. D. Westerheide, R. I. Morimoto, *J. Biol. Chem.* **280**, 33097 (2005).
12. M. Schroder, R. J. Kaufman, *Annu. Rev. Biochem.* **74**, 739 (2005).
13. T. Gidalevitz, A. Ben-Zvi, K. H. Ho, H. R. Brignull, R. I. Morimoto, *Science* **311**, 1471 (2006).
14. Q. Zhang *et al.*, *Proc. Natl. Acad. Sci. U.S.A.* **101**, 4752 (2004).
15. A. C. Massey, R. Kiffin, A. M. Cuervo, *Cell Cycle* **5**, 1292 (2006).
16. R. R. Erickson, L. M. Dunning, J. L. Holtzman, *J. Geront. A: Biol. Sci. Med. Sci.* **61A**, 435 (2006).
17. B. K. Derham, J. J. Harding, *Biochem. J.* **328**, 763 (1997).
18. F. E. Cohen, J. W. Kelly, *Nature* **426**, 905 (2003).
19. B. H. Qu, E. H. Strickland, P. J. Thomas, *J. Biol. Chem.* **272**, 15739 (1997).
20. J. F. Morley, H. R. Brignull, J. J. Weyers, R. I. Morimoto, *Proc. Natl. Acad. Sci. U.S.A.* **99**, 10417 (2002).
21. J. F. Morley, R. I. Morimoto, *Mol. Biol. Cell* **15**, 657 (2004).
22. C. Kenyon, *Cell* **120**, 449 (2005).
23. A. Hsu, C. T. Murphy, C. Kenyon, *Science* **300**, 1142 (2003).
24. www.clinicaltrials.gov.
25. S. D. Westerheide *et al.*, *J. Biol. Chem.* **279**, 56053 (2004).
26. M. Boyce *et al.*, *Science* **307**, 935 (2005).
27. X. Wang *et al.*, *Cell* **127**, 803 (2006).
28. E. Fiebigler *et al.*, *Mol. Biol. Cell* **15**, 1635 (2004).
29. T.-W. Mu, D. M. Fowler, J. W. Kelly, *PLoS Biol.* **6**, e26 (2008).
30. T. E. Golde, D. Dickson, M. Hutton, *Curr. Alzheimer Res.* **3**, 421 (2006).
31. P. K. Auluck, H. Y. Chan, J. Q. Trojanowski, V. M. Lee, N. M. Bonini, *Science* **295**, 865 (2002).
32. Y. Namba, M. Tomonaga, K. Ohtsuka, M. Oda, K. Ikeda, *Brain Nerve* **43**, 57 (1991).
33. S. Tam, R. Geller, C. Spiess, J. Frydman, *Nat. Cell Biol.* **8**, 1155 (2006).
34. A. Kitamura *et al.*, *Nat. Cell Biol.* **8**, 1163 (2006).
35. C. Behrends *et al.*, *Mol. Cell* **23**, 887 (2006).
36. U. Ozcan *et al.*, *Science* **313**, 1137 (2006).
37. X. L. Liu *et al.*, *J. Am. Soc. Nephrol.* **15**, 1731 (2004).
38. R. Geller, M. Vignuzzi, R. Andino, J. Frydman, *Genes Dev.* **21**, 195 (2007).
39. C. Dai, L. Whitesell, A. B. Rogers, S. Lindquist, *Cell* **130**, 1005 (2007).
40. S. H. Panowski *et al.*, *Nature* **447**, 550 (2007).
41. N. A. Bishop, L. Guarente, *Nature* **447**, 545 (2007).
42. We thank D. Fowler, A. Murray, C. Fearn, L. Wiseman, and E. Powers for their critical comments on the manuscript, and E. Powers and J. Zhu for help with the figures. Discussions about proteostasis with S. Lindquist, U. Hartl, P. Walter, A. Horwich, J. Brodsky, and J. Frydman helped clarify our thinking. We appreciate support from NIH (DK46336, NS50636, DK75295, AG04342, AG 18917, GM38109, and AG026647); the Skaggs Institute of Chemical Biology; and the Lita Annenberg Hazen, Bundy, Ellison, and McKnight Foundations, whose collective support enabled the research that led to the ideas outlined here. J.K. is a founder of, holds equity in, and has a paid consulting relationship with FoldRx Pharmaceuticals, Inc., a biotechnology company that specializes in the discovery and development of drug therapies for diseases of protein misfolding and amyloidosis

10.1126/science.1141448

Emergence of Anoxia in the California Current Large Marine Ecosystem

F. Chan,^{1*} J. A. Barth,² J. Lubchenco,¹ A. Kirincich,² H. Weeks,³ W. T. Peterson,⁴ B. A. Menge¹

Eastern boundary current systems are among the most productive large marine ecosystems in the world. Their productivity arises from wind-driven upwelling of nutrient-rich water into the photic zones of coastal oceans and supports 20% of global fishery yield (1). Upwelling also transports oxygen-poor waters onto productive continental shelves, where respiration can further reduce water-column dissolved oxygen (DO) content and thus subject coastal ecosystems to the risk of hypoxia or anoxia.

Of the world's four major eastern boundary current systems, water-column shelf anoxia is previously known for only the Humboldt and Benguela Current systems (2). Because oxygen deficit can be a critical determinant of fishery, ecological, and biogeochemical processes (3, 4), the rise or expansion of hypoxia and anoxia represent major perturbations to the structure and functioning of coastal marine ecosystems. Here, we report the intensification of severe inner-shelf hypoxia (defined here as $\leq 0.5 \text{ ml l}^{-1}$) and the novel rise of water-column anoxia in the California Current large marine ecosystem (CCLME) along the U.S. West Coast.

Following changes in upwelling-favorable winds in 2006, we measured the emergence of anoxia along the central Oregon coast. Anoxia was evident in inner-shelf ($< 50 \text{ m}$) stations situated within 2 km of the surf zone (Fig. 1C). The onset of anoxia was accompanied by the expansion of severe hypoxia across broad sections of the central Oregon shelf. At its largest, hypoxia prevailed across all cross-shelf transect lines between 44.25°N and 45.00°N, extending from the shelf break to the inner shelf and encompassing at least 3000 km². Hypoxia was

also exceptional in its vertical and temporal extents, occupying up to 80% of the water column in shallow (60 m) shelf waters and persisting over mid- and inner-shelf waters from June to October.

Although severe hypoxia is a permanent feature of the oxygen minimum zone (OMZ) that intersects the continental slope ($> 600 \text{ m}$ in this system), there are no prior records of anoxia over the continental shelf or within the OMZ (Fig. 1A). In contrast to OMZ marine life that possess adaptations to severe oxygen stress (3), demersal fish and benthic invertebrate communities in these shallow shelf waters were acutely affected by seasonally persistent anoxia and severe hypoxia. In August 2006, submersible-based surveys along the same previously monitored (2000 to 2004) transect lines revealed the complete absence of all fish from rocky reefs that normally serve as habitats for diverse rockfish (*Sebastes* species) communities that are of current fishery management concern. Our surveys also revealed near-complete mortality of macroscopic benthic invertebrates and an accompanying rise of putative sulfide-oxidizing bacterial mats in shallow (50 m) waters (movie S1).

The rise of anoxia has occurred against a backdrop of recent increases in the frequency and severity of shelf hypoxic events in this system (Fig. 1B). Five decades of available records show little evidence of shelf hypoxia and no evidence of severe inner-shelf hypoxia before 2000 (Fig. 1A). Recent studies indicate that the onset of shelf hypoxia can reflect basin-scale fluctuations in atmosphere-ocean processes that alter the oxygen content of upwelled water, the intensity of upwelling wind stress, and productivity-driven increases in coastal respi-

ration (5, 6). Strongly coupled atmospheric and oceanic circulation underpins ecosystem dynamics in wind-driven upwelling shelves and ecosystem susceptibility to modulations of upwelling wind stress from climate warming (7, 8). The present-day global distribution of shelf anoxia reflects broad cross-system differences in vertical proximity to OMZs, shelf productivity, and circulation. The novel rise of shelf anoxia in the CCLME highlights the potential for rapid reorganization in the distribution of anoxia and the sensitivity of productive upwelling shelves to discontinuous ecosystem change.

References and Notes

1. D. Pauly, V. Christensen, *Nature* **374**, 255 (1995).
2. J. Helly, L. A. Levin, *Deep Sea Res.* **51**, 1159 (2004).
3. J. J. Childress, B. A. Seibel, *J. Exp. Biol.* **201**, 1223 (1998).
4. L. A. Levin, *Oceanogr. Mar. Biol. Annu. Rev.* **41**, 1 (2003).
5. B. A. Grantham *et al.*, *Nature* **429**, 749 (2004).
6. A. Bakun, S. J. Weeks, *Ecol. Lett.* **7**, 1015 (2004).
7. H. V. McGregor, M. Dima, H. W. Fischer, S. Mulitza, *Science* **315**, 637 (2007).
8. J. A. Barth *et al.*, *Proc. Natl. Acad. Sci. U.S.A.* **104**, 3719 (2007).
9. We thank M. Robart, W. Miller, S. Pierce, and J. Peterson for their assistance. This paper is contribution 273 of the Partnership for Interdisciplinary Studies of Coastal Oceans (PISCO; funded by the David and Lucile Packard Foundation and the Gordon and Betty Moore Foundation) and contribution 582 of the U.S. Global Ocean Ecosystem Dynamics program (funded by NSF and National Oceanic and Atmospheric Administration). Additional support was provided by NSF, the A. W. Mellon Foundation, the Wayne and Gladys Valley Foundation, and the Robert and Betty Lundeen Marine Biology Fund.

Supporting Online Material

www.sciencemag.org/cgi/content/full/319/5865/920/DC1
Movie S1

9 August 2007; accepted 28 November 2007
10.1126/science.1149016

¹Department of Zoology, Oregon State University, Corvallis, OR 97331, USA. ²College of Oceanic and Atmospheric Sciences, Oregon State University, Corvallis, OR 97331, USA. ³Oregon Department of Fish and Wildlife, Newport, OR 97365, USA. ⁴Northwest Fisheries Science Center, National Oceanic and Atmospheric Administration, Newport, OR 97365, USA.

*To whom correspondence should be addressed. E-mail: chanft@science.oregonstate.edu

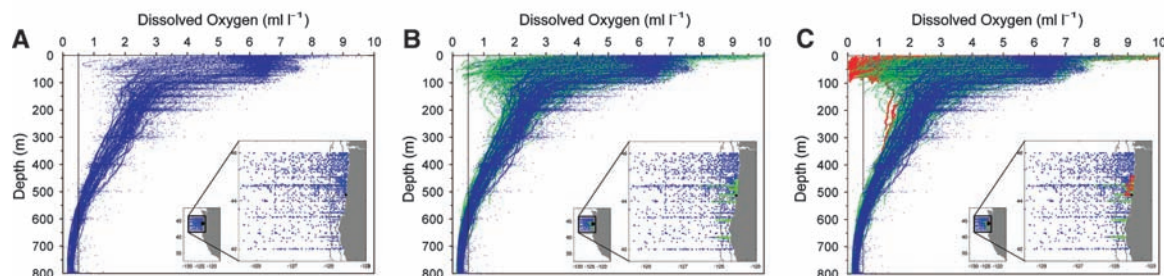


Fig. 1. Dissolved oxygen profiles during the upwelling season (mid-April to mid-October) in the upper 800 m of the continental shelf and slope of Oregon (42.00°N to 46.00°N). (A) 1950 to 1999 from the World Ocean Database and Oregon State University archives ($n = 3101$ hydrocasts, blue). (B) (A) with additional data for 2000 to 2005 ($n = 834$

hydrocasts, green). (C) (A) and (B) plus data for 2006 ($n = 220$ hydrocasts, red). The black vertical line denotes the 0.5 ml l^{-1} threshold. (Insets) Overlapping locations of hydrographic (blue, green, and red) and remotely operated vehicle (black) stations through time and the 100-m and 1000-m isobaths.

Identification of Host Proteins Required for HIV Infection Through a Functional Genomic Screen

Abraham L. Brass,^{1,2} Derek M. Dykxhoorn,^{3*} Yair Benita,^{4*} Nan Yan,³ Alan Engelman,⁵ Ramnik J. Xavier,^{2,4} Judy Lieberman,³ Stephen J. Elledge^{1†}

HIV-1 exploits multiple host proteins during infection. We performed a large-scale small interfering RNA screen to identify host factors required by HIV-1 and identified more than 250 HIV-dependency factors (HDFs). These proteins participate in a broad array of cellular functions and implicate new pathways in the viral life cycle. Further analysis revealed previously unknown roles for retrograde Golgi transport proteins (Rab6 and Vps53) in viral entry, a karyopherin (TNPO3) in viral integration, and the Mediator complex (Med28) in viral transcription. Transcriptional analysis revealed that HDF genes were enriched for high expression in immune cells, suggesting that viruses evolve in host cells that optimally perform the functions required for their life cycle. This effort illustrates the power with which RNA interference and forward genetics can be used to expose the dependencies of human pathogens such as HIV, and in so doing identify potential targets for therapy.

HIV-1 encodes only 15 proteins (1) and thus must exploit multiple host cell functions for successful infection (2). Viral entry depends on binding to the receptor CD4 and either of two co-receptors, CXCR4 or CCR5. Upon membrane fusion, the viral core, containing the viral capsid and nucleocapsid along with the viral genome, reverse transcriptase (RT), integrase (IN), protease (PR), and the viral accessory proteins Vif, Nef, and Vpr, is released into the cytoplasm. Collectively called the reverse transcription complex (RTC), this assembly binds to actin, triggering the synthesis of a double-stranded viral DNA complement that forms the preintegration complex (PIC), which moves along microtubules to the nucleus and enters via a nuclear pore.

IN binds to host lens epithelium-derived growth factor (LEDGF) and catalyzes HIV DNA integration. Proviral transcription depends on the viral factor Tat, which binds to the trans-activation response element (TAR) in the proviral RNA and promotes elongation by recruiting cyclin T1, HIV-1 Tat specific factor 1 (HTATSF1), and Cdk9. Unspliced and partially spliced HIV transcripts require the viral Rev protein for nuclear export. HIV buds directly from the plasma membrane through association with the host class E

Vps proteins (3). Because of the complexity of the retroviral life cycle and the small number of viral proteins, important viral-host relationships likely remain to be discovered. Toward this goal, we performed a genome-wide RNA interference screen to identify host factors involved in HIV-1 infection.

The siRNA screen. We developed a two-part screen to detect host proteins needed for HIV infection (Fig. 1A) (4). Part one consisted of infecting small interfering RNA (siRNA)-transfected cells with the IIIB strain of HIV-1 [HIV-IIIB (4); SOM Text] and 48 hours later staining for p24, produced from the HIV *gag* gene. This screen detects host proteins needed from viral entry through Gag translation, but is less sensitive for factors affecting viral assembly and budding. To identify late-acting factors, we performed part two by incubating culture supernatants from part one with fresh reporter cells and assaying for Tat-dependent reporter gene expression after 24 hours. For the screen, we used HeLa-derived TZM-bl cells, which express endogenous CXCR4, transgenic CD4, and CCR5, and an integrated Tat-dependent β -galactosidase (β -Gal) reporter gene. The screen was optimized with siRNAs against Tat, CD4, and Rab9p40; Rab9p40 is required for HIV particle release (5). siRNAs targeting CD4 or Tat produced a more than threefold decrease in p24 expression (Fig. 1, B and C). Only modest protection was seen upon Rab9p40 depletion (Fig. 1C, part one). However, after incubation of fresh TZM-bl cells with transferred cultured supernatant, the depletion of Rab9p40 scored convincingly (Fig. 1C, part two).

This platform was used for a genome-wide screen. The siRNA library contains 21,121 pools of four siRNAs per gene. Pools were classified as hits if they decreased the percentage of p24-positive cells or β -Gal activity by ≥ 2 SDs from the plate mean [table S2, column E (4)]. We also

required that the siRNAs did not decrease viable cells by >2 SDs. These criteria were met by 386 pools (1.8%). We next rescreened the four siRNAs from each pool separately. In this validation screen, 273 pools (71%) were confirmed with at least one siRNA scoring in either part one or two. There was a strong correlation between parts one and two. Only 28 genes appeared specifically in part two, suggesting that these factors act in late stages of infection (table S2, SOM Text).

HDF bioinformatics analysis. Of the confirmed HDFs, we identified 36 host factors (13%) previously implicated in HIV pathogenesis (table S1), including CD4, CXCR4, NMT1, Rab9p40, and components of the NF- κ B and CREB trans-activation pathways. Among the 237 remaining genes, more than 100 had two or more individual siRNAs score, reducing the likelihood of off-target effects (table S2). Subcellular localization, gene ontology (GO) biological processes, and molecular functions of the candidates are shown (Fig. 1, D and E; fig. S1, A and B; and table S3). One hundred and thirty-six GO biological process terms, assigned to 103 genes, were significantly enriched. Analysis of GO molecular functions identified enrichment for 17 nonredundant statistically significant terms assigned to 86 genes.

Several macromolecular complexes were also detected. The nuclear pore complex (NPC) Nup160 subcomplex had four of six subunits identified (Nup85, Nup107, Nup133, and Nup160). Because Nup160 subcomplexes are NPC scaffolds, their loss may impede HIV nuclear access (6). Depletion of components of Mediator (Med4, Med6, Med7, Med14, and Med28), which directly couples transcription factors to RNA polymerase II (Pol II) (7), inhibited infection, perhaps shedding light on the requirements for activators that bind the viral long terminal repeat (LTR). Two endoplasmic reticulum (ER)-Golgi-associated assemblages, the conserved oligomeric Golgi (COG) complex (8), and the transport protein particle (TRAPP) I complex (9), also scored with multiple components, perhaps due to HIV's dependency on transmembrane glycoproteins for nuclear entry. Three of the late-acting HDFs found in part two, OST48, STT3A and DPM1, encode enzymes involved in glycosylation (10, 11). HIV Env requires glycosylation to be infectious (12). Early studies showed that glycosylation inhibitors prevent Env modification and blocked HIV fusion (13, 14).

Among the unexpected associations was autophagy, a process essential for the degradation and recycling of cellular components. Targeted substrates are encapsulated in membrane-bound autophagosomes by two protein conjugation pathways (15). HIV infection depended on the presence of members of both pathways [Atg7, Atg8 (GABARAPL2), Atg12, and Atg16L2]. In addition, lysosomal-associated

¹Department of Genetics, Center for Genetics and Genomics, Brigham and Women's Hospital, Howard Hughes Medical Institute, Harvard Medical School, Boston, MA 02115, USA.

²Gastrointestinal Unit, Massachusetts General Hospital, Harvard Medical School, Boston, MA 02114, USA. ³Immune Disease Institute and Department of Pediatrics, Harvard Medical School, Boston, MA 02115, USA. ⁴Center for Computational and Integrative Biology, Harvard Medical School, Boston, MA 02114, USA. ⁵Dana-Farber Cancer Institute, Division of AIDS, Harvard Medical School, Boston, MA 02115, USA.

*These authors contributed equally to this work.

†To whom correspondence should be addressed. E-mail: selledge@genetics.med.harvard.edu

HDFs (CLN3, and LapTM5) may also be required for autophagy.

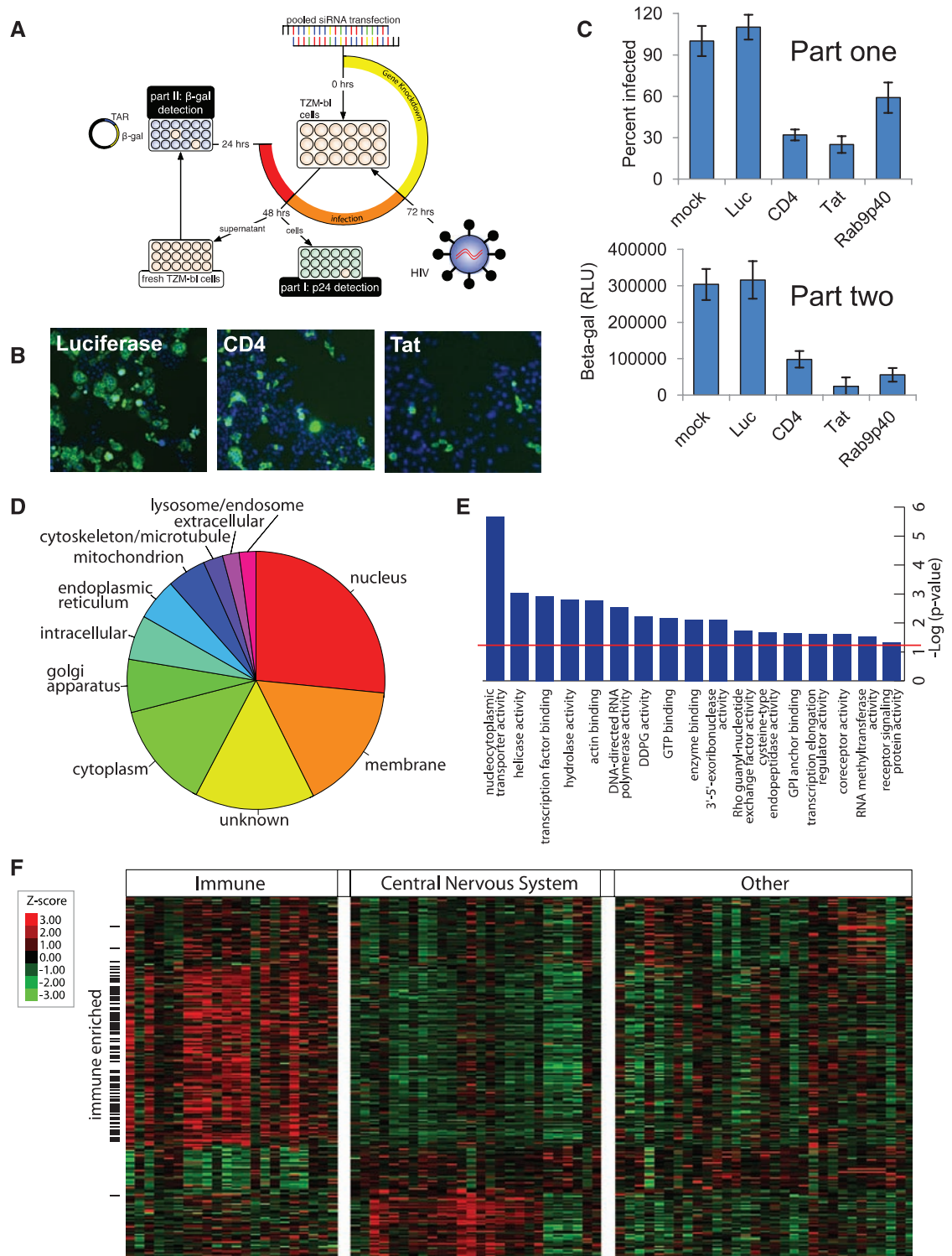
HeLa cells are not the natural host for HIV. We wondered whether HDFs showed an expression bias in other cell types that might explain HIV tropism. We assessed the expression of 239 genes that were expressed in at least one of the 79

tissues in the Genomic Institute of the Novartis Research Fund (GNF) data set and found that 79 of 239 (33%) were enriched for high expression in immune cells [$P < 0.001$, top 7% expression; Fig. 1F and table S3 (4)].

HIV entry requires retrograde vesicular transport. Rab6A regulates retrograde Golgi

transport and is important for recycling of Golgi-resident enzymes (16, 17). Three of four siRNAs were confirmed in the validation round for both Rab6A and Rab6A', which differ by three amino acids due to alternative splicing (table S2) (16). Rab6A' controls endosomal trafficking and is the homolog of the yeast Ypt6

Fig. 1. siRNA screen for HDFs required for HIV infection with bioinformatics analyses. **(A)** Schematic representation of the screen. Arrayed pools of siRNAs were transfected into TZM-bl cells in a 384-well format. After 72 hours, HIV-III_B virus was added, and 48 hours after infection, cultured supernatant was removed and added to fresh TZM-bl cells. In part one, 48 hours after infection, the siRNA transfected cells were fixed, permeabilized, stained, and imaged for HIV p24 protein and DNA. In part two, cells were cultured for 24 hours after the addition of supernatant, then lysed, exposed to a luminescent β -Gal substrate, and relative light units (RLU) recorded. **(B)** siRNAs against CD4 or Tat inhibit HIV infection (green: HIV p24; blue: cell nuclei). Magnification, $\times 4$. **(C)** Screen part one measuring p24 staining, and part two measuring infectious virus production with the indicated siRNAs. (Percent infected is relative to control throughout.) Values represent the mean \pm SD, $N \geq 4$. **(D)** Subcellular localization. Genes were manually curated on the basis of subcellular localization annotated in UniProt and GO. The localization for each protein is provided in table S3. **(E)** Molecular function analysis. The significance threshold is indicated by a red line at $1.3 = -\log(P = 0.05)$. DDPG, dolichyl-diphosphooligosaccharide-protein glycotransferase; GPI, glycosylphosphatidylinositol. **(F)** Expression profiles across 79 tissues (in duplicate) of 239 HDFs. Expression values for each probe set were Z-score-transformed across all arrays (table S3). Of the 239 probes in duplicate in GNF, 79 probes were significantly ($P < 0.05$) higher when expressed in immune tissues compared to all other tissues and are indicated by black bars on the left. Gene names and P -values are provided in table S3.



(16); both isoforms will hence be referred to as Rab6. Ypt6 mutants are defective in retrograde Golgi transport, particularly recycling of glycosyltransferases (17, 18). Depletion of the homolog of Rgp1p, a guanine nucleotide exchange factor required for Ypt6 function, also decreased HIV infection [table S2 (19)].

We generated cells stably expressing short hairpin RNA (shRNAs) directed against Rab6. All three shRNAs decreased infection proportional to Rab6 depletion (Fig. 2, A to C) in the first phase of the life cycle because Rab6 depletion inhibited Tat-dependent reporter expression 20 hours after infection (Fig. 2B). Expression of Rab6-GFP (green fluorescent protein) lacking the Rab6 3'-untranslated region targeted by the shRNAs rescued susceptibility to infection (Fig. 2, A to C, and fig. S2). Given Rab6's role in vesicular transport, we examined surface expression of CD4 and CXCR4 by fluorescence-activated cell sorting (FACS) in the Rab6 knockdown (Rab6-KD) lines. CXCR4 expression showed minor variations that did not correlate with resistance to HIV or Rab6 depletion and were not restored upon Rab6 repletion (fig. S3, A and B). CD4 levels were unaltered (fig. S3C). Thus, something other than receptor expression is defective in Rab6-KD cells.

To characterize the block to infection further, we infected Rab6-KD cells with either HIV-IIIIB or an HIV strain pseudotyped with the vesicular stomatitis virus G envelope protein (VSV-G), containing a yellow fluorescent protein (YFP) reporter in place of *nef* (HIV-YFP). Only HIV-IIIIB infection was inhibited (Fig. 2D). In addition, VSV-G-pseudotyped Moloney leukemia virus-enhanced GFP (MLV-EGFP) infection was unperturbed. HIV envelope proteins promote fusion of the virus to the cell membrane. In contrast, VSV-G pseudotypes are endocytosed, with endosomal acidification triggering fusion. Thus, our initial observations suggested that Rab6 acted early in infection. HIV-IIIIB has tropism for the co-receptor CXCR4. To determine whether inhibition was restricted to CXCR4 virus, we examined the effect of Rab6 silencing on infection with HIV-Bal, a CCR5-tropic virus. Targeting Rab6 did not alter surface CCR5 expression (fig. S3G), but did inhibit HIV-Bal infection (Fig. 2E). Therefore, Rab6 plays a role in infection by both CCR5 and CXCR4 viruses.

Rab6 was required for late reverse transcription of the viral genome, indicating an early block (Fig. 2F). We therefore tested Rab6's role in fusion by coculturing HL2/3 HeLa cells, which express Tat and HIV receptor proteins gp41 and gp120, with T2M-bl cells. HL2/3 viral receptors interact with CD4 and CXCR4 on T2M-bl cells, prompting cellular fusion via the same mechanism used by HIV. Upon fusion, Tat activates β -Gal expression. Decreased Rab6 levels correlated with diminished β -Gal activity, consistent with inhibition of viral fusion [Fig. 2G and fig. S4C (4)]. To test Rab6's role in HIV infection in a more physiological cell, we trans-

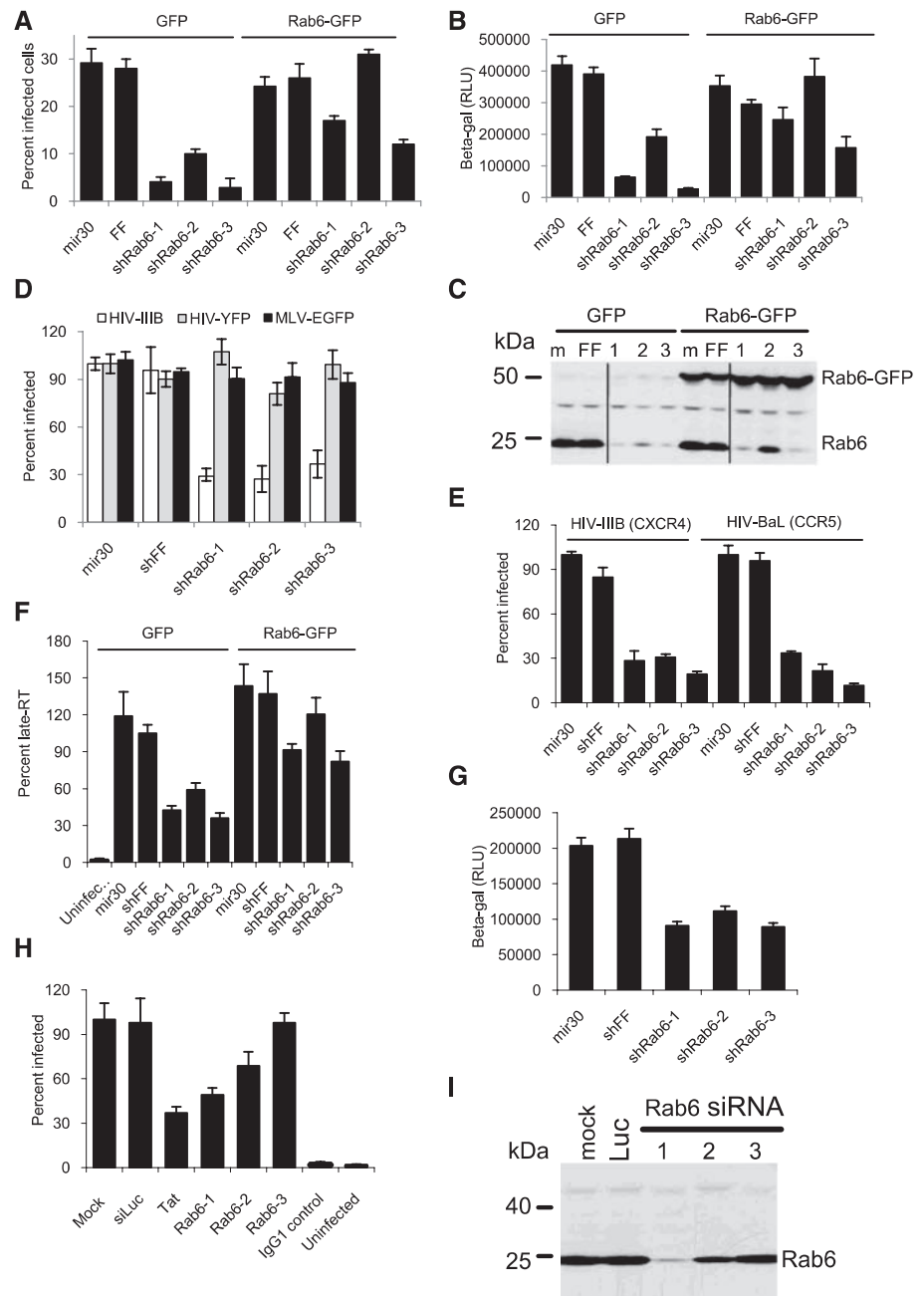


Fig. 2. Rab6-depleted cells resist HIV infection. (A and B) T2M-bl HeLa cells stably expressing the indicated shRNAs, and either the control green fluorescence protein (GFP) or a Rab6-GFP fusion (Rab6-GFP), were infected with HIV-IIIIB and analyzed for (A) p24 at 48 hours after infection or (B) Tat-dependent β -Gal expression at 20 hours after infection. Empty vector (mir30), firefly luciferase (FF), shRNAs against Rab6 (shRab6-1, 2, and 3). Values represent the mean \pm SD, $N \geq 3$. (C) Western blots for Rab6 and Rab6-GFP levels for cells shown in (A) and (B). (D) Rab6 depletion specifically inhibits WT-enveloped HIV. The indicated cell lines were infected with either HIV-IIIIB, VSV-G pseudotyped HIV-YFP, or MLV-EGFP. Infection was monitored by immunofluorescence (IF) of p24 (HIV-IIIIB) or the reporter genes (EGFP, YFP) at 48 hours after infection. Percent infected cells is relative to control throughout. (E) HIV infection via either the CXCR4 or CCR5 co-receptor is attenuated by Rab6 depletion. Cells were infected with either HIV-IIIIB or HIV-Bal and p24 stained at 48 hours after infection. (F) Rab6 depletion blocks HIV before late reverse transcription. Cell lines indicated were infected with HIV-IIIIB, and the late reverse transcription products (late RT) were assessed by qPCR. Percent late-RT product is relative to control. (G) Rab6 loss inhibits cell fusion. The indicated T2M-bl cell lines containing a Tat-dependent β -Gal reporter were layered for 6 hours with HL2/3 cells expressing HIV-1 Env and Tat proteins. The relative amount of cell fusion was quantified by assaying β -Gal activity. (H) Rab6 depletion protects T cells from HIV. Jurkat cells were transfected with the indicated siRNAs for 72 hours, then infected with HIV and analyzed by FACS with antibodies to either p24 (anti-p24) or an isotype matched control (immunoglobulin G1, IgG1) antibody at 48 hours after infection. (I) Cells from (H) were examined for Rab6 protein by Western blotting.

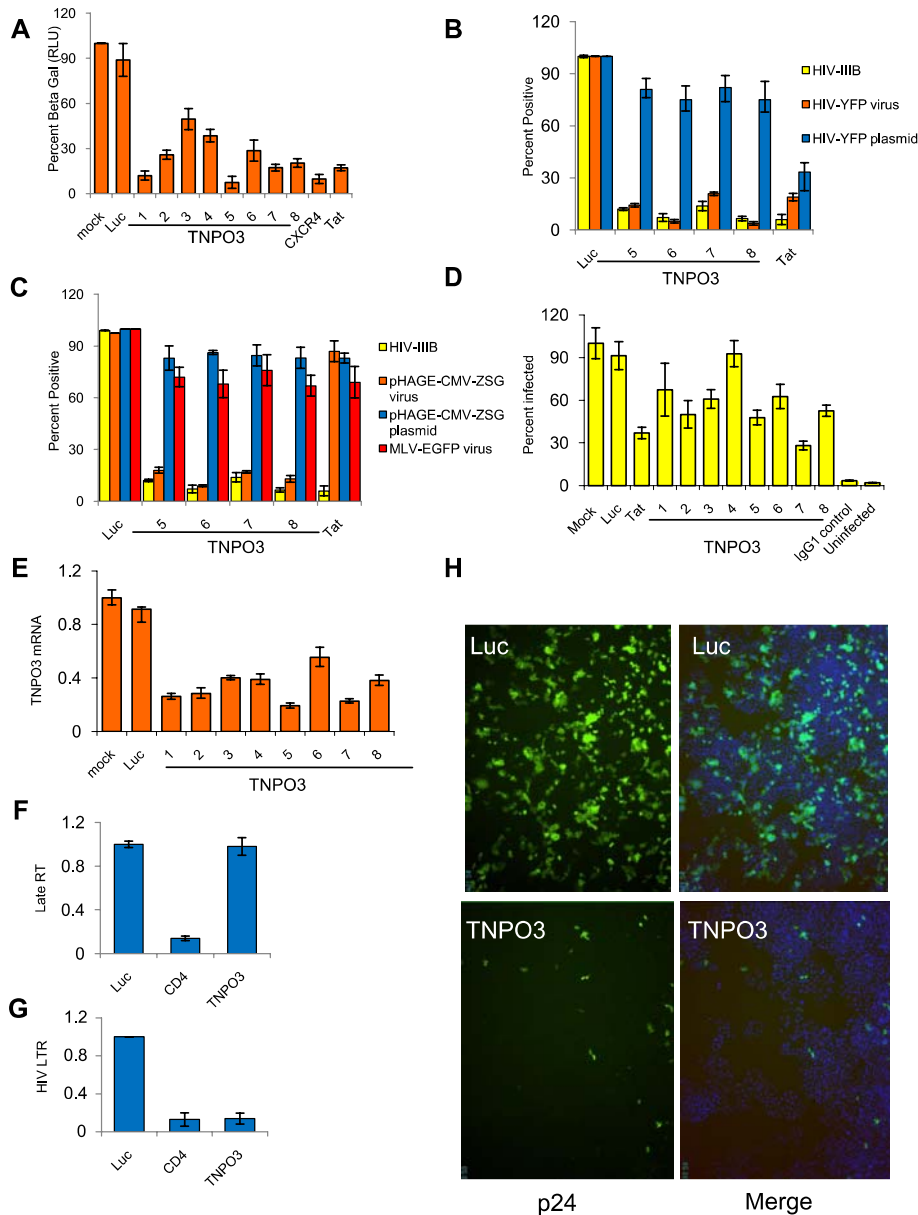


Fig. 3. TNPO3 is required for HIV infection. (A) Cells were transfected with the indicated siRNAs for 72 hours, then infected with HIV-IIIB. After 20 hours, β -Gal activity was measured. Values represent the mean \pm SD, $N \geq 3$ throughout. (B) Cells were transfected with the indicated siRNAs for 72 hours, then infected with either HIV-IIIB or pseudotyped HIV-YFP, or transfected with the HIV-YFP plasmid. After 48 hours, the percentage of positive cells was determined by p24 (HIV-IIIB) or YFP expression (HIV-YFP virus and plasmid). (C) TNPO3 depletion preferentially affects lentiviruses. T2M-bl cells were transfected with the indicated siRNAs for 72 hours, then infected with the indicated viruses or transfected with the Tat-independent pHAGE-CMV-ZSG plasmid. After 48 hours, levels of p24, ZSG, or EGFP were measured. (D) TNPO3 depletion protects T cells from HIV. Jurkat cells were transfected with the indicated siRNAs for 72 hours, then infected with HIV-IIIB and analyzed by FACS with either anti-p24 or an isotype control antibody at 48 hours after infection. (E) TNPO3 mRNA reduction by siRNAs. T2M-bl cells were transfected with the indicated siRNAs for 72 hours, then cDNA was prepared and TNPO3 expression levels were measured by qPCR. (F and G) TNPO3 depletion inhibits HIV after reverse transcription, but before integration. T2M-bl cells were transfected with the indicated siRNAs (TNPO3, siRNAs 5 to 8 pooled) and infected with HIV 72 hours later. Late RT levels were assessed by qPCR, and integrated viral DNA (HIV LTR) was quantified by nested Alu-PCR. (H) IF images showing the block to HIV infection with loss of TNPO3. Cells were treated as described in (B), with either the luciferase (Luc), negative control siRNA; or TNPO3, siRNA #8 targeting TNPO3. "Merge" denotes the combined image for nuclei (blue) and HIV p24 (green).

fecting a T cell line, Jurkat, with Rab6 siRNAs, then infected the cells with HIV. Reduced infection was seen after transfection with two of three Rab6 siRNAs tested (Fig. 2H), correlating with Rab6 depletion (Fig. 2I). No effect on receptor levels was observed in the transfected T cells (fig. S3, E and F).

Similar results were obtained for Vps53 (figs. S4, A to F, and S5). Yeast Vps53 is a component of the Golgi-associated retrograde protein (GARP) complex. GARP targets transport vesicles trafficking from endosomes to the trans-Golgi network in a Ypt6-dependent manner (20–23). Together, these data suggest that retrograde vesicular trafficking is needed for HIV infection, possibly at viral entry.

A role for a karyopherin in HIV replication.

Transportin 3 (TNPO3), a karyopherin, imports multiple proteins into the nucleus, including histone mRNA stem-loop binding protein [SLBP (24)], serine/arginine-rich proteins (SR proteins) that regulate splicing of mRNA (25), and repressor of splicing factor [RSF1 (26)]. Eight of eight TNPO3 siRNAs lowered infection in HeLa cells (Fig. 3, A and H). TNPO3 mRNA reduction, as determined by quantitative polymerase chain reaction (qPCR), correlated with the inhibition of infection (Fig. 3E). Prevention of infection by TNPO3 silencing was independent of HIV envelope (Fig. 3B). TNPO3 depletion also inhibited infection of Jurkat cells (Fig. 3D).

TNPO3 depletion did not significantly affect MLV-EGFP (Fig. 3C). This could be explained if TNPO3 depletion impaired SR protein-dependent splicing of Tat, which is required for efficient HIV, but not γ -retroviral, transcription. However, Tat-dependent reporter gene expression from a transiently transfected HIV-YFP plasmid was only weakly affected by TNPO3 depletion (Fig. 3B). Additionally, an HIV derivative, pHAGE-CMV-ZSG, that contains HIV Gag and Pol, but expresses a fluorescent reporter protein from an internal CMV promoter, also showed a dependency on TNPO3 upon viral infection, but not plasmid transfection (Fig. 3C).

These observations suggest that TNPO3 is needed before viral mRNA splicing. Assays for late RT products and integrated viral DNA in TNPO3-depleted cells showed that the block occurred after reverse transcription but before integration (Fig. 3, F and G). Thus, diminished TNPO3 produces a lentiviral-specific preintegration block, perhaps at the stage of PIC nuclear import. Whether TNPO3 directly interacts with the virus or indirectly, via altered import or splicing of an HDF required for integration, remains to be determined.

The Mediator complex in HIV infection.

Depletion of several components of Mediator inhibited HIV infection. We focused on Med28 because all four Med28 siRNAs inhibited first-round HIV infection (Fig. 4A and fig. S6). Med28 depletion also protected Jurkat cells and

efficiently decreased target gene protein levels (Fig. 4, C and D). Loss of Med28 appeared to specifically affect HIV because it inhibited both HIV-IIIB and HIV-YFP, but not MLV (Fig. 4B). We found no decreases in reverse-transcribed cDNA or integrated proviral DNA upon Med28 depletion (Fig. 4, E and F). However, Med28 loss also decreased YFP expression from a transiently transfected HIV-YFP plasmid (Fig. 4G). Therefore, we conclude that Med28 is required for transcription of viral genes, consistent with its connection to RNA Pol II.

Discussion. Judging from the diverse cellular processes detected in our screen, the exploitation of host cell functions by HIV is extensive. The functional clustering and confirmation of HDFs provide internal validation for our screen and suggest that most of the 237 proteins identified with no previous links to

HIV are likely to play relevant roles in HIV pathogenesis. We have portrayed the HIV viral life cycle along with the presumed subcellular locations and functions of the novel and known HDFs in Fig. 5 [rationale provided in table S4 (4)].

Additional validation comes from the analysis of the enrichment of genes connected to known proteins implicated in HIV function. We find a strong enrichment for connectivity to this data set [fig. S7 and table S5 (4)]. Furthermore, although the screen was performed in HeLa cells, one-third of the confirmed HDFs were significantly enriched for high expression in immune cells. This suggests that immune cells are especially proficient for the functions HIV needs for optimal replication and became the selected host for that reason. It will be interesting to determine if the virus is especially reliant on this

set of proteins and whether the tropism of other viruses can be similarly explained.

Rab6 and Vps53 are required for viral fusion to the membrane through an unknown mechanism. Although we have ruled out alteration of host co-receptor cell surface expression, several alternative explanations exist. There could exist a previously undetected co-receptor, dependent on Rab6 and Vps53. The screen identified more than 30 transmembrane proteins with no known HIV association (table S2). Modification of host receptors may be aberrant. However, no modification of either CD4 or CXCR4 is known to be required for infection (27, 28). Alternatively, the plasma membrane composition may be affected, possibly due to alterations in the major supplier of membrane, the Golgi. Among the candidates affected by such a perturbation are the glycosphingolipids (GSLs), which are required for HIV-host cell fusion (29–31). GSLs are synthesized by ER and Golgi enzymes (32) that depend on retrograde vesicular transport for recycling (18, 33). Rab6/Ypt6 mutants are defective in retrograde Golgi transport, resulting in vesicular scattering and lysosomal degradation of many Golgi resident enzymes, possibly altering GSL homeostasis (18, 20) (SOM Text).

The HIV PIC accesses our genome through the NPC. A candidate for the PIC-associated karyopherin is TNPO3, depletion of which profoundly blocked provirus formation. This effect might be indirect if TPNO3 is required for the activity of another HDF. However, a simpler model involves the PIC binding to TNPO3, then entering the nucleus via interactions with two NPC proteins detected in the screen, RanBP2 and Nup153 (34). Although speculative, these are examples of the kinds of detailed hypotheses that can be generated from a highly validated, functionally derived data set.

A key pharmacological strategy for treating individuals living with HIV has been to simultaneously target multiple virus-encoded enzymes required for replication to overcome emergence of drug resistance. We have taken a parallel strategy by identifying host factors required for the HIV life cycle. Such proteins represent therapeutic targets that are not plagued by the twin problems of viral diversity and escape mutation that interfere with the effectiveness of conventional antiretroviral drugs. We anticipate that HIV would be hard-pressed to evolve resistance to drugs targeting cellular proteins, because it would have to evolve a new capability, not simply mutate a drug-binding site. This is analogous to blocking angiogenesis in nontumor cells to deprive cancer of a blood supply (35). Support for the notion that these HDFs may represent potential therapeutic targets arises in part from a recent genome association study reporting that single-nucleotide polymorphisms in ZNRD1 are associated with slowed HIV disease progression (36). Our screen found that ZNRD1 depletion inhibited HIV (table S2). This suggests that variants in other HDFs might modulate HIV in-

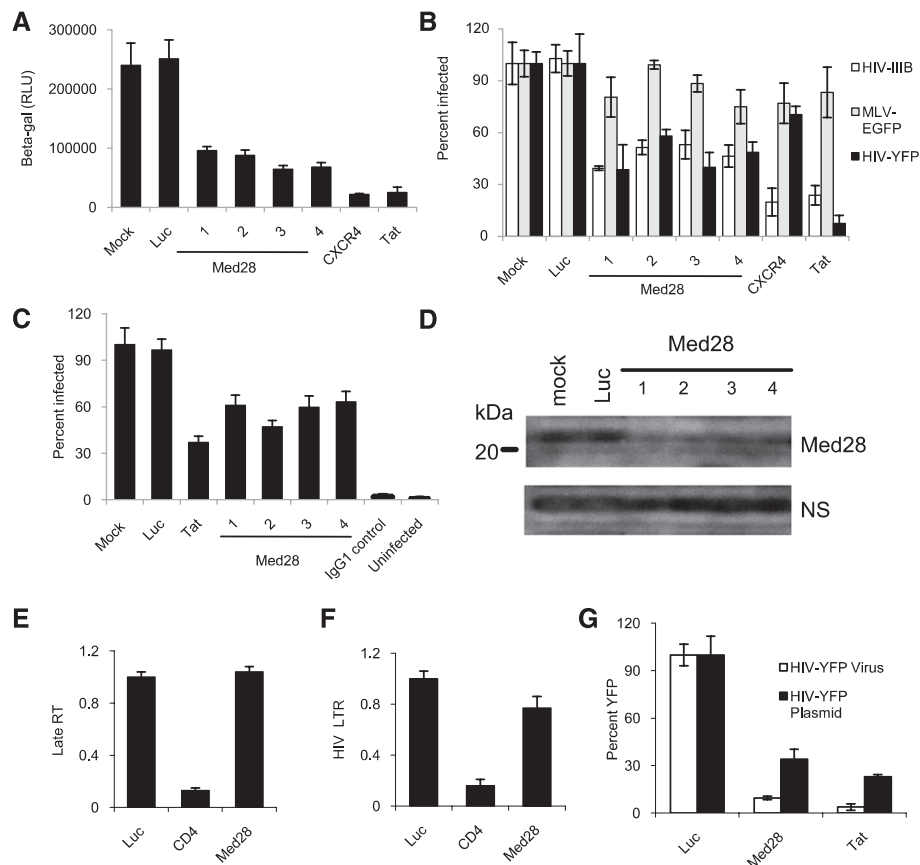


Fig. 4. Med28 silencing inhibits HIV replication. (A) Cells were transfected with the indicated siRNAs for 72 hours, then infected with HIV-IIIB. After 20 hours, β -Gal activity was measured. Values represent the mean \pm SD, $N \geq 3$, throughout. (B) Loss of Med28 inhibits WT-enveloped and VSV-G-pseudotyped HIV. T2M-bl cells were transfected with the indicated siRNAs, and then infected with the indicated viruses 72 hours after transfection. Infection was monitored by IF staining for p24 or reporter expression 48 hours after infection. (C and D) Med28 depletion protects T cells from HIV. Jurkat cells were transfected with the indicated siRNAs for 72 hours, then infected with HIV and analyzed by FACS with either anti-p24 or an isotype antibody control at 48 hours after infection. Jurkat cells from these cultures were also assessed for Med28 protein by Western blotting (D); NS, nonspecific band. (E and F) Med28 depletion inhibits HIV transcription. T2M-bl cells were transfected with the indicated siRNAs (Med28, siRNAs 1 to 4 pooled) and infected with HIV 72 hours later. Late RT product levels were assessed by qPCR (E), and integrated viral DNA (HIV LTR) was quantitated by nested Alu-PCR (F). (G) T2M-bl cells were transfected with the indicated siRNA pools for 72 hours, then infected with HIV-YFP virus or transfected with HIV-YFP plasmid. Levels of YFP reporter protein were monitored by IF 48 hours later.

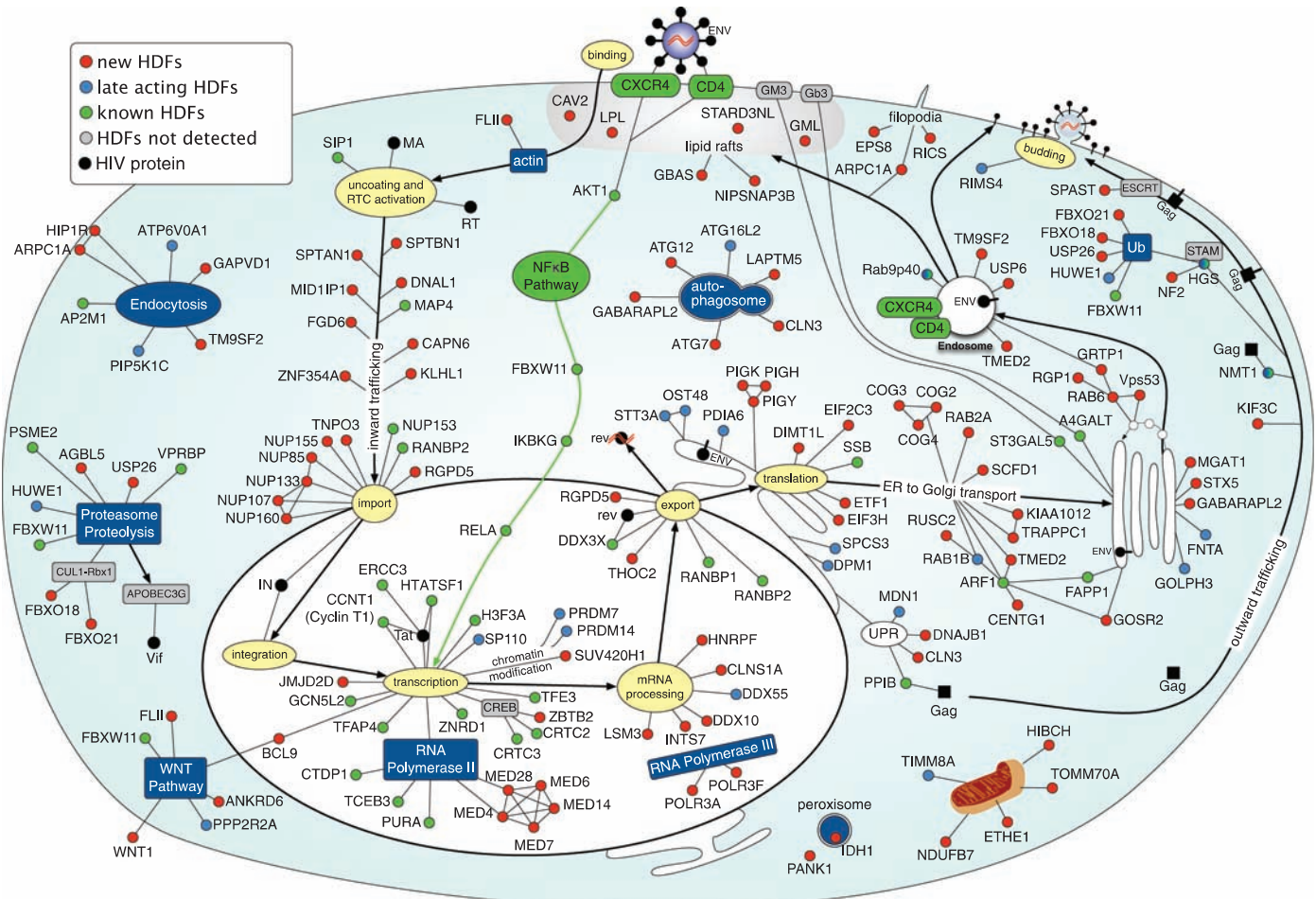


Fig. 5. Model of HDF roles in the HIV life cycle. With the stages of the HIV life cycle as a framework, each HDF was placed at the position most likely to elicit HIV dependency. The function and subcellular location of HDFs were determined with the use of multiple databases (rationale, table S4). Some proteins are in multiple locations to represent more than one possible role in

the HIV life cycle. Newly identified HDFs (red or blue, the latter if they inhibited HIV in part two only); previously implicated HDFs detected in the screen (green), or not detected but with a relevant interaction (gray); HIV protein (black): matrix (MA), reverse transcriptase (RT), integrase (IN), envelope (gp41, gp120) (ENV). Unfolded protein response, UPR.

fection, and drugs inhibiting their functions may prove protective.

References and Notes

1. A. D. Frankel, J. A. Young, *Annu. Rev. Biochem.* **67**, 1 (1998).
2. S. P. Goff, *Nat. Rev. Microbiol.* **5**, 253 (2007).
3. E. Morita, W. I. Sundquist, *Annu. Rev. Cell Dev. Biol.* **20**, 395 (2004).
4. Materials and methods are available as supporting material on Science Online.
5. J. L. Murray *et al.*, *J. Virol.* **79**, 11742 (2005).
6. A. Harel *et al.*, *Mol. Cell* **11**, 853 (2003).
7. R. D. Kornberg, *Trends Biochem. Sci.* **30**, 235 (2005).
8. D. Ungar, T. Oka, M. Krieger, F. M. Hughson, *Trends Cell Biol.* **16**, 113 (2006).
9. Y. G. Kim *et al.*, *Cell* **127**, 817 (2006).
10. H. Ashida, Y. Maeda, T. Kinoshita, *J. Biol. Chem.* **281**, 896 (2006).
11. D. J. Kelleher, R. Gilmore, *Glycobiology* **16**, 47R (2006).
12. T. Wolk, M. Schreiber, *Med. Microbiol. Immunol. (Berl.)* **195**, 165 (2006).
13. H. A. Blough *et al.*, *Biochem. Biophys. Res. Commun.* **141**, 33 (1986).
14. J. Balzarini, *Nat. Rev. Microbiol.* **5**, 583 (2007).
15. N. Mizushima, *Genes Dev.* **21**, 2861 (2007).
16. E. Del Nery *et al.*, *Traffic* **7**, 394 (2006).
17. A. Girod *et al.*, *Nat. Cell Biol.* **1**, 423 (1999).
18. Z. Luo, D. Gallwitz, *J. Biol. Chem.* **278**, 791 (2003).
19. S. Siniossoglou, S. Y. Peak-Chew, H. R. Pelham, *EMBO J.* **19**, 4885 (2000).
20. E. Conibear, T. H. Stevens, *Mol. Biol. Cell* **11**, 305 (2000).
21. N. R. Quenneville, T. Y. Chao, J. M. McCaffery, E. Conibear, *Mol. Biol. Cell* **17**, 1859 (2006).
22. S. Siniossoglou, H. R. Pelham, *EMBO J.* **20**, 5991 (2001).
23. S. Siniossoglou, H. R. Pelham, *J. Biol. Chem.* **277**, 48318 (2002).
24. J. A. Erkmann *et al.*, *Mol. Biol. Cell* **16**, 2960 (2005).
25. M. C. Lai, R. I. Lin, S. Y. Huang, C. W. Tsai, W. Y. Tarn, *J. Biol. Chem.* **275**, 7950 (2000).
26. E. Allemann, S. Dokudovskaya, R. Bordonne, J. Tazi, *Mol. Biol. Cell* **13**, 2436 (2002).
27. D. J. Chabot, H. Chen, D. S. Dimitrov, C. C. Broder, *J. Virol.* **74**, 4404 (2000).
28. J. Wang *et al.*, *Virology* **324**, 140 (2004).
29. P. Hug *et al.*, *J. Virol.* **74**, 6377 (2000).
30. A. Puri *et al.*, *AIDS* **18**, 849 (2004).
31. P. N. Nehete *et al.*, *Antiviral Res.* **56**, 233 (2002).
32. A. H. Futerman, H. Riezman, *Trends Cell Biol.* **15**, 312 (2005).
33. R. Conde, G. Pablo, R. Cueva, G. Larriba, *Yeast* **20**, 1189 (2003).
34. N. Sabri *et al.*, *J. Cell Biol.* **178**, 557 (2007).
35. J. Folkman, *Exp. Cell Res.* **312**, 594 (2006).
36. J. Fellay *et al.*, *Science* **317**, 944 (2007).
37. We thank the Institute of Chemistry and Cell Biology (ICCB)-Longwood: C. Shamu, S. Rudnicki, S. Johnston, D. Fletcher, K. Schulberg, and M. Tsui. We also thank F. Diaz-Griffero, J. Walsh, A. Balazs, R. Mulligan, R. Sutton, V. Ramesh, and A. Puri for reagents and guidance; B. Glick, G. Hu, E. R. McDonald III, A. Smorgorzewska, N. Solimini, M. Krishnan, and members of the Elledge lab for help and advice; A. Liao, A. Landry, and Z. Wu for technical assistance; and E. Golde for facilitating collaborations. Funding for this study was provided by a Crohns and Colitis Foundation of America fellowship (A.L.B.), a Center for Computational and Integrative Biology fellowship (Y.B.), and the Harvard Center for AIDS Research (CFAR) scholar award (N.Y.). J.L. (U19-AI056900), R.J.X. (AI062773), and A.E. (AI052014) are supported by NIH grants. D.M.D. was funded by a grant from the Harvard CFAR to J.L. and S.J.E. S.J.E. is an Investigator with the Howard Hughes Medical Institute.

Supporting Online Material

www.sciencemag.org/cgi/content/full/1152725/DC1
Material and Methods
SOM Text
Figs. S1 to S7
Tables S1 to S5
References

7 November 2007; accepted 21 December 2007
Published online 10 January 2008;
10.1126/science.1152725
Include this information when citing this paper.

Discovery of a Jupiter/Saturn Analog with Gravitational Microlensing

B. S. Gaudi,^{1*} D. P. Bennett,² A. Udalski,³ A. Gould,¹ G. W. Christie,⁴ D. Maoz,⁵ S. Dong,¹ J. McCormick,⁶ M. K. Szymański,³ P. J. Tristram,⁷ S. Nikolaev,⁸ B. Paczyński,^{9†} M. Kubiak,³ G. Pietrzyński,^{3,10} I. Soszyński,³ O. Szewczyk,³ K. Ulaczyk,³ Ł. Wyrzykowski,^{3,11} (The OGLE Collaboration); D. L. DePoy,¹ C. Han,¹² S. Kaspi,⁵ C.-U. Lee,¹³ F. Mallia,¹⁴ T. Natusch,⁴ R. W. Pogge,¹ B.-G. Park,¹³ (The μ FUN Collaboration); F. Abe,¹⁵ I. A. Bond,¹⁶ C. S. Botzler,¹⁷ A. Fukui,¹⁵ J. B. Hearnshaw,¹⁸ Y. Itow,¹⁵ K. Kamiya,¹⁵ A. V. Korpela,¹⁹ P. M. Kilmartin,⁷ W. Lin,¹⁶ K. Masuda,¹⁵ Y. Matsubara,¹⁵ M. Motomura,¹⁵ Y. Muraki,²⁰ S. Nakamura,¹⁵ T. Okumura,¹⁵ K. Ohnishi,²¹ N. J. Rattenbury,²² T. Sako,¹⁵ To. Saito,²³ S. Sato,²⁴ L. Skuljan,¹⁶ D. J. Sullivan,¹⁹ T. Sumi,¹⁵ W. L. Sweatman,¹⁶ P. C. M. Yock,¹⁷ (The MOA Collaboration); M. D. Albrow,¹⁸ A. Allan,²⁵ J.-P. Beaulieu,²⁶ M. J. Burgdorf,²⁷ K. H. Cook,⁸ C. Coutures,²⁶ M. Dominik,²⁸ S. Dieters,²⁹ P. Fouqué,³⁰ J. Greenhill,²⁹ K. Horne,²⁸ I. Steele,²⁷ Y. Tsapras,²⁷ (From the PLANET and RoboNet Collaborations); B. Chaboyer,³¹ A. Crocker,³² S. Frank,¹ B. Macintosh⁸

Searches for extrasolar planets have uncovered an astonishing diversity of planetary systems, yet the frequency of solar system analogs remains unknown. The gravitational microlensing planet search method is potentially sensitive to multiple-planet systems containing analogs of all the solar system planets except Mercury. We report the detection of a multiple-planet system with microlensing. We identify two planets with masses of ~ 0.71 and ~ 0.27 times the mass of Jupiter and orbital separations of ~ 2.3 and ~ 4.6 astronomical units orbiting a primary star of mass ~ 0.50 solar mass at a distance of ~ 1.5 kiloparsecs. This system resembles a scaled version of our solar system in that the mass ratio, separation ratio, and equilibrium temperatures of the planets are similar to those of Jupiter and Saturn. These planets could not have been detected with other techniques; their discovery from only six confirmed microlensing planet detections suggests that solar system analogs may be common.

Nearly 250 extrasolar planets (1) have been discovered by measuring a variety of effects: reflex motion of the host star using pulsar timing or precision Doppler measurements (2–4); periodic dimming of the parent star as the planet transits in front (5, 6); and planet-induced perturbations to microlensing light curves in which the host star acts as the primary gravitational lens (7–11). These detections have uncovered an enormous range of planetary properties, indicating that planetary systems very unlike our own are common throughout the Galaxy (12).

To date, ~ 25 multiple-planet systems have been detected (13), all but one (2) using the Doppler method. Because Doppler surveys must monitor the host star's reflex motion over the planet's orbital period, they are limited by the finite duration as well as the sensitivity of the measurements. Hence, they are only just now becoming sensitive to Jupiter analogs and are not yet sensitive to Saturn analogs (nor, ipso facto, Jupiter/Saturn systems). Thus, all multiple-planet systems discovered so far are very dissimilar from our own, and the frequency of solar system analogs remains unknown.

Because microlensing relies on the direct perturbation of light from distant stars by the gravitational field of the planet, it is “instantaneously” able to detect planets without requiring observations over a full orbit. For a primary star of mass M , microlensing sensitivity peaks for planets in the range $\sim [1-5](M/0.3 M_{\odot})^{1/2}$ astronomical units (AU) (14). For solar-mass stars, this is exactly the

range of the solar system gas giants, so microlensing provides a method to probe solar system analogs (14, 15).

As pointed out by Griest and Safizadeh (16), the very rare class of high-magnification (>100) microlensing events provides an extremely sensitive method of detecting planets. Near the peak of high-magnification events, the two images created by the primary star are highly magnified and distorted and form a complete or nearly complete Einstein ring. A planetary companion to the primary star lying reasonably near the Einstein ring will distort the symmetry of the ring. As the host passes very close to the source line-of-sight, the images sweep around the Einstein ring, thus probing this distortion. Although the total number of high-magnification events is small, the instantaneous chance of detection in each is much higher than for the more common low-magnification events. Equally important, the interval of high sensitivity (i.e., high magnification) is predictable from the evolution of the light curve (16–19). This permits concentration of scarce observing resources on these events. Furthermore, the high-magnification makes it possible to acquire high signal-to-noise ratio photometry of the peak of the events using relatively small-aperture (and so plentiful) telescopes. As a result, four (9, 11) of the six planets (8, 10) discovered to date in microlensing events were in high-magnification events.

Almost immediately after Griest and Safizadeh (16) pointed out the sensitivity of high-

magnification events, Gaudi *et al.* (20) derived an important corollary: Because planets in the neighborhood of the Einstein ring are revealed with near-unit probability in high-magnification events, multiple-planet systems lying in this region will be revealed with almost the same probability.

The Optical Gravitational Lens Experiment (OGLE) (21) and Microlensing Observations in Astrophysics (MOA) (19) collaborations together identify ~ 700 ongoing microlensing events per year. Two collaborations, a joint venture of the Probing Lensing Anomalies Network (PLANET) (22) and RoboNet (23) collaborations, and the Microlensing Follow-Up Network (μ FUN) (24),

¹Department of Astronomy, Ohio State University, 140 West 18th Avenue, Columbus, OH 43210, USA. ²Department of Physics, 225 Nieuwland Science Hall, Notre Dame University, Notre Dame, IN 46556, USA. ³Warsaw University Observatory, Aleje Ujazdowskie 4, 00-478 Warszawa, Poland. ⁴Auckland Observatory, Post Office Box 24-180, Auckland, New Zealand. ⁵School of Physics and Astronomy, Raymond and Beverley Sackler Faculty of Exact Sciences, Tel-Aviv University, Tel Aviv 69978, Israel. ⁶Farm Cove Observatory, 2/24 Rapallo Place, Pakuranga, Auckland 1706, New Zealand. ⁷Mt. John Observatory, Post Office Box 56, Lake Tekapo 8770, New Zealand. ⁸Institute of Geophysics and Planetary Physics, Lawrence Livermore National Laboratory, 7000 East Avenue, Livermore, CA 94550, USA. ⁹Princeton University Observatory, Princeton, NJ 08544, USA. ¹⁰Universidad de Concepción, Departamento de Física, Casilla 160-C, Concepción, Chile. ¹¹Institute of Astronomy, University of Cambridge, Madingley Road, Cambridge CB3 0HA, UK. ¹²Program of Brain Korea, Department of Physics, Chungbuk National University, 410 Seongbong-Rho, Hungduk-Gu, Cheongju 371-763, Korea. ¹³Korea Astronomy and Space Science Institute, 61-1 Hwaam-Dong, Yuseong-Gu, Daejeon 305-348, Korea. ¹⁴Campo Catino Astronomical Observatory, Guaricino, Frosinone 03016, Italy. ¹⁵Solar-Terrestrial Environment Laboratory, Nagoya University, Nagoya, 464-8601, Japan. ¹⁶Institute for Information and Mathematical Sciences, Massey University, Private Bag 102-904, Auckland 1330, New Zealand. ¹⁷Department of Physics, University of Auckland, Private Bag 92-019, Auckland 1001, New Zealand. ¹⁸University of Canterbury, Department of Physics and Astronomy, Private Bag 4800, Christchurch 8020, New Zealand. ¹⁹School of Chemical and Physical Sciences, Victoria University, Wellington, New Zealand. ²⁰Department of Physics, Konan University, Nishiokamoto 8-9-1, Kobe 658-8501, Japan. ²¹Nagano National College of Technology, Nagano 381-8550, Japan. ²²Jodrell Bank Centre for Astrophysics, The University of Manchester, Manchester M13 9PL, UK. ²³Tokyo Metropolitan College of Aeronautics, Tokyo 116-8523, Japan. ²⁴Department of Physics and Astrophysics, Faculty of Science, Nagoya University, Nagoya 464-8602, Japan. ²⁵School of Physics, University of Exeter, Stocker Road, Exeter EX4 4QL, UK. ²⁶Institut d'Astrophysique de Paris, Centre National de la Recherche Scientifique, Université Pierre et Marie Curie UMR7095, 98bis Boulevard Arago, 75014 Paris, France. ²⁷Astrophysics Research Institute, Liverpool John Moores University, Twelve Quays House, Egerton Wharf, Birkenhead CH41 1LD, UK. ²⁸Scottish Universities Physics Alliance, University of St. Andrews, School of Physics and Astronomy, North Haugh, St. Andrews KY16 9SS, UK. ²⁹University of Tasmania, School of Mathematics and Physics, Private Bag 37, Hobart, TAS 7001, Australia. ³⁰Observatoire Midi-Pyrénées, Laboratoire d'Astrophysique, UMR 5572, Université Paul Sabatier-Toulouse 3, 14 avenue Edouard Belin, 31400 Toulouse, France. ³¹Department of Physics and Astronomy, Dartmouth College, 6127 Wilder Laboratory, Hanover, NH 03755, USA. ³²University of Oxford, Denys Wilkinson Building, Keble Road, Oxford OX1 3RH, UK.

*To whom correspondence should be addressed. E-mail: gaudi@astronomy.ohio-state.edu
†Deceased.

then monitor a subset of these events to search for planets. μ FUN focuses almost entirely on high-magnification events, including two events originally identified by OGLE that proved to have a Jupiter-mass (9) and a Neptune-mass (11) planet, respectively. Here, we report on the detection of a multiplanet system using this approach.

On 28 March 2006 [heliocentric Julian day (HJD) \sim 3822], the OGLE Early Warning System (EWS) (21) announced OGLE-2006-BLG-109 as a nonstandard microlensing event possibly indicative of a planet. This immediately triggered follow-up observations by μ FUN and RoboNet, which gained intensity as the event approached high magnification. On 5 April, the event underwent a deviation from the single-lens form indicative of a binary lens. Within 12 hours of this deviation, a preliminary model indicated a jovian-class planet, which was predicted to generate an additional peak on 8 April. The 8 April peak occurred as predicted, but in the meantime, there was an additional peak on 5 to 6 April, which turned out to be due to a second jovian-class planet.

Figure 1 shows the data from 12 observatories, including 8 from μ FUN [the Auckland 0.35 m and Farm Cove 0.25 m in New Zealand (clear filter), the Wise 1 m in Israel (clear), the Cerro Tololo Inter-American Observatory (CTIO) Small and Moderate Aperture Research Telescope System (SMARTS) 1.3 m in Chile (*I*-band and *H*-band), the Aro8 0.3 m in New Mexico operated by the Campo Catino Astronomical Observatory (clear), and the MDM 2.4 m (*I*-band) and Mt. Lemmon 1.0 m (*I*-band) in Arizona], the OGLE Warsaw 1.3 m (*I*-band) in Chile, the MOA Mt. John 0.6 m (*I*-band) in New Zealand, the PLANET/Canopus 1 m (*I*-band) in Tasmania, and the RoboNet/Liverpool 2 m (*R*-band) in the Canary Islands. There are a total of 2642 data points. In addition, there are 29 V-band data points from OGLE and CTIO/SMARTS that we use to determine the source color.

The qualitative character of the event can be read directly from the light curve, primarily from the five distinctive features shown in Fig. 2. Consider the first three features: the low-amplitude anomaly (OGLE, HJD \sim 3823) that triggered the OGLE EWS alert, the gentle “shoulder” during the first rise (MOA, HJD \sim 3830), and the first peak (Auckland, HJD \sim 3831). Together, these can only be produced by, respectively, passage close to or over a weak cusp, entrance into a weak caustic, and exit from a strong caustic. (The magnification diverges when a point source crosses a closed concave caustic curve, where additional images are created on entry or destroyed on exit of the enclosed area. Caustics are strong or weak depending on the brightness of these images. The concave curves meet at cusps that produce sharp spikes of magnification when crossed by the source.) Such a sequence requires a topology similar to the one shown in the inset to Fig. 1. The specific strengths of each feature require the

specific caustic topology shown. In particular, the narrow mouth of the caustic toward the bottom generates a very strong caustic. This was essentially the argument used to predict the fifth feature (OGLE/MDM/Lemmon/Auckland/FarmCove/Tasmania, HJD \sim 3834), corresponding to a moderately strong cusp passage (Fig. 1). The size and strength of this caustic imply a jovian-class planet lying very close to the Einstein ring, although detailed modeling is required to derive the precise planet/star mass ratio. The fourth feature (Wise/OGLE, HJD \sim 3831.5) cannot be explained by considering the caustic generated by this jovian-class planet alone. This feature occurs near the time when the source approaches closest to the center-of-mass of the planet/star system; this is exactly the time at which the central-caustic bumps due to additional planets are expected to occur (20). The inset in Fig. 1 highlights the

additional caustic feature due to a second planet that is required to explain this bump. This caustic feature is smaller than the main caustic, which implies that the planet, also of jovian class, lies farther from the Einstein ring, so it is subject to the standard (16) $b \leftrightarrow b^{-1}$ degeneracy, where b is the planet-star projected separation in units of the Einstein radius. A detailed analysis shows the mass is three times as great as that of the first planet and that the $b < 1$ solution is favored by $\Delta\chi^2 = 11.4$. We label these planets OGLE-2006-BLG-109Lc and OGLE-2006-BLG-109Lb, respectively. Although the caustics of the individual planets do interact to form a single caustic curve, their effects are nevertheless mostly independent (25, 18, 26), so the parts of the caustic associated with the individual planets can be identified, as shown in Fig. 1. Modeling the light curve in detail with a three-body lens yields $m_b/M = 1.35 \times$

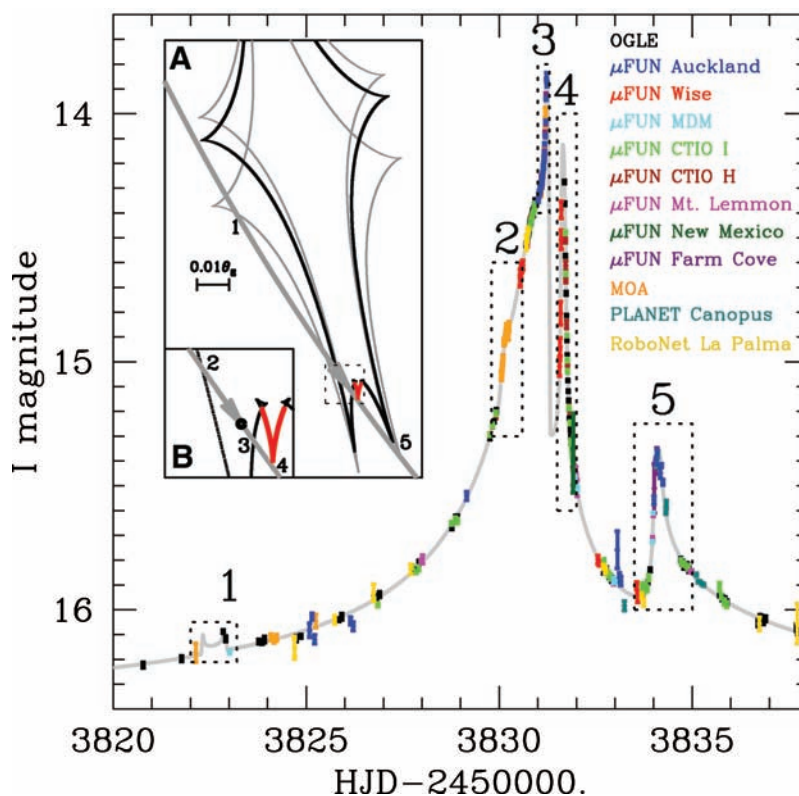


Fig. 1. Data and best-fit model of the OGLE-2006-BLG-109Lb,c two-planet system. The data have been binned for clarity, although the fitting procedures used the unbinned data. Data from each different observatory/filter combination (as indicated by the color scheme) have been aligned using a linear fit to the magnification, which introduces negligible uncertainties. Only data near the peak of the event are shown (the unlensed magnitude is $I = 16.42$). (A) The source trajectory through the caustic created by the two-planet system is shown as the dark gray curve with the arrow indicating the direction of motion. The horizontal line shows an angular scale of $0.01 \theta_E$ or $\sim 15 \mu\text{as}$. The shape and orientation of the caustic due to both planets at the peak of the event is shown by the black curve. The five light-curve features detailed in Fig. 2 are caused by the source crossing or approaching the caustic; the approximate locations of the features are labeled with numbers. The majority of the caustic (in black) is due to only the outer (Saturn-analog) planet; this portion of the caustic explains four of the five features. The portion arising from the second (Jupiter-analog) planet is highlighted in red. This additional cusp in the caustic is required to explain the fourth feature in the light curve; as such, the fourth feature signals the presence of a second (Jupiter-analog) planet. Because of the orbital motion of the Saturn-analog planet, the shape and orientation of the caustic changes over the course of the event. The light gray curves show the caustic at the time of features 1 and 5. (B) A zoom of the source trajectory and caustic near the times of the second, third, and fourth features. The circle shows the size of the source.

10^{-3} , $m_c/m_b = 0.36$ for the mass ratio of the planets and their host, very similar to $m_j/M_\odot = 0.96 \times 10^{-3}$ and $m_s/m_j = 0.30$ for Jupiter, Saturn, and the Sun. The ratio of projected separations $r_{\perp,b}/r_{\perp,c} = 0.60$ is also very similar to the Jupiter/Saturn value of $a_j/a_s = 0.55$.

Two subgroups of authors conducted independent searches for alternative solutions. Both found that no single-planet solution is consistent with the light-curve topology. We also successively eliminated each of the five features to see whether the remaining four features could be fit by a single planet. We found that only the elimination of the fourth feature produced successful single-planet models. By contrast, similar procedures in other events (11, 27) led to many independent solutions. OGLE-2006-BLG-109 differs from these in that it has five well-covered features.

Several higher-order effects are apparent in this event that permit us to extract much more detailed information about the system from the light curve. We only briefly sketch these here. For over 95% of microlensing events observed

from the ground, the lens parameters are determined only relative to the angular Einstein radius θ_E , whose absolute scale remains unknown. Here, $\theta_E = \sqrt{(4GM)/(c^2D)}$, where M is the mass of the lens, $1/D = 1/D_1 - 1/D_s$, and D_1 and D_s are the distances to the lens and the source, respectively. However, in this event the effect of the finite size of the source star during caustic exit allows us to measure the source radius relative to the Einstein radius, $\rho = \theta_*/\theta_E$ (28). From the source color and flux, we can determine its angular size θ_* , and thus θ_E (24).

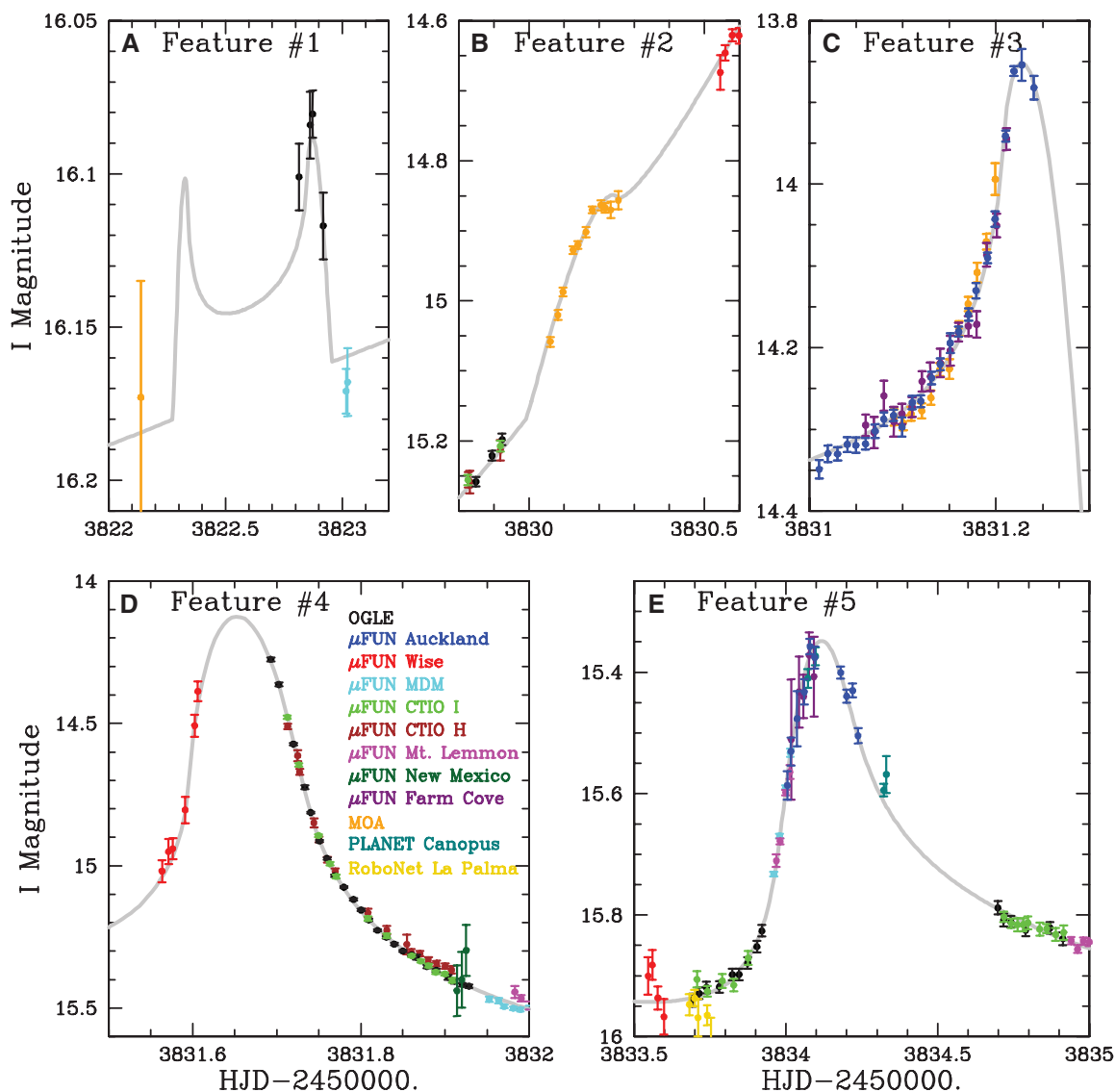
The acceleration of Earth in its orbit about the Sun induces subtle distortions on the light curve called microlens parallax, which yields the physical size of the Einstein radius projected onto the observer plane, $r_E = \theta_E D$ (29). This is usually measured only in the roughly 3% of events that are extremely long, but this event happens to be long and so displays clear distortions arising from parallax.

Combining these two measures of the Einstein radius allows us to triangulate the event and so determine the host star distance, $D_1 = 1/(\theta_E/r_E +$

$1/D_s)$, and mass, $M = (c^2/4G)r_E\theta_E$. We assume $D_s = 8$ kpc, although our results are insensitive to this assumption. From a preliminary analysis, we infer $D_1 \cong 1.5$ kpc and $M \cong 0.5 M_\odot$. Based on high-resolution Keck AO *H*-band images, we detect light from the lens and infer its magnitude to be $H = 17.17 \pm 0.25$, consistent with the mass estimate from the light curve. We subsequently incorporate the lens flux constraint in the light curve analysis, which allows us to derive more precise estimates of $D_1 = 1.49 \pm 0.13$ kpc and $M = 0.50 \pm 0.05 M_\odot$. The planet masses are $m_b = 0.71 \pm 0.08$ and $m_c = 0.27 \pm 0.03$ times the mass of Jupiter.

Finally, we also detect the orbital motion of the outer planet; this motion both rotates and changes the shape of the larger caustic shown in the top inset to Fig. 1. We are able to constrain the two components of the projected velocity of the planet relative to the primary star. Together with the estimate of the stellar mass, they completely determine the outer planet's orbit (including inclination) under the assumption that it is cir-

Fig. 2. Five features of light curve from Fig. 1, which determine planetary geometry. (A) Feature 1, weak cusp crossing. (B) Feature 2, weak caustic entrance. (C) Feature 3, strong caustic exit. (D) Feature 4, strong cusp approach. (E) Feature 5, moderate cusp approach. Features 1, 2, 3, and 5, are explained by the black portion of the caustic seen in Fig. 1A. Feature 4 requires an additional cusp in the caustic, which is shown as the red curve. Data have been binned for clarity.



cular, up to a twofold degeneracy. The solution presented here is marginally favored by the data at $\Delta\chi^2 = 4.8$ via the effect of the planet's acceleration on the light curve. Thus, we can estimate the full (three-dimensional) separation of planet c (again assuming a circular orbit) and also of planet b (assuming a coplanar and circular orbit). We find $a_b = 2.3 \pm 0.2$ AU and $a_c = 4.6 \pm 0.5$ AU. A more refined estimate of these parameters and their uncertainties will require a detailed analysis, including the combined effects of finite sources, parallax, and orbital motion of the planets.

The OGLE-2006-BLG-109L planetary system bears a remarkable similarity to our own solar system. Although the primary mass is only half solar, the mass ratio of the two planets (0.37) and separation ratio (0.50) are similar to those of Jupiter and Saturn. We infer their equilibrium temperatures to be $T_{\text{eq}} \sim 82 \pm 12$ K and $T_{\text{eq}} \sim 59 \pm 7$ K, $\sim 30\%$ smaller than those of Jupiter and Saturn.

Before the detection of extrasolar planets, planet formation theories generally predicted that other systems should resemble our solar system. In the core-accretion paradigm, the most massive giant planet forms at the "snow line," the point in the protoplanetary disk exterior to which ices are stable. Immediately beyond the snow line, the surface density of solids is highest and the dynamical time is the shortest, and therefore the time scale for planet formation is the shortest. Beyond the snow line, the formation time scale increases with distance from the host star. Thus, in this "classical" picture of planet formation, one would expect planet mass to decrease with increasing distance beyond the snow line, as is observed in our solar system (30). The discovery of a population of massive planets well interior to the snow line demonstrated that this picture of planet formation is incomplete, and considerable inward migration of planets must occur (31). Nevertheless, this classical picture may still be applicable to our solar system and some fraction of other systems as well. The OGLE-2006-BLG-109L planetary system represents just such a "scaled version" of our own solar system, with a less-massive host. This system preserves the mass-distance correlation in our solar system, and the scaling with primary mass is consistent with the core-accretion paradigm in which giant planets that form around lower-mass stars are expected to be less massive but form in regions of the protoplanetary disk with similar equilibrium temperatures and are therefore closer to their parent star (32).

The majority of the ~ 25 known multiplanet systems are quite dissimilar to the OGLE-2006-BLG-109L system and to our own solar system. Many of these systems have the very close-in massive planets indicative of large-scale planetary migration, or they have a "normal hierarchy," in which the masses of the giant planets increase with distance from the parent star. There are two multiplanet systems with properties roughly similar to those of OGLE-2006-BLG-109L. The 47 UMa and 14 Her systems each

contain a giant planet at a semimajor axis of ~ 3 AU and a second, less massive giant planet at a separation of ~ 7 AU (33). However, because of their higher-mass primaries, the equilibrium temperatures of these planets are considerably higher than those of OGLE-2006-BLG109L or Jupiter and Saturn, so these systems cannot be considered close analogs of our solar system.

OGLE-2006-BLG109Lb and OGLE-2006-BLG109Lc are the fifth and sixth planets to be detected by microlensing. Although, given the detection of planet c, the a priori probability of detecting planet b in this event was high, it was not unity. Furthermore, only two other jovian-mass planets have been detected by microlensing (8, 9), and neither event had substantial sensitivity to multiple planets. These facts may indicate that the stars being probed by microlensing that host jovian-mass companions are also likely to host additional giant planets. If the OGLE-2006-BLG-109L planetary system is typical, these systems may have properties similar to our solar system. Regardless, the detection of the OGLE-2006-BLG-109L planetary system demonstrates that microlensing surveys will be able to constrain the frequency of solar system analogs throughout the Galaxy.

References and Notes

- J. Schneider; <http://vo.obspm.fr/exoplanetes/encyclo/encycl.html> (2006).
- A. Wolszczan, D. A. Frail, *Nature* **355**, 145 (1992).
- M. Mayor, D. Queloz, *Nature* **378**, 355 (1995).
- G. W. Marcy, R. P. Butler, *Astrophys. J.* **464**, L147 (1996).
- A. Udalski et al., *Acta Astron.* **52**, 1 (2002).
- M. Konacki et al., *Nature* **421**, 507 (2003).
- S. Mao, B. Paczynski, *Astrophys. J.* **374**, L37 (1991).
- I. A. Bond et al., *Astrophys. J.* **606**, L155 (2004).
- A. Udalski et al., *Astrophys. J.* **628**, L109 (2005).
- J.-P. Beaulieu et al., *Nature* **439**, 437 (2006).
- A. Gould et al., *Astrophys. J.* **644**, L37 (2006).
- D. A. Fischer, J. Valenti, *Astrophys. J.* **622**, 1102 (2005).
- R. P. Butler et al., *Astrophys. J.* **646**, 505 (2006).
- A. Gould, A. Loeb, *Astrophys. J.* **396**, 104 (1992).
- D. B. Bennett, S. H. Rhie, *Astrophys. J.* **574**, 985 (2002).
- K. Griest, N. Safizadeh, *Astrophys. J.* **500**, 37 (1998).
- S. H. Rhie et al., *Astrophys. J.* **533**, 378 (2000).
- N. J. Rattenbury, I. A. Bond, J. Skuljan, P. C. M. Yock, *Mon. Not. R. Astron. Soc.* **335**, 159 (2002).
- F. Abe et al., *Science* **305**, 1264 (2004).
- B. S. Gaudi, R. M. Naber, P. D. Sackett, *Astrophys. J.* **502**, L33 (1998).
- A. Udalski, *Acta Astron.* **53**, 291 (2003).
- M. Albrow, *Astrophys. J.* **509**, 687 (1998).
- M. J. Burgdorf et al., *Planet. Space Sci.* **55**, 582 (2007).
- J. Yoo et al., *Astrophys. J.* **603**, 139 (2004).
- J. Wambsganss, *Mon. Not. R. Astron. Soc.* **284**, 172 (1997).
- C. Han, *Astrophys. J.* **629**, 1102 (2005).
- S. Dong et al., *Astrophys. J.* **664**, 862 (2007).
- A. Gould, *Astrophys. J.* **421**, L71 (1994).
- A. Gould, *Astrophys. J.* **392**, 442 (1992).
- J. J. Lissauer, *Icarus* **69**, 249 (1987).
- D. N. C. Lin, P. Bodenheimer, D. C. Richardson, *Nature* **380**, 606 (1996).
- S. Ida, D. N. C. Lin, *Astrophys. J.* **626**, 1045 (2005).
- R. A. Wittenmyer, *Astrophys. J.* **654**, 625 (2007).
- We acknowledge the following support: NSF AST-042758 (A.G., S.D.); NASA NNG04GL51G (D.L.D., A.G., R.W.P.); NASA/JPL 1226901 (D.L.D., B.S.G., A.G.); Polish Ministerstwo Nauki i Szkolnictwa Wyższego MNiSW N20303032/4275 (OGLE); NSF AST-0708890 and NASA NNX07AL71G (D.P.B.); Science Research Center, Korea Science and Engineering Foundation (C.H.); Korea Astronomy and Space Science Institute (B.-G.P.); Deutsche Forschungsgemeinschaft (C.S.B.); Particle Physics and Astronomy Research Council (PPARC), European Union Sixth Framework Programme ANGLES (L.W., N.J.R.); PPARC (RoboNet); Israel Science Foundation (D.M.); Marsden Fund of New Zealand; Japan Ministry of Education, Culture, Sports, Science and Technology; and Japan Society for the Promotion of Science (MOA). RoboNet-1.0 is funded by the Science and Technology Facilities Council (STFC) and operates in conjunction with the eScience Telescopes for Astronomical Research project, which supports A.A. and which is jointly funded by the Department of Trade and Industry, STFC, and the Engineering and Physical Sciences Research Council. K.H.C.'s, S.N.'s and B.M.'s work was performed under the auspices of the U.S. Department of Energy by Lawrence Livermore National Laboratory under contract DE-AC52-07NA27344. M.D. is a Royal Society University Research Fellow. We thank the MDM staff for their support. We thank D. Warren for financial support for the Mt. Canopus Observatory and M. Bode, D. Bramich, C. Mottram, S. Fraser, and C. Snodgrass for contributions to the RoboNet data.

19 October 2007; accepted 9 January 2008
10.1126/science.1151947

Imaging Phonon Excitation with Atomic Resolution

H. Gawronski,* M. Mehlhorn, K. Morgenstern

Inelastic electron tunneling spectroscopy at low temperatures was used to investigate vibrations of Au(111) and Cu(111). The low-energy peaks at 9 millielectron volts (meV) on Au(111) and 21 meV on Cu(111) are attributed to phonons at surfaces. On Au(111), the phonon energy is not influenced by the different stacking of the surface atoms, but it is considerably influenced by different atomic distances within the surface layer. The spatial variation of the phonon excitation is measured in inelastic electron tunneling maps on Au(111), which display atomic resolution. This atomic resolution is explained in terms of site-specific phonon excitation probabilities.

Phonons, which are vibrational modes of crystal lattices, play a key role in a variety of disciplines. They influence the physical properties in a material's characteristics, such as

its thermal and electrical conductivities. Electron-phonon interactions are investigated to understand light scattering or energy relaxation in semiconductors and influence surface chemical

reactions through vibrational heating or cooling of atoms and molecules.

In this report, we concentrate on surface phonon modes that have been intensely investigated both experimentally and theoretically for the past 4 decades (1), and the phonon spectra of many metal surfaces are well known (2). However, phonon modes are generally determined for an entire surface; their variation over a surface has proven more difficult to determine.

Scanning tunneling microscopy (STM) (3) is a well-established technique for investigating topographic and electronic properties of conducting surfaces (4). The resolution of a STM permits obtaining spatial information that is typically not accessible in surface science methods that are usually used for the study of surface vibrations, such as helium atom scattering for phonons or electron energy loss spectroscopy for molecular vibrations. The STM method was recently extended to detect molecular vibrations in order to investigate properties of molecules on surfaces by measuring the energy loss in inelastic electron tunneling spectroscopy (IETS) (5–11). The recording of vibrational maps by measuring the derivative of the conductance (d^2I/dV^2 signal) for each point of a STM image as first demonstrated for a C_2HD molecule adsorbed on the (100) faces of Cu and Ni gave unprecedented spatial information about such molecular vibrations (12). IETS has so far been applied once only to substrate phonons (13). In this study, the d^2I/dV^2 spectra of the highly oriented polygraphite (HOPG) surface was compared to the calculated vibrational density of states to identify acoustic and optical phonon modes.

The requirement for measuring molecular spectra by IETS is a noise level below 5% of the peak signal (14). For typical signals of molecules, this requirement demands stability in z direction better than 0.5 pm. However, the surface phonon signal of our study is more than one order of magnitude smaller than the signal from a molecule [Supporting Online Material (SOM) text]. Our recently developed low-temperature STM (15) has the stability needed to detect such a small signal.

In this report, we demonstrate a previously unknown type of atomic resolution based on d^2I/dV^2 mapping in the energy range of surface phonons. We show that surface phonon excitation results in a decrease of the IETS signal in the low-energy region. A peak shift of ≈ 12 meV between spectra on Au(111) and Cu(111) excludes effects of the tungsten tip as the origin of the low-energy feature. We explain the atomic resolution in d^2I/dV^2 maps by a lateral variation in the probability of surface phonon excitations. Lastly, we discuss the influence of different

stacking and different atomic distances on the phonon spectrum.

The measurements were performed with a custom-built low-temperature STM that operates at 5 K (15). It is optimized for stability and facilitates measurements below 1 pA. For Au(111) the energy range of phonon modes extends from 0 up to 18 meV, whereas on Cu(111) they range up to 32 meV (16, 17). We chose the surfaces of Au and Cu because this shift of their phonon spectra of 14 meV lies well above our resolution limit. The single crystalline Au(111) and Cu(111) samples were prepared by cycles of sputtering with Ne^+ at 1.3 keV (5×10^{-5} mbar, $I = 2 \mu A$) and annealing at 850 K. Inelastic electron tunneling (IET) spectra and maps were taken by measuring the second derivation of the tunneling current in lock-in technique (18) with a modulation voltage of 6 mV for d^2I/dV^2 spectroscopy and 8 mV for d^2I/dV^2 mapping. Whereas the signal resulting from a 6-mV modulation is sufficient for the lock-in amplifier to detect the signal during a spectrum taken within several minutes, a 1-min residual drift demands a slightly higher modulation voltage for the ≈ 40 min of mapping. A modulation frequency of 361.1 Hz was used in

both cases. All figures show nonfiltered original single spectra.

In constant-current imaging, the tip follows the contour of the constant local density of states (LDOS). Thus, the resulting image is a superposition of topologic and electronic effects. Conventional atomic resolution in STM images results from a height variation of the tip at atomic distances because of changes in the LDOS (4). On close-packed surfaces, an additional contribution is also necessary to achieve atomic resolution: a perturbation of the surface by tip forces that are enhanced when approaching the tip to the surface (19). Another possibility to achieve atomic resolution is to transfer a molecule from the sample to the tip, which leads to a sharpening of tip states (20).

Conventional atomic resolution images of the two investigated face-centered cubic (fcc) (111) surfaces of Au and Cu are shown in Fig. 1. In both cases, the atomic resolution is a result of a variation in LDOS. For Au(111) (Fig. 1A), the atomic resolution is superimposed by a geometric effect because of partial dislocations that separate fcc from hexagonal close-packed (hcp) stacking in the well-known herringbone recon-

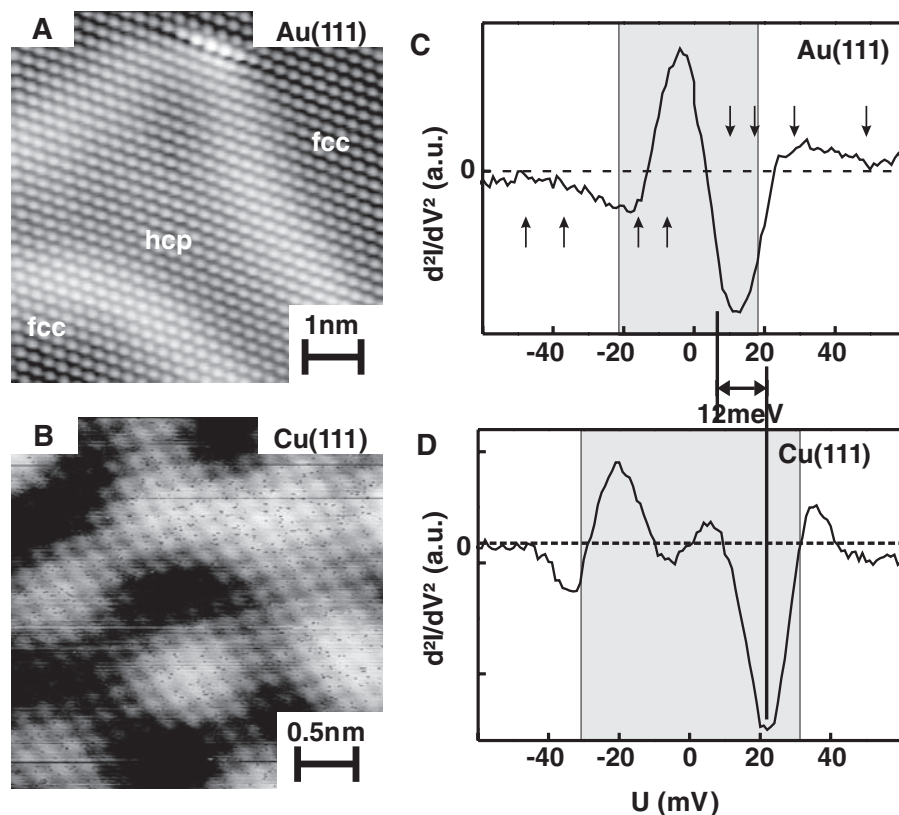


Fig. 1. STM images and IETS spectra measured at 5 K. (A and B) Images in constant-current mode showing atomic resolution (A) in an elbow region of the reconstructed clean Au(111) surface. The atomic resolution is superimposed by the herringbone reconstruction, $I_T = 0.13$ nA, $U_T = 10$ mV, (B) on the Cu(111) surface with adsorbed CO molecules outside the imaged region producing an electron standing wave pattern, which is superimposed to the atomic resolution, $I_T = 1.3$ nA, $U_T = 26$ mV. (C and D) IETS spectra taken (C) on fcc domain of Au(111) surface and (D) on Cu(111) surface; gray shaded regions represent the region of calculated and measured phonon energies integrated over the entire Brillouin zone. Arrows point to the energies where the maps (shown in Fig. 2) were recorded. a.u., arbitrary units. U indicates voltage.

Institute of Solid State Physics, Department of Surface Science, Leibniz University Hannover, Appelstrasse 2, D-30167 Hannover, Germany.

*To whom correspondence should be addressed. E-mail: gawronski@fkp.uni-hannover.de

struction (21). On Cu(111), the atomic resolution is superimposed by an electronic contribution, the standing wave pattern of defect-scattered surface-state electrons (22) (Fig. 1B).

We will describe an approach for achieving an atomic resolution that has its origin in phonon excitation. We first identify phonon-related maxima in the d^2I/dV^2 spectra taken between -50 and $+50$ meV.

The vibrational spectrum taken on Au(111) (Fig. 1C) shows point symmetric maxima centered at an energy of around ± 9 meV with a full width at half maximum (FWHM) of 12 meV. The peaks are well within the energy range of phonons on the Au(111) surface integrated over the entire Brillouin zone (gray shaded region) (2, 16). Note that the exact shape in the positive region is a dip followed by a small protrusion at higher energy, consistent with a Fano line shape. Both the resonant-scattering model proposed by Baratoff and Persson (23), which assumes tunneling to adsorbate-induced resonant states and the formation of temporary negative ions, and the model by Lorente *et al.* (24) that uses the impact scattering framework have been found to describe Fano line shapes in IETS. In both cases, IET occurs when the electron energy matches the vibrational energy of an adsorbate vibration $\hbar\omega$. At this energy, the so-called inelastic tunneling channel opens. That increases the conductivity and thus the tunneling current. However, because of many-body effects, the elastic channel is reduced at the same energy. It depends on the relative magnitude of these two changes in conductivity whether a vibrational excitation leads to a dip, to a peak, or to an intermediate Fano line shape.

The appearance of dips and peaks in a spectrum is corroborated by recent STM point-contact spectroscopy measurements on gold that identify phonon modes of atomic gold wires at energies of 10 and 18 meV for the transversal and longitudinal phonon modes, respectively, with the same symmetry as found here (25, 26).

If the maxima seen on Au(111) were related to surface phonons, they should lie at higher energies for the Cu(111) surface (16, 17). In-

deed, on the Cu(111) surface, we identify similar maxima but centered at an energy of ± 21 meV with a FWHM of 11 meV, that is, about 12 meV higher than on Au(111) (Fig. 1D). This shift is much greater than the thermal and modulation voltage broadening of ± 5.3 meV (for more details on peak broadening, see SOM text). The difference in peak position is in good agreement with the calculated difference in energy of 14 meV between Cu(111) and Au(111) (16, 17). Both the position and the shift in energy corroborate that the peaks on Au and Cu result from surface phonon states, which thus can be measured by IETS.

We next investigated the phonon excitation further on the reconstructed Au(111) surface by spatially mapping the second derivation of the tunneling current at a given sample voltage for each point in the STM image. STM images (I is constant) and simultaneously taken d^2I/dV^2 maps at sample voltages between 49 and -46 meV are shown in Fig. 2 (for the complete series of images, see fig. S5). In all of the STM images (first row), the only visible feature even at highest contrast is a reconstruction line of the Au(111) surface that separates an fcc from an hcp region. Beyond the energy of the surface phonon modes (49 meV), the only feature in the d^2I/dV^2 map (Fig. 2A, second row) is a dark line at the position of the reconstruction line. The

origin is the reconstruction line, which leads to a change in tip height clearly visible as a line in the I/V image and thus to a decrease in the d^2I/dV^2 signal. The observed dark line is an artifact of the I is constant measurement (for a more detailed explanation, see SOM text). Thus, at 49 meV, the d^2I/dV^2 map is structureless. However, in the region related to the Fano profile in the d^2I/dV^2 spectra, the d^2I/dV^2 maps show protrusions and depressions at atomic distances (Fig. 2, B to G) with the hexagonal symmetry as found in the conventional atomic resolution (compare to Fig. 1A).

What accounts for atomic resolution in this case? Phonons are collective motions of atoms and should thus not be localized on the atomic scale. In addition, the individual motion of the atoms is by far too fast to be detected by STM. This atomic resolution thus does not arise from variations in the electronic LDOS as in conventional atomic resolution but from variations in the phonon excitation probability. Depending on the relative tip position to the atomic nuclei, the phonons are excited with different efficiencies. Whether the transition matrix elements are greater in on-top or in hollow sites is not yet known and can only be solved in sophisticated theoretical calculations of the excitation process.

For voltages beyond the phonon peak, the atomic resolution vanishes (Fig. 2H). There is

Fig. 3. IETS: spectra taken on different sites of the reconstructed Au(111) surface. Different intensities are caused by different current offsets: 19 pA on the domains and 21 pA on the boundary.

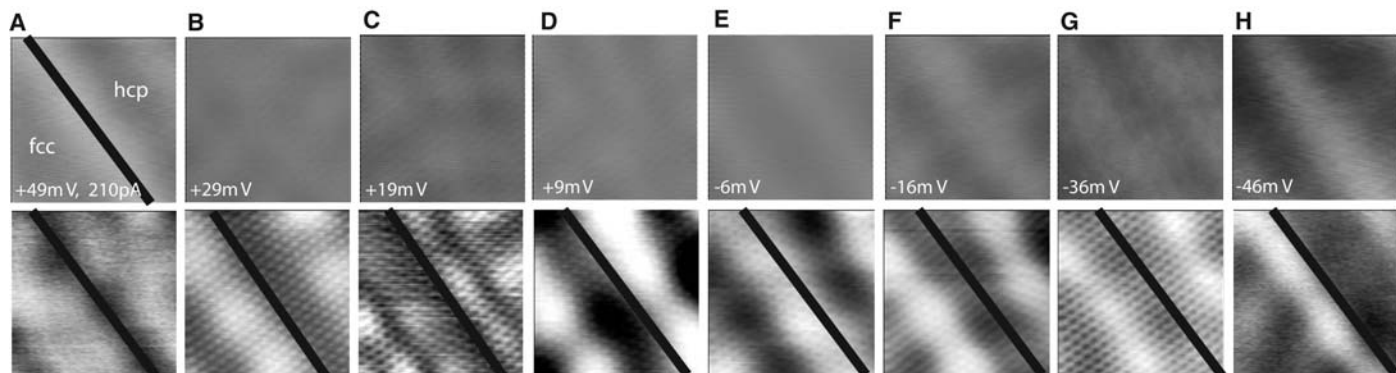
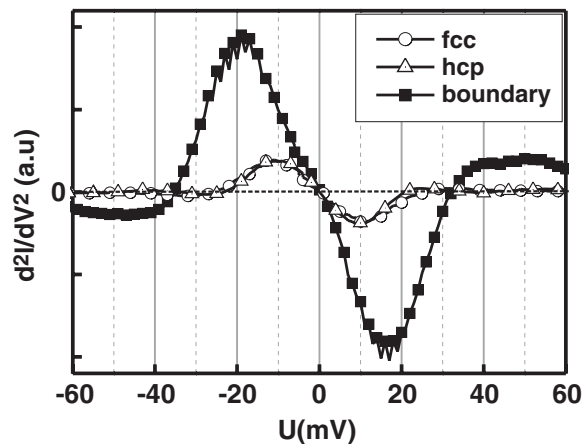


Fig. 2. (A to H) Phonon mapping on Au(111) (3.4 nm by 3.4 nm). The images are taken at different bias voltages as indicated, $I_T = 0.21$ nA. Top row shows I/V images, bottom row shows simultaneously recorded d^2I/dV^2

maps. Diagonal lines indicate the position of the reconstruction line separating a fcc from a hcp region. Because of higher signals at low energies, the gray scale is different at these energies.

no trace of atomic resolution in the topographic STM images even at the highest contrast. Thus, we exclude any effects due to tip-height variation to be at the origin of the atomic resolution in the phonon maps (SOM text).

Another feature in the d^2I/dV^2 maps in Fig. 2 is a stripelike intensity variation perpendicular to the reconstruction line that varies with energy. This intensity variation suggests differences in the phonon spectra on the different domains, which exist on Au(111) (21). In the so-called fcc domains, the atoms are on regular bulk sites; in the hcp domains, the distances between the atoms correspond to the bulk distances, but they are displaced with respect to the underlying second layer to hcp sites; within the domain boundaries, the atoms are both displaced from regular fcc sites and have their in-plane distances reduced by $\approx 12\%$ from 0.288 to 0.254 nm (21). Figure 3 shows spectra taken on the fcc and hcp domains as well as on the domain boundaries. Only for the latter is the peak considerably shifted in energy. Although the phonon peak maximum is situated at 10 meV on both the fcc and hcp sites, it lies at 18 meV on the domain boundaries, which is only 3 meV lower than on Cu(111). This shift is a result of the reduction of the atomic distances in the domain boundaries to almost the atomic distance of Cu(111) ($a = 0.255$ nm). We thus see no influence of the stacking with respect to the second layer on the phonon energy but a large influence of the smaller in-plane atomic distances of atoms within the domain boundaries.

On Au(111), the large energy shift between phonon modes on the domains and the boundaries confines phonons mostly within the domains, that is, into one dimension. We would thus expect a standing wave pattern, similar to the one seen for surface-state electrons scattered off defects (22). However, the wavelength of the standing wave pattern is too large to be observed. Instead, we observe a standing wave pattern parallel to the domain boundaries with a wavelength of 4.3 ± 0.5 nm, which is of the order of the domain width. This we attribute to the scattering of the phonons off the elbows (see fig. S4 for an overview image). This pattern might be enhanced by adsorption of molecules (SOM text). Again, there are no corresponding features in the I/V images. Thus, the standing wave pattern is no artifact.

Lastly, we comment on the stripelike domain structure with respect to the domain boundary for different voltages (Fig. 2). These stripes are asymmetric with respect to translation symmetry. This feature might reflect the nonsymmetric arrangement of the topmost atoms to the underlying layer in the domain boundary and thus be a hint for a slight influence of the second layer onto the surface phonons.

The investigation of surface phonons is potentially rich and should result in a better understanding of vibrational excitation and coupling of surface atoms, such as in the detection of

edge and corner modes, the investigation of phonons near an impurity atom within the surface, and studies of the coupling of different molecules to the surface by analyzing the induced local shift in phonon energy.

References and Notes

- W. Kress, F. W. de Wette, *Surface Phonons*, vol. 21 of *Springer Series in Surface Science* (Springer, Heidelberg, Germany, 1991).
- U. Harten, J. P. Toennies, Ch. Wöll, *Faraday Discuss. Chem. Soc.* **80**, 137 (1985).
- G. Binnig, H. Rohrer, *Helv. Phys. Acta* **55**, 726 (1982).
- R. Wiesendanger, Ed., *Scanning Probe Microscopy* (Springer-Verlag, Berlin, 1998).
- B. C. Stipe, M. A. Rezaei, W. Ho, *Science* **280**, 1732 (1998).
- H. J. Lee, W. Ho, *Science* **286**, 1719 (1999).
- J. I. Pascual *et al.*, *Phys. Rev. Lett.* **86**, 1050 (2001).
- Y. Kim, T. Komeda, M. Kawai, *Phys. Rev. Lett.* **89**, 126104 (2002).
- K. Morgenstern, K.-H. Rieder, *J. Chem. Phys.* **116**, 5746 (2002).
- X. H. Qiu, G. V. Nazin, W. Ho, *Phys. Rev. Lett.* **92**, 206102 (2004).
- H. Gawronski, K. Morgenstern, K.-H. Rieder, *Eur. Phys. J. D* **35**, 349 (2005).
- B. C. Stipe, M. A. Rezaei, W. Ho, *Phys. Rev. Lett.* **82**, 1724 (1999).
- L. Vitali, M. A. Schneider, L. Wirtz, A. Rubio, K. Kern, *Phys. Rev. B* **69**, 121414 (2004).
- L. J. Lauhon, W. Ho, *Rev. Sci. Instrum.* **72**, 216 (2001).
- M. Mehlhorn, H. Gawronski, L. Nedelmann, A. Grujic, K. Morgenstern, *Rev. Sci. Instrum.* **78**, 033905 (2007).
- C. S. Jayanthi, H. Bilz, W. Kress, G. Benedek, *Phys. Rev. Lett.* **59**, 795 (1987).
- S. D. Borisova *et al.*, *Phys. Rev. B* **74**, 165412 (2006).
- B. C. Stipe, M. A. Rezaei, W. Ho, *Rev. Sci. Instrum.* **70**, 137 (1999).
- W. A. Hofer, A. J. Fisher, R. A. Wolkow, P. Grütter, *Phys. Rev. Lett.* **87**, 236104 (2001).
- L. Bartels, G. Meyer, K.-H. Rieder, *Surf. Sci.* **432**, L621 (1999).
- S. Narasimhan, D. Vanderbilt, *Phys. Rev. Lett.* **69**, 1564 (1992).
- M. F. Crommie, C. P. Lutz, D. M. Eigler, *Nature* **363**, 524 (1993).
- B. N. J. Persson, A. Baratoff, *Phys. Rev. Lett.* **59**, 339 (1987).
- N. Lorente, M. Persson, *Phys. Rev. Lett.* **85**, 2997 (2000).
- N. Agraït, C. Untiedt, G. Rubio-Bollinger, S. Vieira, *Phys. Rev. Lett.* **88**, 216803 (2002).
- C. Untiedt, G. Rubio-Bollinger, S. Viera, N. Agraït, *Phys. Rev. B* **62**, 9962 (2000).
- We gratefully acknowledge E. Chulkov and M. Persson for helpful discussions. For funding we thank the Deutsche Forschungsgemeinschaft.

Supporting Online Material

www.sciencemag.org/cgi/content/full/319/5865/930/DC1

SOM Text

Figs. S1 to S5

1 November 2007; accepted 10 January 2008

10.1126/science.1152473

Spin-Dependent WIMP Limits from a Bubble Chamber

E. Behnke,¹ J. I. Collar,^{2*} P. S. Cooper,³ K. Crum,² M. Crisler,³ M. Hu,³ I. Levine,¹ D. Nakazawa,² H. Nguyen,³ B. Odom,² E. Ramberg,³ J. Rasmussen,² N. Riley,² A. Sonnenschein,³ M. Szydagis,² R. Tschirhart³

Bubble chambers were the dominant technology used for particle detection in accelerator experiments for several decades, eventually falling into disuse with the advent of other techniques. We report here on a new application for these devices. We operated an ultraclean, room-temperature bubble chamber containing 1.5 kilograms of superheated CF_3I , a target maximally sensitive to spin-dependent and -independent weakly interacting massive particle (WIMP) couplings. An extreme intrinsic insensitivity to the backgrounds that commonly limit direct searches for dark matter was measured in this device under operating conditions leading to the detection of low-energy nuclear recoils like those expected from WIMPs. Improved limits on the spin-dependent WIMP-proton scattering cross section were extracted during our experiments, excluding this type of coupling as a possible explanation for a recent claim of particle dark-matter detection.

With approximately 85% of the total matter of the universe in a form that still eludes direct detection, the need for large-mass background-insensitive detectors that are able to explore the very small couplings expected from weakly interacting massive particles (WIMPs) is urgent. A member of this family of hypothetical particles, the lightest supersymmetric partner, stands out as one of the most likely candidates for composing the dark matter in galaxies (1, 2), but its predicted interaction rate via low-energy elastic scattering off nuclei is much less than one event per kg·day for any target. In some unfavorable (yet entirely plausible) models, this can become a dismayingly small

rate of less than one event per ton·year, which is so small that the next generation of massive [O(100)kg] WIMP detectors would necessarily suffer from a penury of statistics from any dark matter signal they might register. Information about WIMP properties (such as the mass of the particle) will be scarce. Thus, we require a variety of detec-

¹Department of Physics and Astronomy, Indiana University South Bend, South Bend, IN 46634, USA. ²Department of Physics, Enrico Fermi Institute, and Kavli Institute for Cosmological Physics, University of Chicago, Chicago, IL 60637, USA.

³Fermi National Accelerator Laboratory, Batavia, IL 60510, USA.

*To whom correspondence should be addressed. E-mail: collar@uchicago.edu

tion techniques and massive targets that can both improve sensitivity and allow the unequivocal identification of these particles (3).

Superheated liquids, in the form of bubble chambers, were extensively used as the detection medium of choice in accelerator experiments for more than three decades. These chambers led to numerous discoveries and provided an unprecedented ability to visualize fundamental particles and their interactions (4, 5). However, the advent of newer technologies led to their progressive obsolescence during the 1970s. In a bubble chamber, the heat deposited by ionizing radiation particles along their paths produces local nucleations of the vapor phase in a delicate (metastable) superheated liquid. Rapidly growing bubbles form along these paths and are photographed, and the chamber is then reset by fast recompression to the stable liquid phase. Decompression follows, bringing the target below its vapor pressure at the operating temperature, sensitizing it to radiation and starting the cycle anew. In accelerator experiments, it was sufficient to maintain the superheated state during the few milliseconds corresponding to the bunched arrival of incident beam particles. Uncontrollable boiling on porous materials (such as gaskets and metallic surfaces) prevented serious consideration of the use of this type of detector in searches for rare events, where the time of arrival of the signal is not known.

Having taken several precautions to deactivate inhomogeneous bubble nucleation centers, we have recently shown that it is possible to achieve what is in principle indefinitely long stability in moderately superheated bubble chambers (6), thereby allowing their use in direct WIMP searches. There are several advantages to the use of this device. Most important is the fact that the superheated liquid can be tuned to respond exclusively to particles having large stopping power (dE/dx , energy loss per unit of path distance). Muons, gamma rays, x-rays, β particles, etc., all fall well below the bubble nucleation threshold, which is typically $dE/dx > 50 \text{ keV}/\mu\text{m}$ during a WIMP search (Fig. 1). The target liquids are nevertheless sensitive to nuclear recoils of a few kilo–electron volts, such as those expected from the scattering of WIMPs, given their much denser energy deposition. The process of radiation-induced bubble nucleation is described within the framework of the classical "hot spike" model (7): For the phase transition to occur, the energy deposited by the particle must be larger than the thermodynamical work of formation of a critically sized protobubble. Additionally, this energy must also be lost over a distance comparable to the size of the protobubble; that is, a minimum stopping power condition must be fulfilled. This condition leads to an insensitivity to the listed minimum ionizing backgrounds that normally plague WIMP searches (Figs. 1 and 2) (8–10). As for the probability of spontaneous (homogeneous) bubble nucleation in the bulk of a superheated fluid, it only becomes sizeable at a few degrees below the critical tem-

Fig. 1. Instantaneous stopping power versus energy for different particles in CF_3I , including its three recoiling species. Plotted as horizontal and vertical lines are the calculated dE/dx and energy thresholds for bubble nucleation at temperature (T) = 40°C and two different operating pressures. According to the hot spike nucleation model (7), only radiations in the top right (colored) quadrants can lead to bubbles. Notice the absence of this possibility for electrons even toward the end of their range, in conditions that nonetheless lead to a sensitivity to recoils of just a few kilo–electron volts, such as those expected from WIMP interactions, and the presence of their emitters must therefore be avoided.

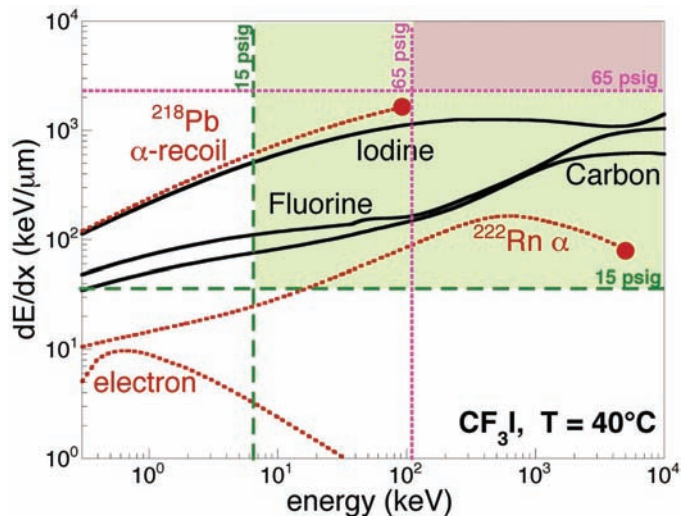


Fig. 2. Families of events in a 1.5-kg CF_3I bubble chamber. At high degrees of superheat (~60°C and atmospheric pressure for this compound), minimum ionizing cosmic ray events reminiscent of those observed in early bubble chambers (4) are visible (A). At moderate superheats (~30°C, 1 atm) the chamber is sensitive strictly to high dE/dx radiation such as nuclear recoils. Whereas neutrons can give rise to simultaneous separate bubbles each corresponding to a scatter (B), WIMPs are expected to produce single bubbles only (C) because of their extremely small probability of interaction. The mean free path between scatters is just a few centimeters for neutrons, leading to an excellent ability to reject neutron-induced recoils in large chambers.

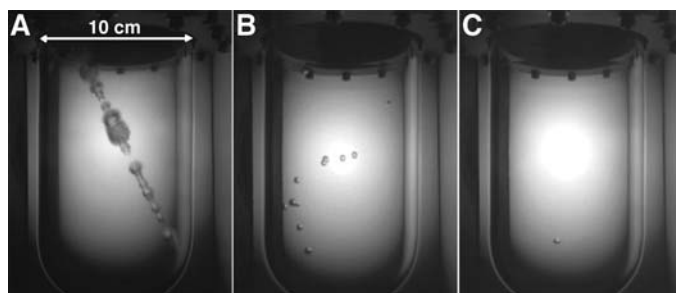
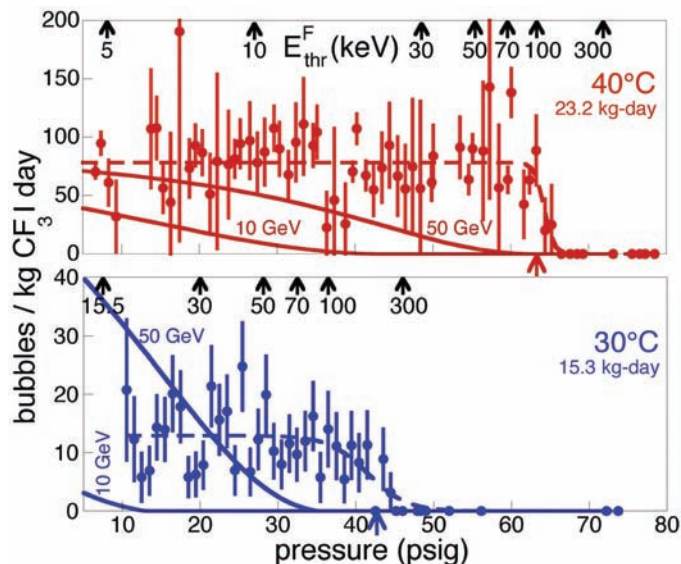


Fig. 3. Distribution of single bulk bubble nucleation rate versus operating pressure for two different running temperatures. Rates display a flat behavior up to a pressure end point. This is characteristic of the response to monochromatic alpha particles and ~100 keV alpha recoils [here from ^{222}Rn emanations (SOM text)]. Colored arrows along the bottom axes indicate the predicted onset of sensitivity to these particles, in good agreement with observations. As a reference, solid lines correspond to the expected signal rate from WIMPs with a mass of 10 and 50 GeV/c^2 and a 3-picobarn cross section for their spin-dependent coupling to protons. Also shown is the response function to ^{222}Rn and progeny (dashed lines). Calculated energy thresholds (in kilo–electron volts) for bubble nucleation by fluorine recoils are shown along the top axes. The error bars include the systematic effect from correlated triple alpha emission after ^{222}Rn decay (fig. S3 and discussion in SOM). This has a conservative effect on the dark matter limits obtained from the data.



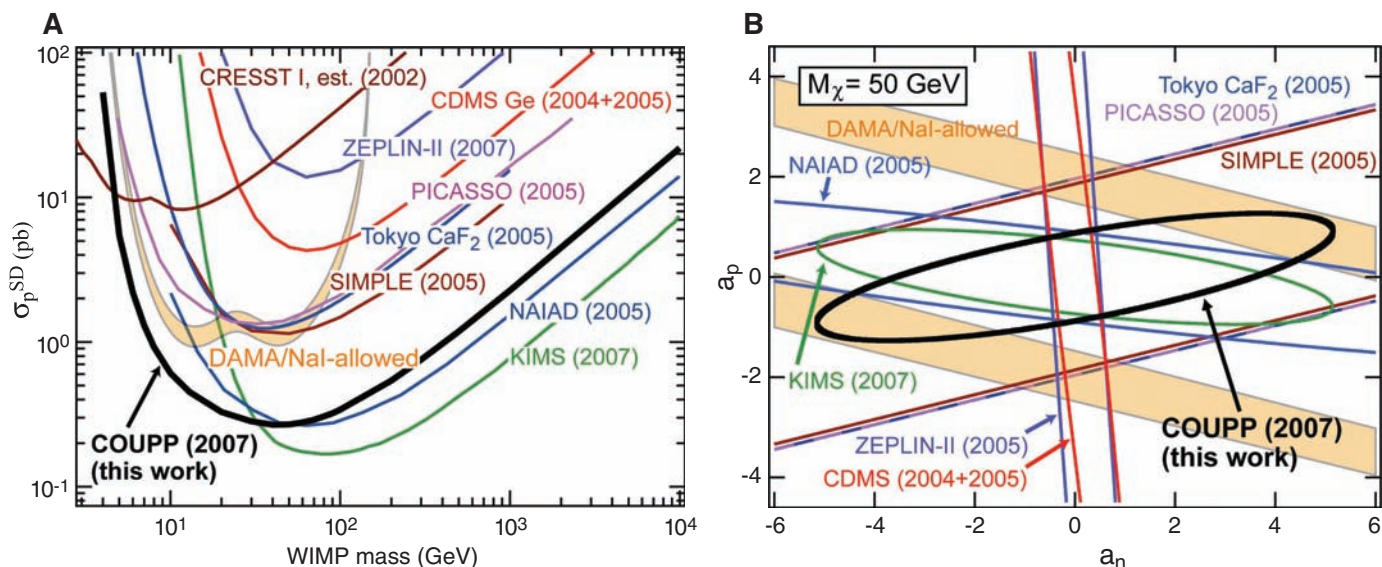


Fig. 4. (A) Improved limits on spin-dependent (pure) proton-WIMP interaction cross section ($\sigma_{p,SD}$, expressed in picobarns) versus WIMP mass from this experiment (COUPP, the Chicagoland Observatory for Underground Particle Physics). Couplings above the line would have produced signals above observed backgrounds and are excluded to a 90% confidence level. Limits from other experiments (labeled by name and year of publication) are also shown (25), as well as the region (DAMA/Nal-allowed) favored as a possible explanation for an

existing claim of WIMP observation (19, 21), a hypothesis now contradicted by this experiment. **(B)** Similar limits for spin-dependent coupling parameters (a_p and a_n), where no assumption is made about the relative strength of the coupling to neutrons and protons, but a WIMP mass M_χ must be chosen (50 GeV/ c^2 here) (26, 27). The region outside of the ellipses is excluded by each experiment. These bounds arise from the weighted average (14) of analyses performed on three independent large data sets adding up to 52 kg·days of exposure.

perature of the target compound (11). Under normal operating conditions for a dark-matter search, this source of instability is entirely negligible.

The supporting online material (SOM) provides details on the underground operation of a prototype chamber containing 1.5 kg of CF₃I, calibrations of this device using neutron and gamma sources, and the origin of the background radiation (²²²Rn α decay) observed during engineering runs.

Even before any precautions against α -emitting backgrounds were taken, an improved sensitivity to the spin-dependent WIMP-proton coupling was obtained from the first data collected. This is possible because of the extreme sensitivity to this mode of interaction afforded by the large mass fraction of fluorine (29%) (12) and the operation of the chamber in conditions where only nuclear recoils (α -, neutron-, or WIMP-induced) can produce bubbles. WIMP-induced bubble nucleation rates were computed for different WIMP masses and operating conditions (chamber pressure and temperature), using the bubble nucleation thresholds predicted by the hot spike model (top axis in Fig. 3) (13). The WIMP recoil rate integrated above the threshold was derived using common methods (14) and customary dark matter halo parameters (15). These calculations have been validated by their ability to predict the response of the chamber to Am/Be neutron recoils (16) (SOM text). Following the procedure described in (17), experimental bulk bubble nucleation rates versus pressure, such as those depicted in Fig. 3, were fitted with a model containing two free parameters: the signal from a WIMP of a given mass, scalable by a free spin-dependent cross

section, and the response to ²²²Rn α particles, expressed as a logistic function with a free overall normalization (SOM). The minimization was performed with the MINUIT package (18), and its output was cross-checked via a standard error matrix analysis. The best fits favored the null hypothesis alone (response to ²²²Rn α particles only).

We obtained improved bounds on spin-dependent WIMP couplings (Fig. 4) by applying an old technology, bubble chambers, to a new problem, that of dark-matter detection. The Dark Matter (DAMA) collaboration has claimed to have observed (19) a characteristic annual modulation in detection rates expected from WIMP interactions (20). The importance of this claim, which if correct would effectively amount to the discovery of particle dark matter, encourages the examination of all possible interpretations. It has been postulated (21) that spin-dependent WIMP interactions may account for the DAMA effect, bypassing in this way the constraints placed by all other experiments. Spin-independent and spin-dependent couplings to neutrons are essentially exhausted as possibilities (21, 22), but a region in spin-dependent coupling to protons for WIMPs below 10 GeV/ c^2 in rest mass has remained beyond experimental reach until now (Fig. 4). This possibility is now excluded by the data at hand, making a WIMP interpretation of the DAMA observations very difficult.

References and Notes

- G. Jungman, M. Kamionkowski, K. Griest, *Phys. Rep.* **267**, 195 (1996).
- R. J. Gaitskill, *Annu. Rev. Nucl. Part. Sci.* **54**, 315 (2004).
- G. Bertone, D. G. Cerdono, J. I. Collar, B. Odom, *Phys. Rev. Lett.* **99**, 151301 (2007).

- D. A. Glaser, *Nucl. Phys. B Proc. Suppl.* **36**, 3 (1994).
- C. Rubbia, *Nucl. Phys. B Proc. Suppl.* **36**, xvii (1994).
- W. J. Bolte et al., *Nucl. Instr. Methods* **A577**, 569 (2007).
- F. Seitz, *Phys. Fluids* **1**, 2 (1958).
- J. I. Collar, *Phys. Rev. D* **54**, R1247 (1996).
- J. I. Collar et al., *Phys. Rev. Lett.* **85**, 3083 (2000).
- J. I. Collar et al., *New J. Phys.* **2**, 14.1 (2000).
- M. Blander, J. L. Katz, *Am. Inst. Chem. Eng. J.* **21**, 833 (1975).
- J. Ellis, R. A. Flores, *Phys. Lett. B* **263**, 259 (1991).
- Although fluorine is dominant, the small (20% or less) contribution from iodine to this coupling is also included. Spin parameters for iodine (Bonn A model) are taken from (23).
- J. D. Lewin, P. F. Smith, *Astropart. Phys.* **6**, 87 (1996).
- A local WIMP density of 0.3 GeV/cm³, halo velocity dispersion of 230 km/s, Earth-halo velocity of 244 km/s, and escape velocity of 650 km/s were used.
- The classical theory of radiation-induced boiling (7, 24) predicts, perhaps naively, sharp (step function) bubble nucleation thresholds. In contrast to (17), where soft (sigmoidal) thresholds are invoked to interpret neutron calibrations, we have observed no need to deviate from the predictions of this theory. In dedicated experiments using smaller devices and neutron-induced recoils, we have ascertained that, at least for a CF₃I bubble chamber, thresholds are very close to steplike. The rapid onset of full response to α recoils observed in this larger chamber (Fig. 3) is another indication of the same. Adoption of a sigmoidal threshold would result in an enhanced WIMP sensitivity, most noticeably for light WIMP masses.
- M. Barnabe-Heider et al., *Phys. Lett. B* **624**, 186 (2005).
- F. James, in *Proceedings of the 1972 CERN Computing and Data Processing School*, Pertisau, Austria, 10 to 24 September 1972.
- R. Bernabei et al., *Riv. Nuovo Cimento* **26N1**, 1 (2003).
- A. K. Drukier, K. Freese, D. N. Spergel, *Phys. Rev. D* **33**, 3495 (1986).
- C. Savage, P. Gondolo, K. Freese, *Phys. Rev. D* **70**, 123513 (2004).
- P. Gondolo, G. Gelmini, *Phys. Rev. D* **71**, 123520 (2005).
- M. T. Ressell, D. J. Dean, *Phys. Rev.* **C56**, 535 (1997).
- C. R. Bell et al., *Nucl. Sci. Eng.* **53**, 458 (1974).

25. <http://dmtools.brown.edu>
 26. D. R. Tovey *et al.*, *Phys. Lett. B* **488**, 17 (2000).
 27. F. Giuliani, *Phys. Rev. Lett.* **93**, 161301 (2004).
 28. We gratefully acknowledge the effort and outstanding technical support of the Fermilab staff. This work is supported by NSF CAREER award PHY-0239812, NSF grants PHY-0707298 and PHY-0555472, the Indiana

University South Bend R&D committee, the Kavli Institute for Cosmological Physics through grant NSF PHY-0114422, and the U.S. Department of Energy.

Supporting Online Material
www.sciencemag.org/cgi/content/full/319/5865/933/DC1

SOM Text
 Figs. S1 to S3
 References

31 August 2007; accepted 4 January 2008
 10.1126/science.1149999

Electron-Driven Acid-Base Chemistry: Proton Transfer from Hydrogen Chloride to Ammonia

Soren N. Eustis,¹ Dunja Radisic,¹ Kit H. Bowen,^{1*} Rafał A. Bachorz,^{2,3} Maciej Haranczyk,^{3,4} Gregory K. Schenter,³ Maciej Gutowski^{3,4,5*}

In contrast to widely familiar acid-base behavior in solution, single molecules of NH₃ and HCl do not react to form the ionic salt, NH₄⁺Cl⁻, in isolation. We applied anion photoelectron spectroscopy and ab initio theory to investigate the interaction of an excess electron with the hydrogen-bonded complex NH₃⋯HCl. Our results show that an excess electron induces this complex to form the ionic salt. We propose a mechanism that proceeds through a dipole-bound state to form the negative ion of ionic ammonium chloride, a species that can also be characterized as a deformed Rydberg radical, NH₄⁻, polarized by a chloride anion, Cl⁻.

When vapors from open bottles of concentrated hydrochloric acid and ammonium hydroxide intermingle, a white cloud consisting of tiny ammonium chloride particles forms. Yet for many years the question of how individual molecules of HCl and NH₃ interact ranked as a fundamental problem in acid-base chemistry. Essentially, two main types of interactions were posited: either a hydrogen-bonded, ClH⋯NH₃ complex, or a proton-transferred (ionic) molecule, NH₄⁺Cl⁻, classified respectively by Mulliken as outer and inner complexes (*1*). Competition between covalent and ionic bonding, as well as the role of hydrogen bonding and proton transfer, made the HCl/NH₃ system a particularly attractive model for exploring the interplay between major concepts in chemistry. Eventually, the following question came into focus: Can a single molecule of NH₃ interacting with a single molecule of HCl undergo proton transfer to form NH₄⁺Cl⁻, or does the formation of such ionic species require the assistance of environmental, cooperative effects, like those found in the condensed phase?

For a time, the prevailing evidence leaned toward the proton-transferred outcome. In a series of experiments 20 years ago, however, Legon

showed conclusively by rotational spectroscopy that in beams of neutral [(HCl)(NH₃)] heterodimers (*2*, *3*), no appreciable proton transfer occurs; instead, the spectra are consistent with linear, hydrogen-bonded ClH⋯NH₃ complexes. Modern theoretical studies agree (*4–11*). Therefore, as counterintuitive as it may seem, ammonia and hydrogen chloride do not react under isolated conditions. This finding also made it clear, however, that the appearance of the white clouds required outside interactions to induce proton transfer and thus salt formation. As a result, the answer to one question had raised another: Can local environmental effects, such as collisions with other molecules or interactions with electrons, ions, or even photons, trigger proton transfer in acid-base complexes such as these?

Here, we focus on a particular aspect of this general question: Can a single electron, the most fundamental entity in chemistry, cause the ClH⋯NH₃ complex to undergo proton transfer to form an ionic salt? Although the synergy between electron and proton transfer is recognized as a fundamental process in biophysics, materials science, and catalysis (*12*, *13*), the detailed mechanisms responsible for many of these processes remain unresolved. The system under study can be viewed as undergoing a process quite similar to proton-coupled electron transfer (PCET). PCET reactions are commonly defined as those involving the concerted transfer of an electron and a proton in a given complex (*12*, *14*). However, there are variants of the PCET model that account for stepwise transfer (ET→PT, or PT→ET). These PCET reactions generally occur on nanosecond time scales, depending on the pathway and the overall driving force for the reaction. The present study is not time resolved,

but the flight time of ions in our instrument ensures that all processes measured occur on a time scale less than ~100 μs.

Experimentally, we used anion photoelectron spectroscopy to study these species. Anion photoelectron spectroscopy is conducted by crossing a mass-selected beam of negative ions with a fixed-frequency photon beam and analyzing the energy of the resultant photodetached electrons. Photodetachment is a direct process that is governed by the energy-conserving relation, $h\nu = \text{EBE} + \text{EKE}$, where $h\nu$ is the photon energy, EBE is the electron binding energy, and EKE is the electron kinetic energy. The known photon energy and measured electron kinetic energies yield the electron binding energies (anion-to-corresponding neutral transition energies). The anionic complexes of interest were generated in a nozzle-ion source. In this device, an ammonia/argon (15%/85%) mixture at 25°C and 2 atm was expanded through a 20-μm orifice into high vacuum, while a HCl/argon (10%/90%) mixture at a few Torr flowed from a small tube into the expansion region immediately outside the nozzle. Into this confluence of gases, low-energy electrons were injected from a biased filament nearby. This arrangement brought the three main components together in vacuum but very near the nozzle, where plentiful cooling collisions with argon atoms carried away the excess energy of the products. The nozzle and its stagnation chamber were biased at -500 V, and the entire region between the nozzle and the skimmer was subjected to a weak, axial magnetic field to enhance the stability of the microplasma. The resultant anions were then extracted and transported by a series of lenses through a 90° magnetic sector, which served as a mass analyzer and selector. By sweeping the magnet current and thus the magnetic field, anions were detected by a Faraday cup further downstream and a mass spectrum was thereby recorded. Ions of interest were then focused through an aperture and transported into the ion-laser interaction region, where they crossed a beam of ~200 W of 488-nm (2.540 eV) photons from an argon ion laser. Some of the resultant photodetached electrons then entered the optics of a hemispherical electron energy analyzer, where they were counted as a function of their electron kinetic energy. Our apparatus has been described in further detail elsewhere (*15*).

For the theoretical analysis, we used high-level, ab initio, quantum chemistry methods implemented with MOLPRO (*16*) and Gaussian03 (*17*) to characterize potential energy surfaces of the neutral and the anion. The potential energy surfaces were explored at the coupled cluster level

¹Department of Chemistry, Johns Hopkins University, Baltimore, MD 21218, USA. ²Center for Functional Nanostructures (CFN) and Institute of Physical Chemistry, Universität Karlsruhe (TH), D-76128 Karlsruhe, Germany. ³Chemical and Materials Sciences Division, Pacific Northwest National Laboratory, Richland, WA 99352, USA. ⁴Department of Chemistry, University of Gdańsk, 80-952 Gdańsk, Poland. ⁵Department of Chemistry, Heriot-Watt University, EH14 4AS Edinburgh, UK.

*To whom correspondence should be addressed. E-mail: kbowen@jhu.edu (K.H.B.); m.gutowski@hw.ac.uk (M.G.)

of theory (18) with extended basis sets (19). The coupled cluster calculations included single and double excitations (CCSD) when producing potential energy maps and determining minimum energy structures, whereas additional perturbative triple excitations [CCSD(T)] were included when calculating the adiabatic electron affinity and vertical detachment energy (VDE). Two-dimensional (2D) potential energy surfaces were calculated for the neutral and the anion, with the geometrical variables being the H-Cl distance, which characterizes the extent of intermolecular proton transfer, and the N-Cl distance along which the low-frequency intermolecular stretching vibration occurs. The 2D vibrational problems were solved for the pseudo three-body system (Cl, H, NH₃) with the use of scaled skewed coordinates (20) and a discrete variable representation of the potentials (21), resulting in

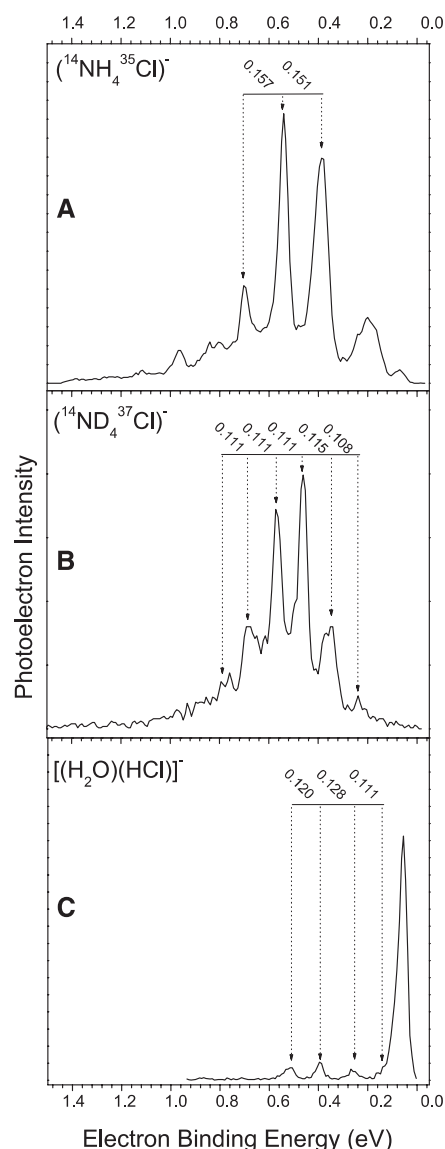


Fig. 1. Photoelectron spectra of (A) (NH₄Cl)⁻, (B) (ND₄Cl)⁻, and (C) the mixed dimer [(H₂O)(HCl)]⁻. All spectra were recorded with 2.540-eV photons.

anharmonic energy levels for the neutral and the anion that take into account the coupling between the proton and dimer stretches. All vibrational modes were taken into account when calculating the Franck-Condon (FC) factors between the ground vibrational state of the anion and various energy states of the neutral. These calculations were performed in harmonic approximation, and molecular Hessians were determined at the second-order Møller-Plesset level of theory.

Because the dipole moment of the ClH⁺⋯NH₃ complex is known from Stark-effect measurements to be substantial (4.06 D) (22), one might predict the anionic complex to be dipole bound (23, 24). However, the photoelectron spectrum of [(NH₃)(HCl)]⁻ (Fig. 1A) differs drastically from the spectrum of [(H₂O)(HCl)]⁻ (Fig. 1C), which is the water analog of the [(NH₃)(HCl)]⁻ anionic complex and a genuine dipole-bound system (25). Because dipole-bound electrons interact weakly with their nuclear frameworks, their characteristic binding energies are typically very low. Moreover, for the same reason, there is little structural difference between dipole-bound anions and their neutral counterparts, which results in high FC overlap between the anion and its neutral counterpart during photodetachment and thus a single dominant peak in their photoelectron spectra. In this context, two observations make it clear that the photoelectron spectrum of [(NH₃)(HCl)]⁻ is not that of a dipole-bound state. First, the well-developed set of vibrational features (FC profile) in the spectrum of [(NH₃)(HCl)]⁻ is indicative of a notable structural difference between the anion and its corresponding neutral. Second, for the [(NH₃)(HCl)]⁻ complex, the position of the maximum in the vibrational envelope corresponds to an EBE, which is an order of magnitude larger

than that for the dipole-bound [(H₂O)(HCl)]⁻ complex.

How, then, should we interpret the vibrational progression in the spectrum of the [(NH₃)(HCl)]⁻ complex? More specifically, if the FC distribution of peak intensities is characteristic of potential energy surfaces of the neutral and the anion that differ appreciably along some geometrical degree of freedom, what is the nature of this degree of freedom? We hypothesize that excess electron attachment to the hydrogen-bonded ClH⁺⋯NH₃ complex is accompanied by intermolecular proton transfer, with the final product being (NH₄⁺Cl)⁻. Furthermore, (NH₄⁺Cl)⁻ can be characterized as (NH₄⁰Cl)⁻, where (NH₄⁰) is the ammonium Rydberg (neutral) radical. The ammonium Rydberg radical, NH₄⁰, is a hydrogenic system in which an electron is bound to a closed-shell NH₄⁺ cation core (26).

Our calculations support this hypothesis in revealing profound differences between the neutral and anionic potential surfaces (Figs. 2 and 3). Both systems have C_{3v} equilibrium structures, but the N⁺⋯H⁺⋯Cl proton is coordinated to Cl in the neutral and to N in the anionic complex. Moreover, the Cl-N distance decreases by 0.249 Å from the neutral to the anion. Other geometrical degrees of freedom are much less affected (table S1). The calculated dipole moment of the [(NH₃)(HCl)] system increases from 4.15 to 9.82 D upon the intermolecular proton transfer, indicative of the formation of the ionic pair, (NH₄⁺Cl)⁻. The binding of the excess electron by the cationic site and the formation of the NH₄⁰Cl radical anion are responsible for the very different peak profiles in the [(H₂O)(HCl)]⁻ and [(NH₃)(HCl)]⁻ spectra. Thus, the computational results predict that the qualitative differences

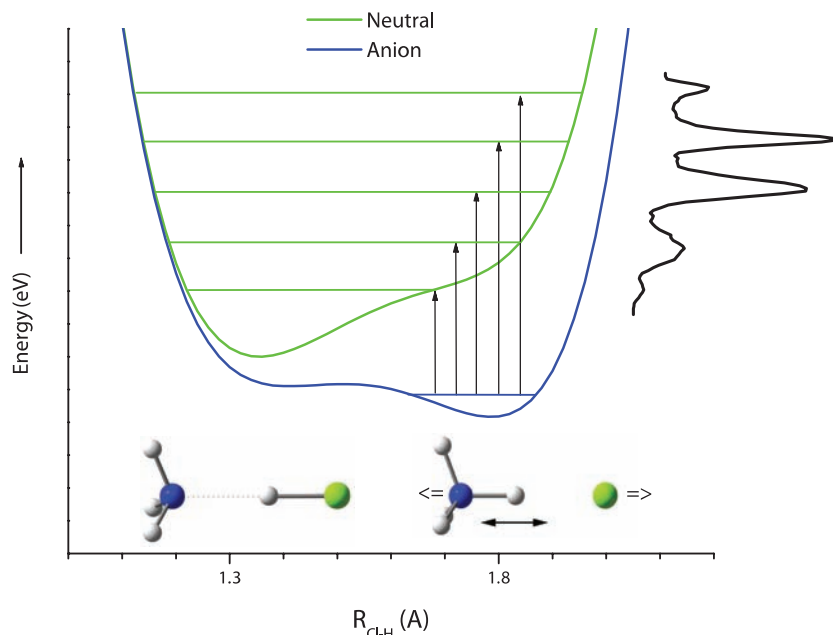
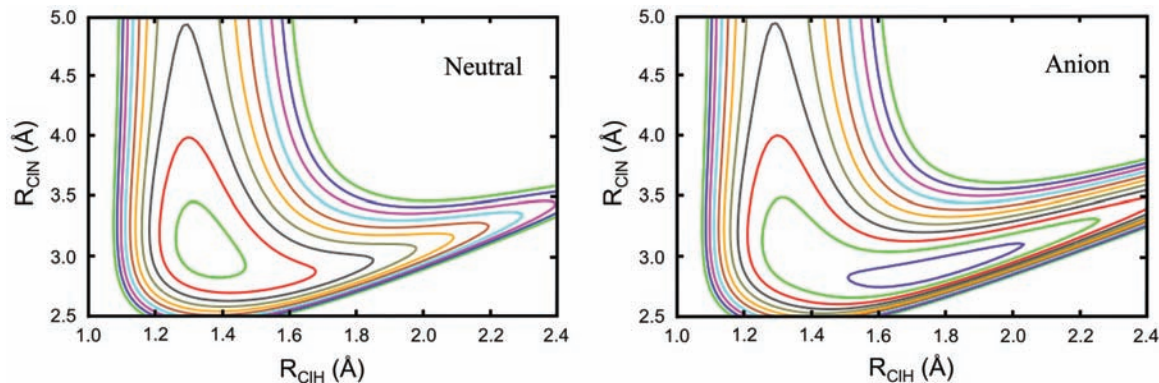


Fig. 2. One-dimensional potential energy curves for the neutral (upper) and anionic (lower) forms of ClH⁺⋯NH₃ and NH₄Cl. The two potential curves have been shifted in energy for clearer presentation. Figure 1A is presented alongside the neutral potential energy surface.

Fig. 3. Two-dimensional potential energy curves mapping the N-Cl and Cl-H bond lengths for the neutral (left) and anionic species (right). The contour line spacing is 0.005 Hartree.



in the photoelectron spectra of $[(\text{H}_2\text{O})(\text{HCl})]^-$ and $[(\text{NH}_3)(\text{HCl})]^-$ result primarily from the intermolecular proton transfer from HCl to NH_3 .

Quantitatively, the experimental and computational results are in excellent agreement. The EBE at the maximum of the most intense peak is 0.541 ± 0.010 eV, where the computed EBE value for the most prominent peak is predicted to be 0.512 eV. Essentially, these values are experimental and computational measures of VDE, the vertical detachment energy (the EBE of optimal FC overlap). Additionally, the transition between the lowest-energy vibrational level of the anionic state and the lowest-energy vibrational level of its neutral counterpart provides the value of the system's adiabatic electron affinity, and based on our spectral assignment, this value of 0.075 ± 0.020 eV agrees perfectly with the computed value of 0.075 eV.

How does the $\text{ClH}\cdots\text{NH}_3$ complex evolve, upon electron attachment, into the NH_4^0 Rydberg radical perturbed by Cl^- ? As illustrated in Fig. 4, we envision a two-step process. Because the dipole moment of the neutral $\text{ClH}\cdots\text{NH}_3$ complex is easily big enough to trap an excess electron, the first step likely involves the formation of an incipient dipole-bound anionic complex. This is in contrast to our previous theoretical work on proton transfer in the formic acid dimer anion, in which the dipole moment is too low (1.74 D for the neutral monomer and zero for the dimer) to trap an electron (27). Our calculations show that the excess electron is held in an extremely diffuse cloud off the ammonia end of the $\text{ClH}\cdots\text{NH}_3$ complex and is vertically bound by only 0.03 eV (Fig. 4A). In the second step, this extra negative charge serves to facilitate the barrier-free transfer of the proton from HCl to NH_3 , forming the $(\text{NH}_4^+\text{Cl}^-)$ anion (Fig. 4B). Thus, the dipole-bound anionic complex may be viewed as a stepping-stone to the more anionic salt NH_4^0Cl^- . In isolation, the NH_4^0 radical would be essentially spherical (Fig. 4C) with a calculated ionization potential (IP) of 5.08 eV, but in NH_4^0Cl^- , the unpaired electron is polarized and destabilized by the presence of the nearby Cl^- anion, and the electron binding energy decreases to 0.51 eV.

Our initial calculations revealed profound differences between the neutral and anionic poten-

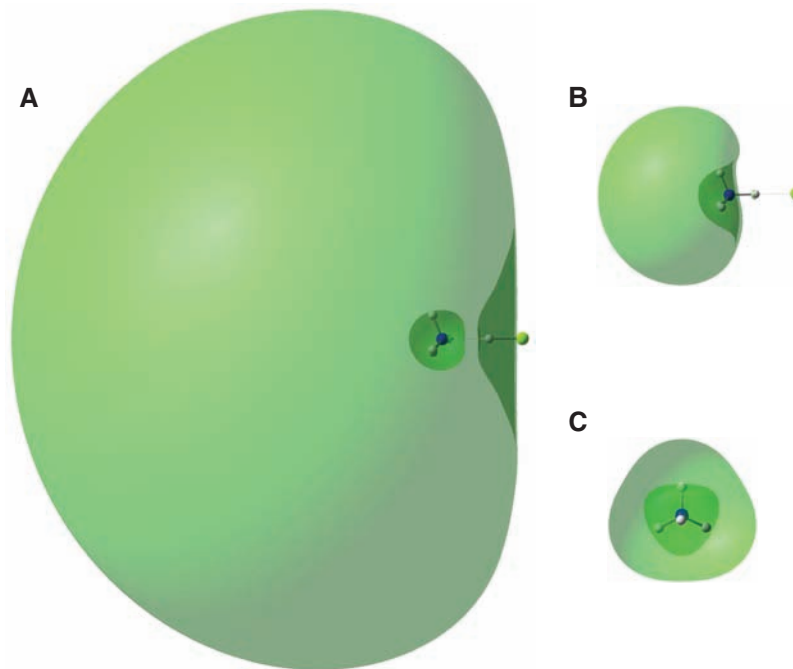


Fig. 4. Singly occupied molecular orbitals for (A) the dipole-bound intermediate $(\text{ClH}\cdots\text{NH}_3)^-$, (B) the proton-transferred species $(\text{NH}_4^+\text{Cl}^-)$, and for comparison (C) the neutral Rydberg radical (NH_4^0) . Orbitals were generated with ChemCraft (32), and the resulting contours enclose 50% of the total excess electron density in each case. Calculated VDE values for (A) and (B) are 0.03 and 0.51 eV, respectively, and the calculated IP value for (C) is 5.08 eV.

tial surfaces for this system, and slices of these surfaces along the hydrogen-chlorine distance, $R_{\text{Cl-H}}$, are shown schematically in Fig. 2. The neutral surface exhibits a well that corresponds to the $\text{ClH}\cdots\text{NH}_3$ hydrogen-bonded complex, with no local minimum at the geometry of the neutral NH_4^+Cl^- molecule. On the same distance scale, the corresponding anion surface exhibits a well at the geometry of $(\text{NH}_4^+\text{Cl}^-)$, and a ledge (without an associated local minimum) that corresponds to the hydrogen-bonded complex $(\text{ClH}\cdots\text{NH}_3)$. Thus, whereas the $(\text{NH}_4^+\text{Cl}^-)$ anion can exist as a stable entity in isolation, the neutral NH_4^+Cl^- ionic molecule cannot, collapsing thermodynamically into a complex between intact molecules of NH_3 and HCl. Figure 2 also depicts the vertical photodetachment transitions from the potential well of the $(\text{NH}_4^+\text{Cl}^-)$ anion to the corresponding neutral potential surface. It

is clear there is FC overlap, albeit small, between the $\nu = 0$ levels of the anion and neutral wells. Also, the most intense peaks in the experimental spectral profile can be assigned to transitions from the region near the center of the anion's well to the ledge portion of the neutral potential. These transitions correspond to highly excited vibrations within the greater anharmonic well of the neutral $\text{NH}_3\cdots\text{HCl}$ complex.

The $(\text{ND}_4^+\text{Cl}^-)$ spectrum exhibits the same major progressions as does the $(\text{NH}_4^+\text{Cl}^-)$ spectrum, but with smaller energy spacings (Fig. 1, A and B). The most intense peaks show typical spacings of 0.154 eV (1242 cm^{-1}) in the $(\text{NH}_4^+\text{Cl}^-)$ spectrum and 0.111 eV (895 cm^{-1}) in the $(\text{ND}_4^+\text{Cl}^-)$ spectrum. The 1.387 ratio between the above spacings is quite close to $2^{1/2}$, the expected ratio for a H/D substitution in a hydrogen stretching mode. Infrared spectroscopic measurements of

NH₃/HCl and ND₃/DCl mixtures condensed in an argon matrix have been reported (28). Their spectra yield ($\nu = 0 \rightarrow 1$) vibrational transition values of 1371 and 1113 cm⁻¹, respectively, for the N...H/D...Cl stretching modes of the proton-transferred species, NH₄⁺Cl⁻ and ND₄⁺Cl⁻. Because our spacings are extracted from highly anharmonic parts of the progressions and the (0 \rightarrow 1) vibrational frequencies are strongly affected by matrix effects (28, 29), the agreement is satisfactory. The first three calculated spacings between the energy levels associated with various excitations of the central hydrogen atom are 1718 (0 to 1), 1171 (1 to 2), and 1214 (2 to 3) cm⁻¹. The latter value of 1214 cm⁻¹ matches very well the spacing between the two most prominent peaks [1218 cm⁻¹ (0.151 eV)], suggesting that the two strongest peaks in the (NH₄⁺Cl⁻)⁻ spectrum can be assigned as transitions from $\nu'' = 0$ in the anionic complex to $\nu' = 2$ and 3, respectively, in the neutral manifold (ν'' denotes vibrational quantum numbers in the anion, ν' signifies those in the neutral).

The secondary vibrational structure in the photoelectron spectra is likely associated with low-frequency vibrational modes, a prime candidate being the Cl-N intermolecular stretching mode. This is supported by the calculated decrease of the Cl-N distance by 0.249 Å from the neutral to the anion (Fig. 3). Both for the neutral and the anion, the theoretical calculations showed strong coupling between the central hydrogen and intermolecular stretching modes. (These two modes are schematically depicted in Fig. 2.) We calculated anharmonic spacings in the 155 to 172 cm⁻¹ range (~0.02 eV) for the first five energy levels of the intermolecular stretching mode in the neutral complex.

These intermolecular stretching progressions are similar to those seen by Lineberger and co-workers (30) in their seminal work measuring the photoelectron spectra of the alkali halide anions. There are clear similarities between the current system, NH₄⁰Cl⁻, and the alkali halide anions, (MX)⁻, which have also been described as M⁰X⁻. Their spectra, however, are dominated by the only available degree of freedom, the M-X stretch, whereas in the ammonia-hydrogen chloride system, transitions from that mode are far less prominent, with the N...H/D...Cl stretch giving rise to the dominant transitions.

References and Notes

- R. S. Mulliken, W. B. Person, *Molecular Complexes, A Lecture and Reprint Volume* (Wiley-Interscience, New York, 1969).
- N. W. Howard, A. C. Legon, *J. Chem. Phys.* **88**, 4694 (1988).
- A. C. Legon, *Chem. Soc. Rev.* **22**, 153 (1993).
- B. Cherg, F.-M. Tao, *J. Chem. Phys.* **114**, 1720 (2001).
- F.-M. Tao, *J. Chem. Phys.* **110**, 11121 (1999).
- R. Cazar, A. Jamka, F.-M. Tao, *Chem. Phys. Lett.* **287**, 549 (1998).
- I. Alkorta, I. Rozas, O. Mo, M. Yanez, J. Elguero, *J. Phys. Chem. A* **105**, 7481 (2001).
- A. Brciz, A. Karpfen, H. Lischka, P. Schuster, *Chem. Phys.* **89**, 337 (1984).

- A. Famulari, M. Sironi, M. Raimondi, in *Quantum Systems in Chemistry and Physics* (Springer, Netherlands, 2000), vol. 1, pp. 361–379.
- Z. Latajka, S. Sakai, K. Morokuma, H. Ratajczak, *Chem. Phys. Lett.* **110**, 464 (1984).
- G. Corongiu *et al.*, *Int. J. Quant. Chem.* **59**, 119 (1996).
- S. Y. Reece, J. M. Hodgkiss, J. Stubbe, D. G. Nocera, *Philos. Trans. R. Soc. B* **361**, 1351 (2006).
- D. Radisic *et al.*, *J. Am. Chem. Soc.* **127**, 6443 (2005).
- J.-Y. Fang, S. Hammes-Schiffer, *J. Chem. Phys.* **106**, 8442 (1997).
- J. V. Coe, J. T. Snodgrass, C. B. Friedhoff, K. M. McHugh, K. H. Bowen, *J. Chem. Phys.* **87**, 4302 (1987).
- MOLPRO, version 2006.1, a package of ab initio programs; H. J. Werner *et al.* (www.molpro.net).
- Gaussian 03, Revision C.02; M. J. Frisch *et al.*, Gaussian, Inc., Wallingford CT, 2004.
- P. R. Taylor, *Lecture Notes in Quantum Chemistry II*, B. O. Roos, Ed. (Springer-Verlag, Berlin, 1994).
- We used augmented, polarized, correlation consistent basis sets of double- and triple-zeta quality (31) supplemented with additional diffuse s and p functions centered on the nitrogen atom with exponents chosen to describe the excess electron-charge distribution in the dipole-bound anion (ClH⁻NH₃)⁻.
- B. C. Garrett, D. G. Truhlar, *J. Am. Chem. Soc.* **101**, 5207 (1979).
- D. T. Colbert, W. H. Miller, *J. Chem. Phys.* **96**, 1982 (1992).
- C. S. Brauer *et al.*, *J. Phys. Chem. A* **110**, 10025 (2006).
- C. Desfrancois *et al.*, *Phys. Rev. Lett.* **72**, 48 (1994).
- R. N. Compton *et al.*, *J. Chem. Phys.* **105**, 3472 (1996).
- P. Skurski, M. Gutowski, *J. Chem. Phys.* **111**, 3004 (1999).
- G. Herzberg, *Annu. Rev. Phys. Chem.* **38**, 27 (1987).
- R. A. Bachorz, M. Haranczyk, I. Dabowska, J. Rak, M. Gutowski, *J. Chem. Phys.* **122**, 204304 (2005).
- A. J. Barnes, T. R. Beech, Z. Mielke, *J. Chem. Soc. Faraday Trans. II* **80**, 455 (1984).
- M. J. T. Jordan, J. E. Del Bene, *J. Am. Chem. Soc.* **122**, 2101 (2000).
- T. M. Miller, D. G. Leopold, K. K. Murray, W. C. Lineberger, *J. Chem. Phys.* **85**, 2368 (1986).
- R. A. Kendall, T. H. Dunning Jr., R. J. Harrison, *J. Chem. Phys.* **96**, 6796 (1992).
- ChemCraft Version 1.5 (build 276), www.chemcraftprog.org.
- This material is based in part on work supported by National Science Foundation grant CHE-0517337 (K.H.B.). We also thank the Polish State Committee for Scientific Research (KBN) for support under grants DS/8000-4-0026-8 (M.G.) and N204 127 31/2963 (M.H.) and the U.S. Department of Energy (DOE) Office of Basic Energy Sciences Chemical Sciences program (M.G. and G.K.S.). The research of R.A.B. was supported by the Deutsche Forschungsgemeinschaft (DFG) through the Center for Functional Nanostructures (CFN, Project No. C3.3) and by a grant from the Ministry of Science, Research and the Arts of Baden-Württemberg (Az: 7713.14-300). M.H. is a holder of an award from the Foundation for Polish Science (FNP). This research was performed in part at the Molecular Science Computing Facility in the William R. Wiley Environmental Molecular Sciences Laboratory at Pacific Northwest National Laboratory, operated for the U.S. DOE by Battelle.

Supporting Online Material

www.sciencemag.org/cgi/content/full/319/5865/936/DC1
Table S1

11 October 2007; accepted 21 December 2007
10.1126/science.1151614

High-Throughput Synthesis of Zeolitic Imidazolate Frameworks and Application to CO₂ Capture

Rahul Banerjee,^{1*} Anh Phan,¹ Bo Wang,¹ Carolyn Knobler,¹ Hiroyasu Furukawa,¹ Michael O'Keeffe,² Omar M. Yaghi^{1*}

A high-throughput protocol was developed for the synthesis of zeolitic imidazolate frameworks (ZIFs). Twenty-five different ZIF crystals were synthesized from only 9600 microreactions of either zinc(II)/cobalt(II) and imidazolate/imidazolate-type linkers. All of the ZIF structures have tetrahedral frameworks: 10 of which have two different links (heterolinks), 16 of which are previously unobserved compositions and structures, and 5 of which have topologies as yet unobserved in zeolites. Members of a selection of these ZIFs (termed ZIF-68, ZIF-69, and ZIF-70) have high thermal stability (up to 390°C) and chemical stability in refluxing organic and aqueous media. Their frameworks have high porosity (with surface areas up to 1970 square meters per gram), and they exhibit unusual selectivity for CO₂ capture from CO₂/CO mixtures and extraordinary capacity for storing CO₂: 1 liter of ZIF-69 can hold ~83 liters of CO₂ at 273 kelvin under ambient pressure.

High-throughput methods are routinely used in screening for activity of drug molecules and catalysts, but their use in the synthesis of new crystalline solid-state compounds remains relatively undeveloped. Often, the products are either known compounds or ones with condensed extended structures (1–7). For multicomponent chemical systems, such as in the synthesis of porous metal-organic structures, it would be reasonable to assume that the most energetically favored structures

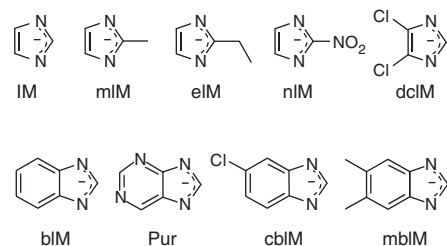
would result and that these would be known structures and topologies. Another challenge in solid-state synthesis is overcoming the propen-

¹Center for Reticular Chemistry at California NanoSystems Institute, Department of Chemistry and Biochemistry, University of California at Los Angeles, 607 East Charles E. Young Drive, Los Angeles, CA 90095, USA. ²Department of Chemistry and Biochemistry, Arizona State University, Tempe, AZ 85287, USA.

*To whom correspondence should be addressed. E-mail: rahul@chem.ucla.edu (R.B.); yaghi@chem.ucla.edu (O.M.Y.)

sity for producing multiple phases when mixed linkers are used in the synthesis (i.e., several phases each containing one kind of linker, rather than one phase containing mixed “hetero” linkers).

We show that high-throughput methods can be successfully applied to developing a robust synthesis protocol for ZIFs. Not only does this approach consistently yield only tetrahedral porous ZIF structures, but it also allows access to ZIF topologies previously un-



Scheme 1.

realized in ZIFs or in other zeolite materials. We also show that ZIFs with heterolinks can be produced that provide a greater level of complexity into the pore composition and structure, thus impacting the selectivity and multifunctionality of the pores. Specifically, the high-throughput syntheses and structures of 25 ZIFs are described and studied. All are open tetrahedral structures: 10 have heterolinks, 16 are previously unreported compositions and structures, and 5 have topologies heretofore unobserved in zeolite science. Among them are ZIFs with large (>10 Å) aperture pores, which opens up possibilities for application of these materials. We show that their synthesis is scalable to multigram quantities, using the same conditions used in the high-throughput method, and that the frameworks have extraordinary thermal and chemical stability, as well as high porosity. We find that several ZIFs with heterolinks have pores that can affect exceptional selective capture and storage of CO_2 .

We (8, 9) and others (10–14) have recently reported the synthesis of ZIFs in which (i) transition metal atoms (M, specifically Zn and Co) replace T atoms (tetrahedral linkers such as Si, Al, and P) and (ii) imidazolates (IMs) (Scheme 1) replace bridging oxides in zeolites. Given that the M–IM–M angle is near 145° and that it is coincident with the Si–O–Si angle preferred and commonly found in many zeolites, we were hopeful that the class of ZIF materials would at least be as extensive as that of zeolites (15, 16). We set out to develop the ZIF portfolio and quickly found that the traditional synthesis used to discover the original ZIFs was tedious, unpredictable, and time consuming, and that it required wastefully large amounts of solvents and reagents (8, 9). We targeted, among other goals, structures with heterolinks (Scheme 1) based on a wide variety of available IM units and studied their application to the selective capture of CO_2 .

The general ZIF reaction examined is composed of one or two of these nine different

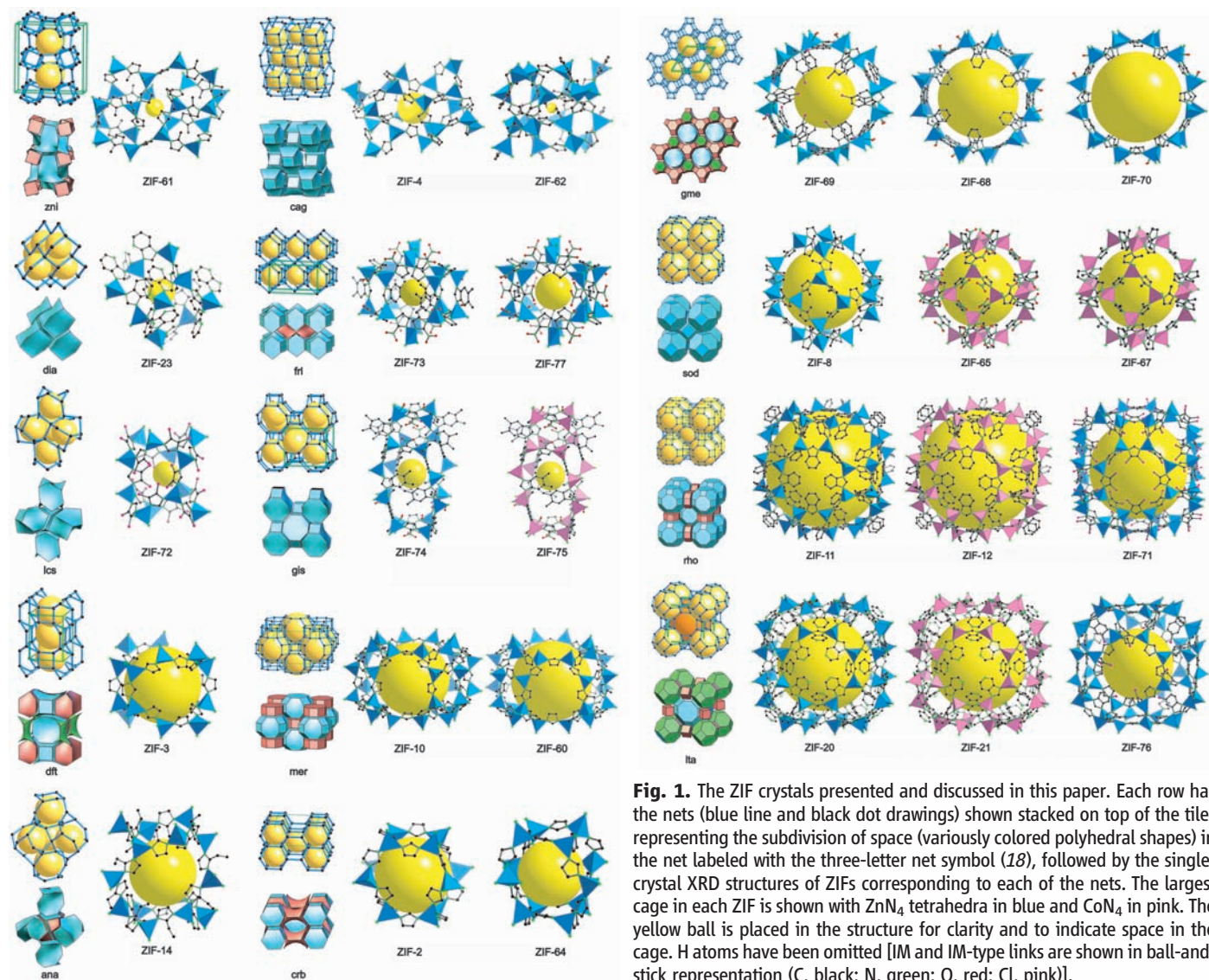


Fig. 1. The ZIF crystals presented and discussed in this paper. Each row has the nets (blue line and black dot drawings) shown stacked on top of the tiles representing the subdivision of space (variously colored polyhedral shapes) in the net labeled with the three-letter net symbol (18), followed by the single-crystal XRD structures of ZIFs corresponding to each of the nets. The largest cage in each ZIF is shown with ZnN_4 tetrahedra in blue and CoN_4 in pink. The yellow ball is placed in the structure for clarity and to indicate space in the cage. H atoms have been omitted [IM and IM-type links are shown in ball-and-stick representation (C, black; N, green; O, red; Cl, pink)].

IM-type links, which were reacted with either zinc(II) nitrate or cobalt(II) nitrate in *N,N'*-dimethylformamide or *N,N'*-diethylformamide. In total, we used 100 plates (9600 wells, 0.30 ml reactant volume per well) [supporting online material (SOM) text S1]. The metal-to-linker mole ratio was varied from 1:1 to 1:12. These amounts were dispensed with an automated dispensing unit charged with a stock solution whose concentration was also varied from 0.075 to 0.20 M for both reactants. After loading the mixture of reactants into the wells, the plates were covered with a polytetrafluoroethylene sheet, sealed, and then heated to a temperature range of 65° to 150°C for 48 to 100 hours. Crystalline products of ZIFs were obtained in this temperature range. Photographic images of wells containing crystals (0.1 to 1.0 mm) are shown in SOM text S2. After a preliminary analysis by automated powder x-ray diffraction (PXRD) (17), crystals for single-crystal x-ray diffraction (XRD) studies were then selected from those wells containing new materials (SOM text S2). In general, we found that a concentration level of 0.20 M, a reaction time of 72 hours, and an isothermal temperature of 85° or 100°C were optimal for ZIF synthesis and crystallization.

We isolated 25 different crystals using this protocol for single-crystal structural characterization (Table 1, Fig. 1, and SOM text S2). Among the 25 crystal structures, 9 are based on ZIFs already discovered by the traditional method (ZIF-2 to ZIF-23) (8, 9), whereas 16 have a new composition

Table 1. The ZIFs discovered by high-throughput synthesis. Dashes indicate no zeolite symbol.

ZIF- <i>n</i>	Composition	Net (18)	Zeolite (15)	<i>T/V</i> (nm ⁻³)	<i>d_a</i> (Å)	<i>d_p</i> (Å)	<i>N</i> †	Transitivity	Cage
2	Zn(IM) ₂	crb	BCT	2.80	6.4	6.9	12	1232	[6 ² .8 ²]
3*	Zn(IM) ₂	dft	DFT	2.66	4.6	6.0	16	1353	[6 ² .8 ⁴]
4	Zn(IM) ₂	cag	-	2.04	2.0	2.1	20	1431	[4 ² .6 ⁸]
8	Zn(mIM) ₂	sod	SOD	2.47	3.4	11.6	24	1121	[4 ⁶ .6 ⁸]
10	Zn(IM) ₂	mer	MER	2.25	8.2	12.1	24	1463	[4 ¹² .8 ⁶]
11	Zn(bIM) ₂	rho	RHO	2.01	3.0	14.6	48	1242	[4 ¹² .6 ⁸ .8 ⁶]
12	Co(bIM) ₂	rho	RHO	2.01	3.0	14.6	48	1242	[4 ¹² .6 ⁸ .8 ⁶]
14	Zn(eIM) ₂	ana	ANA	2.47	2.2	2.2	24	1132	[6 ² .8 ³]
20	Zn(Pur) ₂	lta	LTA	2.04	2.8	15.4	48	1343	[4 ¹² .6 ⁸ .8 ⁶]
21	Co(Pur) ₂	lta	LTA	2.03	2.8	15.4	48	1343	[4 ¹² .6 ⁸ .8 ⁶]
23*	Zn(abIM) ₂	dia	-	3.31	1.1	4.2	10	1111	[6 ⁴]
60	Zn(IM) _{1.5} (mIM) _{0.5}	mer	MER	2.24	7.2	9.4	24	1463	[4 ¹² .8 ⁶]
61	Zn(IM)(mIM)	zni	-	4.62	0.7	0.7	20	1342	[6 ³ .12 ²]
62	Zn(IM) _{1.75} (bIM) _{0.25}	cag	-	3.52	1.4	1.3	20	1431	[4 ² .6 ⁸]
64	Zn(IM) ₂	crb	BCT	3.62	2.5	7.9	12	1232	[6 ² .8 ²]
65	Co(nIM) ₂	sod	SOD	2.32	3.4	10.4	24	1121	[4 ⁶ .6 ⁸]
67	Co(mIM) ₂	sod	SOD	2.46	3.4	11.6	24	1121	[4 ⁶ .6 ⁸]
68	Zn(bIM)(nIM)	gme	GME	2.12	7.5	10.3	24	1463	[4 ⁶ .8 ³ .12 ²]
69	Zn(cbIM)(nIM)	gme	GME	2.09	4.4	7.8	24	1463	[4 ⁶ .8 ³ .12 ²]
70	Zn(lm) _{1.13} (nIM) _{0.87}	gme	GME	2.10	13.1	15.9	24	1463	[4 ⁶ .8 ³ .12 ²]
71	Zn(dclIM) ₂	rho	RHO	2.06	4.2	16.5	48	1242	[4 ¹² .6 ⁸ .8 ⁶]
72	Zn(dclIM) ₂	lcs	-	3.16	1.9	1.9	12	1121	[6 ⁵]
73	Zn(nIM) _{1.74} (mbIM) _{0.26}	frl	-	3.20	1.0	1.0	16	2342	[4 ⁴ .6 ² .8 ²]
74	Zn(nIM)(mbIM)	gis	GIS	2.66	1.2	2.6	20	1231	[4 ⁶ .8 ⁴]
75	Co(nIM)(mbIM)	gis	GIS	2.66	1.2	2.62	20	1231	[4 ⁶ .8 ⁴]
76	Zn(IM)(cbIM)	lta	LTA	2.05	5.4	12.2	48	1343	[4 ¹² .6 ⁸ .8 ⁶]
77	Zn(nIM)	frl	-	3.22	2.9	3.6	16	2342	[4 ⁴ .6 ² .8 ²]

*Discovered by traditional synthesis methods. †*N* is the number of vertices of the largest cage.

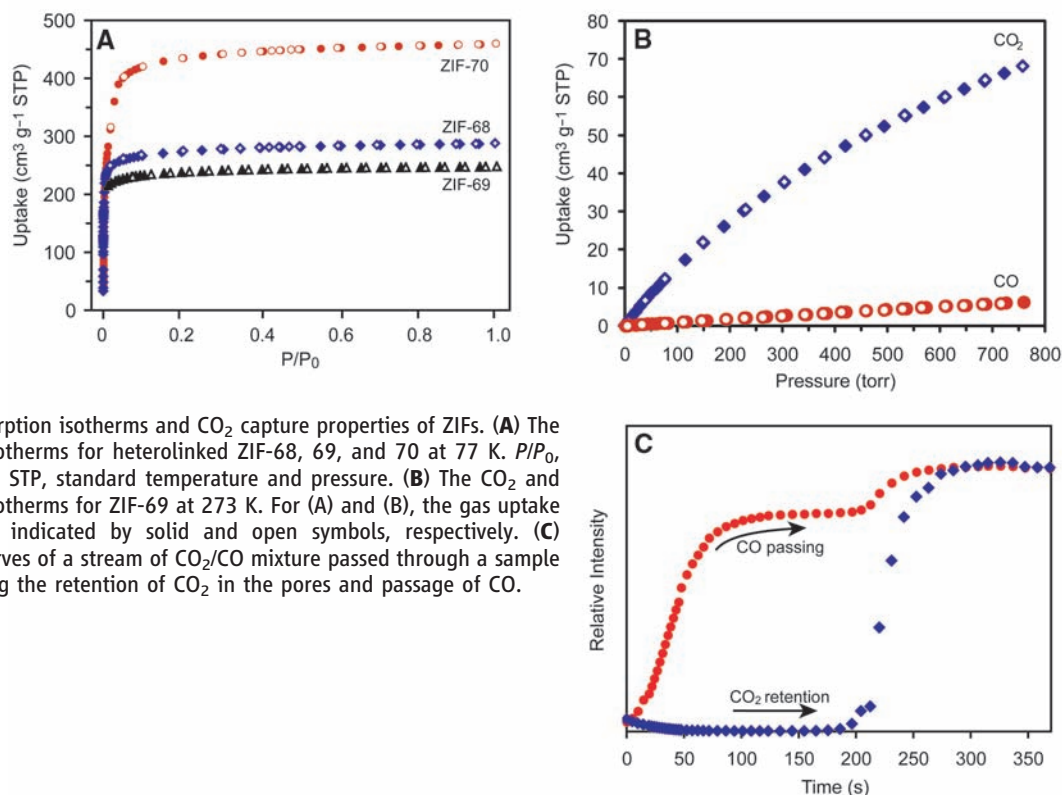


Fig. 2. Gas adsorption isotherms and CO₂ capture properties of ZIFs. (A) The N₂ adsorption isotherms for heterolinked ZIF-68, 69, and 70 at 77 K. *P/P₀*, relative pressure; STP, standard temperature and pressure. (B) The CO₂ and CO adsorption isotherms for ZIF-69 at 273 K. For (A) and (B), the gas uptake and release are indicated by solid and open symbols, respectively. (C) Breakthrough curves of a stream of CO₂/CO mixture passed through a sample of ZIF-68 showing the retention of CO₂ in the pores and passage of CO.

and a new structure (ZIF-60 to 77). Three (ZIF-68 to 70) have structures based on a zeolite topology (**gme**), which heretofore has not been achieved in metal-organic compounds, and five have tetrahedral topologies (**dia**, **cag**, **frl**, **lcs**, and **zni**) not occurring in zeolites. The nets of the structures are denoted by a bold lowercase three-letter symbol (*l8*) that is often the same as that of the corresponding zeolite net (Table 1). Furthermore, 10 structures (ZIF-60 to 62, 68 to 70, and 73 to 76) contain two chemically different imidazolate links (i.e., heterolinks). In the Cambridge Structural Database (version 5.28, January 2007), only 24 ZIF structures have been reported in the past 12 years; however, using the methodology described here, in 3 months, we optimized the reaction and identification conditions and produced crystals of ZIF-2 to 77 from the examination of only 9600 wells.

We analyze the complexity of the nets in terms of their natural tiling, which is a unique partition of space into tiles such that the set of edges and vertices of the tiles is the same as that of the net (*19*). A useful measure of structural complexity is the transitivity *pqrs*, which records that the tiling has *p* kinds of vertices, *q* kinds of edges, *r* kinds of faces, and *s* kinds of tiles. Of the 14 topologies recorded in Table 1 and shown in Fig. 1, all but one (**frl**) have just one kind of vertex (uninodal). Of the 176 recognized zeolite topologies, 21 are uninodal; we have found 9 of these in this study. Of the uninodal zeolite nets, only three (GIS, SOD, and ABW) have just one kind of tile (isohedral), and we have found two of them.

Of the five nonzeolite nets found and mentioned above, four are uninodal and three are isohedral. In contrast to the synthesis of zeolites, in ZIF chemistry, we are selecting the simpler nets in the synthesis. Indeed, the most complex zeolite net has transitivity 24 27 41 19 (*20*), which suggests that there is vast potential for the use of this high-throughput method in accessing ZIFs with structures based on more complex zeolites. The only binodal net (**frl**) found is of interest because it is simply related to the net (**sra**) of the missing isohedral zeolite net ABW, as detailed elsewhere (*21*). The topology (**lcs**) of ZIF-72 is also of interest because it is that of an invariant lattice complex (symbol *S*), but, despite its simplicity, it has not been previously reported in any tetrahedral structure.

We tabulate the density of the ZIFs using the traditional zeolite measure of the number of tetrahedral vertices per unit volume (*T/V*) (Table 1). The density (*T/V*) of an IM analog (i.e., ZIF) is

typically one-eighth that of a silicate zeolite because, in an IM framework containing zinc(II), the Zn...Zn distance is ~6.0 Å, whereas the corresponding Si...Si distance in a silicate is ~3.0 Å. For the structures reported here, *T/V* is in the range 2.0 to 4.6 nm⁻³; whereas the density for oxide zeolites is 12 to 20 nm⁻³. This difference indicates that ZIF frameworks are more open and more amenable to functionalization of their pores.

The existence of two different types of IMs with a side chain (especially an NO₂ or a CH₃ group) or an aromatic ring on the link makes the pore heterogeneously functionalized across the series (Fig. 1). Furthermore, the diameter of the largest sphere that will pass through that pore (*d_a*) ranges from as low as 0.7 Å to as high as 13.1 Å, whereas the diameter of the largest sphere that will fit into the cavities (*d_p*) varies from 0.7 to 15.9 Å. With the exception of ZIF-69, 71, 72, and 77, H atoms are nearest to the center of the cavity, and we have used a van der Waals radius of 1.2 Å for H in determining the appropriate sphere size. For ZIF-69, 71, 72, and 77, where the atoms nearest to the center of the cages are either Cl (69, 71, and 72) or O (77), van der Waals radii of 1.8 Å (Cl) and 1.5 Å (O) were used. The values of *d_a* and *d_p* provide a lower limit to the cage volume because, in some cases, the cages are ellipsoidal. The number of vertices of the largest cage in each structure ranges from 10 (**dia**) to 48 (**lta**). The cage face symbol (in which [...*m*...]) signifies that the cage has *m* faces that are *n* rings) and the transivities of the nets are given in Table 1.

In all of the ZIFs, a Zn or Co atom is connected to four IM or substituted IM linkers to create a corresponding tetrahedron (Fig. 1 and SOM text S2). The tetrahedra are linked by corner-sharing into different three-dimensional zeolitic frameworks. However, these ZIFs differ in the nature of the functional groups decorating the pores and in the metrics of their pore structure (Table 1). Across the series, the metrics are systematically varied in increments of less than 1 Å; such tunability is unusual and potentially useful in gas adsorption and separation. We first needed to show for the ZIFs of interest that the microscale synthesis and the reaction conditions used for their discovery in the high-throughput instrument could be translated into multigram-scale bulk synthesis. For seven chosen ZIFs of heterolinks (ZIF-60, 61, 68 to 70, 74, and 76), we found that the microsynthesis conditions are scalable to 10-g scale and pure ZIF materials can thus be obtained (SOM text S1).

We targeted ZIF-68, 69, and 70 for adsorption studies because they all have the same topology (**gme**) and large pores (7.2, 10.2, and 15.9 Å in diameter for ZIF-69, 68, and 70, respectively) connected through tunable apertures (4.4, 7.5, and 13.1 Å). These ZIFs are permanently porous metal-organic frameworks in which the pore walls contain heterogeneous link functionality. We first examined the structural, thermal, and chemical stability, as well as the porosity, of these ZIFs. Thermal gravimetric analysis (TGA) was performed on the as-synthesized, solvent-exchanged, and activated ZIF products of ZIF-68 to 70, which revealed a thermal stability range of up to 390°C. Specifically, the TGA trace for these ZIFs showed a gradual weight-loss step between 25° and 168°C. A plateau between 150° and 390°C indicates that the evacuated framework has high thermal stability (SOM text S3). The evacuated frameworks of ZIF-68 to 70 thus produced have PXRD patterns that are coincident with the corresponding patterns simulated from single-crystal XRD structures (SOM text S3), which indicates that heterolinked ZIF frameworks have high structural and thermal stability. Examination of their chemical stability was performed by heating the samples in boiling benzene, methanol, and water for 7 days: conditions that reflect potential extreme industrial requirements. Notably, all of the ZIFs retained their structures under these conditions, as evidenced by the sharp, unshifted diffraction lines in their PXRD patterns (SOM text S4).

The permanent porosity of these ZIFs was also demonstrated by N₂ adsorption measurements (*8*) (SOM text S5), which showed that they exhibit type I adsorption isotherm behavior typical of materials of permanent porosity (Fig. 2A). The Langmuir surface areas were 1220, 1070, and 1970 m² g⁻¹ for ZIF-68, 69, and 70, respectively; these surface areas are more than double those of the most porous zeolites (*22*) and significantly higher than those of other reported ZIFs (*8*, *9*).

The exceptional stability and metric attributes of these ZIFs led us to evaluate their behavior for a particularly difficult gas separation: CO₂ from CO. The adsorption isotherms for all three ZIFs show a disproportionately high affinity and capacity for CO₂ (SOM text S5), with ZIF-69 outperforming ZIF-68 and ZIF-70, as well as the state-of-the-art material BPL carbon (*23*) (Table 2 and Fig. 2B). Adsorption is completely reversible, and we calculate that 1 liter of ZIF-69 can store 82.6 liters (162 g) of CO₂ at 273 K. The selectivity is further supported by preliminary breakthrough experiments, which show complete retention of CO₂ and passage of CO through the pores of ZIF-68, 69, and 70 when they are exposed to streams containing a binary mixture of CO₂/CO (50:50 v/v) at room temperature (Fig. 2C and SOM text S5). In comparison

Table 2. Comparison of gas separation selectivity of ZIFs and BPL carbon (SOM text S5).

Material	Gas pairs	ZIFs selectivity	BPL carbon selectivity (23)	Ratio ZIFs/BPL carbon
ZIF-68	CO ₂ /CO	19.2	7.5	2.6
ZIF-69	CO ₂ /CO	20.9	7.5	2.8
ZIF-70	CO ₂ /CO	37.8	7.5	5.0

with that of BPL carbon, ZIFs have higher selectivity (Table 2). In terms of storage capacity and selectivity to CO₂, ZIF-69 and 70 outperform BPL carbon and all the other ZIFs that we have examined.

References and Notes

- D. E. Akporiaye, I. M. Dahl, A. Karlsson, R. Wendelbo, *Angew. Chem. Int. Ed.* **37**, 609 (1998).
- J. Klein, C. W. Lehmann, H. W. Schmidt, W. F. Maier, *Angew. Chem. Int. Ed.* **37**, 3369 (1998).
- K. Choi, D. Gardner, N. Hilbrandt, T. Bein, *Angew. Chem. Int. Ed.* **38**, 2891 (1999).
- R. Lai, B. S. Kang, G. R. Gavalas, *Angew. Chem. Int. Ed.* **40**, 408 (2001).
- M. Forster, N. Stock, A. K. Cheetham, *Angew. Chem. Int. Ed.* **44**, 7608 (2005).
- N. Stock, T. Bein, *Angew. Chem. Int. Ed.* **43**, 749 (2004).
- A. Corma, M. J. Díaz-Cabanas, J. L. Jordá, C. Martínez, M. Moliner, *Nature* **443**, 842 (2006).
- K. S. Park *et al.*, *Proc. Natl. Acad. Sci. U.S.A.* **103**, 10186 (2006).
- H. Hayashi, A. P. Côté, H. Furukawa, M. O'Keeffe, O. M. Yaghi, *Nat. Mater.* **6**, 501 (2007).
- R. Lehnert, F. Seel, *Z. Anorg. Allg. Chem.* **464**, 187 (1980).
- S. J. Rettig, V. Sánchez, A. Storr, R. C. Thompson, J. Trotter, *J. Chem. Soc. Dalton Trans.* **2000**, 3931 (2000).
- Y. Liu, V. Ch. Kravtsov, R. Larsena, M. Eddaoudi, *Chem. Commun.* **2006**, 1488 (2006).
- J.-P. Zhang, X.-M. Chen, *Chem. Commun.* **2006**, 1689 (2006).
- Y.-Q. Tian *et al.*, *Chem. Eur. J.* **13**, 4146 (2007).
- C. Baerlocher, L. B. McCusker, Database of Zeolite Structures (www.iza-structure.org/databases).
- M. E. Davis, *Nature* **417**, 813 (2002).
- The isolation of the sample array is accomplished in parallel by sonication and transfer in a custom-designed shallow metal plate, which allows the presence of a small amount of solvent during the PXRD data collection. The samples were then analyzed by a Bruker D8 DISCOVER high-throughput PXRD instrument with a movable horizontal x-y stage for automated analysis and an image plate detector system. The data collection time was 3 to 6 min per sample. The PXRD patterns thus collected were compared against an in-house library of PXRD patterns of known ZIFs and other network-type materials.
- Reticular Chemistry Structure Resource (<http://rcsr.anu.edu.au>).
- O. Delgado-Friedrichs, M. O'Keeffe, O. M. Yaghi, *Acta Crystallogr. A* **59**, 22 (2003).
- V. A. Blatov, O. Delgado-Friedrichs, M. O'Keeffe, D. M. Proserpio, *Acta Crystallogr.* **A63**, 418 (2007).
- N. L. Rosi *et al.*, *J. Am. Chem. Soc.* **127**, 1504 (2005).
- F. Rouquerol, J. Rouquerol, K. Sing, *Adsorption by Powders and Porous Solids* (Academic Press, London, 1999).
- S. Sircar, T. C. Golden, M. B. Rao, *Carbon* **34**, 1 (1996).
- The work was supported by Badische Anilin und Soda Fabrik (BASF) Ludwigshafen for synthesis, the U.S. Department of Energy (DEFG0206ER15813) for adsorption and separations studies, and the U.S. Department of Defense (W911NF-061-0405) for equipment used for breakthrough experiments. Crystallographic data for the structures reported in this paper have been deposited with the Cambridge Crystallographic Data Centre under reference numbers CCDC 671067 to 671089. These data can be obtained free of charge via www.ccdc.cam.ac.uk/conts/retrieving.html (or from the Cambridge Crystallographic Data Centre, 12 Union Road, Cambridge CB2 1EZ, UK).

Supporting Online Material

www.sciencemag.org/cgi/content/full/319/5865/939/DC1
SOM Text S1 to S5
Figs. S1 to S86
Tables S1 to S23

2 November 2007; accepted 3 January 2008
10.1126/science.1152516

Rogue Mantle Helium and Neon

Francis Albarède

The canonical model of helium isotope geochemistry describes the lower mantle as undegassed, but this view conflicts with evidence of recycled material in the source of ocean island basalts. Because mantle helium is efficiently extracted by magmatic activity, it cannot remain in fertile mantle rocks for long periods of time. Here, I suggest that helium with high ³He/⁴He ratios, as well as neon rich in the solar component, diffused early in Earth's history from low-melting-point primordial material into residual refractory "reservoir" rocks, such as dunites. The difference in ³He/⁴He ratios of ocean-island and mid-ocean ridge basalts and the preservation of solar neon are ascribed to the reservoir rocks being stretched and tapped to different extents during melting.

Helium-4 is a radiogenic nuclide produced in Earth and other planetary bodies by the alpha decay of uranium and thorium. In contrast, most of the ³He present is a regular stable nuclide. The relative abundances of the two isotopes in oceanic basalts therefore reflect the evolution of the parent/daughter ratio (U+Th)/He. These three elements are strongly incompatible (i.e., excluded from the structure of the major silicate materials), but one of them (He) is markedly affected by outgassing. Helium preferentially partitions not only into any gas phase present, but also into liquid during melting (1). Contribution from primitive undegassed mantle gives basalts very low ⁴He/³He ratios. The canonical model holds that high ⁴He/³He ratios characterize high (U+Th)/He mantle sources, such as the mantle underneath mid-ocean ridges, which were degassed during successive melting events. If He is less incompatible than both Th and U, however, these

low ³He/⁴He regions could instead signal mantle that was depleted in incompatible elements upon melting (1, 2). However, the abundances of rare gases differ between these two models, being high for undegassed mantle and very low for residual mantle.

For historical reasons, He isotopic compositions are reported upside down as R/R_{atm}, where R denotes the ³He/⁴He ratio and the subscript signals the normalization to the atmospheric ratio. More than 30 years of observations have shown that mid-ocean ridge basalts (MORBs) are characterized by a narrow range of ³He/⁴He ratios clustering about 8 R_{atm}, whereas values in excess of 20 R_{atm} are found nearly exclusively in ocean-island basalts (OIBs) (3–6). These data support the idea that MORBs are derived from parts of Earth's mantle that are significantly more degassed than the source of OIBs (5, 7, 8). If pushed to the extreme, the assertion that OIBs are tapping a deep, largely undegassed part of the mantle implies that the lower mantle is pristine and that mantle convection takes place as separate layers (9, 10).

This canonical view, however, conflicts with several critical observations on OIBs. Nearly every isotopic system involving lithophile elements—notably ⁸⁷Rb-⁸⁷Sr, ¹⁴⁷Sm-¹⁴³Nd, ¹⁷⁶Lu-¹⁷⁶Hf, and ¹⁸⁷Re-¹⁸⁷Os—indicates that the mantle source of MORB and OIB is de-

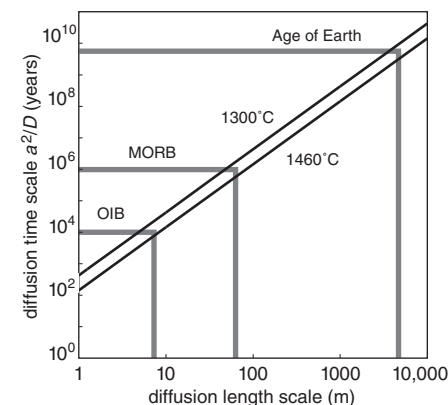


Fig. 1. Relationship between the time and length scales of diffusion in olivine, using the data of Shuster *et al.* (20) at two different temperatures. The two isotopes of He have comparable diffusion rates. At a temperature of 1460°C, He and Ne have the same diffusivity in quartz, which suggests that He and Ne diffusivity at mantle temperatures in mantle minerals may not be very different. The set of values labeled "Age of Earth" show that over the geological ages, He and Ne may have moved by diffusion over distances in excess of several kilometers. Assuming that melting takes place in the uppermost 100 km and an upwelling velocity of 10 m year⁻¹ beneath OIBs and 10 cm year⁻¹ beneath MORBs gives time scales for diffusion; the corresponding distances of diffusion relevant to melt extraction for MORB and OIB can be read from the curve (see text).

pleted in fertile components with respect to chondrites. Even stronger evidence against primitive mantle is the surprisingly large range of $\delta^{18}\text{O}$ values in Hawaiian basalts, which attest to the OIB source holding a component that went through low-temperature alteration, and the correlation of $^{187}\text{Os}/^{186}\text{Os}$ with $\delta^{18}\text{O}$ (11). The correlation between Hf and Pb isotopes further indicates the presence of pelagic sediments in the source of the Hawaiian plume (12). These observations raise the question of how Hawaiian basalts, which carry the embodiment of a primordial gas signature, at the same time can provide such strong evidence of surface material recycling. They are not explained by geodynamic models in which high $^3\text{He}/^4\text{He}$ ratios in oceanic basalts reflect a contribution from blobs of primordial material drifting in the mantle flow field (13).

A solution to this conundrum may lie in an analogy with oil genesis: ^3He is unlikely to escape melting events and magmatic outgassing for billions of years of whole-mantle convection if it resides in fertile, low-melting-point rocks, but large quantities may remain buried at depth if He migrates into refractory reservoir rocks. Because there can be no free gas phase percolating at pressures in excess of olivine carbonation at ~ 3 GPa (14), He must be largely redistributed by diffusion. Given the lack of isotopic evidence for the persistence of large swaths of primordial mantle, the dual fate of He must consist in being hosted either by fertile material, from

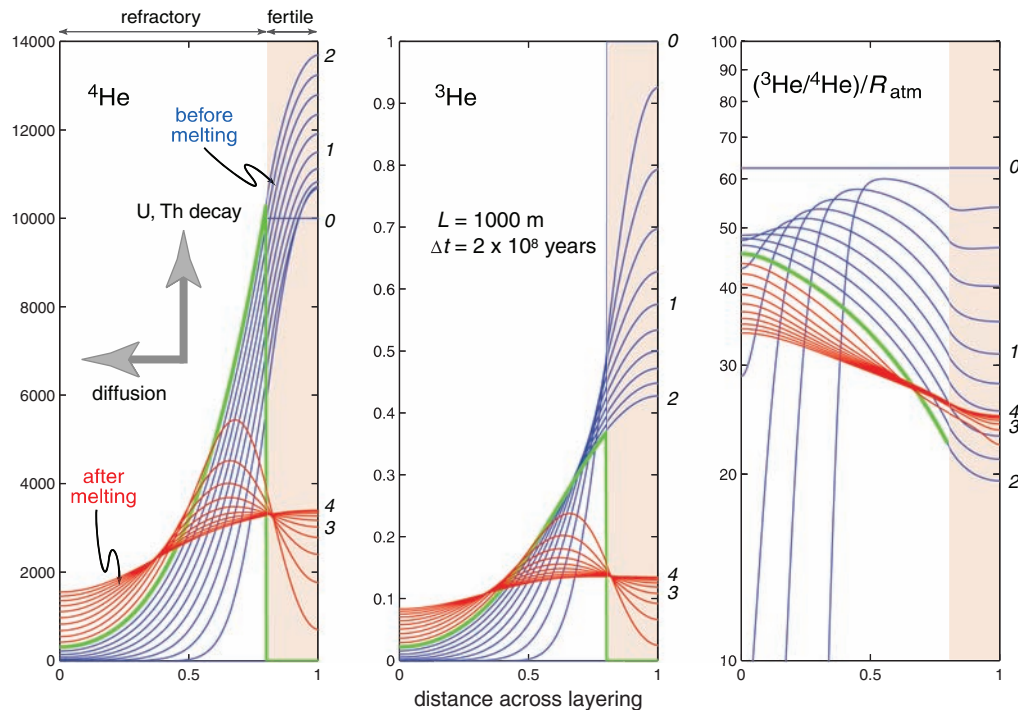
which it is eventually extracted to the atmosphere upon decompressional melting, or by refractory rocks.

Very different gradients of ^3He and ^4He across the system favor the increase of $^3\text{He}/^4\text{He}$ in refractory rocks. Helium-3 was originally present in frozen He-rich material evolved from the early magma ocean, such as pyroxenites and fertile peridotite. Throughout Earth's history, ^3He migrated deeper and deeper into thick layers of He-poor refractory rocks, first in cumulates of the magma ocean (15, 16) and subsequently in olivine-rich dunites and harzburgites formed under mid-ocean ridges (17). Changes in the mineralogy of the alternating layers with depth are not relevant as long as melt is not present. The persistence of high $^3\text{He}/^4\text{He}$ mantle regions therefore boils down to two simple questions: (i) how He migrated into deep-seated refractory reservoirs in the first place, and (ii) how it was extracted from its reservoir upon melting. The "helium-recharged depleted mantle" model of Ellam and Stuart (18) assumes conservative mixing between depleted and undegassed mantle. Inefficient He extraction does not result from the persistence of abundant gas cavities during shallow melting (19), because bubbles would need to hold back exceedingly large amounts of rare gases. The case for He-poor, high- $^3\text{He}/^4\text{He}$ residues implied by the assumption that He is slightly less incompatible than U and Th during melting (1) is, by contrast, fully compatible with the present model.

Figure 1 shows the overall scaling of He diffusion in mantle rocks. The He volume diffusivity in olivine was recently redetermined, and ^3He and ^4He were shown to diffuse at comparable rates (20). Because of the exponential dependence of diffusivity on the inverse of temperature, the results are virtually independent of the choice of a particular mantle temperature. At 1300° to 1400°C , it only takes He $\sim 10^4$ years to migrate over ~ 10 m and 10^8 years to cover 1 km.

A quantitative model illustrates how rogue mantle rare gases move around (Fig. 2). I assume that mantle material consists of alternating thin layers of low-melting-point rocks, either primordial fertile peridotite or pyroxenites, embedded in thicker layers of refractory dunite and harzburgite (21). The model assumes radiogenic ^4He ingrowth from U and Th. Initially, ^3He , U and Th are much more concentrated in the fertile layers than in residual rocks. For simplicity, I assume that the mantle is homogeneously striped, so that, by symmetry, a no-flux condition applies at the center of both the pyroxenite and dunite layers. The model described in Fig. 2 postulates that ^3He initially hosted in a 200-m-thick layer of primordial material diffuses into the 800-m-thick ^3He -poor refractory layer for 2×10^9 years. At this point, a small fraction of melt is removed from the fertile layer entraining its He, U, and Th, possibly during one of the mantle events suggested by Parman (22). I further assume that either the residuum of the fertile layer is preserved or that it is replaced

Fig. 2. A two-stage history of He in the marble-cake mantle made of fertile (e.g., U- and Th-rich "pyroxenite" in beige) and refractory (e.g., U- and Th-poor "dunite" in green) rocks. The figure represents He diffusion over 4×10^9 years, with a double-layer geometry and a melting event at 2×10^9 years ago. The curves show He profiles across the system every 2×10^8 years; the labels in italic along the right edges indicate numbers of years ($\times 10^9$) before the present. The thicknesses of the refractory and the fertile layers are 800 and 200 m, respectively ($L = 1000$ m). The He diffusion coefficient is taken to be $10^{-12} \text{ m}^2 \text{ s}^{-1}$ (20). Helium-3 concentrations are normalized to their initial value in the fertile layer. The initial $^4\text{He}/^3\text{He}$ ratio of Earth is taken as 8000. Fertile material has a $^{238}\text{U}/^3\text{He}$ ratio of 15,000 before melting and 500 after melting. $^3\text{He}/^4\text{He}$ ratios are normalized to the modern atmospheric ratio $R_{\text{atm}} = 1.4 \times 10^{-6}$. It is assumed that ^3He is introduced at $t = 0$ into the system with the fertile layer before significant ingrowth of radiogenic ^4He . A core of helium with a high $^3\text{He}/^4\text{He}$ ratio moves into the dunite (right panel). The episode of melting (green curves) removes helium with a low $^3\text{He}/^4\text{He}$ ratio from the fertile layer and therefore helps to maintain isotopic gradients across the system. After melting (red curves), helium



with a high $^3\text{He}/^4\text{He}$ ratio diffuses back from the dunite into the still fertile, but no longer pristine and undegassed, pyroxenite layer. Refractory He-, U-, and Th-poor dunite therefore acts as a long-term reservoir for He and Ne.

by an equivalent layer of subducted pyroxenite, which is a simple way of maintaining the double-layer structure. The diffusion equations were solved using an implicit finite-difference scheme. In the absence of relevant data, I assume that the high- and low-pressure forms of these rocks behave identically with respect to He diffusion.

In the interval from 2×10^9 years ago to the present (in blue in Fig. 2), significant radiogenic ^4He has not yet accumulated in the fertile layer, and the core of helium diffusing into the U- and Th-poor refractory layer therefore has a high $^3\text{He}/^4\text{He}$ ratio. At 2×10^9 years ago, the episode of melting (in green) removes helium with a low $^3\text{He}/^4\text{He}$ ratio from the fertile layer, which thereby helps maintain isotopic gradients across the system. The interval from 2×10^9 to 4×10^9 years ago (in red) shows how the fertile layer, regardless of its origin, is replenished in helium with a high $^3\text{He}/^4\text{He}$ ratio by the refractory layer.

The contrast between MORB and OIB sources can thus be accounted for simply by different proportions of high- $^3\text{He}/^4\text{He}$ reservoir rocks being unaffected by the melt extraction process. Assuming for simplicity that melts begin forming over the uppermost 100 km with an upwelling rate of 10 m year^{-1} beneath OIBs and 10 cm year^{-1} beneath mid-ocean ridges, the characteristic times of melt extraction in these two environments are 10^4 years and 10^6 years, respectively, and the maximum thicknesses of refractory layers contributing their He to the magmas are 10 m and 100 m, respectively (Fig. 1). For OIBs, both the existence of high- $^3\text{He}/^4\text{He}$ regions and the coexistence of high- and low- $^3\text{He}/^4\text{He}$ magmas are adequately explained by the variable stretching of refractory layers present in the upwelling region. Because of temperature-dependent viscosity, shear is maximum along the edge of conduits: Outgassing of large lumps of residual material down to a dimension of $<100 \text{ m}$ should allow for a quick transfer of the high- $^3\text{He}/^4\text{He}$ signature to their surroundings, including the fertile components, which eventually melt and form OIBs. The highest $^3\text{He}/^4\text{He}$ ratios (>30) are found in the infant volcano of Loihi on the southeastern flank of Hawaii (8) and in the northwesternmost lavas of Selaldalur in Iceland (23). Pyroxenite layers not brought into contact with such initially large lumps of residues, in contrast, could be parent to low- $^3\text{He}/^4\text{He}$ basalts, which provides an alternative to the interpretation that the source of low- $^3\text{He}/^4\text{He}$ hot spots, such as Gough or Tristan, is dominated by recycled crustal material (8).

The flow regime beneath mid-ocean ridges is expected to be laminar, with weaker velocity gradients and only mild shearing. The distribution of the spacing between alternating values of Hf isotopes along the Southeast Indian Ridge implies an exponential distribution of layer thicknesses (24). The $^3\text{He}/^4\text{He}$ ratio of MORB therefore represents an aver-

age value of thinly to moderately marbled mantle ($<100 \text{ m}$). Thick refractory lumps are not expected to contribute to the He measured in MORB, nor are their $^3\text{He}/^4\text{He}$ ratios anticipated to be affected by ridge activity. Unusually low $^3\text{He}/^4\text{He}$ ratios are observed in MORB along the ultraslow-spreading Southwest Indian Ridge (25), where the crust is unusually thin (26). I suggest that the low $^3\text{He}/^4\text{He}$ ratios simply result from a lesser contribution of the thickest refractory layers to the magmatic He.

The presence of solar (high- $^{20}\text{Ne}/^{22}\text{Ne}$) neon in oceanic basalts (27) can be explained by the same rogue component. Neon diffusivity in olivine is unknown, but Ne and He diffusivities in quartz are identical at 1460°C (28), which justifies the assumption that at high temperatures, the diffusion coefficients of these two gases may be comparable in mantle minerals. As for primordial ^3He , the presence of solar neon in MORB is not expected from a severely degassed mantle reservoir unless it is held back during melting. More than any other argument, the correlation between $^3\text{He}/^4\text{He}$ and $^{21}\text{Ne}/^{22}\text{Ne}$ ratios in OIB (29) and MORB (30) implies that a primordial component is present in the mantle and that diffusion out of the refractory reservoir is incapable of efficiently separating Ne from He. The similarity of rare gas diffusivities simply reflects that the crossover temperature of Arrhenius plots predicted by the Meyer-Neldel-Winchell compensation law for diffusion falls in the range of mantle temperatures. The isotopic abundances of oxygen and lithophile radiogenic nuclides (^{87}Sr , ^{143}Nd , ^{176}Hf , ^{206}Pb , etc.) in oceanic basalts attest to a complex history and cannot be reconciled with a primordial holding tank of rare gases that would have escaped melting processes. In contrast to He, which does not accumulate in the atmosphere, and to Ne, whose radiogenic ingrowth is slow, Ar is perfectly accounted for by a binary mixture of atmospheric and radiogenic sources, and does not lend itself to a breakdown of separate mantle components.

The present interpretation of mantle He isotope geochemistry turns the rationale behind the canonical model upside down. It views high $^3\text{He}/^4\text{He}$ ratios as attesting to the presence of recycled refractory residues rather than to that of primordial fertile mantle. The refolded parts of the mantle are weak and intensely stretched by mantle flow, and they must be quickly depleted in ^3He by repeated melting events. In contrast, thicker layers of residual material constitute a resistant reservoir for helium with a high $^3\text{He}/^4\text{He}$ ratio: Whichever process removed the fertile constituents from such rocks in the first place (ridge activity, accumulation from an early magma ocean) should have also removed most of their water, making them particularly rigid and resistant to further stretching by mantle convection (31). Old fragments of oceanic lithosphere and refractory cumulates from the magma ocean, rather than

primordial mantle “nuggets,” should host most of the primordial He and Ne observed today in oceanic basalts. Helium with high $^3\text{He}/^4\text{He}$ ratios may contain a component of primordial origin but may not necessarily reflect the reservoir in which it has been residing for most of Earth’s history.

References and Notes

1. S. W. Parman, M. D. Kurz, S. R. Hart, T. L. Grove, *Nature* **437**, 1140 (2005).
2. D. Graham, J. Lupton, F. Albarède, M. Condomines, *Nature* **347**, 545 (1990).
3. H. Craig, J. E. Lupton, *Earth Planet. Sci. Lett.* **31**, 369 (1976).
4. I. Kaneoka, N. Takaoka, *Science* **208**, 1366 (1980).
5. C. J. Allegre, T. Staudacher, P. Sarda, M. Kurz, *Nature* **303**, 762 (1983).
6. D. W. Graham, *Rev. Mineral. Geochem.* **47**, 247 (2002).
7. I. Kaneoka, *Nature* **302**, 698 (1983).
8. M. D. Kurz, W. J. Jenkins, S. R. Hart, *Nature* **297**, 43 (1982).
9. R. K. O’Nions, L. N. Tolstikhin, *Earth Planet. Sci. Lett.* **139**, 213 (1996).
10. C. J. Allegre, *Earth Planet. Sci. Lett.* **150**, 1 (1997).
11. J. C. Lassiter, E. H. Hauri, *Earth Planet. Sci. Lett.* **164**, 483 (1998).
12. J. Blichert-Toft, F. A. Frey, F. Albarède, *Science* **285**, 879 (1999).
13. T. W. Becker, J. B. Kellogg, R. J. O’Connell, *Earth Planet. Sci. Lett.* **171**, 351 (1999).
14. P. J. Wyllie, W. L. Huang, *Contrib. Mineral. Petrol.* **54**, 79 (1976).
15. C. B. Agee, J. Li, M. C. Shannon, S. Circone, *J. Geophys. Res.* **100**, 17 (1995).
16. E. Ohtani, T. Kato, H. Sawamoto, *Nature* **322**, 352 (1986).
17. P. B. Kelemen, N. Shimizu, V. J. M. Salters, *Nature* **375**, 747 (1995).
18. R. M. Ellam, F. M. Stuart, *Earth Planet. Sci. Lett.* **228**, 511 (2004).
19. D. L. Anderson, *Proc. Natl. Acad. Sci. U.S.A.* **95**, 9087 (1998).
20. D. L. Shuster, K. A. Farley, J. M. Sistierson, D. S. Burnett, *Earth Planet. Sci. Lett.* **217**, 19 (2004).
21. C. J. Allegre, D. L. Turcotte, *Nature* **323**, 123 (1986).
22. S. W. Parman, *Nature* **446**, 900 (2007).
23. D. R. Hilton, K. Gronvold, C. G. Macpherson, P. R. Castillo, *Earth Planet. Sci. Lett.* **173**, 53 (1999).
24. D. W. Graham, J. Blichert-Toft, C. J. Russo, K. H. Rubin, F. Albarède, *Nature* **440**, 199 (2006).
25. J. E. Georgan, M. D. Kurz, H. J. B. Dick, J. Lin, *Earth Planet. Sci. Lett.* **206**, 509 (2003).
26. T. A. Minshull, R. S. White, *Geophys. J. Int.* **125**, 139 (1996).
27. M. Honda, I. McDougall, D. B. Patterson, A. Doulgeris, D. Clague, *Earth Planet. Sci. Lett.* **349**, 149 (1991).
28. D. L. Shuster, K. A. Farley, *Geochim. Cosmochim. Acta* **69**, 2349 (2005).
29. M. Honda, I. McDougall, D. Patterson, *Lithos* **30**, 257 (1993).
30. M. D. Kurz et al., *Earth Planet. Sci. Lett.* **232**, 125 (2005).
31. G. Hirth, D. L. Kohlstedt, *Earth Planet. Sci. Lett.* **144**, 93 (1996).
32. The idea defended in this manuscript appeared during discussions with I. Kaneoka while the author was a visiting professor at the Earthquake Research Institute of Tokyo. I thank D. Shuster for sharing helpful information on his diffusion data, and J. Blichert-Toft, D. Graham, and S. Parman for reviewing the manuscript.

4 September 2007; accepted 7 January 2008

Published online 17 January 2008;

10.1126/science.1150060

Include this information when citing this paper.

The Premetazoan Ancestry of Cadherins

Monika Abedin¹ and Nicole King^{1,2*}

Cadherin-mediated cell adhesion and signaling is essential for metazoan development and yet is absent from all other multicellular organisms. We found cadherin genes at numbers similar to those observed in complex metazoans in one of the closest single-celled relatives of metazoans, the choanoflagellate *Monosiga brevicollis*. Because the evolution of metazoans from a single-celled ancestor required novel cell adhesion and signaling mechanisms, the discovery of diverse cadherins in choanoflagellates suggests that cadherins may have contributed to metazoan origins.

The evolution of animals (metazoans) from their single-celled ancestors required genomic innovations that allowed cells to adhere and communicate (1–3). Cadherins are critical mediators of metazoan cell adhesion and signaling and provide the structural basis for vital developmental processes, including tissue morphogenesis and maintenance, cell sorting, and cell polarization (4–8). However, despite their importance for metazoan multicellularity, cadherins are apparently lacking from all nonmetazoan multicellular organisms (e.g., plants and fungi). Indeed, cadherins have only been found in metazoans and their closest single-celled relatives, the choanoflagellates (9, 10), which suggests that the study of choanoflagellate cadherins may illuminate the transition from single-celled organisms to multicellular metazoans.

Choanoflagellates are unicellular and colony-forming organisms that use a single apical flagellum surrounded by a collar of actin-filled microvilli to swim and capture bacterial prey. Both the cell morphology and feeding strategy of choanoflagellates are nearly indistinguishable from those of feeding cells (choanocytes) in sponges (11, 12). In contrast to sponges and other metazoans, however, all choanoflagellates have a unicellular stage in their life history. Furthermore, choanoflagellates are not metazoans and did not evolve from sponges or more recently derived metazoan phyla (13–16). Thus, the common ancestor of choanoflagellates and metazoans was probably unicellular or, at most, capable of forming simple colonies.

Given the absence of overt cell adhesion in *M. brevicollis*, one might expect choanoflagellates to have fewer cadherin genes than metazoans. We identified cadherins in the recently sequenced *M. brevicollis* genome and compared them with those in four metazoan genomes: *Nematostella vectensis* (phylum Cnidaria), *Drosophila melanogaster* (phylum Arthropoda), *Ciona intestinalis* (phylum Chordata), and *Mus musculus* (phylum Chordata) (17). Cadherin gene numbers range from 17 in *D. melanogaster* to 127 in *M. musculus* (representing from 0.12

to 0.39% of the gene catalog; Table 1). Similarly, 23 putative cadherin genes (representing 0.25% of the gene catalog) are present in *M. brevicollis*, revealing that the absolute and relative abundances of cadherins in choanoflagellates are comparable to those of diverse metazoan genomes despite a lesser degree of morphological complexity (Table 1 and table S1 and fig. S1). In contrast, the numbers of extracellular cadherin (EC) repeats (the defining domain of cadherins) in *M. brevicollis* and *N. vectensis* cadherins exceed those of more recently derived metazoans (Table 1).

Cadherins containing epidermal growth factor (EGF), laminin G (LamG), and transmembrane domains linked to EC repeats [proteins with these four linked domains are classified as Fat cadherins (18)] are observed in *M. brevicollis*, sponges, sea urchins, and humans, among others (Fig. 1, A and B), which suggests that cadherins with these physically linked domains are ubiquitous and predate metazoan origins. Additionally, *M. brevicollis*, the sponge *Amphimedon queenslandica*, and *N. vectensis* (19) share cadherins with EC repeats linked to the Src homology 2 (SH2), Hedgehog N-terminal peptide (N-hh), immunoglobulin (Ig), and von Willebrand type A domains, which suggests that cadherins containing these domains evolved before metazoans. Because SH2 domains bind sites of tyrosine phosphorylation (20), choanoflagellate and cnidarian cadherins containing cytoplasmic SH2 domains [MBCDH1 and 2 and NvHedgling

(19); Fig. 1, A and C] could connect extracellular cues to intracellular processes such as cell cycle regulation and cellular metabolism. The presence of a protein tyrosine phosphatase domain in two *M. brevicollis* cadherins, MBCDH21 and MBCDH7 (Fig. 1, A and B, and fig. S1), provides further evidence of a connection between choanoflagellate cadherins and tyrosine kinase signaling. Likewise, the presence of an N-hh domain at the amino termini of cadherins in choanoflagellates, sponges, and cnidarians (Fig. 1, A and C) suggests an ancestral connection between cadherins and hedgehog signaling components important in metazoan development (21).

The linkage of EC repeats to SH2 and N-hh domains in *M. brevicollis* and *N. vectensis* appears to be absent in more recently derived lineages, which suggests that this ancient protein architecture was lost relatively early in metazoan evolution. In contrast, the connection between metazoan cadherins and β -catenin, part of the Wnt developmental signaling pathway (6, 22) and an important regulator of cadherin-mediated adhesion (23, 24), seemingly represents a metazoan innovation that evolved after the divergence of choanoflagellate and metazoan lineages. Unlike *M. brevicollis*, metazoan classical cadherins contain a highly conserved cadherin cytoplasmic domain (CCD) with binding sites for β -catenin. *N. vectensis* has five CCDs (fig. S2), and we found that a previously identified sponge cadherin also contains a cadherin CCD domain (Fig. 1B) (17, 25). This indicates that CCD-containing cadherins evolved before the origin of Bilateria.

Monosiga brevicollis leads a unicellular lifestyle and is not known to form cell-cell contacts. Therefore, the biological processes mediated by choanoflagellate cadherins remain enigmatic. We investigated the subcellular localization of MBCDH1 and MBCDH2, two nearly identical cadherins (note S1 in supporting online text and fig. S3) with domain contents resembling those of inferred ancestral cadherins (Fig. 1C). Antibodies raised against an extracellular portion of MBCDH1, which has 95% sequence identity to

Table 1. Cadherin abundance and number of EC repeats in *M. brevicollis* and diverse eukaryotes. *Atha*, *Arabidopsis thaliana*; *Ddis*, *Dictyostelium discoideum*; *Scer*, *Saccharomyces cerevisiae*; *Mbre*, *Monosiga brevicollis*; *Nvec*, *Nematostella vectensis*; *Dmel*, *Drosophila melanogaster*; *Cint*, *Ciona intestinalis*; *Mmus*, *Mus musculus*. Normalized cadherin abundance is the percentage of EC repeat-encoding genes in the draft gene catalog.

	Metazoa							
	Plant	Slime mold	Fungus	Choanoflagellate	Bilateria			
					Cnidarian	Arthropod	Ascidian	Vertebrate
Genomic content	<i>Atha</i>	<i>Ddis</i>	<i>Scer</i>	<i>Mbre</i>	<i>Nvec</i>	<i>Dmel</i>	<i>Cint</i>	<i>Mmus</i>
Genes/genome	27,273	13,607	6,609	9,196	18,000	13,601	14,182	32,661
Cadherins/genome	0	0	0	23	46	17	32	127
Normalized cadherin abundance	0	0	0	0.26%	0.12%	0.13%	0.23%	0.39%
EC repeats/cadherin (average)	N/A	N/A	N/A	14.7	11	12.2	6.2	5.2

¹Department of Molecular and Cell Biology and Center for Integrative Genomics, University of California at Berkeley, Berkeley, CA 94720, USA. ²Department of Integrative Biology, University of California at Berkeley, 142 Life Sciences Addition, Mail Code 3200, Berkeley, CA 94720, USA.

*To whom correspondence should be addressed. E-mail: nking@berkeley.edu

MBCDH2, recognized a single protein band of the predicted size (~191 kD; figs. S3 and S4) that presumably represents both MBCDH1 and MBCDH2. Subcellular cadherin localization was revealed by probing cells with the antibody either before or after cell membrane permeabilization. MBCDH1 and MBCDH2 were detected in four regions of the choanoflagellate cell: the apical collar of actin-filled microvilli, the basal pole of the cell, an unidentified structure at the apical end of the cell, and puncta within the cell body (Fig. 2, A to J). Antibodies bound to extracellular MBCDH1 and MBCDH2 colocalized with polymerized actin, most strikingly in the apical collar and, to a lesser extent, near the

basal end of the cell (Fig. 2, F, G, and I). The colocalization of actin filaments and *M. brevicollis* cadherins suggests that associations between cadherins and actin filaments predate the diversification of choanoflagellates and metazoans. Metazoan SH2 domain-containing proteins, such as mammalian Nck, interact with actin-binding proteins through phosphorylated tyrosines (26, 27), which suggests that the cytoplasmic tails of MBCDH1 and MBCDH2 might indirectly interact with the underlying actin cytoskeleton.

On the basis of the shared domain content of *M. brevicollis* and metazoan cadherins (Fig. 1), cadherins in the last common ancestor of choanoflagellates and metazoans had, among others,

SH2, N-hh, LamG, EGF, immunoglobulin, and transmembrane domains. The functions of these domains suggest that some choanoflagellate cadherins may mediate intracellular signaling. For example, the SH2 domain interacts with targets of tyrosine kinase phosphorylation, one of the few metazoan-type signaling networks found in choanoflagellates (9, 28). In metazoan epithelial cells, recruitment of β -catenin facilitates essential interactions between classical cadherins and the actin cytoskeleton to establish and maintain cell shape and polarity (29, 30). If *M. brevicollis* cadherins associate with the local actin cytoskeleton, as suggested by their colocalization, this interaction merits further investigation as

Fig. 1. (A) Venn diagram analysis of domains linked to EC repeats in *M. brevicollis*, *N. vectensis*, and *M. musculus* cadherins. (B) Representative composition of Fat-related cadherins from *M. brevicollis* and diverse metazoan taxa. The cladogram depicts relations among metazoan phyla (34, 35). Green boxes highlight clusters of EGF and LamG domains, and EC repeats are shown in blue. (C) Protein domains shared by *M. brevicollis* MBCDH1 and 2, MBCDH10, and MBCDH11; the sponge cadherin AmqHedgling; and the cnidarian cadherin NvHedgling. These domains are absent from *M. musculus* cadherins. Blue boxes contain SH2 domains, yellow boxes contain immunoglobulin domains, and red boxes contain N-hh and VWA domains. (Key) Symbols used in (B) and (C). LCA, last common ancestor. LamN and LamG domains in MBCDH21 are below the SMART e-value threshold but above the Pfam threshold (36, 37). See fig. S1 for the complete domain structure of MBCDH21, table S2 for protein identifiers and species names, and table S3 for domain abbreviations.

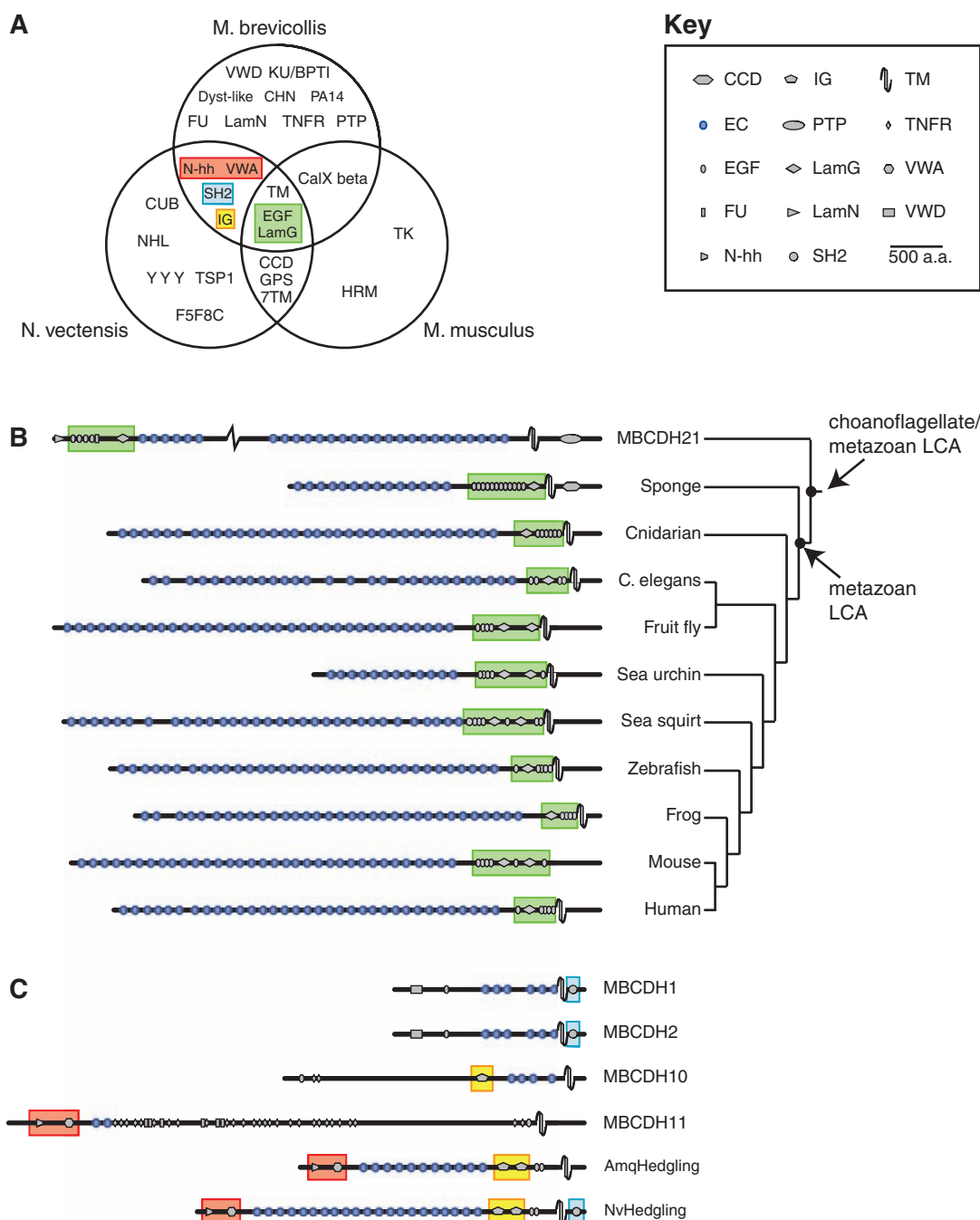
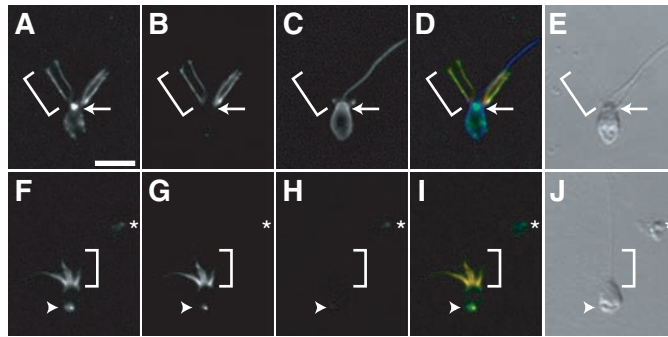


Fig. 2. Subcellular localization of MBCDH1 and MBCDH2 (A and F), compared with polymerized actin stained with rhodamine-phalloidin (B and G), or antibodies against β -tubulin (C and H). Cells were exposed to antibodies against MBCDH1 after (A to E) or before (F to J) permeabilization. Overlay of MBCDH1 and MBCDH2



(green), actin (red), and β -tubulin (blue) reveals colocalization of MBCDH1 and MBCDH2 with actin (yellow) on the collar and at the basal pole (D and I). Differential interference contrast microscopy shows cell morphology (E and J). Brackets, collar of microvilli; arrow, apical organelle; arrowhead, basal pole; asterisk, cluster of autofluorescent bacterial detritus.

MBCDH1 and MBCDH2 lack the CCD and the *M. brevicollis* genome lacks a β -catenin ortholog.

Metazoan E-cadherins and flamingo cadherins are bound by pathogenic bacteria which exploit them as extracellular tethers during host cell invasion (31–33). It is possible that choanoflagellate cadherins fill an equivalent role in binding bacterial prey for recognition or capture, functions consistent with the enrichment of MBCDH1 and MBCDH2 on the feeding collar (Fig. 2). If ancient cadherins bound bacteria in the unicellular progenitor of choanoflagellates and metazoans, cadherin-mediated cell adhesion in metazoans may reflect the co-option of a class of proteins whose earliest function was to interpret and respond to cues from the extracellular milieu. Indeed, the transition to multicellularity likely rested on the co-option of diverse transmembrane and secreted proteins to new functions in intercellular signaling and adhesion.

References and Notes

1. S. Tyler, *Integr. Comp. Biol.* **43**, 55 (2003).
2. N. M. Brooke, P. W. Holland, *Curr. Opin. Genet. Dev.* **13**, 599 (2003).
3. N. King, *Dev. Cell* **7**, 313 (2004).
4. M. J. Wheelock, K. R. Johnson, *Curr. Opin. Cell Biol.* **15**, 509 (2003).
5. R. A. Foty, M. S. Steinberg, *Int. J. Dev. Biol.* **48**, 397 (2004).
6. W. J. Nelson, R. Nusse, *Science* **303**, 1483 (2004).
7. B. M. Gumbiner, *Nat. Rev. Mol. Cell Biol.* **6**, 622 (2005).
8. J. M. Halbleib, W. J. Nelson, *Genes Dev.* **20**, 3199 (2006).
9. N. King, C. T. Hittinger, S. B. Carroll, *Science* **301**, 361 (2003).
10. E. T. Steenkamp, J. Wright, S. L. Baldauf, *Mol. Biol. Evol.* **23**, 93 (2006).
11. H. James-Clark, *Annu. Mag. Natl. Hist.* **1**, 133–142; 188–215; 250–264 (1868).
12. D. J. Hibbert, *J. Cell Sci.* **17**, 191 (1975).
13. G. Burger, L. Forget, Y. Zhu, M. W. Gray, B. F. Lang, *Proc. Natl. Acad. Sci. U.S.A.* **100**, 892 (2003).
14. D. V. Lavrov, L. Forget, M. Kelly, B. F. Lang, *Mol. Biol. Evol.* **22**, 1231 (2005).
15. A. Rokas, D. Kruger, S. B. Carroll, *Science* **310**, 1933 (2005).
16. E. Jimenez-Guri, H. Philippe, B. Okamura, P. W. Holland, *Science* **317**, 116 (2007).
17. Materials and methods are available as supporting material on Science Online.
18. T. Tanoue, M. Takeichi, *J. Cell Sci.* **118**, 2347 (2005).
19. M. Adamska et al., *Curr. Biol.* **17**, R836 (2007).
20. L. E. Marengere, T. Pawson, *J. Cell Sci. Suppl.* **18**, 97 (1994).
21. J. Gerhart, *Teratology* **60**, 226 (1999).
22. C. Jamora, E. Fuchs, *Nat. Cell Biol.* **4**, E101 (2002).

23. R. Kemler, *Trends Genet.* **9**, 317 (1993).
24. B. M. Gumbiner, *J. Cell Biol.* **148**, 399 (2000).
25. O. Sakarya et al., *PLoS ONE* **2**, e506 (2007).
26. N. Jones et al., *Nature* **440**, 818 (2006).
27. G. M. Rivera et al., *Proc. Natl. Acad. Sci. U.S.A.* **103**, 9536 (2006).
28. Y. Segawa et al., *Proc. Natl. Acad. Sci. U.S.A.* **103**, 12021 (2006).
29. M. Perez-Moreno, C. Jamora, E. Fuchs, *Cell* **112**, 535 (2003).

30. R. W. Carthew, *Curr. Opin. Genet. Dev.* **15**, 358 (2005).
31. J. Mengaud, H. Ohayon, P. Gounon, R. M. Mege, P. Cossart, *Cell* **84**, 923 (1996).
32. E. C. Boyle, B. B. Finlay, *Curr. Opin. Cell Biol.* **15**, 633 (2003).
33. K. Blau et al., *J. Infect. Dis.* **195**, 1828 (2007).
34. M. J. Telford, *Curr. Biol.* **16**, R981 (2006).
35. Tree of Life Web Project, www.tolweb.org/tree [accessed 10 December 2007].
36. I. Letunic et al., *Nucleic Acids Res.* **34**, D257 (2006).
37. A. Bateman et al., *Nucleic Acids Res.* **32**, D138 (2004).
38. We thank S. Nichols, J. Nelson, A. Rokas, N. Patel, C. Tabin, and J. Reiter for critical reading of the manuscript and J. Chapman, A. Morris, and our laboratory for technical support and advice. Supported by the Gordon and Betty Moore Foundation Marine Microbiology Initiative and the Pew Scholars Program. N.K. is a Scholar in the Canadian Institute for Advanced Research. The *M. brevicollis* genome assembly and annotation data are deposited at DBJ/EMBL/GenBank under the project accession ABFJ00000000. See tables S2, S3, and S4 and notes S1 and S2 for nucleotides, proteins, accession numbers, and sequences.

Supporting Online Material

www.sciencemag.org/cgi/content/full/319/5865/946/DC1
Materials and Methods
SOM Text
Figs. S1 to S4
Tables S1 to S5
References

28 September 2007; accepted 13 December 2007
10.1126/science.1151084

A Global Map of Human Impact on Marine Ecosystems

Benjamin S. Halpern,¹ Shaun Walbridge,^{1*} Kimberly A. Selkoe,^{1,2,*} Carrie V. Kappel,¹ Fiorenza Micheli,³ Caterina D'Agrosa,⁴ John F. Bruno,⁵ Kenneth S. Casey,⁶ Colin Ebert,¹ Helen E. Fox,⁷ Rod Fujita,⁸ Dennis Heinemann,⁹ Hunter S. Lenihan,¹⁰ Elizabeth M. P. Madin,¹¹ Matthew T. Perry,¹ Elizabeth R. Selig,^{6,12} Mark Spalding,¹³ Robert Steneck,¹⁴ Reg Watson¹⁵

The management and conservation of the world's oceans require synthesis of spatial data on the distribution and intensity of human activities and the overlap of their impacts on marine ecosystems. We developed an ecosystem-specific, multiscale spatial model to synthesize 17 global data sets of anthropogenic drivers of ecological change for 20 marine ecosystems. Our analysis indicates that no area is unaffected by human influence and that a large fraction (41%) is strongly affected by multiple drivers. However, large areas of relatively little human impact remain, particularly near the poles. The analytical process and resulting maps provide flexible tools for regional and global efforts to allocate conservation resources; to implement ecosystem-based management; and to inform marine spatial planning, education, and basic research.

Humans depend on ocean ecosystems for important and valuable goods and services, but human use has also altered the oceans through direct and indirect means (1–5). Land-based activities affect the runoff of pollutants and nutrients into coastal waters (6, 7) and remove, alter, or destroy natural habitat. Ocean-based activities extract resources, add pollution, and change species composition (8). These human activities vary in their intensity of impact on the ecological condition of communities (9) and in their spatial distribution across the seascape. Understanding and quantifying, i.e., mapping, the spatial distribution of human impacts is needed for the evaluation of trade-offs (or compatibility) between human uses of the oceans and protection of ecosystems and the

services they provide (1, 2, 10). Such mapping will help improve and rationalize spatial management of human activities (11).

Determining the ecological impact of human activities on the oceans requires a method for translating human activities into ecosystem-specific impacts and spatial data for the activities and ecosystems. Past efforts to map human impacts on terrestrial ecosystems (12), coral reefs (13), and coastal regions (14–16) used either coarse categorical or ad hoc methods to translate human activities into impacts. We developed a standardized, quantitative method, on the basis of expert judgment, to estimate ecosystem-specific differences in impact of 17 anthropogenic drivers of ecological change (table S1) (9). The results provided impact weights (table S2) used to

combine multiple drivers into a single comparable estimate of cumulative human impact on 20 ecosystem types (17). We focused on the current estimated impact of humans on marine ecosystems

¹National Center for Ecological Analysis and Synthesis, 735 State Street, Santa Barbara, CA 93101, USA. ²Hawai'i Institute of Marine Biology, Post Office Box 1346, Kane'o'he, HI 96744, USA. ³Hopkins Marine Station, Stanford University, Oceanview Boulevard, Pacific Grove, CA 93950–3094, USA. ⁴Wildlife Conservation Society, 2300 Southern Boulevard, Bronx, NY 10460, USA. ⁵Department of Marine Sciences, University of North Carolina at Chapel Hill, Chapel Hill, NC 27599–3300, USA. ⁶National Oceanographic Data Center, National Oceanic and Atmospheric Administration (NOAA), 1315 East-West Highway, Silver Spring, MD 20910, USA. ⁷Conservation Science Program, World Wildlife Fund—United States, 1250 24th Street NW, Washington, DC 20037, USA. ⁸Environmental Defense, 5655 College Avenue, Suite 304, Oakland, CA, 94618, USA. ⁹Ocean Conservancy, 1300 19th Street, NW, Washington, DC 20006, USA. ¹⁰Bren School of Environmental Science and Management, University of California, Santa Barbara, CA 93106, USA. ¹¹Department of Ecology, Evolution, and Marine Biology, University of California, Santa Barbara, CA 93106, USA. ¹²Curriculum in Ecology, University of North Carolina at Chapel Hill, Chapel Hill, NC 27599–3275, USA. ¹³Conservation Strategies Division, the Nature Conservancy, 93 Centre Drive, Newmarket, CB8 8AW, UK. ¹⁴School of Marine Sciences, University of Maine, Darling Marine Center, Walpole, ME 04353, USA. ¹⁵Fisheries Center, 2202 Main Mall, University of British Columbia, Vancouver, V6T 1Z4, Canada.

*These authors contributed equally to this work.

†Present address: School of Life Sciences, Arizona State University, Tempe, AZ 85287–4501, USA.

‡To whom correspondence should be addressed. E-mail: halpern@nceas.ucsb.edu, selkoe@nceas.ucsb.edu

(within the last decade), as past impacts and future scenarios of human impacts are less tractable, though also important (17).

Predicted cumulative impact scores (I_C) were calculated for each 1 km² cell of ocean

as follows: $I_C = \sum_{i=1}^n \sum_{j=1}^m D_i * E_j * \mu_{i,j}$ where D_i is

the log-transformed and normalized value [scaled between 0 and 1 (17)] of an anthropogenic driver at location i , E_j is the presence or absence of ecosystem j (either 1 or 0, respectively), and $\mu_{i,j}$ is the impact weight for the anthropogenic driver i and ecosystem j [range 0 to 4 (table S2)], given $n = 17$ drivers and $m = 20$ ecosystems (fig. S1). We modeled the distribution of several intertidal and shallow coastal ecosystems lacking global data (17). Weighting anthropogenic drivers by their estimated ecological impact in this way resulted in a different picture of ocean condition compared with simply mapping the footprints of human activities or drivers (fig. S1). Summing across ecosystems allows cells with multiple ecosystems to have higher potential scores than areas with fewer ecosystems; sensitivity analyses showed that summing or averaging across ecosystems within cells resulted in similar global pictures of human impacts on marine ecosystems (17). The global impact of a

particular driver (I_D) is $I_D = \sum_{i=1}^n D_i * E_j * \mu_{i,j}$ and

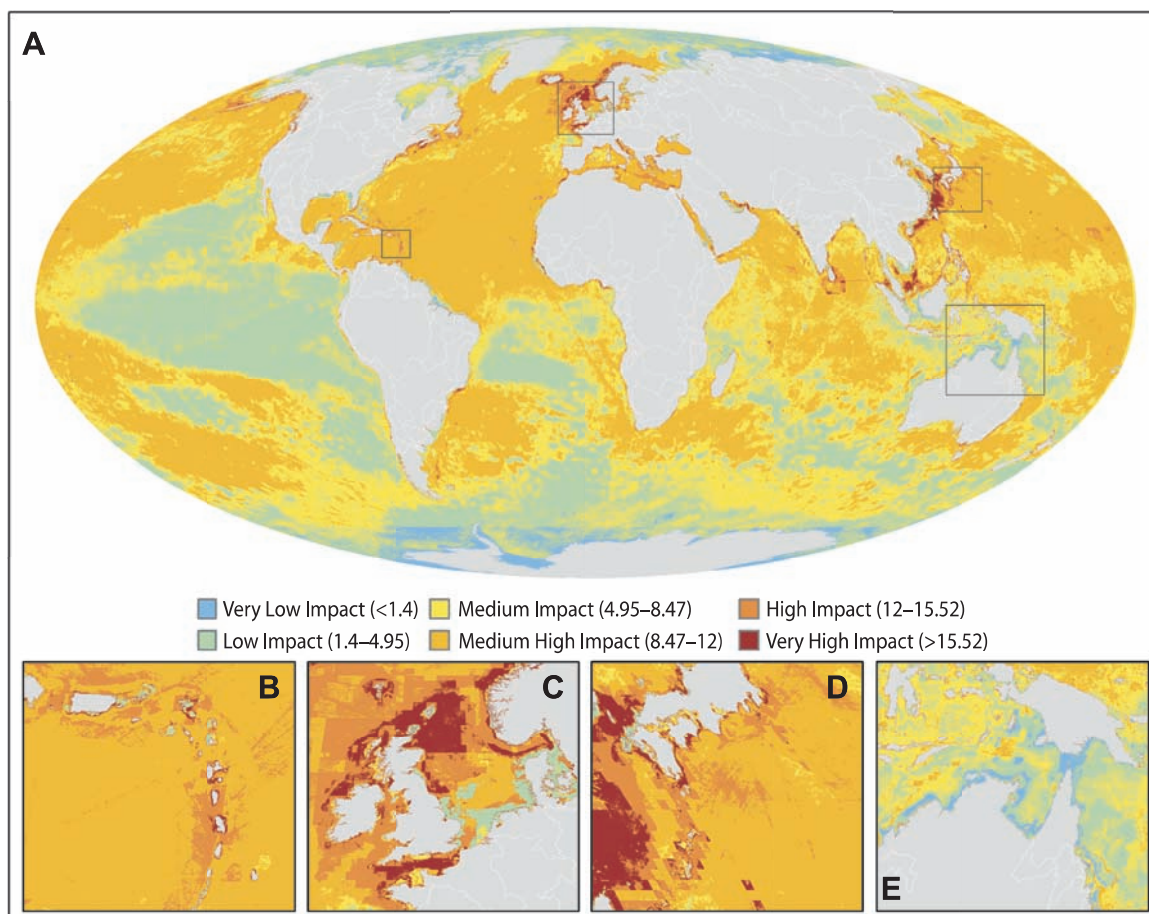
of all drivers on a particular ecosystem type (I_E)

is $I_E = \sum_{j=1}^m D_i * E_j * \mu_{i,j}$. This method produced

I_C scores ranging from 0.01 to 90.1. The I_C scores were significantly correlated with independent estimates of ecological condition in 16 mixed-ecosystem regions containing coral reefs (17, 18). The linear equation relating the two scores [$R^2 = 0.63$, $P = 0.001$ (fig. S5)] was then used to divide I_C scores into six categories of human impact ranging from very low impact ($I_C < 1.4$) to very high impact ($I_C > 15.5$) (17).

Predicted human impact on the oceans shows strong spatial heterogeneity (Fig. 1) with a roughly bimodal distribution of per-cell I_C scores (Fig. 2), but with every square kilometer affected by some anthropogenic driver of ecological change. Over a third (41%) of the world's oceans have medium high to very high I_C scores [>8.5 (17)], with a small fraction (0.5%) but relatively large area (~2.2 million km²) experiencing very high impact ($I_C > 15.5$). Most of the highest predicted cumulative impact is in areas of continental shelf and slope, which are subject to both land- and ocean-based anthropogenic drivers. Large areas of high predicted impact occur in the North and Norwegian seas, South and East China seas, Eastern Caribbean, North American eastern seaboard, Mediterranean, Persian Gulf, Bering Sea, and the waters around Sri Lanka (Fig. 1).

Fig. 1. Global map (A) of cumulative human impact across 20 ocean ecosystem types. (Insets) Highly impacted regions in the Eastern Caribbean (B), the North Sea (C), and the Japanese waters (D) and one of the least impacted regions, in northern Australia and the Torres Strait (E).



Ecoregions, a classification of coastal (<200 m depth) areas based on species composition and biogeography (19), also showed variation in scores indicating differential risks to unique marine assemblages (table S3).

The majority of very low impact areas (3.7% of the oceans) occurs in the high-latitude Arctic and Antarctic poles (Fig. 1), in areas with seasonal or permanent ice that limits human access. However, our analyses did not account for illegal, unregulated, and unreported (IUU) fishing,

which may be extensive in the Southern Ocean (20), or atmospheric pollution, which may be particularly high in the Arctic (21). Furthermore, projections of future polar ice loss (22) suggest that the impact on these regions will increase substantially. In general, small human population and coastal watershed size predict light human impact (Fig. 1E) but do not ensure it, as shipping, fishing, and climate change affect even remote locations—e.g., impact scores are relatively high in the international waters of the Patagonian

shelf. In some places, predicted impact scores may be higher than anticipated because many anthropogenic drivers are not readily observable. Conversely, impact scores may seem unexpectedly low in other locations because a more abundant but less-sensitive ecosystem (e.g., soft sediment) surrounds a sensitive, but rare, ecosystem (e.g., coral reefs).

Ecosystems with the highest predicted cumulative impact scores include hard and soft continental shelves and rocky reefs (Fig. 3). Coral reefs, seagrass beds, mangroves, rocky reefs and shelves, and seamounts have few to no areas remaining anywhere in the world with $I_C < 1.5$ (Fig. 3). Indeed, our data suggest that almost half of all coral reefs experience medium high to very high impact (13, 17, 23). Shallow soft-bottom and pelagic deep-water ecosystems had the lowest scores (>50% of these ecosystems have $I_C < 1.1$ and 1.2, respectively), partly because of the lower vulnerability of these ecosystems to most anthropogenic drivers (table S2). Overall, these results highlight the greater cumulative impact of human activities on coastal ecosystems.

Perhaps not surprisingly, anthropogenic drivers associated with global climate change are distributed widely (Fig. 4A) and are an important component of global cumulative impact scores, particularly for offshore ecosystems. Other drivers, in particular commercial fishing, are also globally widespread but have smaller cumulative impacts because of their uneven distribution. Land-based anthropogenic drivers have relatively small spatial extents and predicted cumulative impacts (Fig. 4A), but their cumulative impact scores approach those of other more widespread drivers within coastal areas where they occur (Fig. 4B). The spatial distribution of land-based impacts is highly heterogeneous but positively spatially correlated. Therefore, management of coastal waters must contend with multiple drivers in concert. Coordination with regulating agencies for urban and agricultural runoff is warranted, although such efforts can be challenging when watersheds cross jurisdictional boundaries. Where anthropogenic drivers tend to be spatially distinct (uncorrelated), as with commercial shipping versus pelagic high-bycatch fishing, management will require independent regulation and conservation tools. Assessing positive and negative spatial correlations among drivers can help anticipate potential interactions (24) and provides guidance in adjusting spatial management accordingly.

Our approach may be used to identify regions where better management of human activities could achieve a higher return-on-investment, e.g., by reducing or eliminating anthropogenic drivers with high impact scores (fig. S2). It may also be used to assess whether or how human activities can be spatially managed to reduce their negative impacts on ecosystems. For example, fishing zones have been shifted to decrease impacts on sensitive ecosystems (25), and navigation lanes have been rerouted to protect sensitive areas of the ocean (26). Wide-ranging fish stocks

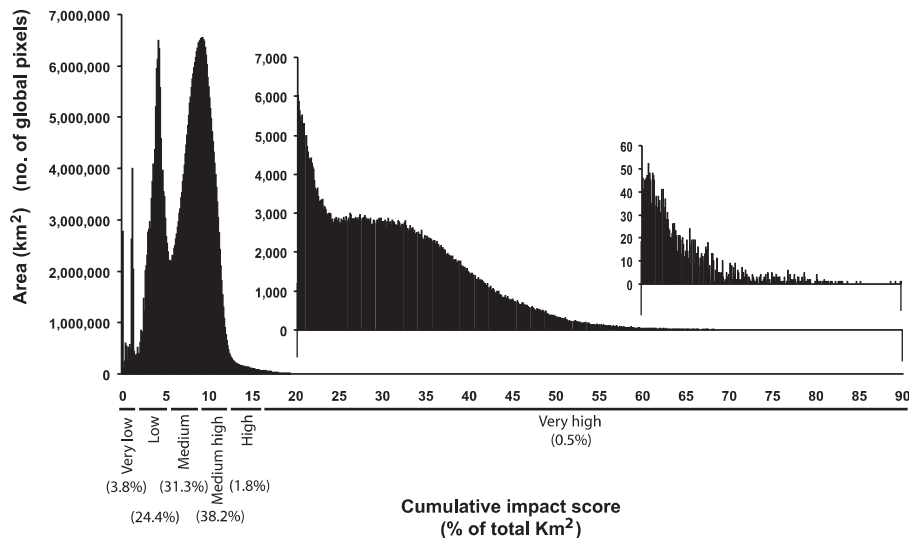
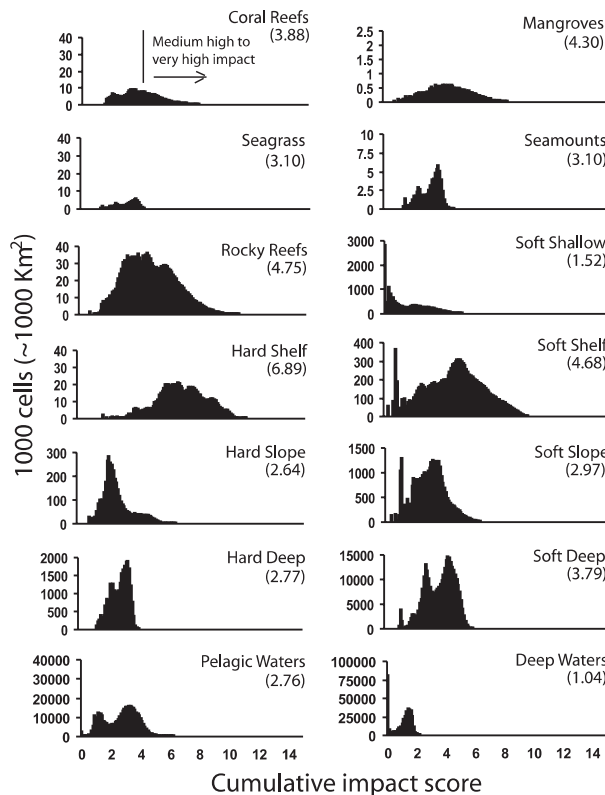


Fig. 2. Histogram of cumulative impact scores depicting the fraction of global area that falls within each impact category. There are no zeros; histogram bars are in bins of 0.1. Categories described in (17). (Insets) Expanded views of the tail of values.

Fig. 3. The distribution of cumulative impact scores for each ecosystem in our analyses (means in parentheses). Individual ecosystem scores have a smaller range of values than cumulative impact scores (Fig. 2) because the latter sum all ecosystem-specific scores within a cell. Ground-truthed estimates of coral reef condition (17) were used to identify I_E values at which coral reefs experience medium high to very high impact, as indicated on the coral reef histogram. Note differences in y-axis scales.



and those that occur primarily in international waters present challenges in determining who must take responsibility for management. If ecosystem-specific weighting values ($\mu_{i,j}$) are excluded, we can also evaluate the distribution, or footprint, of summed anthropogenic drivers of ecosystem change. This global footprint of drivers correlates with the distribution of cumulative impact scores ($R^2 = 0.83$), but ignores the important small-scale spatial patterns that emerge when accounting for ecosystem vulnerability (fig. S1) (17).

Our results represent the current best estimate of the spatial variation in anthropogenic impacts. Although these estimates are conservative and incomplete for most of the ocean, they potentially inflate human impacts on coastal areas because we used an additive model (17). Averaging impacts across ecosystems produced highly correlated results, very similar to those from the additive model (17), which suggests such inflation is limited, if it exists. Furthermore, the large extent of the ocean that our model predicts to be negatively affected by human activities will likely increase once additional drivers, their historical effects, and possible

synergisms are incorporated into the model. Key activities with significant impacts on marine ecosystems but without global data include recreational fishing (27), aquaculture (28, 29), disease (30), coastal engineering (habitat alteration), and point-source pollution (31). Most of these activities primarily affect intertidal and nearshore ecosystems rather than offshore ecosystems, which suggests that our estimates for nearshore areas are particularly conservative. In addition, the spatial data for many anthropogenic drivers were derived from valid but inexact modeling approaches (17). Ecosystem data were highly variable in quality, both within and among ecosystem types, and in many cases, we may have underestimated the full extent of these ecosystems and, therefore, the cumulative impact scores. Furthermore, many changes occurred in the past with lasting negative effects, but the drivers no longer occur at a particular location, e.g., historical overfishing (4) or past coastal habitat destruction (32). Although we used a conservative, additive model, some drivers may have synergistic effects (24). Despite these limitations, this analysis provides a framework and baseline that can be built upon with future

incorporation or refinement of data. It is noteworthy that the data gaps emphasize the need for research on the most basic information, such as distribution of habitat types and whether and how different anthropogenic drivers interact.

Humans depend heavily on goods and services from the oceans, and these needs will likely increase with a growing human population (10). Our approach provides a structured framework for quantifying the ecological trade-offs associated with different human uses of marine ecosystems and for identifying locations and strategies to minimize ecological impact and maintain sustainable use. In some places, such strategies can benefit both humans and ecosystems, for example, using shellfish aquaculture both to provide food and to improve water quality. Our analytical framework can easily be applied to local- and regional-scale planning where better data are available and can be extended by incorporating other types of information, such as species distribution or diversity data (33–35) to identify hot spots with both high diversity and high cumulative human impacts that perhaps deserve conservation priority. A key next research step will be

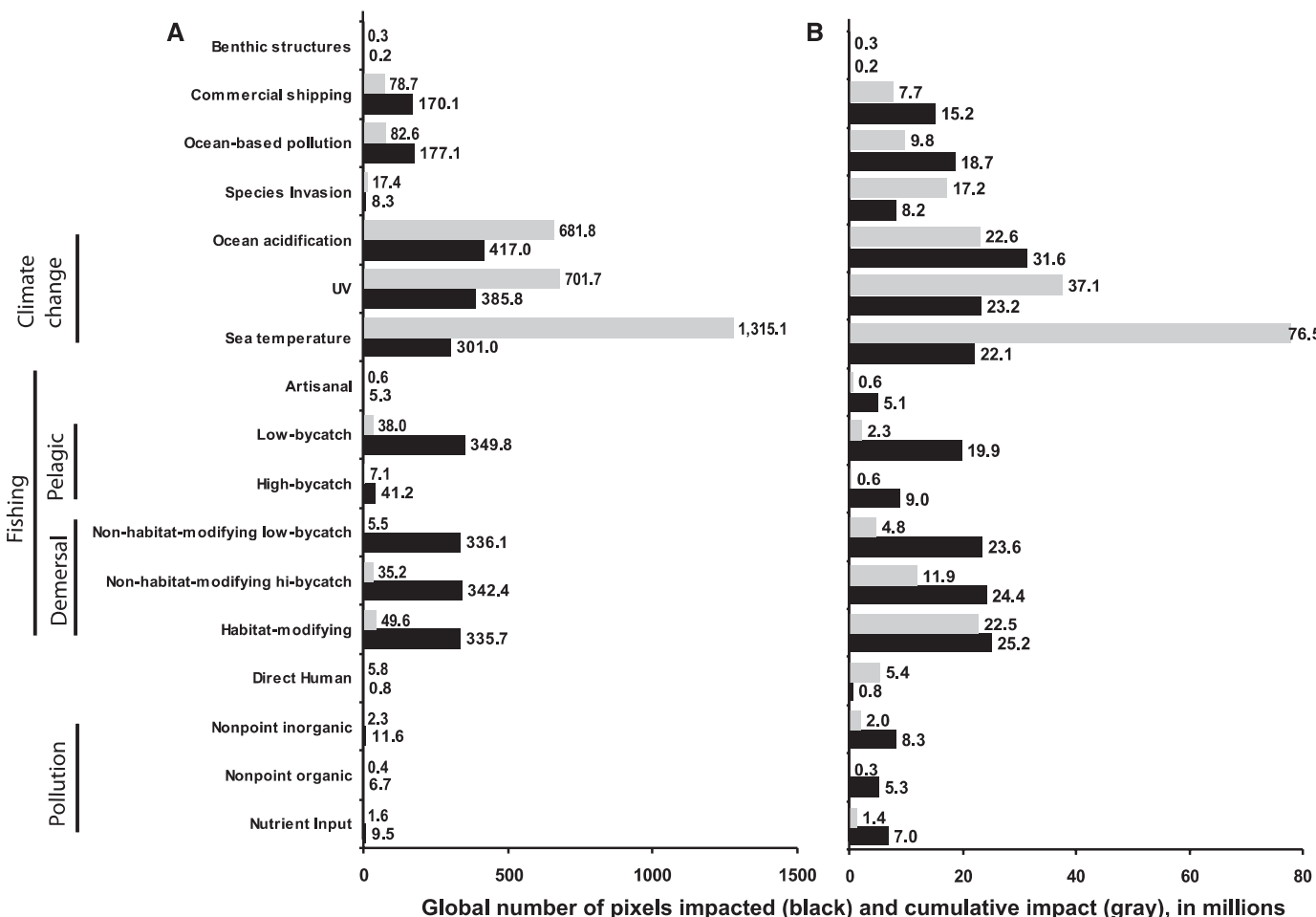


Fig. 4. Total area affected (square kilometers, gray bars) and summed threat scores (rescaled units, black bars) for each anthropogenic driver (A) globally and (B) for all coastal regions <200 m in depth. Values for each bar are reported in millions.

to compile regional and global databases of empirical measurements of ecosystem condition to further validate the efficacy of our approach.

References and Notes

- Pew Oceans Commission (POC), *America's Living Oceans: Charting a Course for Sea Change* (POC, Arlington, VA, 2003).
- U.S. Commission on Ocean Policy, *An Ocean Blueprint for the 21st Century: Final Report to the President and Congress* (U.S. Commission on Ocean Policy, Washington, DC, 2004).
- R. A. Myers, B. Worm, *Nature* **423**, 280 (2003).
- J. B. C. Jackson *et al.*, *Science* **293**, 629 (2001).
- H. K. Lotze *et al.*, *Science* **312**, 1806 (2006).
- J. P. M. Syvitski, C. J. Vorosmarty, A. J. Kettner, P. Green, *Science* **308**, 376 (2005).
- P. M. Vitousek *et al.*, *Ecol. Appl.* **7**, 737 (1997).
- D. Pauly, R. Watson, J. Alder, *Philos. Trans. R. Soc. London Ser. B* **360**, 5 (2005).
- B. S. Halpern, K. A. Selkoe, F. Micheli, C. V. Kappel, *Conserv. Biol.* **21**, 1301 (2007).
- W. V. Reid *et al.*, *Millennium Ecosystem Assessment: Ecosystems and Human Well-Being—Synthesis Report* (World Resources Institute, Washington, DC, 2005).
- L. B. Crowder *et al.*, *Science* **313**, 617 (2006).
- E. W. Sanderson *et al.*, *Bioscience* **52**, 891 (2002).
- D. Bryant, L. Burke, J. McManus, M. Spalding, *Reefs at Risk: A Map-Based Indicator of Threats to the World's Coral Reefs* (World Resources Institute, Washington, DC, 1998).
- N. Ban, J. Alder, *Aquat. Conserv.: Mar. Freshwat. Ecosyst.* **16**, 10.1002/iaqc (2007).
- M. W. Beck, M. Odaya, *Aquat. Conserv.: Mar. Freshwat. Ecosyst.* **11**, 235 (2001).
- D. Vander Schaaf *et al.*, *A Conservation Assessment of the Pacific Northwest Coast Ecoregion* (The Nature Conservancy of Canada, Victoria, BC, and Washington Department of Fish and Wildlife, Olympia, WA, 2006).
- Materials and methods are available as supporting material on *Science* Online.
- J. M. Pandolfi *et al.*, *Science* **307**, 1725 (2005).
- M. D. Spalding *et al.*, *Bioscience* **57**, 573 (2007).
- U. R. Sumaila, J. Alder, H. Keith, *Mar. Policy* **30**, 696 (2006).
- A. Clarke, C. M. Harris, *Environ. Conserv.* **30**, 1 (2003).
- J. E. Overland, M. Y. Wang, *Geophys. Res. Lett.* **34**, L17705 (2007).
- J. M. Pandolfi *et al.*, *Science* **301**, 955 (2003).
- B. S. Halpern, K. L. McLeod, A. A. Rosenberg, L. B. Crowder, *Ocean Coast. Manage.* 10.1016/j.ocecoaman.2007.08.002 (2008).
- D. Witherell, C. Pautzke, D. Fluharty, *ICES J. Mar. Sci.* **57**, 771 (2000).
- S. D. Kraus *et al.*, *Science* **309**, 561 (2005).
- F. C. Coleman, W. F. Figueira, J. S. Ueland, L. B. Crowder, *Science* **305**, 1958 (2004).
- R. L. Naylor *et al.*, *Nature* **405**, 1017 (2000).
- R. Dalton, *Nature* **431**, 502 (2004).
- K. D. Lafferty, J. W. Porter, S. E. Ford, *Annu. Rev. Ecol. Evol. Systemat.* **35**, 31 (2004).
- M. Shahidul Islam, M. Tanaka, *Mar. Pollut. Bull.* **48**, 624 (2004).
- L. Airoldi, M. W. Beck, *Annu. Rev. Oceanogr. Mar. Biol.* **45**, 347 (2007).
- A. P. Kerswell, *Ecology* **87**, 2479 (2006).
- A. R. G. Price, *Mar. Ecol. Prog. Ser.* **241**, 23 (2002).
- C. M. Roberts *et al.*, *Science* **295**, 1280 (2002).
- This work was funded by the National Center for Ecological Analysis and Synthesis (NCEAS) and supported by the National Science Foundation and a grant from the David and Lucile Packard Foundation to NCEAS to evaluate ecosystem-based management in coastal oceans. Thanks to J. Hutton at U.N. Environmental Programme World Conservation Monitoring Centre for sharing coral reef, mangrove, and seagrass ecosystem data, J. Guinotte and the Marine Conservation Biology Institute for providing ocean acidification data, E. Sanderson for comments on earlier drafts, and support from the Pew Charitable Trusts to the Sea Around Us Project for development of mapped fisheries data. R. Myers participated in this project but passed away before it was completed; we are grateful for his contributions.

Supporting Online Material

www.sciencemag.org/cgi/content/full/319/5865/948/DC1

Materials and Methods

Figs. S1 to S6

Tables S1 to S6

References

16 August 2007; accepted 11 December 2007

10.1126/science.1149345

Effects of Predator Hunting Mode on Grassland Ecosystem Function

Oswald J. Schmitz

The way predators control their prey populations is determined by the interplay between predator hunting mode and prey antipredator behavior. It is uncertain, however, how the effects of such interplay control ecosystem function. A 3-year experiment in grassland mesocosms revealed that actively hunting spiders reduced plant species diversity and enhanced aboveground net primary production and nitrogen mineralization rate, whereas sit-and-wait ambush spiders had opposite effects. These effects arise from the different responses to the two different predators by their grasshopper prey—the dominant herbivore species that controls plant species composition and accordingly ecosystem functioning. Predator hunting mode is thus a key functional trait that can help to explain variation in the nature of top-down control of ecosystems.

Species are most likely to have strong effects on ecosystems when they alter factors that regulate key ecosystem functions such as production, decomposition, and nitrogen mineralization (1). These effects can be direct, as when selectively feeding herbivores alter plant community composition and hence alter the quality and quantity of plant material entering the soil organic matter pool to be decomposed and mineralized (1–6); or indirect, as when predators alter the way in which herbivores affect plant community composition (7–10). The exact nature of a species' effect will, however, depend on traits that determine the way it

functions (1, 11). Explaining such trait dependency is an important hurdle to overcome in developing predictive theories of species effects on ecosystem function (1). This endeavor is currently hampered by a limited understanding of what kinds of species' traits control functioning (11–15).

Here I report on a 3-year experiment quantifying the effect of one important functional trait of top predator species—their hunting mode—on the nature of indirect effects emerging at the ecosystem level (Fig. 1). Predators can propagate indirect effects down trophic chains in at least two ways (16). They can alter the numerical abundance of herbivore prey by capturing and consuming them. Alternatively, their mere presence in a system can trigger herbivore prey to modify foraging activity in a manner that reduces predation risk. A general rule, derived

from empirical synthesis, is that these different kinds of effect are related to predator hunting mode, irrespective of taxonomic identity (17). Sit-and-wait ambush predators cause largely behavioral responses in their prey because prey species respond strongly to persistent point-source cues of predator presence. Widely roaming, actively hunting predators may reduce prey density, but they produce highly variable predation risk cues and are thus unlikely to cause chronic behavioral responses in their prey. These hunting mode-dependent herbivore responses should lead to different cascading effects on the composition and abundance of plant species within ecosystems (9, 18) that should further cascade to affect ecosystem function (10). Predator effects do indeed cascade to influence ecosystem functions, and they vary with predator species (10, 19–22). But the basis for variation in predator species effects remains unresolved.

This study was carried out in a grassland ecosystem in northeastern Connecticut. The important plant species in this ecosystem (determined by their interaction strengths) may be effectively represented within three functional groups of plants: (i) the grass *Poa pratensis*, (ii) the competitively dominant herb *Solidago rugosa*, and (iii) a variety of other herb species, including *Trifolium repens*, *Potentilla simplex*, *Rudbeckia hirta*, *Crysanthemum leucanthemum*, and *Daucus carota*. The important animal species are the generalist grasshopper herbivore *Melanoplus femurrubrum* and the spider predators *Pisaurina mira* and *Phidippus rimator* (23). *Pisaurina mira* is a sit-and-wait predator in the upper canopy of the meadow.

School of Forestry and Environmental Studies and Department of Ecology and Evolutionary Biology, Yale University, New Haven, CT 06511, USA. E-mail: oswald.schmitz@yale.edu

Phidippus rimator actively hunts its prey throughout the entire meadow canopy. Under local conditions in this field, these spiders exist approximately in a 1:1 ratio of abundance (23).

The experiment was composed of 14 circular mesocosms, 1.6 m in diameter and 1.5 m high, that were placed over naturally growing vegetation in the field (24). Each treatment (sit-

and-wait predator and actively hunting predator) was randomly assigned to mesocosms in a matched-pairs design. I measured levels of seven key ecosystem properties and the three ecosystem functions aboveground net primary production (ANPP), organic matter decomposition rate (decomposition), and nitrogen mineralization rate (N mineralization), within

each mesocosm when the experiment was initiated and after 3 years (24).

From initially indistinguishable conditions between treatments (table S1), I saw striking directional differences in ecosystem properties and functions between predator treatments (Fig. 2). Relative to initial conditions, actively hunting predators caused a reduction in plant species evenness and enhanced ANPP and N mineralization, whereas sit-and-wait predators had slight positive effects on plant species evenness but reduced ANPP and N mineralization.

These differences were the result of predator hunting mode-dependent effects on plant community composition [multivariate analysis of variance (MANOVA) Wilks' lambda test = 0.393, df = 3, 10, $P < 0.025$]. The biomass of the competitive dominant plant *S. rugosa* was 168% higher in treatments containing the actively hunting predator than in treatments containing the sit-and-wait predator (Fig. 3A). The biomass of other herbs was 47% lower in treatments containing actively hunting predators than in treatments containing sit-and-wait predators (Fig. 3A). There were no treatment effects (both $P > 0.40$) on grass biomass and total plant biomass (Fig. 3A). The shifting composition of *S. rugosa* and other herb species caused plant species evenness to be 14% lower in the actively hunting predator treatments than in the sit-and-wait predator treatments (Fig. 3B). The mechanism driving these differences in plant composition is a tradeoff choice that grasshoppers must make between feeding on grasses and seeking refuge in and feeding on the competitive dominant plant *S. rugosa* when facing predators (18). Grasshoppers tend not to exhibit chronic foraging shifts in response to widely roaming active hunters such as *P. rimator* that present weak and variable cues, whereas they do exhibit chronic foraging shifts when facing sit-and-wait *P. mira*, which provides persistent cues (18). These hunting mode-dependent grasshopper responses in turn determine the nature of the indirect control that spiders exert over the competitive dominant plant *S. rugosa* (Fig. 1).

By indirectly controlling plant community composition, predators altered an important regulating factor (1, 25) that led to hunting mode-dependent differences in ecosystem functions (Fig. 4). ANPP was 163% higher in actively hunting predator treatments than in sit-and-wait predator treatments (Fig. 4A). Plant matter decomposition rate (Fig. 4B) was not different between treatments ($P > 0.40$). N mineralization in actively hunting predator treatments was 33% higher than in sit-and-wait predator treatments (Fig. 4C). To resolve how a lack of difference in plant organic matter decomposition may have translated into differences in N mineralization, I measured the C:N ratio (a measure of quality) of the plant litter subjected to decomposition in the two treatments (24). I found plant litter quality to be 14% higher in active predator treatments than in sit-and-wait predator treatments [C:N in

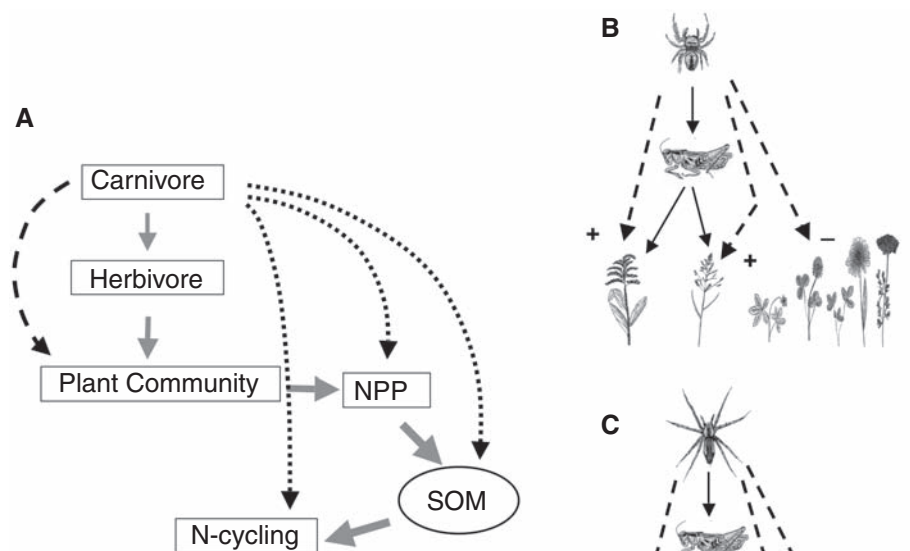
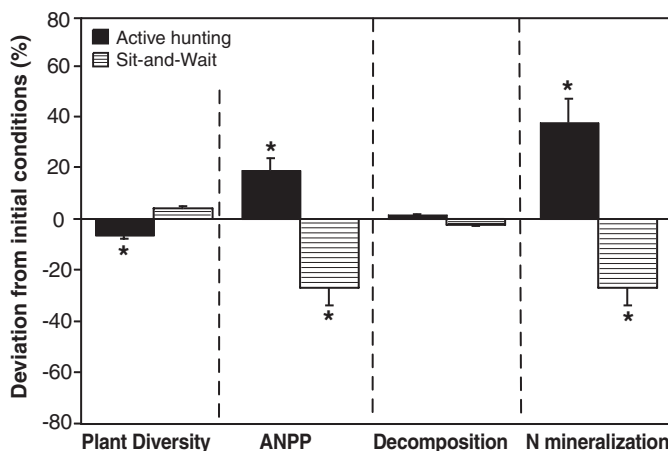


Fig. 1. Hypothesized predator indirect effects on plant community composition (dashed lines) and on ecosystem functions (dotted lines). (A) Predators can influence ecosystem function via the direct causal chain (depicted by solid arrows) running from predators through herbivores through plant community composition. Plant community composition in turn regulates NPP: the quality and quantity of plant matter entering the soil organic matter pool (24) to be decomposed and produce N mineralization. In the study ecosystem, predator indirect effects on plant community composition depended on how predators affect their grasshopper herbivore *M. femurrubrum* prey. (B) The actively hunting spider *P. rimator* causes density reductions of the grasshopper, which leads to indirect positive effects on grass and *S. rugosa* and an indirect negative effect on other herbs because the competitive dominant plant *S. rugosa* suppresses other herbs. (C) The sit-and-wait spider *P. mira* causes grasshopper foraging shifts from preferred nutritious grass to safer *S. rugosa*. This predator has indirect positive effects on grasses and other herbs and an indirect negative effect on *S. rugosa*. These hunting mode-dependent differences in plant composition are predicted to have different effects on ecosystem function.

Fig. 2. Net deviations from initial plant diversity and levels of ecosystem functions in different predator hunting mode treatments. Actively hunting predators suppress plant species evenness and enhance productivity and N mineralization, whereas sit-and-wait predators have opposite effects. Values are mean \pm 1 SD. Determinations of significance for each treatment and variable are based on a one-way *t* test for difference from 0% change, $n = 7$ replicates. * $P = 0.05$.



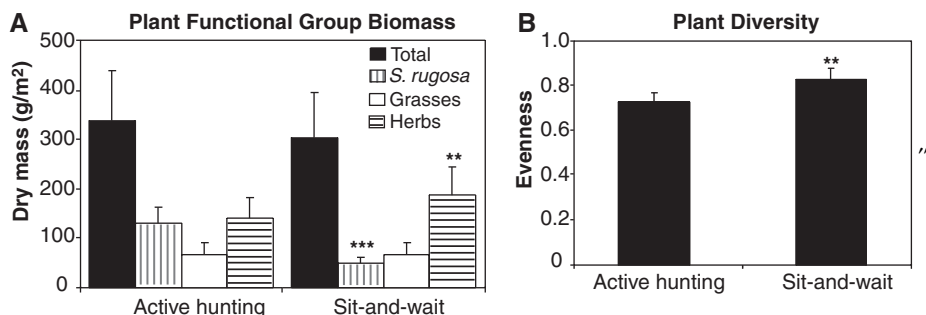


Fig. 3. Effects of manipulating predator hunting mode on the composition of the meadow plant community. **(A)** Actively hunting predator treatments had higher *S. rugosa* abundance and lower abundance of other herbs than did sit-and-wait predator treatments. There were no treatment effects on total plant biomass and grass biomass. **(B)** Changes in plant species functional group composition led to changes in plant species diversity, measured as evenness to account for *S. rugosa* dominance effects. Values are mean \pm 1 SD. Determinations of the effect of treatment differences on the biomass of each plant functional group and on plant diversity are based on one-way paired *t* tests following MANOVA, $n = 7$ replicates. $*0.05 < P < 0.01$, $***P < 0.01$.

active = 34.1 ± 1.7 (SEM) versus C:N in sit-and-wait = 38.9 ± 1.9 (SEM)], indicating that active predator treatments had significantly higher availability of N per unit of plant matter decomposed than did sit-and-wait treatments (one-tailed paired *t* test, $P < 0.05$, $n = 7$ replicates).

This experiment helps to explain why species in higher trophic levels sometimes enhance productivity, decomposition, and elemental cycling and at other times reduce the level of those functions (26). These differences are brought about by a simple causal chain: a predator hunting mode-dependent herbivore response leading to different indirect effects on plant community composition that in turn cascades to affect ecosystem functioning (Fig. 1).

The single-predator experimental treatments in this study are, however, an abstraction of natural system structure in two respects. First, it is not a highly reticulate system, so top-down effects propagate downward fairly linearly. Second, natural systems typically contain coexisting, multiple predator species. Thus, the nature and strength of top-down effects of predator species diversity on ecosystem function, especially when passing through a reticulate network, may be quite different than in single-predator treatments (12, 27, 28). Nevertheless, the current study represents an important precursor to a multiple-predator study in that it elucidates the mechanism and pathway by which an important predator functional trait can influence ecosystem function. Moreover, recent synthesis (29) suggests that the concept of predator hunting mode can be extended to explain variation in top-down effects that arise when different combinations of predator species coexist.

The recognition that predators may play important roles in ecosystems has prompted concern that the loss of top predators will lead to profound changes in the diversity and abundance of species in lower trophic levels of ecosystems, and ultimately in ecosystem functions (1, 7, 12, 20, 25, 30). The normal presumption

in ecosystem science, however, is that predator species cause qualitatively similar kinds of indirect effects on ecosystems (1, 31). This experiment instead shows that we must begin to consider the mechanisms by which predators hunt their prey in order to develop clearer understanding of predator effects on ecosystems and to develop effective ecosystem conservation efforts. An appealing feature of framing theory using hunting mode as a functional trait is that it may offer generalizable understanding about the source of contingency in prey responses to predators (17, 29). Moreover, hunting mode is a trait that is readily ascertained through natural history observation of predators in the field. The link between predator hunting mode and ecosystem function thus offers considerable promise for developing theory aimed at using predator functional traits as a key predictor of ecological dynamics.

References and Notes

- F. S. Chapin *et al.*, *Science* **277**, 500 (1997).
- P. J. McInnes, R. J. Naiman, J. Pastor, Y. Cohen, *Ecology* **73**, 2059 (1992).
- J. Pastor, B. Dewey, R. J. Naiman, P. F. McInnes, Y. Cohen, *Ecology* **74**, 467 (1993).
- D. A. Frank, P. M. Groffman, *Ecology* **79**, 2229 (1998).
- M. E. Ritchie, D. Tilman, J. M. H. Knopps, *Ecology* **79**, 165 (1998).
- G. E. Belovsky, J. B. Slade, *Proc. Natl. Acad. Sci. U.S.A.* **97**, 14412 (2000).
- J. Terborgh *et al.*, *Science* **294**, 1923 (2001).
- L. A. Dyer, D. Letourneau, *Ecol. Lett.* **6**, 60 (2003).
- O. J. Schmitz, *Ecol. Lett.* **6**, 156 (2003).
- O. J. Schmitz, *Ecology* **87**, 1432 (2006).
- D. U. Hooper *et al.*, *Ecol. Monogr.* **75**, 3 (2005).
- J. E. Duffy, *Oikos* **99**, 201 (2002).
- D. R. Chalcraft, W. J. Resettaris, *Am. Nat.* **162**, 390 (2003).
- O. L. Petchey, K. J. Gaston, *Ecol. Lett.* **9**, 741 (2006).
- J. P. Wright *et al.*, *Ecol. Lett.* **9**, 111 (2006).
- O. J. Schmitz, V. Krivan, O. Ovadia, *Ecol. Lett.* **7**, 153 (2004).
- O. J. Schmitz, in *Ecology of Predator-Prey Interactions*, P. Barbosa, I. Castellanos, Eds. (Oxford Univ. Press, Oxford, 2005), pp. 256–278.
- O. J. Schmitz, K. B. Suttle, *Ecology* **82**, 2072 (2001).
- A. L. Downing, M. A. Leibold, *Nature* **416**, 837 (2002).

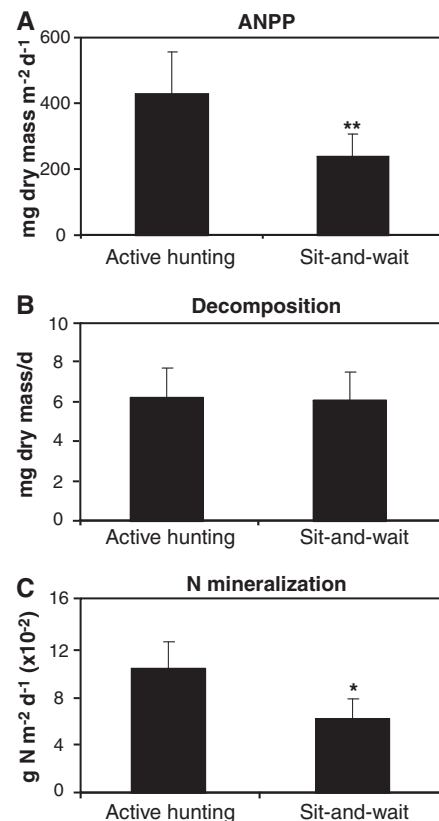


Fig. 4. Effects of manipulating predator hunting mode on three key ecosystem functions. Actively hunting predators caused higher rates of ANPP **(A)** and N mineralization **(C)** than did sit-and-wait predators. Predator treatments had no effect on decomposition **(B)**. Values are mean \pm 1 SD. Determinations of treatment differences are based on one-way paired *t* tests, $n = 7$ replicates. $*P = 0.05$, $**0.05 < P < 0.01$.

- J. E. Duffy, *Ecol. Lett.* **6**, 680 (2003).
- T. Fukami *et al.*, *Ecol. Lett.* **9**, 1299 (2006).
- J. L. Maron *et al.*, *Ecol. Monogr.* **76**, 3 (2006).
- O. J. Schmitz, in *Insects and Ecosystem Function*, W. W. Weisser, E. Siemann, Eds. (Springer Verlag, Berlin, 2004), pp. 277–302.
- See supporting material on Science Online.
- E. Thebault, M. Loreau, *Proc. Natl. Acad. Sci. U.S.A.* **100**, 14949 (2003).
- D. A. Wardle, *Communities and Ecosystems: Linking the Aboveground and Belowground Components* (Princeton Univ. Press, Princeton, NJ, 2002).
- D. R. Strong, *Ecology* **73**, 747 (1992).
- G. A. Polis, D. R. Strong, *Am. Nat.* **147**, 813 (1996).
- O. J. Schmitz, *Ecology* **88**, 2415 (2007).
- A. R. E. Sinclair, A. E. Byrom, *J. Anim. Ecol.* **75**, 64 (2006).
- M. Loreau *et al.*, *Science* **294**, 804 (2001).
- I thank B. Barton, N. David, D. Hawlena, K. Kidd, and J. Lee for help with the field work and D. Hawlena, P. Raymond, D. Skelly, K. Suttle, and anonymous reviewers for comments. Funding was provided by the NSF Ecological Biology program.

Supporting Online Material

www.sciencemag.org/cgi/content/full/319/5865/952/DC1
Materials and Methods
Table S1
References

30 October 2007; accepted 4 January 2008
10.1126/science.1152355

Axle-Less F₁-ATPase Rotates in the Correct Direction

Shou Furuike,^{1*} Mohammad Delawar Hossain,^{1,2*} Yasushi Maki,³ Kengo Adachi,¹ Toshiharu Suzuki,^{4,5} Ayako Kohori,¹ Hiroyasu Itoh,^{6,7} Masasuke Yoshida,^{4,5} Kazuhiko Kinoshita Jr.^{1†}

F₁-adenosine triphosphatase (ATPase) is an ATP-driven rotary molecular motor in which the central γ subunit rotates inside a cylinder made of three α and three β subunits alternately arranged. The rotor shaft, an antiparallel α -helical coiled coil of the amino and carboxyl termini of the γ subunit, deeply penetrates the central cavity of the stator cylinder. We truncated the shaft step by step until the remaining rotor head would be outside the cavity and simply sat on the concave entrance of the stator orifice. All truncation mutants rotated in the correct direction, implying torque generation, although the average rotary speeds were low and short mutants exhibited moments of irregular motion. Neither a fixed pivot nor a rigid axle was needed for rotation of F₁-ATPase.

F₁-ATPase, a water-soluble portion of the enzyme ATP synthase, has been predicted (1, 2) and proved (3) to be an ATP-driven rotary motor. Its minimal subcomplex, active in ATP hydrolysis and rotation, consists of $\alpha_3\beta_3\gamma$ subunits (4, 5), which we refer to here as F₁. A crystal structure (6) of bovine mitochondrial F₁ (MF₁) is shown in Fig. 1A. The central γ subunit is supported by the $\alpha_3\beta_3$ cylinder at the top orifice and bottom (blue and dark green atoms); the bottom support forms a hydrophobic sleeve that could act as a bearing (7). Three catalytic sites for ATP hydrolysis reside at α - β interfaces, primarily hosted by a β subunit. In the original structure (7), one site (hosted by β_{TP} and α_{TP} in Fig. 1) bound an ATP analog; another (β_{DP} and α_{DP}), adenosine 5'-diphosphate (ADP); the third (β_E and α_E), none; and noncatalytic nucleotide-binding sites in the other interfaces bound the ATP analog. The upper portions of β_{TP} and β_{DP} are bent toward, and apparently push, the top of the γ shaft, whereas β_E retracts and pulls the shaft (Fig. 1A). This structure led Wang and Oster (8) to propose a push-pull rotary mechanism in which the γ shaft, which is slightly bent and skewed, makes a conical rotation around the axis shown in black in Fig. 1A. In this mechanism, pivoting of the shaft in the bottom support is essential for torque production. Here, we ask if the pivot, or even the whole shaft, is necessary for rotation.

We used as the wild type a modified (α -C193S, β -His₁₀ at N terminus, γ -S107C, γ -I210C) subcomplex (9) of the thermophilic F₁ (TF₁). Following earlier work (10) on *Escherichia coli* F₁ (EF₁), we previously deleted 21 C-terminal residues of TF₁- γ . The mutant (γ - Δ C21 in Fig. 1B) produced considerable torque (11), but the truncated rotor tip would still touch the bottom support (Fig. 1A), and thus the remaining bottom interactions might have provided the torque. Beyond 21 residues, we failed to obtain an active subcomplex. Here, we find that shorter γ subunits, the shortest two being almost outside the stator cavity (Fig. 1), are expressed at levels similar to that of the wild type (fig. S1), and that we can obtain assembled subcomplexes containing a mutated γ subunit, albeit at lower yields for short mutants (Fig. 2), by omitting heat treatment in the purification procedure and doing column treatments at room temperature (12).

We tested if these mutants rotate, by attaching the β subunits to a glass surface through the histidine residues at the N terminus and putting, as a marker, a 40-nm gold bead or its duplex on the two cysteines of the γ subunit. All mutants, up to γ - Δ N22C43 (Fig. 1, E and F), could rotate the bead in the correct, counterclockwise (viewed from above in Fig. 1) direction for >100 revolutions (Fig. 3A). The probability of finding a rotating bead was low for short mutants: from the wild type up to γ - Δ N7C29, we observed, on average, a few or more rotating beads per field of view (7.1 μ m by 7.1 μ m) when 5 to 10 nM F₁ was infused into the observation chamber at 2 mM ATP; about 0.5 bead per field of view for 10 to 20 nM γ - Δ N11C32; >10 beads per chamber (~6 mm by 18 mm) for 40 nM γ - Δ N14C36; and 1 or 2 beads per chamber for 40 to 100 nM γ - Δ N18C40 or 100 nM γ - Δ N22C43. For the last two mutants, surface bead density was very low, suggesting that most F₁ molecules lacked γ , consistent with the faint γ bands in Fig. 2. The beads that rotated relatively smoothly without much surface obstruction gave time-averaged rotary speeds that were consistent with the rate of ATP hydrolysis (Fig. 4B). The hydrolysis rate

leveled off at the value of γ -less mutant $\alpha_3\beta_3$, which shows hydrolysis activity uncoupled to γ rotation (13). The paucity of γ in samples of the shortest mutants (Fig. 2) explains this asymptotic behavior.

The time-averaged rate of rotation, as well as the rate of ATP hydrolysis, was low in the truncated mutants (Fig. 4B), indicating that the interactions between the γ tip and the lower stator support are important for rapid progress of catalysis. We note the relatively flat portion in Fig. 4B between γ - Δ C21 and γ - Δ N7C29, where the tip would be unable to make strong contacts with the lower support; from γ - Δ N11C32, for which the tip would be completely in the middle of the cavity, the rates decreased again, and we observed irregular movements as described below. We have shown previously that reverse rotation of F₁ by an external force leads to reversal of chemical reactions in the catalytic sites, leading to net ATP synthesis (14). The reversal by manipulation of the γ angle alone implies a γ -dictator mechanism, whereby the γ angle controls which chemical reaction takes place in the three catalytic sites: ATP binding, hydrolysis, and product release (5, 15). Leverage by a short γ , without firm pivoting at the bottom, will be inefficient in driving β (and α) subunits over an activation barrier into the conformation appropriate for the next chemical reaction. A remote possibility is that the $\alpha_3\beta_3$ cylinder alone may undergo ATP-dependent, circular conformational changes without supervision by γ , and that a bead, or even the shortest γ , simply reflects this motion. With $\alpha_3\beta_3$, however, we did not find any bead to rotate. The correlation between the γ length and rotary speed (Fig. 4B) indicates the diminishing but finite contribution of a short γ in the coordination.

At a sufficiently high camera speed, all rotations appeared stepwise even at 2 mM ATP (Fig. 3, C and D). For the wild-type protein, dwells at this saturating ATP concentration are at ~80° past an ATP-waiting angle, where ATP hydrolysis and phosphate release take ~1 ms each at room temperature (9, 15, 16). The dwelling angles of the mutants have not been assigned. The steps of mutants were noisy, indicating larger fluctuation of short γ subunits, and some mutants showed two or more dwelling angles per 120°. The horizontal lines in Fig. 3, C and D, show the angles of the most populated dwells in each mutant. The dwells imply the presence of an activation barrier(s) against a reaction that is to take place at that angle.

In addition to the apparently thermal fluctuations, short mutants exhibited irregular motions where the bead moved toward and stayed near the rotation axis for tens of milliseconds before going back to the rotary track mostly onto the position 120° ahead (Fig. 3B-b), occasionally onto the previous position (Fig. 3B-c), and rarely but notably onto the position 120° backward (Fig. 3B-d). Such behaviors tended to be repetitive, but the total time was usually short and

¹Department of Physics, Faculty of Science and Engineering, Waseda University, Shinjuku-ku, Tokyo 169-8555, Japan.

²Department of Physics, School of Physical Sciences, Shahjalal University of Science and Technology, Sylhet-3114, Bangladesh.

³Department of Physics, Osaka Medical College, Osaka 569-8686, Japan. ⁴Chemical Resources Laboratory, Tokyo Institute of Technology, Nagatsuta 4259, Yokohama 226-8503, Japan.

⁵ATP-Synthesis Regulation Project, International Cooperative Research Project (ICORP), Japan Science and Technology Agency (JST), Aomi 2-41, Tokyo 135-0064, Japan. ⁶Tsukuba Research Laboratory, Hamamatsu Photonics KK, Tokodai, Tsukuba 300-2635, Japan. ⁷Core Research for Evolutional Science and Technology (CREST) "Formation of Soft Nano-Machines" Team 13*, Tokodai, Tsukuba 300-2635, Japan.

*These authors contributed equally to this work.

†To whom correspondence should be addressed. E-mail: kazuhiko@waseda.jp

within the width of the vertical bars in Fig. 3A. Exceptionally long repetitions were also observed (Fig. 3A, two long horizontal rectangles). The bead position near the rotation axis suggests an F_1 conformation(s) quite different from the one in Fig. 1. If the two cysteines on γ (near the black circles in Fig. 1F) bound the bead, a central bead location would require the γ head to become upright, by counterclockwise inclination in Fig. 1F, right. The tip of the γ shaft would then move toward α_{DP} , a movement allowed for a short γ . Alternatively, the coiled-coil portion of a short γ may occasionally melt. To be upright, the γ

head must reposition itself in the concave orifice, breaking all γ -stator interactions seen in the crystal. The F_1 would be in an unclutched state. This scenario based on the wild-type MF_1 structure may not be valid, but some major reorganization must underlie the central bead location.

The shortest mutant (γ - $\Delta N22C43$) exhibited frequent irregular motions and also backward steps (Fig. 3A). It still rotated mainly in the correct direction, which must be driven by an effective positive torque. For the upper and lower curves in Fig. 3A, there were 65 and 44

moments of irregular motion in 100 s, respectively, with the total durations of 2.7 and 2.4 s; there were 368 and 259 forward 120°-steps, compared with 32 and 37 backward steps. The second shortest γ (γ - $\Delta N18C40$), which is also nearly outside the stator cavity, rotated much more steadily.

To estimate the torque of the mutants, we attached larger beads for which the viscous friction is high. γ - $\Delta C21$ could rotate a duplex of 0.49- μ m polystyrene beads with an apparent torque of ~ 20 pN \cdot nm (11), about half the torque of the wild type, but the mutant was unable to rotate a 0.9- μ m bead duplex. γ - $\Delta N4C25$ up to γ - $\Delta N11C32$ could rotate a 0.29- μ m duplex, but not the 0.49- μ m duplex. Rotating duplexes were rare for γ - $\Delta N7C29$ and γ - $\Delta N11C32$, and they tended to detach from the surface during observation. The 0.29- μ m bead, compared with the 40-nm gold bead, likely bumps the glass (or F_1) surface and is detached. When the bead is stuck against a surface in one of the dwelling angles where the activation barrier is high for short mutants, the bead may stop there.

Assuming that the instantaneous rotary speeds of the 0.29- μ m bead duplexes during 120° steps are determined by the balance between the torque of the motor and viscous friction (3, 5, 17), we estimated the torque of γ - $\Delta N4C25$ to γ - $\Delta N11C32$ to be ~ 20 pN \cdot nm (fig. S3A). This estimate may be questioned because the mutants undergo extensive thermal fluctuations and thus 120° excursions may result from occasional large-amplitude fluctuations that are not directly related to the motor torque (a diffusion-and-catch mechanism of rotation). In some duplexes, we observed three 120° steps occurring always in succession (Fig. 4A, arrow), presumably because the F_1 was obliquely attached to the surface. Torque estimated in the 360° excursions (fig. S3B), which cannot be entirely thermal, was at least 8 pN \cdot nm. Also, most duplexes in Fig. 4A rotated with a time-averaged speed exceeding 1 revolution s^{-1} ,

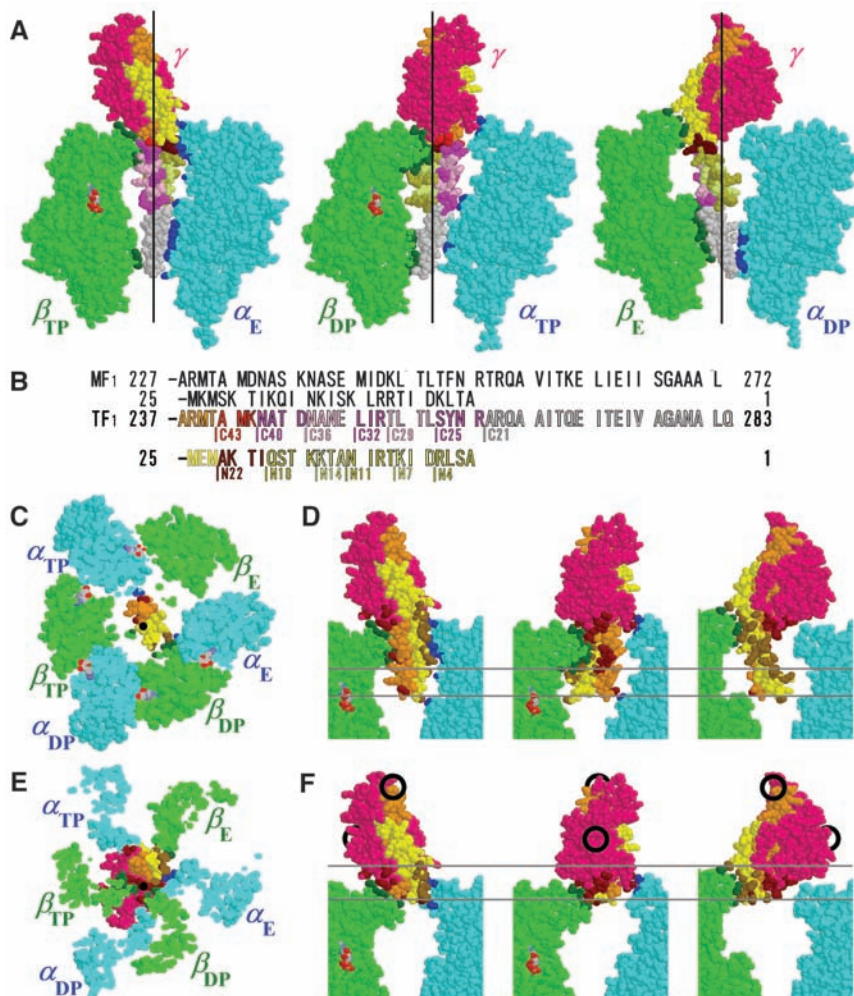


Fig. 1. An atomic structure (δ) of MF_1 . (A) Side views showing the central γ subunit and an opposing α - β pair. The membrane-embedded F_0 portion of ATP synthase would be above the γ subunit. Truncations of the γ subunit are shown with the color scheme in (B); the N- and C-terminal α helices are in yellow and orange, respectively. Those atoms of α and β subunits that are within 0.5 nm from an atom of γ (excluding hydrogens) are colored blue and dark green, respectively. Nucleotides are shown in CPK colors. Black lines [and black dots in (C) and (E)] represent a putative rotation axis (δ). (B) Amino acid sequences at the C and N termini of γ in MF_1 (22) and TF_1 , except that the numbering in (B) starts from Met-1, which is absent in the expressed wild-type protein (23). Abbreviations for the amino acid residues are as follows: A, Ala; D, Asp; E, Glu; F, Phe; G, Gly; I, Ile; K, Lys; L, Leu; M, Met; N, Asn; Q, Gln; R, Arg; S, Ser; T, Thr; V, Val; and Y, Tyr. (C to F) Structures of γ - $\Delta N4C25$ (C and D) and γ - $\Delta N22C43$ (E and F). For γ - $\Delta N4C25$, γ -Met-4 is represented by γ -Lys-4, excluding the ϵ -amino group to mimic Met. For γ - $\Delta N22C43$, γ -Met-22 is represented by γ -Ser-22. (C) and (E) are bottom views of the section between the gray lines in (D) and (F). Atoms of γ that are within 0.5 nm from an atom of α or β are shown in gold and brown (there were none on the C-terminal helix of γ - $\Delta N22C43$). Black circles in (F) show approximate locations of biotinylated cysteines.

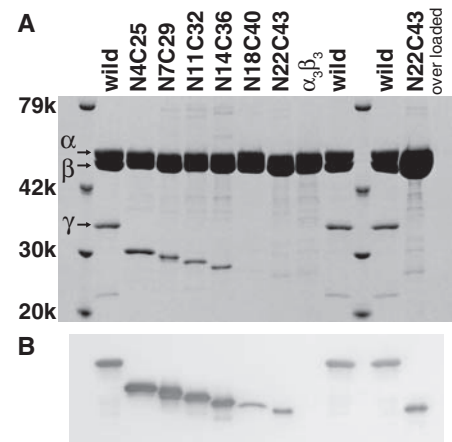


Fig. 2. Confirmation of γ truncations by polyacrylamide gel electrophoresis. (A) A 12.5% gel containing 0.1% SDS, stained with Coomassie Brilliant Blue R-250. (B) Western blot of (A) stained with antibodies to the γ subunit.

implying a lower bound for the effective torque of 2 pN·nm. Torque of the shorter mutants could not be estimated, but the unidirectional character of the rotation implies production of an effective torque in the correct direction.

Most manmade rotary machines rely on a rigid axle held by a static bearing; thanks to the constraint exerted by the bearing, almost any force acting on the axle is converted to a torque through a lever action. Nature seems to have adopted this simple principle for the bacterial flagellar motor (18) and the proton-driven F_0

motor of the ATP synthase (4): Their rotor axis is held stationary by stator bearings, and thus force from one driving unit, acting on only one point on the rotor, suffices to produce torque. For the short γ mutants here, however, the concept of a rigid axle in a static bearing no longer applies. Yet the mutants do rotate.

Rotating the shortest γ is perhaps like rotating an unsupported pen between six fingers, suspending the pen vertically at the very top. The six upper tips of the α and β subunits must play three roles in a highly concerted fashion: mov-

ing the rotor in the correct direction, serving as a fulcrum to convert the motion into torque, and preventing the truncated rotor from escaping. All these functions require contacts between the rotor and tips, but static contacts do not allow full rotation. The grip must be dynamic, yet continuous; a failure for a moment will allow Brownian motion to carry the rotor away. A partial hint may be the $\sim 30^\circ$ twist of γ in some crystal structures (19); the rest of a 120° step might be covered by Brownian rotation. The short γ may indeed be driven by biased diffusion,

Fig. 3. Rotation of 40-nm gold beads attached to the γ subunit. Counterclockwise rotations, viewed from above in Fig. 1A, are plotted as positive revolutions. ATP concentration was 2 mM except for the wild-type protein in (C). (A) Overall time courses for beads that rotated relatively fast. Vertical bars and two horizontal rectangles indicate the period during which irregular motions described in (B) continued. (B) Traces of typical irregular motions where the bead tended to dwell near the rotation center. (a) Regular 120° steps; (b) center then forward; (c) center and turning back; (d) center then backward. (C) Stepping kinetics observed at 8000 frames s^{-1} . Thin dark lines, after 15-point median filtering. Most-populated angles for each mutant (judged over the entire time courses) are on the horizontal lines separated by 120° ; for the wild type at $2 \mu M$ ATP, these are ATP-waiting angles. (D) Stepping kinetics of the shortest four mutants at 125 frames s^{-1} (records taken at higher speeds have been averaged in 8-ms bins). Vertical bars show moments of irregular motions. Crosses, backward steps; arrowhead, succession of two backward steps (a rare event).

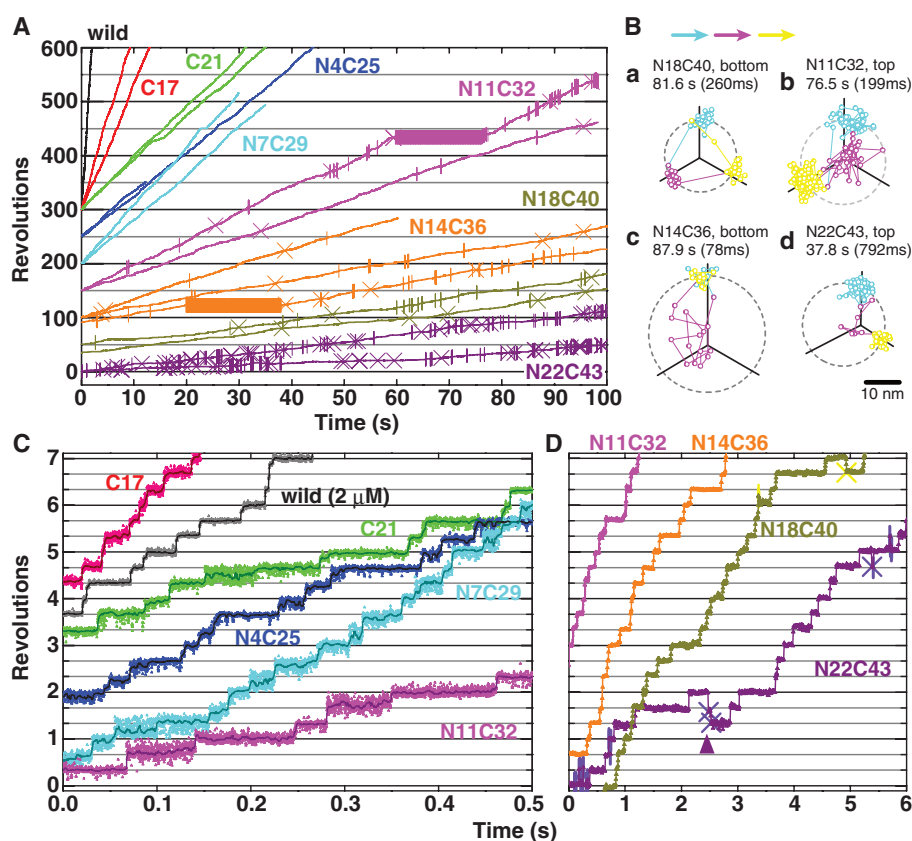
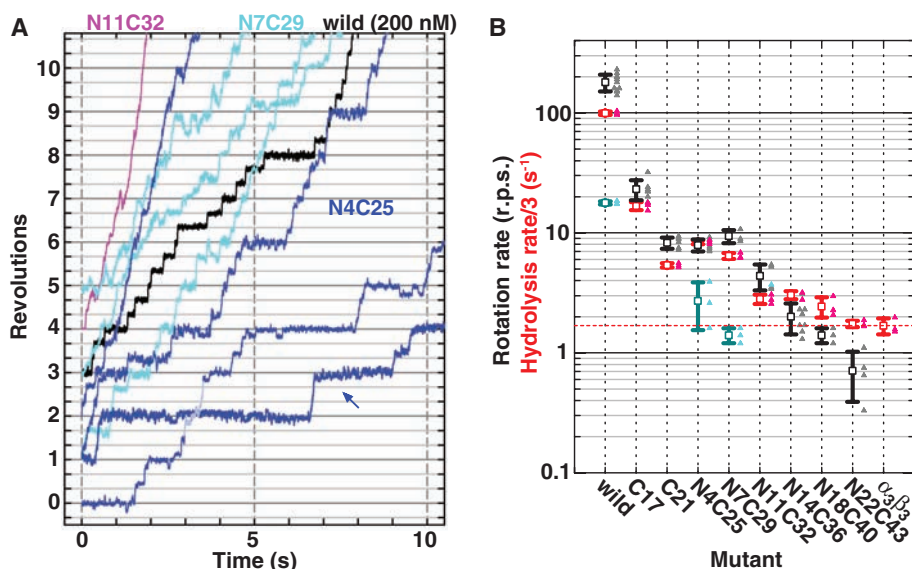


Fig. 4. (A) Rotation time courses for 0.29- μm bead duplexes at 500 frames s^{-1} . Data show relatively fast rotation or clearer stepping. ATP concentration was 2 mM (200 nM for the wild type). (B) Summary of rotation and hydrolysis rates at 2 mM ATP. Black symbols show mean \pm SD for time-averaged rotation rates of 40-nm gold beads that rotated relatively fast; rates of individual beads over >50 (mostly >100) consecutive revolutions are shown in gray triangles. Dark cyan, mean \pm SD for rotation rates of 0.29- μm bead duplexes that rotated relatively fast; cyan, individual rates over 10 revolutions. Red, mean \pm SD for the rate of ATP hydrolysis (fig. S2); three determinations in magenta; red dashed line, mean hydrolysis rate of $\alpha_3\beta_3$. Temperature, $23^\circ C$.



as in the single-head linear motor KIF1A (20) that cannot rely on alternating firm grips allowed for two-head motors. Unlike KIF1A, which diffuses widely, however, diffusion of the truncated γ is largely within 120°, and most 120° steps are in the forward direction (~90% in γ - Δ N22C43 and >99% in γ - Δ N18C40). The orifice somehow blocks backward diffusion, ensuring generation of an effective torque. Clarifying how this is achieved will provide a new paradigm for the design of molecular machines. Why is there superfluous robustness in the rotary mechanism of F_1 ? Perhaps this began as a clumsy device, and then proceeded to sophistication. If so, ring-shaped AAA+ ATPases may all, in principle, be capable of producing torque, as suggested for helicases (21).

References and Notes

- P. D. Boyer, W. Kohlbrenner, in *Energy Coupling in Photosynthesis*, B. R. Selman, S. Selman-Reimer, Eds. (Elsevier, Amsterdam, 1981), pp. 231–240.
- F. Oosawa, S. Hayashi, *Adv. Biophys.* **22**, 151 (1986).
- H. Noji, R. Yasuda, M. Yoshida, K. Kinoshita Jr., *Nature* **386**, 299 (1997).
- M. Yoshida, E. Muneyuki, T. Hisabori, *Nat. Rev. Mol. Cell Biol.* **2**, 669 (2001).
- K. Kinoshita Jr., K. Adachi, H. Itoh, *Annu. Rev. Biophys. Biomol. Struct.* **33**, 245 (2004).
- C. Gibbons, M. G. Montgomery, A. G. W. Leslie, J. E. Walker, *Nat. Struct. Biol.* **7**, 1055 (2000).
- J. P. Abrahams, A. G. W. Leslie, R. Lutter, J. E. Walker, *Nature* **370**, 621 (1994).
- H. Wang, G. Oster, *Nature* **396**, 279 (1998).
- R. Yasuda, H. Noji, M. Yoshida, K. Kinoshita Jr., H. Itoh, *Nature* **410**, 898 (2001).
- M. Müller, O. Pänke, W. Junge, S. Engelbrecht, *J. Biol. Chem.* **277**, 23308 (2002).
- M. D. Hossain et al., *Biophys. J.* **90**, 4195 (2006).
- See supporting material on *Science* Online.
- K. Miwa, M. Yoshida, *Proc. Natl. Acad. Sci. U.S.A.* **86**, 6484 (1989).
- H. Itoh et al., *Nature* **427**, 465 (2004).
- K. Adachi et al., *Cell* **130**, 309 (2007).
- K. Shimabukuro et al., *Proc. Natl. Acad. Sci. U.S.A.* **100**, 14731 (2003).
- N. Sakaki et al., *Biophys. J.* **88**, 2047 (2005).
- H. C. Berg, *Annu. Rev. Biochem.* **72**, 19 (2003).
- V. Kabaleeswaran, N. Puri, J. E. Walker, A. G. W. Leslie, D. M. Mueller, *EMBO J.* **25**, 5433 (2006).
- Y. Okada, H. Higuchi, N. Hirokawa, *Nature* **424**, 574 (2003).
- S. S. Patel, K. M. Picha, *Annu. Rev. Biochem.* **69**, 651 (2000).
- J. E. Walker et al., *J. Mol. Biol.* **184**, 677 (1985).
- S. Ohta et al., *Biochim. Biophys. Acta* **933**, 141 (1988).
- We thank M. Shio for designing a stable microscope stage; K. Shiroguchi and A. Shinohara for gene engineering; R. Shimo-Kon and R. Kanda for sample preparation; N. Sakaki, Y. Onoue, and T. Okamoto for technical support; K. Sakamaki and M. Fukatsu for encouragement and lab management; and members of the Kinoshita lab for help and advice. This work was supported by Grants-in-Aid for Specially Promoted Research and for Young Scientists (B) and the 21st Century Center of Excellence Program from the Ministry of Education, Sports, Culture, Science and Technology, Japan.

Supporting Online Material

www.sciencemag.org/cgi/content/full/319/5865/955/DC1

Materials and Methods

Table S1

Figs. S1 to S3

References

Movies S1 to S6

4 October 2007; accepted 19 December 2007

10.1126/science.1151343

A Mouse Model of Mitochondrial Disease Reveals Germline Selection Against Severe mtDNA Mutations

Weiwei Fan,^{1,2} Katrina G. Waymire,^{1,2} Navneet Narula,³ Peng Li,⁴ Christophe Rocher,^{1,2} Pinar E. Coskun,^{1,2} Mani A. Vannan,⁴ Jagat Narula,⁴ Grant R. MacGregor,^{1,5,6} Douglas C. Wallace^{1,2,7*}

The majority of mitochondrial DNA (mtDNA) mutations that cause human disease are mild to moderately deleterious, yet many random mtDNA mutations would be expected to be severe. To determine the fate of the more severe mtDNA mutations, we introduced mtDNAs containing two mutations that affect oxidative phosphorylation into the female mouse germ line. The severe *ND6* mutation was selectively eliminated during oogenesis within four generations, whereas the milder *COI* mutation was retained throughout multiple generations even though the offspring consistently developed mitochondrial myopathy and cardiomyopathy. Thus, severe mtDNA mutations appear to be selectively eliminated from the female germ line, thereby minimizing their impact on population fitness.

The maternally inherited mitochondrial DNA (mtDNA) has a high mutation rate, and mtDNA base substitution mutations have been implicated in a variety of inherited degenerative diseases including myopathy, cardiomyopathy, and neurological and endocrine disorders (1, 2). Paradoxically, the frequency of mtDNA diseases is high, estimated at 1 in 5000

(3, 4), yet only a few mtDNA mutations account for the majority of familial cases (2). Because mutations would be expected to occur randomly in the mtDNA, the paucity of the most severe mtDNA base substitutions in maternal pedigrees suggests that the severe mutations may be selectively eliminated in the female germ line.

To investigate this possibility, we have developed a mouse model in which the germline transmission of mtDNA point mutations of different severity could be tested. An antimycin A-resistant mouse LA9 cell line was cloned whose mtDNA harbored two homoplasmic (pure mutant) protein-coding gene base change mutations: one severe and the other mild. The severe mutation was a C insertion at nucleotide 13,885 (13885insC), which created a frameshift mutation in the NADH dehydrogenase subunit 6 gene (*ND6*). This frameshift mutation altered codon 63 and resulted in termination at codon 79 (Fig. 1A, top; fig. S1A, bottom). When homoplasmic,

this mutation inactivates oxidative phosphorylation complex I (5). The mild mutation was a missense mutation at nucleotide 6589 (T6589C) in the cytochrome c oxidase subunit I gene (*COI*) that converted the highly conserved valine at codon 421 to alanine (V421A) (fig. S1A, top). When homoplasmic, this mutation reduces the activity of oxidative phosphorylation complex IV by 50% (6, 7).

LA9 cells homoplasmic for both the *ND6* frameshift and *COI* missense mutations were enucleated, and the mtDNAs were transferred by cytoplasm fusion to the mtDNA-deficient (ρ^0) mouse cell line LMEB4, generating the LMJL8 transmitochondrial cybrid (8). LMJL8 mitochondria exhibited no detectable oxygen consumption when provided with NADH-linked complex I substrates (fig. S1B) and no detectable complex I enzyme activity (fig. S1C). However, the same mitochondria exhibited a 43% increase in succinate-linked respiration and a 91% increase in complex II + III activity as well as a 62% increase in complex IV activity (fig. S1, B and C), presumably as a compensatory response to the severe complex I defect (9). Relative to LM(TK⁻) cells, mouse L cell lines homoplasmic for the *COI* missense mutation also showed increased reactive oxygen species (ROS). Cells homoplasmic for both the *ND6* frameshift and *COI* missense mutations produced fewer ROS than did the *COI* mutant cells. However, cells that were 50% heteroplasmic for both the *ND6* frameshift and the *COI* missense mutations had the highest ROS production (fig. S1D).

To analyze the fates of the severe *ND6* frameshift versus moderate *COI* missense mtDNA mutations, we introduced these mutations into the mouse germ line. LMJL8 cybrids were enucleated and the cytoplasts fused to the mouse female embryonic stem (ES) cell line

¹Center for Molecular and Mitochondrial Medicine and Genetics, University of California, Irvine, CA 92697, USA.

²Department of Biological Chemistry, University of California, Irvine, CA 92697, USA. ³Department of Pathology, University of California, Irvine, CA 92697, USA. ⁴Division of Cardiology, Department of Medicine, University of California, Irvine, CA 92697, USA. ⁵Department of Developmental and Cell Biology, University of California, Irvine, CA 92697, USA.

⁶Developmental Biology Center, University of California, Irvine, CA 92697, USA. ⁷Departments of Ecology and Evolutionary Biology and Pediatrics, University of California, Irvine, CA 92697, USA.

*To whom correspondence should be addressed. E-mail: dwallace@uci.edu

CC9.3.1 that had been cured of its resident mitochondria and mtDNAs by treatment with rhodamine 6G (10–12). Of the 96 resulting ES cybrids, four (EC53, EC77, EC95, and EC96) were found to be homoplasmic for the *COI* missense mutation. By quantitative primer

extension–denaturing high-performance liquid chromatography analysis, three of the ES cell cybrids were also found to be homoplasmic for the *ND6* frameshift mutation. However, one ES cell cybrid, EC77, was heteroplasmic (mixture of mutant and normal mtDNAs); 96% of the

mtDNAs harbored the *ND6* frameshift mutation (13885insC), whereas 4% of the mtDNAs had sustained a secondary deletion of the adjacent T (13885insCdelT), restoring the reading frame (Fig. 1A, bottom, and Fig. 1B). This *ND6* revertant mutation encodes the normal amino acid

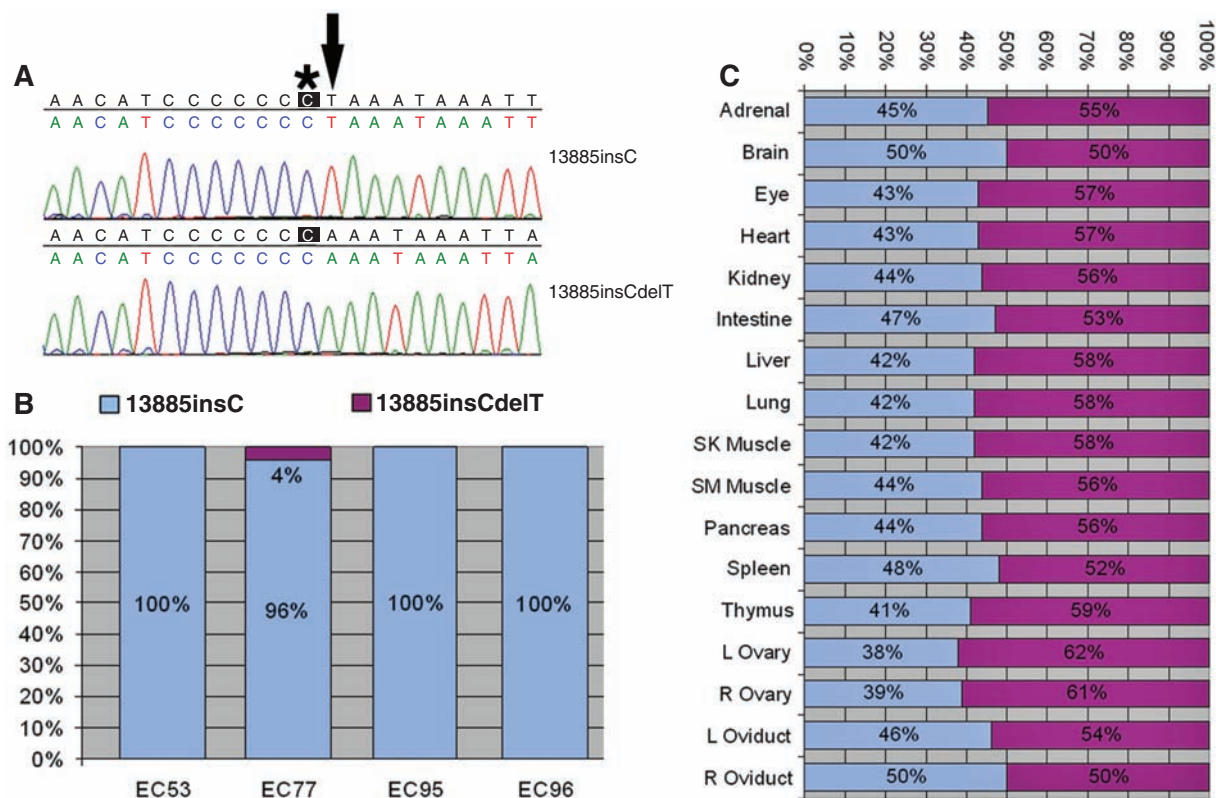
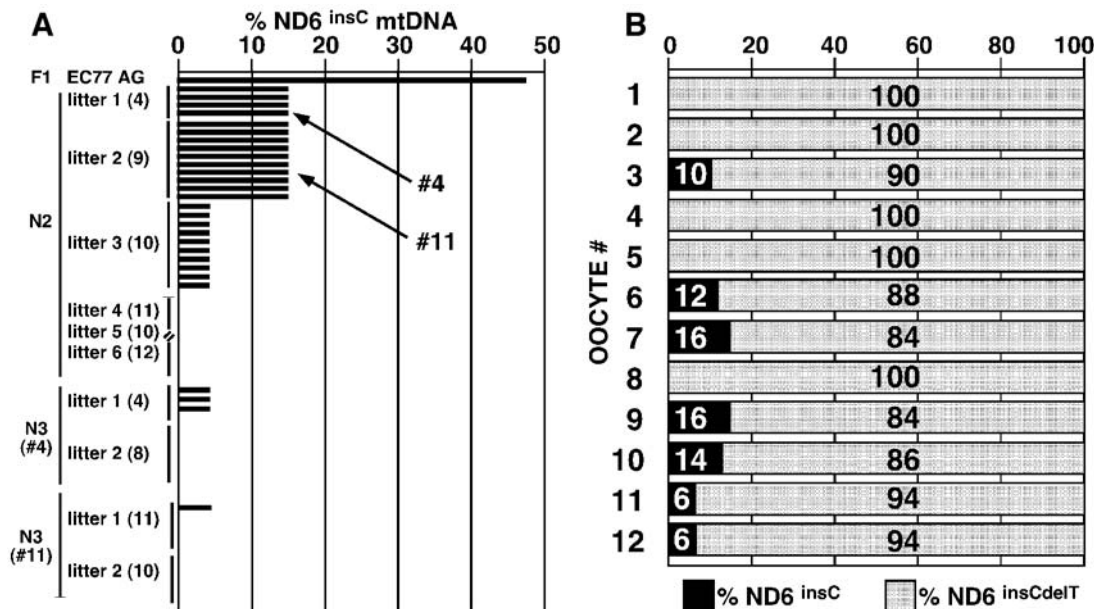


Fig. 1. Qualitative and quantitative analysis of the *ND6* frameshift (13885insC) and *ND6* revertant (13885insCdelT) mutations in mouse ES cell cybrids and tissues of F₁ female EC77-AG. (A) Sequence around nucleotide 13,885 of two clones of mtDNA from EC77 cells. Top (13885insC), the single C insertion causing the frameshift (asterisk); bottom (13885insCdelT), the

T (arrow) deletion that restored the normal reading frame. (B) Percentages of *ND6* frameshift (13885insC, blue) versus revertant (13885insCdelT, purple) in four independent mouse ES cybrids. (C) Proportions of *ND6* frameshift (13885insC) and revertant (13885insCdelT) mtDNAs in the tissues of F₁ female EC77-AG.

Fig. 2. Selective elimination of *ND6* frameshift mtDNA (13885insC) from F₁ female EC77-AG and her offspring. (A) Percentages of *ND6* frameshift (13885insC) mtDNAs in EC77-AG and her offspring, plus the pups of her daughters EC77 #4 and #11. Each offspring was analyzed from multiple litters. Litter sizes are indicated in parentheses. (B) Percentages of the *ND6* frameshift (13885insC, black) and revertant (13885insCdelT, gray) mtDNAs in 12 oocytes isolated from EC77 progeny mice containing 14% of the *ND6* frameshift mutation (13885insC).



sequence but changes leucine codon 60 from TTA to TTG.

EC77 ES cells were injected into female C57BL/6Nhsd blastocysts, and the chimeric embryos were transferred into pseudo-pregnant females (12). Three chimeric females were generated that contained varying proportions of three mtDNA genotypes: *ND6* frameshift + *COI* missense, *ND6* revertant + *COI* missense, and wild type (fig. S2). The chimeras were mated with C57BL/6J (B6) males and produced a total of 111 pups. Only one F₁ agouti female pup, EC77-AG, was generated harboring the mutant mtDNAs. Analysis of tail mtDNA by primer extension and by cloning and sequencing revealed that EC77-AG was homoplasmic for the *COI* mutant allele but heteroplasmic for the *ND6* frameshift (47%) and *ND6* revertant (53%) mtDNAs (fig. S3A). Post mortem analysis at 11 months revealed that all analyzed tissues from EC77-AG had essentially the same genotype, with an average of 44 ± 3% (range 38% to 50%) of the mtDNAs harboring the *ND6* frameshift plus *COI* missense mutations (*ND6* 13885insC + *COI* T6589C) and 56% harboring the *ND6* revertant plus *COI* missense mutations (*ND6* 13885insCdelT + *COI* T6589C). The highest levels of the frameshift mutant mtDNA were found in the brain and right oviduct; the lowest level was found in the left ovary (Fig. 1C).

Throughout the 11 months of her life, EC77-AG displayed no overt phenotype. However, post mortem mitochondrial enzymatic assays revealed a 10% to 33% decrease of complex I activity in brain, heart, liver, and skeletal muscle (fig. S3B), a 56% and 46% decrease of complex IV activity in brain and skeletal muscle (fig. S3B), a 56% and 46% decrease of complex IV activity in brain and skeletal muscle, and a 19% and 39% increase of complex IV activity in heart and liver (fig. S3C). This was associated with structures consistent with lipid droplets in the heart mitochondria by ultrastructural analysis (compare fig. S3, D and E).

To analyze transmission of the heteroplasmic, severe, *ND6* frameshift (*ND6* 13885insC + *COI* T6589C) mtDNA in successive maternal generations, we mated F₁ female EC77-AG, which had 47% *ND6* frameshift tail mtDNA, with B6 males. EC77-AG gave birth to six litters totaling 56 pups (N₂). The proportion of *ND6* frameshift tail mtDNA, as assessed by primer extension analysis, declined to 14% in the first litter of four pups (EC77 #1 to #4) and the second litter of nine pups (EC77 #5 to #13), then to 6% in the third litter of 10 pups (EC77 #14 to #23), and finally was lost (0%) in all subsequent litters (Fig. 2A).

To verify the reproducibility of the progressive loss of the *ND6* frameshift mtDNA, we mated N₂ female EC77 #4, which had 14% *ND6* frameshift mtDNA, with B6 males. EC77 #4 gave birth to two litters totaling 12 pups (N₃) (Fig. 2A). Three of the four pups of the first litter had 6% *ND6* frameshift mtDNA, whereas the remaining pup of the first litter and all eight pups of the second litter had lost the *ND6* frameshift mtDNA (0%). We also mated N₂

female EC77 #11, which had 14% *ND6* frameshift mtDNA, with B6 males. EC77 #11 gave birth to two litters totaling 21 pups. One of the 11 pups of the first litter had 6% *ND6* frameshift mtDNA, whereas the remaining 10 pups of the first litter and all 10 pups of the second litter had lost the frameshift mtDNA (0%). Mating of B6 males with N₃ females, which had 6% *ND6* frameshift mtDNA, only produced pups that lacked the *ND6* frameshift mtDNA. These data suggest that the mtDNA harboring the deleterious *ND6* frameshift mutation (13885insC) was selectively and directionally eliminated from the mouse female germ line within four generations.

To determine whether the *ND6* frameshift plus *COI* missense mtDNA was eliminated from the female germ line in favor of the *ND6* revertant plus *COI* missense mtDNA via selective

loss of those fetuses with the highest percentages of *ND6* frameshift mtDNA, we compared the litter sizes of females with different proportions of *ND6* frameshift mtDNA. Females with higher percentages of *ND6* frameshift mtDNA would be predicted to generate pups with higher proportions of the *ND6* frameshift mtDNA and thus have higher fetal loss rates and smaller litter sizes. We instead observed that the percentage of *ND6* frameshift mtDNA in the mother had no effect on litter size. The average litter size of F₁ female EC77-AG with 47% *ND6* frameshift mtDNA was 9.3 pups per litter, whereas that of two of her daughters with 14% *ND6* frameshift mtDNA was 8.25 pups per litter, and that of her descendants with 6% *ND6* frameshift mtDNAs was 8.75 pups per litter. Given that average litter size usually decreases slightly when backcrossing onto a B6 strain background, the average litter size

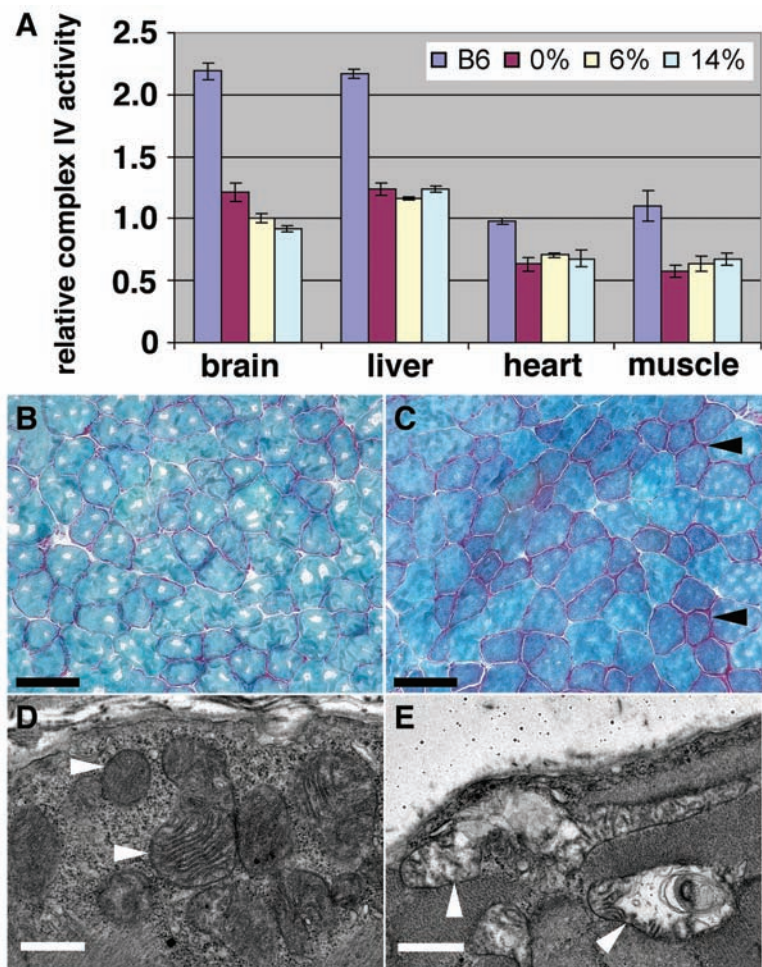


Fig. 3. Decreased mitochondrial complex IV activity and mitochondrial myopathy in *COI* mutant mice. (A) Complex IV activity was reduced to similar extents in various tissues of mutant mice harboring 0%, 6%, or 14% *ND6* frameshift mutations plus 100% *COI* missense. Numbers of animals tested: six B6, seven 0% (0% *ND6* frameshift plus 100% *COI* missense), three 6% (6% *ND6* frameshift plus 100% *COI* missense), and four 14% (14% *ND6* frameshift plus 100% *COI* missense), with three repeats performed for each test on each animal. (B and C) Gomori trichrome staining shows increased ragged red fibers in skeletal muscle of 12-month-old *COI* mutant mice (C) compared to age-matched control (B). (D and E) Electron microscopy (EM) shows altered mitochondrial morphology (arrowheads) in skeletal muscle of 12-month-old *COI* mutant (E) mice compared to age-matched control (D). Scale bars, 75 μ m [(B) and (C)], 1 μ m [(D) and (E)].

appeared unaffected by the proportion of the mother's mtDNA that harbored the *ND6* frameshift mutation, thus arguing against preferential fetal loss as the segregation mechanism.

To determine whether the *ND6* frameshift mtDNA was lost before fertilization or ovulation, we collected and genotyped individual oocytes from superovulated N_2 females containing 14% *ND6* frameshift plus *COI* missense and 86% *ND6* revertant plus *COI* missense mtDNA. Of the 12 oocytes that were successfully genotyped, four retained 10 to 16% of the *ND6* frameshift mtDNA, two retained 6% of the *ND6* frameshift mtDNA, and five had lost the frameshift mtDNA (Fig. 2B). Previous studies on mice heteroplasmic for the normal NZB and Balb/c mtDNAs revealed that these mtDNAs segregated randomly when transmitted through the female germ line (13). If this was the case for mice that were heteroplasmic for the *ND6* frameshift and *ND6* revertant mtDNAs, we would expect that the percentage of frameshift versus total mtDNAs would be normally distributed around the mother's genotype. In fact, none of the oocytes or progeny had a higher proportion of the *ND6*

frameshift mutant mtDNA than the mother. This indicates that proto-oocytes with the higher proportion of frameshift mutant mtDNA must have been eliminated by selection before ovulation.

As seen with the F_1 female EC77-AG, the proportion of *ND6* frameshift mtDNA in the different tissues of three N_2 mice containing 14% *ND6* frameshift and 86% *ND6* revertant mtDNA, all with the *COI* missense mutation, was relatively constant, ranging between 14% and 16% (fig. S4A). Ultrastructural analysis of hearts taken from the 14% *ND6* frameshift plus 100% *COI* missense mice revealed mitochondrial proliferation, evidence of mitochondrial autophagy, and myofibrillar degeneration (fig. S4, B to D). Biochemical analysis of brain, heart, and liver of mice with 14% *ND6* frameshift plus 100% *COI* missense mutant mtDNAs revealed little reduction in complex I activity (fig. S4E); however, complex IV activity in these tissues was reduced by 28%, 70%, and 59%, respectively (fig. S4F).

Comparison of the complex I activity in mice harboring 0%, 6%, and 14% *ND6* frameshift and 100% *COI* missense mtDNAs confirmed that complex I was little affected, with the possible

exception of a modest reduction of complex I in muscle in animals with 14% *ND6* frameshift mtDNAs (fig. S5A). The complex II + III activities were also relatively stable (fig. S5B). However, complex IV was reduced about 50% in brain, liver, heart, and muscle of the 14%, 6%, and 0% *ND6* frameshift plus 100% *COI* missense mutant mice (Fig. 3A). Hence, the predominant biochemical defect in animals with 14% or less *ND6* frameshift mtDNAs can be attributed to the homoplasmic *COI* missense mutation.

Mice that were homoplasmic for the *COI* missense mutation, linked to the *ND6* revertant mutation (13885insCdeIT), transmitted this mtDNA to all of their offspring through multiple backcrosses to B6 males. Although the phenotype of these mice was grossly normal, muscle histology of 12-month-old animals revealed ragged red muscle fibers and abnormal mitochondria characteristic of mitochondrial myopathy (Fig. 3, B to E).

In addition to the mitochondrial myopathy, echocardiographic analysis of 12-month-old *COI* missense mice revealed that 100% of these animals ($n = 7$) had developed a striking cardiomyopathy, as compared to age-matched B6 control mice ($n = 5$) (Fig. 4, A and B). This cardiomyopathy was associated with a 35% increase in left ventricular wall thickness, a 23% reduction in left ventricular inner dimension at end-diastole ($P < 0.001$), and a 27% increase in rotation in association with a 28% reduction in circumferential strain vectors ($P < 0.001$) and a 42% reduction in radial stretch vectors ($P < 0.001$) (fig. S6, A and B). Histology of the *COI* missense mutant hearts revealed the presence of myocyte hypertrophy, myofibrillar lysis, binucleate cells, and interstitial fibrosis (Fig. 4, C and D). Focal inflammation, interstitial edema, and increased blood vessel number and diameter were also observed (fig. S6, C to E). However, no evidence of the myofiber disarray characteristic of hypertrophic cardiomyopathy was seen. Cardiac ultrastructural analysis revealed loss of myofilaments and mitochondrial abnormalities in mutant heart tissue, including mitochondrial proliferation, reduction in mitochondrial matrix density, and cristolysis (Fig. 4F), relative to age-matched controls (Fig. 4E). Hence, the milder mtDNA *COI* missense mutation was successfully transmitted through repeated maternal generations, even though it caused maternally inherited mitochondrial myopathy and cardiomyopathy.

Our studies suggest that the female germ line has the capacity for intraovarian selection against highly deleterious mtDNA mutations such as the *ND6* frameshift mutation, while permitting transmission of more moderate mtDNA mutations such as the *COI* missense mutation. This observation may explain why there is a dearth of severe mtDNA base substitution pedigrees in humans, yet more moderate pathogenic mtDNA mutations are repeatedly seen, such as those causing neurogenic muscle weakness, ataxia, and retinitis pigmentosa (NARP) T8993G (ATP6

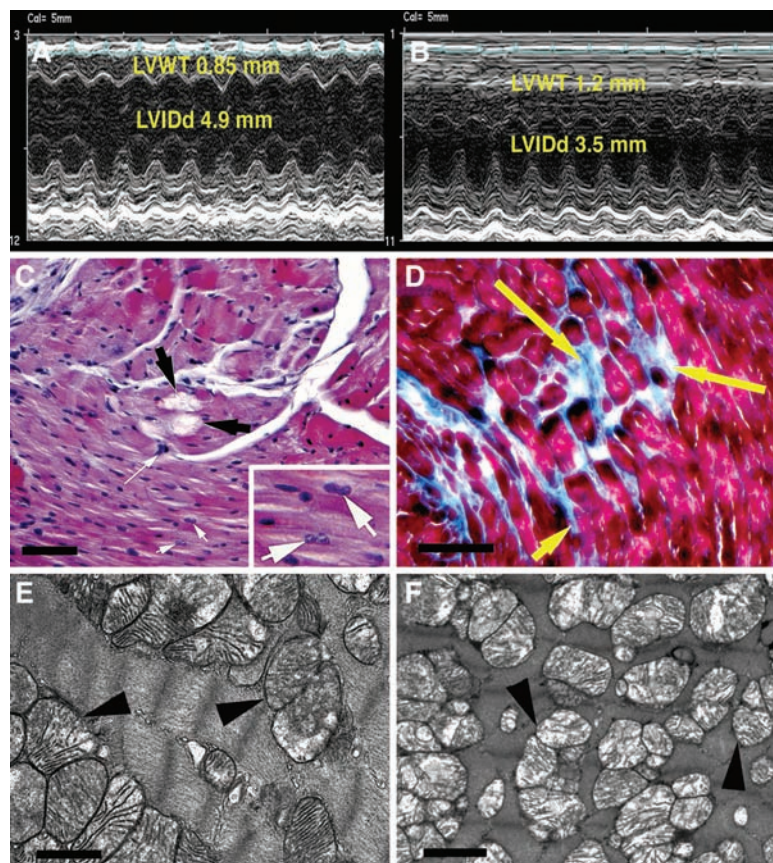


Fig. 4. Mitochondrial cardiomyopathy in 12-month-old mice homoplasmic for *COI* missense mutation. (A) Echocardiographic analysis of control heart. (B) Echocardiographic analysis of mutant heart showing increased left ventricular wall thickness (LVWT) and decreased left ventricular internal dimension in diastole (LVIDd). (C) Hematoxylin and eosin-stained mutant heart showing myofibrillar lysis (black arrows), myocyte hypertrophy (long white arrow), and binucleate cells (inset, white arrows). (D) Masson trichrome-stained mutant heart showing interstitial replacement fibrosis (yellow arrows). (E) EM of mitochondria (arrowheads) in normal heart. (F) EM of mutant heart showing mitochondrial proliferation, reduced matrix density, and cristolysis (arrowheads). Scale bars, 500 μm (C), 100 μm (D), 1 μm [(E) and (F)].

L156R) and Leber hereditary optic neuropathy (LHON) G11778A (ND4 R340H) and T14484C (ND6 M64V) (2).

Although the mechanism by which the severe mtDNA mutations are recognized and eliminated remains unclear, our observation that cells heteroplasmic for both the *ND6* frameshift and the *COI* missense mutations have the highest ROS production provides one possible explanation. It has been proposed that the primordial female germ cells have a limited number of mtDNAs permitting rapid genetic drift toward pure mutant or wild-type mtDNA during the approximately 20 female germline cell divisions (13). At birth, the ovigerous cords reorganize to form single oogonia surrounded by granulosa cells. This would lead to oogonia within fetal ovigerous cords with mtDNA genotypes symmetrically distributed around the maternal mean percent heteroplasmy. Of these oogonia, only about 30% complete meiotic maturation; the remainder undergo apoptosis (14, 15). Because apoptosis in preovulatory follicles is thought to be induced by oxidative stress (16), it is conceivable that the proto-oocytes with the highest percentage of severe mtDNA mutations produce the most ROS and thus are preferentially eliminated by apoptosis. Such a process would then lead to the progressive loss of the more deleterious mtDNA mutations over successive female generations.

Among the pathogenic missense mutations that are observed, the more severe mtDNA mutations such as NARP T8993G remain hetero-

plasmic through successive generations. By contrast, the milder mtDNA mutations, such as LHON G11778A and T14484C, can segregate to homoplasmic mutant (2). Because heteroplasmy would temper the biochemical defect associated with the more severe mutations, this observation supports the concept that the more severe mtDNA defects are eliminated within the maternal germ line.

The existence of a female germline filter for severely deleterious mtDNA mutations makes evolutionary sense. Assuming that mtDNA variation is pivotal to species adaptation to changing environments and that the uniparental mtDNA cannot generate diversity by recombination, then mtDNA diversity must be generated through a high mutation rate (17–19). However, a high mutation rate would generate many highly deleterious mutations that could create an excessive genetic load and endanger species fitness. This dilemma can be resolved by the addition of a graded filter in the female germ line that eliminates the most severe mutations before conception. For such a filter to succeed, multiple cell divisions resulting in a large population of proto-oocytes would be required to segregate out the new mtDNA mutations. This may explain why the mammalian female generates millions of primordial oogonia but ovulates only a few hundred mature oocytes.

References and Notes

1. D. C. Wallace, *Annu. Rev. Genet.* **39**, 359 (2005).
2. D. C. Wallace, M. T. Lott, V. Procaccio, in *Emery and Rimoin's Principles and Practice of Medical Genetics*, D. L. Rimoin, J. M. Connor, R. E. Peyerit, B. R. Korf, Eds.

- (Churchill Livingstone, Philadelphia, ed. 5, 2007), vol. 1, pp. 194–298.
3. A. M. Schaefer, R. W. Taylor, D. M. Turnbull, P. F. Chinnery, *Biochim. Biophys. Acta* **1659**, 115 (2004).
4. A. M. Schaefer et al., *Ann. Neurol.*, 10.1002/ana.21217 (2007).
5. Y. Bai, G. Attardi, *EMBO J.* **17**, 4848 (1998).
6. R. Acin-Perez et al., *Hum. Mol. Genet.* **12**, 329 (2003).
7. A. Kasahara et al., *Hum. Mol. Genet.* **15**, 871 (2006).
8. I. Trounce, D. C. Wallace, *Somat. Cell Mol. Genet.* **22**, 81 (1996).
9. J. E. Kokoszka et al., *Nature* **427**, 461 (2004).
10. S. E. Levy, K. G. Waymire, Y. L. Kim, G. R. MacGregor, D. C. Wallace, *Transgen. Res.* **8**, 137 (1999).
11. J. E. Sliigh et al., *Proc. Natl. Acad. Sci. U.S.A.* **97**, 14461 (2000).
12. G. R. MacGregor, W. W. Fan, K. G. Waymire, D. C. Wallace, in *Embryonic Stem Cells*, E. Notarianni, M. J. Evans, Eds. (Oxford Univ. Press, New York, 2006), pp. 72–104.
13. J. P. Jenuth, A. C. Peterson, K. Fu, E. A. Shoubridge, *Nat. Genet.* **14**, 146 (1996).
14. M. R. Hussein, *Hum. Reprod. Update* **11**, 162 (2005).
15. J. L. Tilly, K. I. Tilly, *Endocrinology* **136**, 242 (1995).
16. M. Tsai-Turton, U. Luderer, *Endocrinology* **147**, 1224 (2006).
17. D. C. Wallace, *Annu. Rev. Biochem.* **76**, 781 (2007).
18. E. Ruiz-Pesini, D. Mishmar, B. Brandon, V. Procaccio, D. C. Wallace, *Science* **303**, 223 (2004).
19. E. Ruiz-Pesini, D. C. Wallace, *Hum. Mutat.* **27**, 1072 (2006).
20. Supported by California Regenerative Medicine Predoctoral Fellowship TI-00008 (W.F.), NIH grant HD45913 (G.R.M.), and NIH grants NS21328, AG13154, AG24373, DK73691, and AG16573 (D.C.W.).

Supporting Online Material

www.sciencemag.org/cgi/content/full/319/5865/958/DC1

Materials and Methods

Figs. S1 to S6

References

13 July 2007; accepted 19 December 2007

10.1126/science.1147786

Metal Chelation and Inhibition of Bacterial Growth in Tissue Abscesses

Brian D. Corbin,¹ Erin H. Seeley,² Andrea Raab,⁶ Joerg Feldmann,⁶ Michael R. Miller,^{2,3} Victor J. Torres,¹ Kelsi L. Anderson,⁴ Brian M. Dattilo,^{2,3} Paul M. Dunman,⁴ Russell Gerads,⁷ Richard M. Caprioli,² Wolfgang Nacken,⁵ Walter J. Chazin,^{2,3} Eric P. Skaar^{1*}

Bacterial infection often results in the formation of tissue abscesses, which represent the primary site of interaction between invading bacteria and the innate immune system. We identify the host protein calprotectin as a neutrophil-dependent factor expressed inside *Staphylococcus aureus* abscesses. Neutrophil-derived calprotectin inhibited *S. aureus* growth through chelation of nutrient Mn²⁺ and Zn²⁺: an activity that results in reprogramming of the bacterial transcriptome. The abscesses of mice lacking calprotectin were enriched in metal, and staphylococcal proliferation was enhanced in these metal-rich abscesses. These results demonstrate that calprotectin is a critical factor in the innate immune response to infection and define metal chelation as a strategy for inhibiting microbial growth inside abscessed tissue.

Abscesses represent an immune response to infection that helps confine the spread of disease through the restriction of microbial growth and dissemination to neighboring tissues (1). *S. aureus* infection results in the formation of abscesses characterized by the extensive accumulation of host neutrophils. Although a role for neutrophils in abscess development is established, the specific host factors that limit

microbial growth within the abscess are incompletely defined.

To identify host factors that limit microbial growth within the abscess, we applied imaging mass spectrometry (IMS) to a mouse model of *S. aureus* infection (2). Kidneys from uninfected and infected animals were sectioned and analyzed by means of IMS. Among the proteins that were present exclusively in abscessed tissue was a

protein exhibiting a mass-to-charge ratio (*m/z*) of 10,165 that displayed the strongest mass-to-charge intensity observed in these experiments; this protein was subsequently identified as S100A8, a component of the calprotectin heterodimer (S100A8/S100A9) (Fig. 1, A and B) (2). Immunohistochemistry with antisera to S100A8 as a probe confirmed that S100A8 was only detectable in tissue from infected mice and localized coordinately with abscesses (Fig. 1C and fig. S1). Furthermore, IMS revealed that S100A8 and S100A9 colocalize to the site of infection, which supports heterodimeric calprotectin as the functional form of these proteins inside tissue abscesses (Fig. 1D). Calprotectin is an S100 EF-hand Ca²⁺-binding protein that accounts for

¹Department of Microbiology and Immunology, Vanderbilt University Medical Center, Nashville, TN 37232, USA.

²Departments of Biochemistry and Chemistry, Vanderbilt University Medical Center, Nashville, TN 37232, USA. ³Center for Structural Biology, Vanderbilt University Medical Center, Nashville, TN 37232, USA. ⁴Department of Pathology and Microbiology, University of Nebraska Medical Center, Omaha, NE 68198, USA. ⁵Institute for Experimental Dermatology, University of Muenster, 48149 Muenster, Germany. ⁶College of Physical Science, University of Aberdeen, Aberdeen AB24 3UE, Scotland, UK. ⁷Applied Speciation and Consulting, Tukwila, WA 98188, USA.

*To whom correspondence should be addressed. E-mail: eric.skaar@vanderbilt.edu

~40% of the cytosolic protein pool of neutrophils (3). This protein was originally identified through its ability to inhibit the growth of a variety of fungal and bacterial pathogens *in vitro* (4). Calprotectin's antimicrobial activity has been proposed to be due to the calprotectin-mediated chelation of nutrient Zn^{2+} (5–7). However, the considerable body of data on the antimicrobial mechanism of calprotectin is largely indirect, and the contribution of calprotectin to the host-pathogen interaction has not been evaluated.

The first step in our approach was to ascertain the cell population responsible for recruitment and/or expression of S100A8 in the staphylococcal abscess. IMS revealed that S100A8 localizes coordinately with staphylococcal kidney and liver abscesses in neutrophil-replete mice. In contrast, infected neutropenic mice do not express S100A8 in the kidney or liver in spite of *S. aureus*-induced lesion formation in these organs (Fig. 1E and figs. S2 and S3). These findings indicate that the presence of S100A8 in infected kidney and liver abscesses is dependent on an intact neutrophil population.

Consistent with a previous report (4), we found that purified calprotectin inhibits *S. aureus* growth in a dose-dependent manner, with complete growth arrest observed at 75 $\mu\text{g/ml}$ (Fig. 2A). The anti-staphylococcal activity of calprotectin is augmented when the protein is purified in the presence of Ca^{2+} (Fig. 2B). This result is consistent with calprotectin's assignment as an S100 EF-hand Ca^{2+} -binding protein (8). We found that neither the S100A9 homodimer, nor the S100A9C3S

homodimer, nor the S100A8/S100A9C3S heterodimer (9) was able to inhibit staphylococcal growth (Fig. 2C), indicating that heterodimerization and the cysteine residue at position 3 in S100A9 are also critical to calprotectin's antimicrobial activity.

The antimicrobial activity of calprotectin is proposed to occur through metal-ion chelation, suggesting that physical contact between calprotectin and *S. aureus* is not required for growth inhibition. We were unable to detect calprotectin-staphylococci interactions using a coprecipitation assay (Fig. 2D), which is consistent with this notion. Moreover, calprotectin (500 $\mu\text{g/ml}$) inhibited staphylococcal growth in the absence of physical contact (Fig. 2E), and *S. aureus* growth was decreased in media transiently treated with calprotectin (Fig. 2F). To determine whether calprotectin chelates nutrient cations, we quantitated calprotectin-dependent cation removal from media using inductively coupled plasma mass spectrometry (ICPMS). These analyses revealed no statistical difference in the number of Fe^{2+} or Mg^{2+} atoms remaining in the medium upon transient treatment with calprotectin (Fig. 3A). In contrast, Mn^{2+} and Zn^{2+} atoms were not detected after calprotectin treatment (Fig. 3A). A significant increase in detectable Ca^{2+} in the medium after calprotectin treatment is likely due to the release of excess Ca^{2+} ions bound to calprotectin in secondary binding sites as a by-product of purification in a Ca^{2+} -rich buffer.

Our data revealed a previously unrecognized role for calprotectin in binding Mn^{2+} . To val-

idate this hypothesis, we examined the Mn^{2+} -binding properties of calprotectin using a fluorescence spectroscopy assay. The shift in the intensity of wavelength of the peak maximum as a result of addition of Mn^{2+} (Fig. 3B) confirmed that calprotectin does bind this metal ion. To determine the sensitivity of *S. aureus* to Zn^{2+} and Mn^{2+} starvation, we grew *S. aureus* in media depleted in either cation. These experiments revealed that *S. aureus* is acutely sensitive to Mn^{2+} deprivation, whereas the bacteria proliferate in media that contain trace levels of Zn^{2+} (Fig. 3C). Addition of excess Mn^{2+} or Zn^{2+} to growth medium rescues calprotectin-mediated inhibition of staphylococcal proliferation, confirming that Mn^{2+} and Zn^{2+} chelation is responsible for the anti-staphylococcal activity of calprotectin (Fig. 3D). Presumably, the ability of individual metals to rescue staphylococcal growth is due to saturation of the Zn^{2+}/Mn^{2+} -binding sites of calprotectin by either excess Zn^{2+} or Mn^{2+} . As a further demonstration that *S. aureus* exposed to calprotectin is Mn^{2+} -starved, *S. aureus* strains were created that are inactivated for the Mn^{2+} -dependent transcriptional repressor ($\Delta mntR$) or the Mn^{2+} uptake system ($\Delta mntA$ and $\Delta mntB$). MntR is a repressor of the MntABC transport system responsible for Mn^{2+} acquisition, and its disruption renders *S. aureus* sensitive to Mn^{2+} -mediated toxicity (10). We found that coincubation with calprotectin alleviates the sensitivity of $\Delta mntR$ to excess Mn^{2+} , whereas strains defective in Mn^{2+} uptake ($\Delta mntA$ or $\Delta mntB$) exhibit increased sensitivity to calprotectin toxicity (fig. S4).

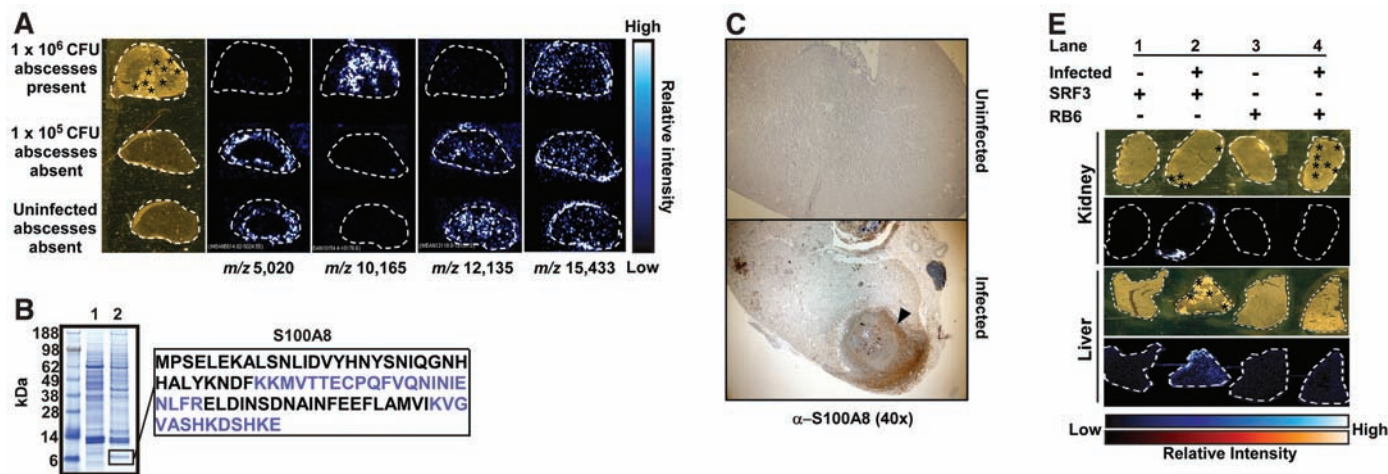
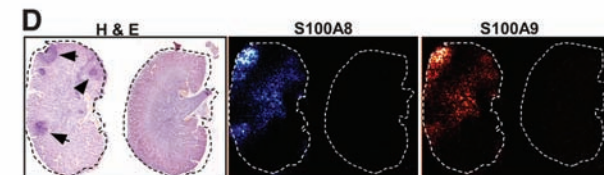


Fig. 1. S100A8 is recruited to staphylococcal abscesses in a neutrophil-dependent manner. (A) IMS of *S. aureus*-infected and uninfected murine kidneys. Optical images of kidney sections mounted on a gold-coated matrix-assisted laser desorption/ionization plate are shown in the far left column. Two-dimensional ion density maps of representative proteins expressed in murine tissue are shown in the four right panels. CFU, colony-forming units. (B) SDS-polyacrylamide gel electrophoresis analysis of material extracted from kidneys of uninfected (lane 1) or infected (lane 2) mice followed by tandem mass spectrometry-based identification of proteins. The band at ~10 kDa was excised and subjected to further analysis. Residues in blue denote peptides that matched the sequence of S100A8. (C) Immunohistochemistry with S100A8 antisera localizes S100A8 to *S. aureus*-infected murine abscesses. Arrowhead denotes abscess. (D) IMS of *S. aureus*-infected and uninfected murine kidneys prepared



as described in (A) showing the distribution of S100A8 (m/z 10,165) and S100A9 (m/z 12,976). Arrows denote abscesses. H&E, hematoxylin and eosin. (E) IMS analysis of S100A8 expression. In each organ set, the top row shows matrix-treated organs and the bottom row shows IMS. Mice were either depleted of neutrophils (RB6) or treated with control antibody (SRF3). Asterisks denote sites of abscess formation.

Fig. 2. Calprotectin inhibits *S. aureus* growth by chelating an essential component from the media. Error bars in (A) to (C), (E), and (F) (some of which are smaller than the symbols) represent the SD of at least three replicates, and all experiments were performed in triplicate. +, $P \leq 0.05$; ++, $P \leq 0.005$ (Student's *t* test). (A) Effect of recombinant calprotectin on *S. aureus* growth. O.D.₆₀₀, optical density at 600 nm. (B) Analysis of *S. aureus* growth in the presence of calprotectin purified with (Ca²⁺) or without (no Ca²⁺) calcium as compared with that in buffer alone (buffer). (C) Analysis of *S. aureus* growth in the presence of S100A8/A9 heterodimers (A8/A9), S100A9 homodimers (A9), S100A8/S100A9C3S heterodimers (A8/A9*), or S100A9C3S homodimers (A9*) as compared with that in buffer alone (buffer). (D) Assessment of calprotectin's ability to coprecipitate with staphylococcal cells. (E) Ability of calprotectin (A8/A9) to inhibit *S. aureus* growth across a dialysis membrane as compared with that in buffer alone (buffer). (F) Growth kinetics of *S. aureus* in media that were pretreated with calprotectin (A8/A9) or buffer control (buffer) and filtered through a centricon column with a 5-kD cutoff.

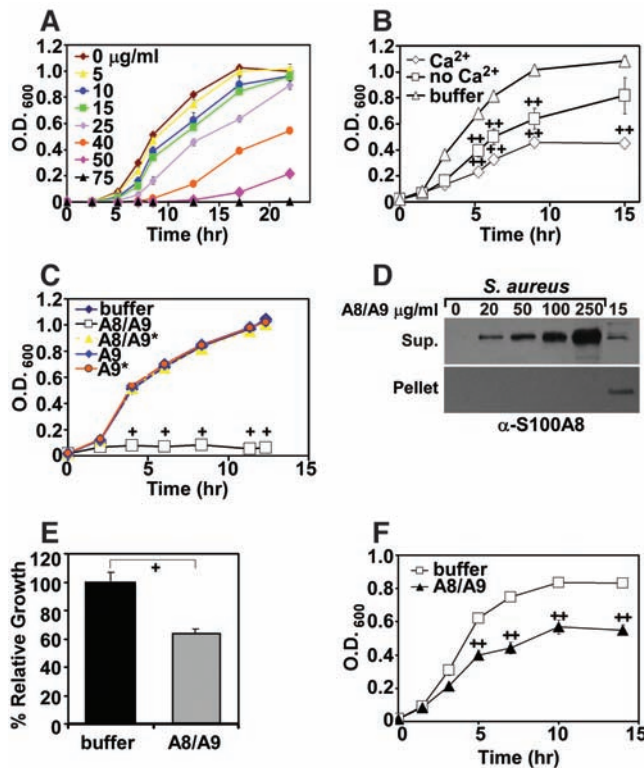
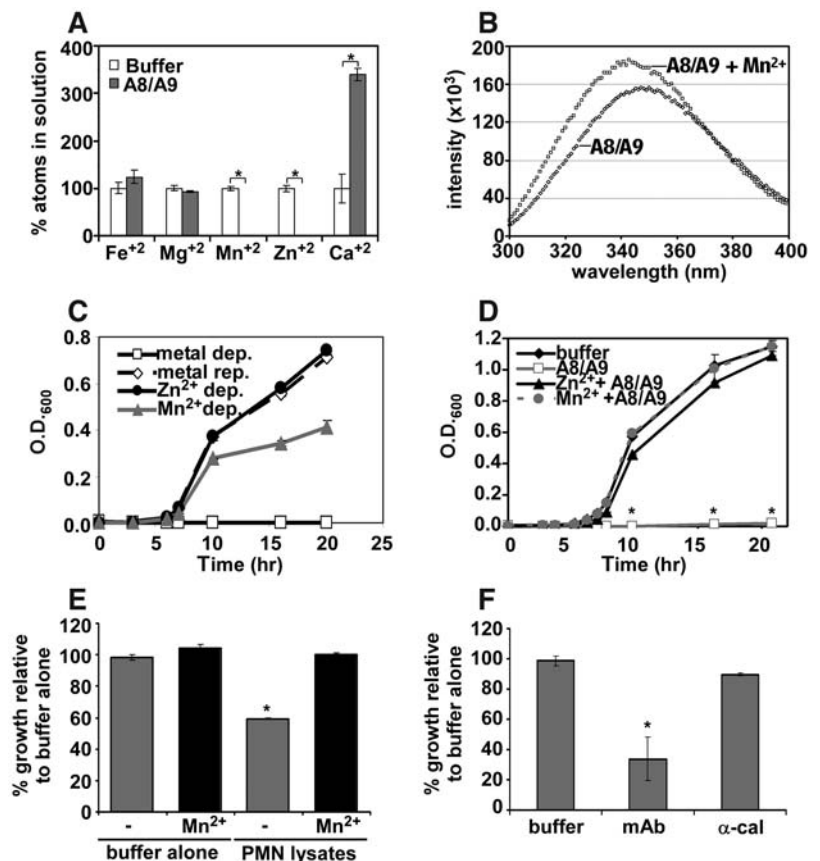
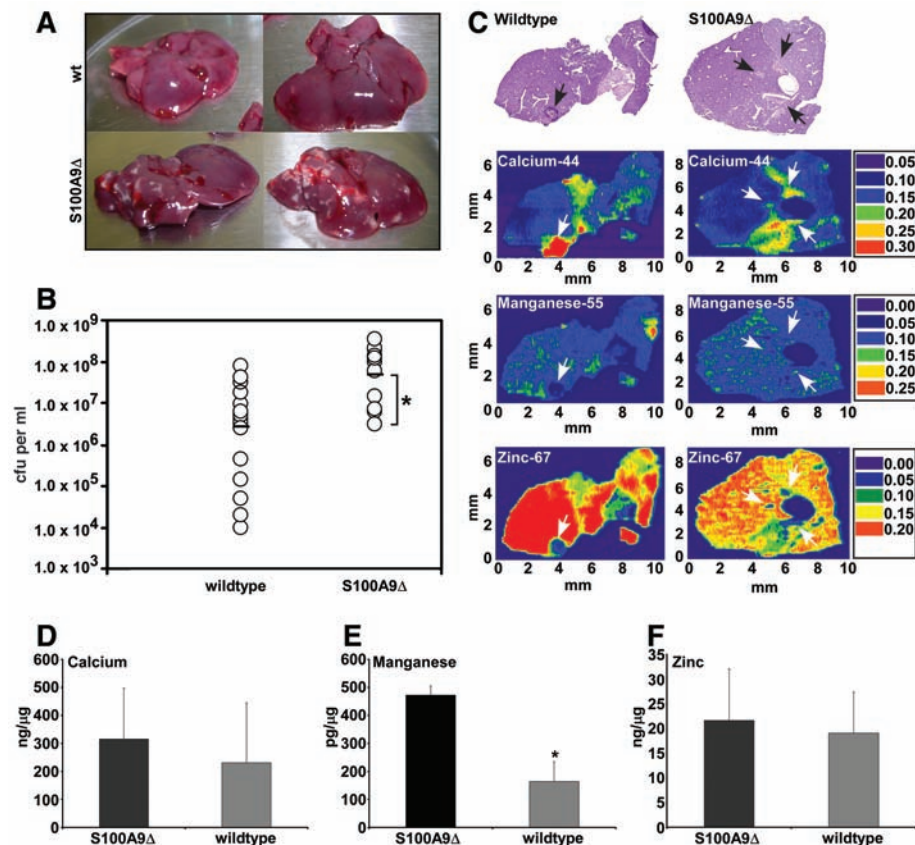


Fig. 3. Calprotectin inhibits staphylococcal growth by chelating Mn²⁺ and Zn²⁺. Error bars in (A) and (C) to (F) represent the SD of at least three replicates. *, $P \leq 0.05$ (Student's *t* test). (A) ICPMS analyses of metals in media after exposure to calprotectin (A8/A9) or buffer alone (buffer). Percent atoms in solution represents the percent of each metal present in medium after treatment as compared with the corresponding percentages in untreated medium. (B) Fluorescence emission spectra of Mn²⁺ (250 μM) and presence (squares) of Mn²⁺ (250 μM). (C) The sensitivity of *S. aureus* to growth in metal-rich media ("metal rep."), media lacking all cations ("metal dep."), media depleted for Zn²⁺ ("Zn²⁺ dep."), or media depleted for Mn²⁺ ("Mn²⁺ dep."). (D) Effect of calprotectin (A8/A9) on *S. aureus* growth in vitro in the presence of excess Zn²⁺ or Mn²⁺. (E) The growth of *S. aureus* upon exposure to neutrophil lysates in the presence or absence of excess Mn²⁺ as compared with that in buffer alone. (F) The growth of *S. aureus* upon exposure to polymorphonuclear leukocyte (PMN) lysates that have been immunodepleted of calprotectin (α-cal), treated with a nonspecific control antibody (mAb), or treated with buffer control (buffer).



Furthermore, comparison of the global gene expression profiles of *S. aureus* exposed to calprotectin with those observed upon Mn²⁺ starvation, Zn²⁺ starvation, heat shock, cold shock, alkaline shock, and acid shock, as well as stringent response-inducing and SOS response-inducing conditions (11), demonstrated that *S. aureus* treated with sub-inhibitory calprotectin elicits an expression profile most closely resembling that of staphylococci starved for Zn²⁺ and Mn²⁺ (fig. S5 and tables S4 to S9). Taken together, these data support a model whereby calprotectin prevents *S. aureus* growth through the chelation of nutrient Mn²⁺ and Zn²⁺. We next sought to determine the contribution of calprotectin to neutrophil-mediated bacterial killing. Neutrophils extracted from wild-type (WT) and calprotectin-deficient mice kill *S. aureus* in vitro with similar efficiency, suggesting that calprotectin does not contribute to phagocytic killing (fig. S6). However, the antimicrobial activity of the cytoplasmic compartment from purified neutrophils is reversible upon the addition of excess Mn²⁺ or immunodepletion of calprotectin (Fig. 3, E and F) (2). These results indicate that neutrophil cytoplasmic extracts containing calprotectin inhibit bacterial growth through metal chelation. In keeping with this, calprotectin is likely directed at bacterial pathogens through targeted secretion systems or upon neutrophil lysis as a posthumous killing mechanism. To determine whether calprotectin-mediated cation chelation inhibits bacterial growth in tissue abscesses, we compared the growth of *S. aureus*

Fig. 4. S100A9 is a vital component of the neutrophil arsenal to inhibit *S. aureus* growth in vivo. **(A)** Photographs of livers dissected from C57BL/6 WT and S100A9 Δ mice infected with *S. aureus* 96 hours after infection. **(B)** *S. aureus* multiplication in infected livers. Each circle represents a positive culture from a single liver. The mean of each group is represented by a horizontal line ($n = 16$ mice for S100A9 Δ , $n = 19$ mice for C57BL/6 wild type). *, $P \leq 0.02$ (Student's *t* test). **(C)** LA-ICPMS of infected organs from WT and calprotectin-deficient (S100A9 Δ) mice. Top panel shows H&E stains. Bottom panels show LA-ICPMS maps for Ca²⁺ ("calcium-44"), Mn²⁺ ("manganese-55"), and Zn²⁺ ("zinc-67"). Arrows denote the site of abscesses. Scales are presented in arbitrary units. **(D to F)** Quantitative determinations of metal concentrations in abscessed tissue from WT or calprotectin-deficient (S100A9 Δ) mice extracted via LCM. The error bars in (D) to (F) represent the SD of three replicates, and the asterisk in (E) denotes statistical significance ($P < 0.05$) as determined by the Student's *t* test.



in abscesses from WT and calprotectin-deficient (S100A9^{-/-}) mice (2). Livers from mice lacking calprotectin exhibit increased abscess formation and bacterial burden as compared with livers from infected WT animals (Fig. 4, A and B). Although we did not detect a significant difference in neutrophil recruitment to the livers of infected animals (fig. S7), additional immunomodulatory functions attributed to calprotectin could contribute to the sensitivity of calprotectin-deficient animals to *S. aureus* infection (12).

To assess the effect of calprotectin on nutrient metal availability inside the abscess, we applied laser ablation ICPMS (LA-ICPMS) mapping to image metal distribution in infected animal tissue (2). LA-ICPMS revealed that staphylococcal liver abscesses from WT mice are enriched in Ca²⁺, which is consistent with robust immune cell infiltrate to the infection site (Fig. 4C). In contrast, these abscesses are devoid of detectable Zn²⁺ and Mn²⁺, unequivocally establishing the abscess as a cation-starved environment (Fig. 4C and fig. S8). Abscesses from mice lacking calprotectin contain appreciable levels of Ca²⁺; however, these levels appear diminished as compared with the levels in abscesses from WT mice, potentially reflecting the Ca²⁺ contribution of calprotectin to the abscess. Furthermore, calprotectin-deficient abscesses contain levels of Mn²⁺ that are equivalent to those in the surrounding healthy tissue, demonstrating the in vivo requirement for calprotectin in Mn²⁺ chelation and removal from the abscess. The absence of

calprotectin did not have a noticeable impact on Zn²⁺ levels in these experiments. To corroborate these results, we extracted abscessed material using laser capture microdissection (LCM) and quantitated Zn²⁺, Mn²⁺, and Ca²⁺ concentrations in isolated abscesses using ICPMS (Fig. 4, D to F). These experiments confirmed that abscesses from mice lacking calprotectin are significantly enriched in Mn²⁺ as compared with those from WT mice (Fig. 4E). Taken together, these results establish calprotectin-mediated metal chelation as an immune defense strategy to prevent bacterial outgrowth in tissue abscesses.

The inhibition of bacterial nutrient uptake represents a promising alternative area of research for the design of new antimicrobials, and the observed calprotectin-mediated metal chelation provides a specific direction to assess the therapeutic potential of this concept. The results reported here suggest that beyond direct treatment of abscesses with calprotectin protein, noncytotoxic bioavailable metal-ion chelators represent a promising area of investigation for inhibitors of microbial growth.

References and Notes

1. F. D. Lowy, *N. Engl. J. Med.* **339**, 520 (1998).
2. See supporting online material.
3. S. Yui, Y. Nakatani, M. Mikami, *Biol. Pharm. Bull.* **26**, 753 (2003).
4. M. Steinbakk *et al.*, *Lancet* **336**, 763 (1990).
5. H. J. Loomans, B. L. Hahn, Q. Q. Li, S. H. Phadnis, P. G. Sohnle, *J. Infect. Dis.* **177**, 812 (1998).

6. D. Lusitani, S. E. Malawista, R. R. Montgomery, *Infect. Immun.* **71**, 4711 (2003).
7. P. G. Sohnle, M. J. Hunter, B. Hahn, W. J. Chazin, *J. Infect. Dis.* **182**, 1272 (2000).
8. I. P. Korndorfer, F. Brueckner, A. Skerra, *J. Mol. Biol.* **370**, 887 (2007).
9. M. J. Hunter, W. J. Chazin, *J. Biol. Chem.* **273**, 12427 (1998).
10. M. J. Horsburgh *et al.*, *Mol. Microbiol.* **44**, 1269 (2002).
11. K. L. Anderson *et al.*, *J. Bacteriol.* **188**, 6739 (2006).
12. M. Benedyk *et al.*, *J. Invest. Dermatol.* **127**, 2001 (2007).
13. We thank members of the Skaar laboratory and F. DeLeo, D. Russell, and H. Seifert for critical reading of this manuscript; the Vanderbilt Pathology Core, Tissue Acquisition Core, O. Aranmolate, L. Zimmerman, M. Reyzer, and S. Joyce for technical assistance; and H. Gresham for providing the monoclonal antibody RB6-8C5. This research was supported by the Searle Scholars Program, NIH R01 GM62112 (to W.J.C.), Engineering and Physical Sciences Research Council GR/S98689/01 (to J.F. and A.R.), NIH 5R01 GM58008-09 and U.S. Department of Defense W81XWH-05-1-0179 (to R.M.C.), and the Vanderbilt-Ingram Cancer Center Core Support Grant NIH P50 CA068485. E.P.S. holds an Investigator in Pathogenesis of Infectious Disease Award from the Burroughs Wellcome Fund. B.D.C., B.M.D., and V.J.T. were supported by NIH training grants T32 HL069765, T32 GM08320, and F32 AI071487, respectively. Minimum Information About a Microarray Experiment-compliant microarray data have been submitted to the Gene Expression Omnibus database under the provisional submission number GSE9828.

Supporting Online Material

www.sciencemag.org/cgi/content/full/319/5865/962/DC1
Materials and Methods
Figs. S1 to S8
Tables S1 to S9
References

1 November 2007; accepted 19 December 2007
10.1126/science.1152449

The Critical Importance of Retrieval for Learning

Jeffrey D. Karpicke^{1*} and Henry L. Roediger III²

Learning is often considered complete when a student can produce the correct answer to a question. In our research, students in one condition learned foreign language vocabulary words in the standard paradigm of repeated study-test trials. In three other conditions, once a student had correctly produced the vocabulary item, it was repeatedly studied but dropped from further testing, repeatedly tested but dropped from further study, or dropped from both study and test. Repeated studying after learning had no effect on delayed recall, but repeated testing produced a large positive effect. In addition, students' predictions of their performance were uncorrelated with actual performance. The results demonstrate the critical role of retrieval practice in consolidating learning and show that even university students seem unaware of this fact.

Ever since the pioneering work of Ebbinghaus (1), scientists have generally studied human learning and memory by presenting people with information to be learned in a study period and testing them on it in a test period to see what they retained. When this procedure occurs over many trials, an exponential learning curve is produced. The standard assumption in nearly all research is that learning occurs while people study and encode material. Therefore, additional study should increase learning. Retrieving information on a test, however, is sometimes considered a relatively neutral event that measures the learning that occurred during study but does not by itself produce learning. Over the years, researchers have occasionally argued that learning can occur during testing (2–6). However, the assumptions that repeated studying promotes learning and that testing represents a neutral event that merely measures learning still permeate contemporary memory research as well as contemporary educational practice, where tests are also considered purely as assessments of knowledge.

Our goal in the present research was to examine these long-standing assumptions regarding the effects of repeated studying and repeated testing on learning. Specifically, once information can be recalled from memory, what are the effects of repeated encoding (during study trials) or repeated retrieval (during test trials) on learning and long-term retention, assessed after a week delay? A second purpose of this research was to examine students' assessments of their own learning. After learning a set of materials under repeated study or repeated test conditions, we asked students to predict their future recall on the week-delayed final test. Our question was, would students show any insight into their own learning?

A final purpose of the experiment was to address another venerable issue in learning and

memory, concerning the relation between the speed with which something is learned and the rate at which it is forgotten. Is speed of learning correlated with long-term retention, and if so, is the correlation positive (processes that promote fast learning also slow forgetting and promote good retention) or negative (quick learning may be superficial and produce rapid forgetting)? Early research led to the conclusion that quick learning reduced the rate of forgetting and improved long-term retention (7), but later critics argued that, when forgetting is assessed more properly than in the early studies, no differences exist between forgetting rates for fast and slow learning conditions (8, 9). By any account, conditions that exhibit equivalent learning curves should produce equivalent retention after a delay (9).

Using foreign language vocabulary word pairs, we examined the contributions of repeated study and repeated testing to learning by comparing a standard learning condition to three dropout conditions. The standard method of measuring learning, used since Ebbinghaus's research (1), involves presenting subjects with information in a study

period, then testing them on it in a test period, then presenting it again, testing on it again, and so on. The dropout learning conditions of the present experiment differed from the standard learning condition in that, once an item was successfully recalled once on a test, it was either (i) dropped from study periods but still tested in one condition, (ii) dropped from test periods but still repeatedly studied in a second condition, or (iii) dropped altogether from both study and test periods in a third condition (Table 1).

Surprisingly, standard learning conditions and dropout conditions have seldom been compared in memory research, despite their critical importance to theories of learning and their practical importance to students (in using flash cards and other study methods). Dropout conditions were originally developed to remedy methodological problems that arise from repeated practice in the standard learning condition (10), but they can also be used to examine the effect of repeated practice in its own right, as we did in the present experiment. If learning happens exclusively during study periods and if tests are neutral assessments, then additional study trials should have a strong positive effect on learning, whereas additional test trials should produce no effect. Further, if repeated study or test practice after an item has been learned does indeed benefit long-term retention, this would contradict the conventional wisdom that students should drop material that they have learned from further practice in order to focus their effort on material they have not yet learned. Dropping learned facts may create the same long-term retention as occurs in standard conditions but in a shorter amount of time, or it may improve learning by allowing students to focus on items they have not yet recalled. This strategy is implicitly endorsed by contemporary theories of study-time allocation (11, 12) and is explicitly encouraged in many popular study guides (13).

Table 1. Conditions used in the experiment, average number of trials within each study or test period, and total number of trials in the learning phase in each condition. S_N indicates that only vocabulary pairs not recalled in the previous test period were studied in the current study period. T_N indicates that only pairs not recalled in the previous test period were tested in the current test period. Students in all conditions performed a 30-s distracter task that involved verifying multiplication problems after each study period.

Condition	Study (S) or test (T) period and number of trials per period								Total number of trials
	1	2	3	4	5	6	7	8	
ST	S 40	T 40	S 40	T 40	S 40	T 40	S 40	T 40	320
$S_N T$	S 40	T 40	S_N 26.8	T 40	S_N 8.0	T 40	S_N 2.0	T 40	236.8
ST_N	S 40	T 40	S 40	T_N 27.9	S 40	T_N 11.8	S 40	T_N 3.3	243.0
$S_N T_N$	S 40	T 40	S_N 27.1	T_N 27.1	S_N 8.8	T_N 8.8	S_N 1.5	T_N 1.5	154.8

¹Department of Psychological Sciences, Purdue University, West Lafayette, IN 47907, USA. ²Department of Psychology, Washington University in St. Louis, St. Louis, MO 63130, USA.

*To whom correspondence should be addressed. E-mail: karpicke@purdue.edu

In the experiment, we had college students learn a list of foreign language vocabulary word pairs and manipulated whether pairs remained in the list (and were repeatedly practiced) or were dropped after the first time they were recalled, as shown in Table 1. All students began by studying a list of 40 Swahili-English word pairs (e.g., *mashua*-boat) in a study period and then testing over the entire list in a test period (e.g., *mashua*-?). All conditions were treated the same in the initial study and test periods. Once a word pair was recalled correctly, it was treated differently in the four conditions. In the standard condition, subjects studied and were tested over the entire list in each study and test period (denoted ST). In a second condition, once a pair was recalled, it was dropped from further study but tested in each subsequent test period (denoted S_NT, where S_N indicates that only nonrecalled pairs were restudied). In a third condition, recalled pairs were dropped from further testing but studied in each subsequent study period (denoted ST_N, where T_N indicates that only nonrecalled pairs were kept in the list during test periods). In a fourth condition, recalled pairs were dropped entirely from both study and test periods (S_NT_N). The final condition represents what conventional wisdom and many educators instruct students to do: Study something until it is learned (i.e., can be recalled) and then drop it from further practice.

At the end of the learning phase, students in all four conditions were asked to predict how many of the 40 pairs they would recall on a final test in 1 week. They were then dismissed and returned for the final test a week later. Of key importance were the effects of the four learning conditions on the speed with which the vocabulary words were learned, on students' predictions of their future performance, and on long-term retention assessed after a week delay (14).

Figure 1 shows the cumulative proportion of word pairs recalled during the learning phase, which gives credit the first time a student recalled

a pair. We also analyzed traditional learning curves (the proportion of the total list recalled in each test period) for the two conditions that required recall of the entire list (ST and S_NT), and the results by the two measurement methods were identical. Thus, we restrict our discussion to the cumulative learning curves on which all four conditions can be compared. Figure 1 shows that performance was virtually perfect by the end of learning (i.e., all 40 English target words were recalled by nearly all subjects). More importantly, there were no differences in the learning curves of the four conditions.

Given the similarity of acquisition performance, it is not too surprising that students in the four conditions did not differ in their aggregate judgments of learning (their predictions of their future performance). On average, the students in all conditions predicted they would recall about 50% of the pairs in 1 week. The mean number of words predicted to be recalled in each condition were as follows: ST = 20.8, S_NT = 20.4, ST_N = 22.0, and S_NT_N = 20.3. An analysis of variance did not reveal significant differences among the conditions ($F < 1$).

Although students' cumulative learning performance was equivalent in the four conditions and predicted final recall was also equivalent, actual recall on the final delayed test differed widely across conditions, as shown in Fig. 2. The results show that testing (and not studying) is the critical factor for promoting long-term recall. In fact, repeated study after one successful recall did not produce any measurable learning a week later. In the learning conditions that required repeated retrieval practice (ST and S_NT), students correctly recalled about 80% of the pairs on the final test. In the other conditions in which items were dropped from repeated testing (ST_N and S_NT_N), students recalled just 36% and 33% of the pairs. It is worth emphasizing that, despite the fact that students repeatedly studied all of the word pairs in every

study period in the ST_N condition, their long-term recall was much worse than students who were repeatedly tested on the entire list. Combining the two conditions that involved repeated testing (ST and S_NT) and combining the two conditions that involved dropping items from testing after they were recalled once (ST_N and S_NT_N), repeated retrieval increased final recall by 4 standard deviations ($d = 4.03$). The distributions of scores in these two groups did not overlap: Final recall in the drop-from-testing conditions ranged from 10% to 60%, whereas final recall in the repeated test conditions ranged from 63% to 95%. Whether students repeatedly studied the entire set or whether they restudied only pairs they had not yet recalled produced virtually no effect on long-term retention. The dramatic difference shown in Fig. 2 was caused by whether or not the pairs were repeatedly tested.

Even though cumulative learning performance was identical in the four conditions, the total number of trials (study or test) in each condition varied greatly. Table 1 shows the mean number of trials in each study and test period and the total number of trials in each condition. The standard condition (ST) involved the most trials (320) because all 40 items were presented in each study and test period. The S_NT_N condition involved the fewest trials (154.8, on average) because the number of trials in each period grew smaller as items were recalled and dropped from further practice. The other two conditions (S_NT and ST_N) involved about the same number of trials (236.8 and 243.0, respectively) but because they differed in terms of whether items were dropped from study or test periods, they produced dramatically different effects on long-term retention. In other words, about 80 more study trials occurred in the ST_N condition than in the S_NT_N condition, but this produced practically no gain in retention. Likewise, about 80 more study trials occurred in the ST condition than in the S_NT condition, and this produced no gain whatsoever in retention. However, when about 80 more test trials occurred in the learning phase (in the ST condition versus the ST_N condition, and in the S_NT condition versus the S_NT_N condition), repeated retrieval practice led to greater than 150% improvements in long-term retention.

The present research shows the powerful effect of testing on learning: Repeated retrieval practice enhanced long-term retention, whereas repeated studying produced essentially no benefit. Although educators and psychologists often consider testing a neutral process that merely assesses the contents of memory, practicing retrieval during tests produces more learning than additional encoding or study once an item has been recalled (15–17). Dropout methods such as the ones used in the present experiment have seldom been used to investigate effects of repeated practice in their own right, but comparison of the dropout conditions to the repeated practice conditions revealed dramatic effects of retrieval practice on learning.

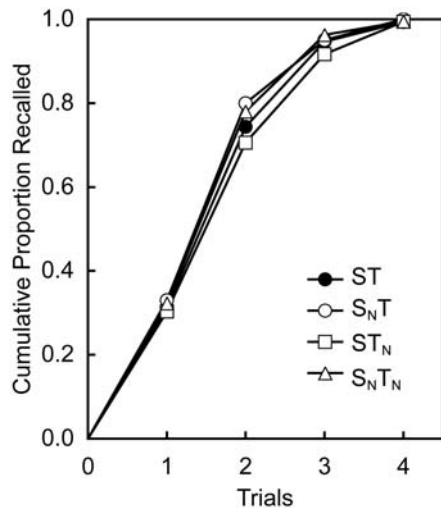


Fig. 1. Cumulative performance during the learning phase.

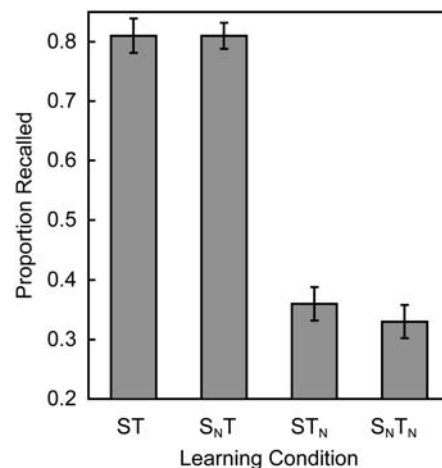


Fig. 2. Proportion recalled on the final test 1 week after learning. Error bars represent standard errors of the mean.

The experiment also shows a striking absence of any benefit of repeated studying once an item could be recalled from memory. A basic tenet of human learning and memory research is that repetition of material improves its retention. This is often true in standard learning situations, yet our research demonstrates a situation that stands in stark contrast to this principle. The benefits of repetition for learning and long-term retention clearly depend on the processes learners engage in during repetition. Once information can be recalled, repeated encoding in study trials produced no benefit, whereas repeated retrieval in test trials generated large benefits for long-term retention. Further research is necessary to generalize these findings to other materials. However, the basic effects of testing on retention have been shown with many kinds of materials (16), so we have confidence that the present results will generalize, too.

Our experiment also speaks to an old debate in the science of memory, concerning the relation between speed of learning and rate of forgetting (7–9). Our study shows that the forgetting rate for information is not necessarily determined by speed of learning but, instead, is greatly determined by the type of practice involved. Even though the four conditions in the experiment produced equivalent learning curves, repeated recall slowed forgetting relative to recalling each word pair just one time.

Importantly, students exhibited no awareness of the mnemonic effects of retrieval practice, as evidenced by the fact that they did not predict they would recall more if they had repeatedly

recalled the list of vocabulary words than if they only recalled each word one time. Indeed, questionnaires asking students to report on the strategies they use to study for exams in education also indicate that practicing recall (or self-testing) is a seldom-used strategy (18). If students do test themselves while studying, they likely do it to assess what they have or have not learned (19), rather than to enhance their long-term retention by practicing retrieval. In fact, the conventional wisdom shared among students and educators is that if information can be recalled from memory, it has been learned and can be dropped from further practice, so students can focus their effort on other material. Research on students' use of self-testing as a learning strategy shows that students do tend to drop facts from further practice once they can recall them (20). However, the present research shows that the conventional wisdom existing in education and expressed in many study guides is wrong. Even after items can be recalled from memory, eliminating those items from repeated retrieval practice greatly reduces long-term retention. Repeated retrieval induced through testing (and not repeated encoding during additional study) produces large positive effects on long-term retention.

References and Notes

1. H. Ebbinghaus, *Memory: A Contribution to Experimental Psychology*, H. A. Ruger, C. E. Bussenius, Transl. (Dover, New York, 1964).
2. R. A. Bjork, in *Information Processing and Cognition: The Loyola Symposium*, R. L. Solso, Ed. (Erlbaum, Hillsdale, NJ, 1975), pp. 123–144.
3. M. Carrier, H. Pashler, *Mem. Cognit.* **20**, 633 (1992).

4. A. I. Gates, *Arch. Psychol.* **6**, 1 (1917).
5. C. Izawa, *J. Math. Psychol.* **8**, 200 (1971).
6. E. Tulving, *J. Verb. Learn. Verb. Behav.* **6**, 175 (1967).
7. J. A. McGeoch, *The Psychology of Human Learning* (Longmans, Green, New York, 1942).
8. N. J. Slamecka, B. McElree, *J. Exp. Psychol. Learn. Mem. Cognit.* **9**, 384 (1983).
9. B. J. Underwood, *J. Verb. Learn. Verb. Behav.* **3**, 112 (1964).
10. W. F. Battig, *Psychon. Sci. Monogr.* **1** (suppl.), 1 (1965).
11. J. Metcalfe, N. Kornell, *J. Exp. Psychol. Gen.* **132**, 530 (2003).
12. K. W. Thiede, J. Dunlosky, *J. Exp. Psychol. Learn. Mem. Cognit.* **25**, 1024 (1999).
13. S. Frank, *The Everything Study Book* (Adams, Avon, MA, 1996).
14. Materials and methods are available as supporting material on Science Online.
15. J. D. Karpicke, H. L. Roediger, *J. Mem. Lang.* **57**, 151 (2007).
16. H. L. Roediger, J. D. Karpicke, *Perspect. Psychol. Sci.* **1**, 181 (2006).
17. H. L. Roediger, J. D. Karpicke, *Psychol. Sci.* **17**, 249 (2006).
18. N. Kornell, R. A. Bjork, *Psychon. Bull. Rev.* **14**, 219 (2007).
19. J. Dunlosky, K. Rawson, S. McDonald, in *Applied Metacognition*, T. Perfect, B. Schwartz, Eds. (Cambridge Univ. Press, Cambridge, 2002), pp. 68–92.
20. J. D. Karpicke, thesis, Washington University, St. Louis, MO (2007).
21. We thank J. S. Nairne for helpful comments on the manuscript. This research was supported by a Collaborative Activity Grant of the James S. McDonnell Foundation to the second author.

Supporting Online Material

www.sciencemag.org/cgi/content/full/319/5865/966/DC1

Materials and Methods

Table S1

References

31 October 2007; accepted 12 December 2007

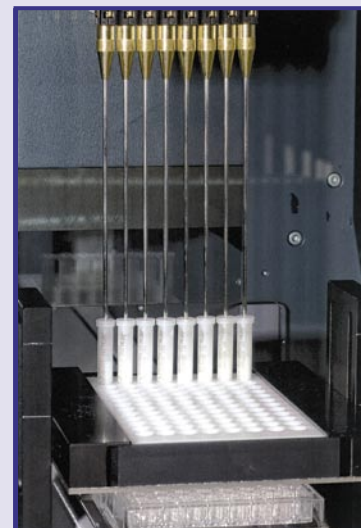
10.1126/science.1152408

High Throughput Bioprocess Development

Tecan and Atoll have successfully integrated Atoll's MediaScout 96-well RoboColumn system with the Tecan Freedom EVO liquid handling workstation to allow fully automated bioprocess parameter screening and high throughput screening of chromatographic resins. The combination simplifies handling of a large number of samples and testing of chromatographic conditions during development of purification methods. MediaScout RoboColumns deliver the separation performance of regular ready-to-use liquid chromatography columns with very high reproducibility. These columns are offered with almost every adsorptive resin available and for multiple sample desalting applications with small pore gel permeation chromatography materials. The configurable Freedom EVO workstation provides precise and reliable liquid handling and accommodates a wide range of devices, including a plate stacker module and a robotic manipulator arm to transfer 96-well plates into a plate reader. Integrating the two technologies removes all manual steps for buffer preparation, sample injection, elution, and detection, allowing 96-well plates to be completely processed in just minutes.

Tecan Group

For information +41 44 922 81 11
www.tecan.com



Literature

Catalogue of Microplates & Microplate Equipment is a 60-page resource that introduces a wealth of versatile, high-performance new products, including Thermobond 2 (a new low-cost plate sealer), Microstream (an innovative plate and tube rack thawing system), and MiniSeal (an entry-level semiautomated thermal sealer developed for laboratories sealing small to medium batches of microplates). The catalog includes an expanded range of microplate seals and several new products extending Porvair Sciences' assay plate range into the ultraviolet range. The catalog is divided into five main sections: solid-phase extraction, life sciences, storage and collection, microplate equipment, and automation.

Porvair Sciences

For information +44 1932 240255
www.porvair-sciences.com

Chemistry Pumping Unit

The PC VARIO 3001 Chemistry Pumping Unit is a new generation of diaphragm pumping system for small- to medium-scale chemistry applications including evaporation, sample concentration, drying, and distillation. The unit combines the proven performance and reliability, even in tough operating conditions, of its predecessor (PC VARIO 2001) with a new highly intuitive vacuum controller. The new controller saves time through simplified operation resulting from easy-to-use jog wheel operation and clear text menus. Through proven low-vacuum chemistry pumping technology, the PC VARIO 3001 sets the standard for reliability, reproducibility, efficiency, and low operational noise in a compact benchtop unit. Providing vacuum down to 2 mbar and a pumping speed of up to 1.7 m³/hour, the unit delivers fast, continuously high evaporation rates, even with high-boiling-point solvents. The unit's automatic boiling point detection and anti-bumping technology mean that it is no longer necessary to constantly monitor the process.

Radleys

For information +44 1799 513320
www.radleys.co.uk

High-Capacity Evaporator

Genevac HT-12 Series II systems are designed to solve evaporation bottlenecks in high throughput and production laboratories. The systems offer options for integration into automated environments, for

handling potentially explosive solvents, and for use with strong acids. Applications include fast lyophilization, combinatorial chemistry, parallel synthesis, compound purification, plate reformatting, and plate replication requiring high throughput evaporation. The unique design of the HT-12 multilayer rotor ensures efficient use of laboratory bench space. The HT-12 instruments incorporate the latest scroll pump technology and do not require any pumping fluid or lubricant to operate, which makes the system suitable for use in harsh chemistry environments. The system incorporates a wide range of sample formats. The stainless steel rotors incorporate 12 "sample swings" to accommodate sample holders for tubes, vials, microtiter plates, and custom sample formats.

Genevac

For information +44 1473 240000.
www.genevac.com

Electrophoresis Interference Removal

PAGE-Perfect removes all interfering agents from protein solutions, allowing the samples to be reproducibly resolved on polyacrylamide gels with higher band visibility, greater protein resolution, and no band distortion. It is a simple two-step method for concentrating, cleaning, and preparing protein solutions for loading on gels. The user simply treats the protein solution with the supplied reagents, resulting in the precipitation of the proteins and removal of interfering agents. It removes detergents, salts, chaotropes, and reducing agents.

G-Biosciences/Genotech

For information 800-628-7730
www.GBiosciences.com

Electronically submit your new product description or product literature information! Go to www.sciencemag.org/products/newproducts.dtl for more information.

Newly offered instrumentation, apparatus, and laboratory materials of interest to researchers in all disciplines in academic, industrial, and governmental organizations are featured in this space. Emphasis is given to purpose, chief characteristics, and availability of products and materials. Endorsement by *Science* or AAAS of any products or materials mentioned is not implied. Additional information may be obtained from the manufacturer or supplier.